

Final Design Report

Stratospheric Aerosol
Geoengineering Aircraft

Final Design Report

Stratospheric Aerosol Geoengineering Aircraft

by

Design Synthesis Exercise Group 2

As part of the course:

AE3200 Design Synthesis Exercise

at Delft University of Technology

Team members:	M. Cruellas Bordes	4277600
	C.J.G. De Petter	4279387
	M. Janssens	4275780
	A.F. van Korlaar	4295951
	L.P. Kulik	4268857
	R. Maselis	4278224
	L.H. Mulder	4305264
	S. Stoev	4273249
	K.J.F. van Vlijmen	4337832
	I.E. de Vries	4305744

Course staff:	Dr. S. J. Hulshoff	Tutor
	D. Rajpal	Coach
	C. M. Souza	Coach

Preface

This report is the concluding report in a series of reports for the *Design Synthesis Exercise*. The *Design Synthesis Exercise* is the conclusion of the undergraduate part of the education in Aerospace Engineering at Delft University of Technology. In this final project students combine all knowledge obtained during the bachelor and enhance their skills in designing, and particularly in designing in a team.

In 11 weeks 10 aerospace engineering students perform the preliminary design of an aircraft suited for the delivery of aerosol to stratospheric altitudes around 20 km, as well as estimations of the initial and operating cost of a fleet of such aircraft capable of delivering 5 million metric tonnes of aerosols per year. A more elaborate discussion of the background of this problem can be found in Chapter 2 and a market analysis is performed in Chapter 3. Readers with a particular interest in the actual final aircraft design, including the design of the aerosol dispersion system, are referred to Chapters 7 and 8. Next to this, the operational concept, the initial concept selection, a sensitivity analysis, risk identification, resource allocation, a RAMS analysis, a sustainable development strategy, a production plan and a planning for future development is included.

Acknowledgments

Our thanks go out to our supervisor Steven Hulshoff and coaches Darwin Rajpal and Carlos Melo Souza. Furthermore, we would like to thank Delft University of Technology for providing us with the opportunity and facilities to participate in this project, in particular the OSCC. Next to that our gratitude is for associate professor of the Politecnico di Milano Sergio Ricci, PhD candidate from Stanford University E. Botero, J. Engel from KURVAL, F. Rijkhold Meesters and P. Siegmend from the Royal Netherlands Meteorological Institute (KNMI). Finally we are grateful for the help of associate professor R. de Breuker, associate professor C. Kassapoglou, associate professor J.L.A. Dubbeldam, PhD candidate L. Azzini and PhD candidate K. van AS, all from Delft University of Technology.

Summary

The concern of global warming is present more than ever. The efforts to stop global warming focus on solving the problem in the long term, by reducing emissions and capturing currently present greenhouse gases. Future scenarios depend on many aspects, making the prediction of greenhouse gas concentrations and the climate's response uncertain. If the most pessimistic trends unfold, an unacceptable temperature increase before long term solutions kick in may occur. A temporary intervention to manage global temperatures and prevent this whilst working on the implementation of a permanent solution may therefore be required. Stratospheric geoengineering, more specifically, solar radiation management (SRM), offers such a temporary solution. A possible implementation of SRM is the injection of aerosols in the stratosphere, producing stratospheric clouds which reflect part of the incoming sunlight. This report aims to describe the preliminary technical and operational design a fleet of purpose-built Stratospheric Aerosol Geoengineering Aircraft (SAGA) to deliver five megatons of aerosol per year to altitudes between 18.5 and 19.5km to gain insight in the costs and impact of such a system.

A fleet of almost 350 aircraft with a range of 7000km is proposed to deliver five megatons of aerosol to the stratosphere. With a payload of 35 tons, two regional flights per aircraft per day meet this requirement. For optimal aerosol activity, the injection is proposed in the tropical region, where seven airports will facilitate SAGA operations. The aerosol consists of sulfuric acid – H₂SO₄.

The technical aircraft constraints for the SAGA mission require a very specific design. The high altitude and high payload create the need for a high aspect ratio of 13, a wing surface area of 700 m² and 4 engines each capable of providing in excess of 600 kN of sea level thrust. Following from these requirements, the structural weight and aeroelastic effects are critical design drivers, requiring a 28.2 metric ton strut-braced wing. An aerosol storage and dispersion system requiring ground pre-heating and 1.65 MW of engine-supplied power ensures a constant evaporation of 2.1 kg/s. SAGA will also be unmanned.

Care for the environment is a social responsibility, thus economical profits are not the goal of the SAGA mission. SAGA is therefore proposed as a worldwide program, in which governments form a supervising and funding consortium. A maximum total development cost of \$100 billion and a maximum yearly operating cost of \$11 billion are expected to meet the operations.

Finally, the environmental impact of the aerosol in the stratosphere is estimated to reduce solar influx to counteract a 25% increase in CO₂ concentration, while SAGA's contribution to atmospheric sulfur compounds is estimated to 4%. SAGA's contribution to worldwide fuel consumption is determined to 0.03% only.

The SAGA project concludes that an aircraft-based platform for stratospheric geoengineering is feasible in terms of technical design, costs and environmental impact. It is a realistic, short-term achievable option with a high technological readiness level. While several design risks remain at this stage of development, a detailed design phase and careful future planning may facilitate implementation of SAGA in 7 years.

Contents

Preface	i
1 Introduction	1
2 Problem background	2
3 Market analysis	4
3.1 Funding concept	4
3.2 Public opinion	5
3.3 State-of-the-art and cost estimation	5
3.4 Possible alternatives/competition	6
3.5 Market analysis conclusion	6
4 Operations and logistic concept description	8
4.1 General Considerations	8
4.1.1 Injection Location	8
4.1.2 Payload	8
4.1.3 Dispersion rate.	9
4.2 Operational concept	9
4.2.1 Operational range	9
5 Concept trade offs	12
5.1 Concepts, trade-off criteria and weights	12
5.2 Trade-off results and discussion.	13
5.2.1 Conventional concept analysis.	13
5.2.2 Blended wing body concept	14
5.2.3 Twin body aircraft	14
5.2.4 Second trade-off and final design decision.	14
6 Functional analysis	16
6.1 Functional breakdown structure	16
6.2 Functional flow diagrams	16
7 Final design	18
7.1 Description of final design	18
7.2 Drawings	19
8 Analysis and evaluation SAGA concept	21
8.1 Design framework and overview	21
8.1.1 Risk-oriented design focus.	21
8.1.2 Design methodology.	22
8.1.3 Design insights.	23
8.2 Performance	23
8.2.1 SUAVE mission analysis	24
8.2.2 Design choices.	24
8.2.3 SUAVE results	26
8.2.4 Verification and Validation.	28
8.2.5 Sensitivity analysis.	30
8.3 Aerodynamics.	34
8.3.1 Aerodynamic design drivers	34
8.3.2 First-order aerodynamic model	34
8.3.3 Wing design	35
8.3.4 Horizontal tail	38
8.3.5 Vertical tail.	38
8.3.6 Strut	39
8.3.7 Detailed analysis.	39
8.3.8 Sensitivity analysis.	41
8.3.9 Verification and Validation.	42
8.4 Propulsion and power.	43
8.4.1 General design choices.	43

8.4.2 Engine design	43
8.4.3 Verification and validation	47
8.4.4 Sensitivity analysis	48
8.5 Structures and materials	48
8.5.1 Design choices	49
8.5.2 Verification and validation	55
8.5.3 Material characteristics	56
8.6 Aeroelasticity	58
8.6.1 Results	58
8.6.2 Recommendations to handle aeroelastic problems	58
8.6.3 Verification & Validation	60
8.6.4 Sensitivity analysis	63
8.6.5 Conclusion	65
8.7 Stability and control	65
8.7.1 Tail sizing	66
8.7.2 Control surface sizing	67
8.7.3 Verification and validation	69
8.7.4 Sensitivity analysis	71
8.8 Systems	72
8.8.1 Fuel system	73
8.8.2 Hydraulic System	73
8.8.3 Electrical system	73
8.8.4 Communication system	73
8.8.5 Hardware/software system	74
8.8.6 Data handling system	75
8.9 Aerosol handling system	77
8.9.1 Aerosol design choices, motivations and consequences	77
8.9.2 Verification and validation	82
8.9.3 Sensitivity analysis	83
9 Verification and validation	84
9.1 Handling of discrepancies	84
9.2 Verification strategies	84
9.2.1 Unit tests	84
9.2.2 System tests	84
9.3 Verification results	85
9.4 Validation strategies and current results	85
9.5 Requirements compliance matrix	86
9.5.1 Feasibility analysis	90
10 Sensitivity analysis	91
11 Risk identification	92
11.1 Risk map scales	92
11.2 Aircraft risks	92
11.3 Operational risks	96
11.4 Aerosol-related risks	98
11.5 Remaining design risks	100
11.6 Design margins	103
12 Resource allocation	104
12.1 Cost breakdown	104
12.2 Budget breakdown	109
13 Reliability, availability, maintainability and safety analysis	114
13.1 Required level of reliability	114
13.2 Safety critical functions	114
13.3 Redundancy philosophy	115
13.4 Expected reliability level	116
13.5 Expected availability level	117
13.6 Maintenance activities	117
14 Sustainability strategy and analysis	118
14.1 Strategies for sustainability	118

14.2 Sustainable conceptual design choices	118
14.3 Sustainable preliminary design choices	119
14.4 Environmental effects of SAGA	119
15 Production plan	122
15.1 Main considerations	122
15.2 Manufacturing, assembly and integration of SAGA	122
16 Future planning	125
16.1 Project design and development logic.	125
16.2 Project Gantt chart	127
17 Conclusion and recommendations	128
17.1 Recommendations	128
Bibliography	130
Nomenclature	134
List of Figures	137
List of Tables	139
A SUAVE inputs and outputs	141

1. Introduction

Global warming is advancing faster than models from just a decade ago predicted. Ongoing emissions of carbon dioxide and other greenhouse gases have caused a significant rise in the average Earth's temperature over the past century and might lead to positive feedback effects which further exacerbate the consequences of global warming. Recent efforts to counteract climate change focus on solving the problem in the long term, by reducing the emissions of and capturing greenhouse gases. Future scenarios depend on many aspects, making the prediction of greenhouse gas concentrations and the climate's response very uncertain. The possibility of an unacceptable temperature increase before long term solutions become effective necessitates the development of a system capable of managing global temperatures as a means of temporary risk control, whilst long term solutions are being implemented. An active way of adjusting the climate, should it be necessary, is presented by geoengineering. Geoengineering is an overarching term for the intentional manipulation of the environment, particularly manipulation intended to reduce the undesired effects of anthropogenic climate change. A geoengineering method to counteract the global temperature increase is solar radiation management (SRM). SRM counteracts warming of the Earth's surface by reducing incident solar radiation. Several possibilities to reduce solar irradiation exist, including e.g. space mirror placement, marine cloud brightening and stratospheric aerosol injection. This report provides a possible implementation strategy, detailed analysis and design of a stratospheric aerosol injection platform using aircraft.

The aim of the Stratospheric Aerosol Geoengineering Aircraft (SAGA) is to deliver aerosol material to the stratosphere, in order to establish an Earth-covering stratospheric cloud of particles that scatters part of the incoming sunlight. Different possible methods to deliver aerosol material to the stratosphere have been identified, however, detailed feasibility analyses and proposed implementation strategies for realistic methods are not abundant. The SAGA project focuses on one method only for stratospheric aerosol delivery, namely the use of a fleet of purpose-built aircraft. An operational scenario is created, as well as a preliminary design of an aircraft, using a purpose-specific approach, designed to meet all functional requirements identified to perform the mission. In addition, a cost-analysis of both development and operational cost of the SAGA mission features in this study. This study is intended to contribute to already available literature on geoengineering methods by providing a specific, in-depth analysis of one realistic SRM technique, available and implementable on relatively short notice.

The report starts with an elaboration of the topic background in Chapter 2, before a market analysis is conducted in Chapter 3. This is followed by a proposition for an operational and logistic concept in Chapter 4. The report then turns to the aircraft development process, first through a summary of aircraft concept trade offs in Chapter 5, then in terms of its functional breakdown and flow in Chapter 6 and finally through a final design presented in Chapter 7 and analysed in terms of its technical disciplines in Chapter 8. Subsequently, the verification and validation procedures and results, as well as a requirements verification of the technical analyses are outlined in Chapter 9, before Chapter 10 discusses the overall sensitivity of the final design to important mission parameters. A risk analysis follows in Chapter 11, followed by a resource allocation to estimate costs and other budgets in Chapter 12. Reliability, availability, maintainability and safety are addressed in Chapter 13, and SAGA's sustainability strategy is presented in Chapter 14. Finally, suggestions for further progression along the path set in this report are included in terms of a production plan in Chapter 15 and a future planning in Chapter 16, resulting in the overall conclusion and recommendations of the SAGA project in Chapter 17.

2. Problem background

As briefly mentioned in the introduction, the SAGA mission is a venture of temporary nature. It is essential to point out that this mission is no solution to the problem of global warming. Anthropogenic contribution to the rising concentration of greenhouse gases in the atmosphere causes an increase in the Earth's surface temperature and climate change. The most adequate way to tackle this problem is not cooling down the earth by an opposite anthropogenic intervention, but rather eliminating the cause of excessive heating. Solutions to climate change and global warming should therefore be focused on reducing the emission of greenhouse gases and possibly capturing them to reduce their concentration. History has shown that changing the current society habits to low-emission, sustainable ones cannot be achieved overnight. This inertia of society must be taken into account when developing a strategy to halt or reverse global warming. Additionally, even if emissions can be drastically reduced in a short amount of time, the expected decrease in concentration of greenhouse gases will not occur simultaneously, as the current concentration is the sum of emissions over the past decades, and thus not directly affected by an instantaneous reduction of emissions. Accordingly, the temperature will not change instantly upon reduction of emissions. This slow response indicates it is likely that the anthropogenic temperature and climate effects will not be eliminated in the short term. In 2009, following the Conference of the Parties in Copenhagen, it was concluded a 2 K increase in temperature with respect to pre-industrial levels should be considered dangerous [1]. According to an ongoing temperature analysis conducted by NASA's Goddard Institute for Space Studies (GISS), the average global temperature on Earth has increased by about 0.8 K since 1880. This number is still well below the 2 K specified in 2009, however, alarming is that two-thirds of the warming has occurred since 1975, at a rate of roughly 0.15-0.20 K per decade [2]. In Fig. 2.1 and 2.2 the temperature anomalies observed in 1880 and in 2014 are shown. The rate of temperature increase necessitates active reforms, however, the mentioned societal inertia and the variety of aspects affecting temperature and climate require attention. The future of the climate is not accurately predictable, which creates a need for a range of possible interventions in case unacceptable scenarios become the reality.

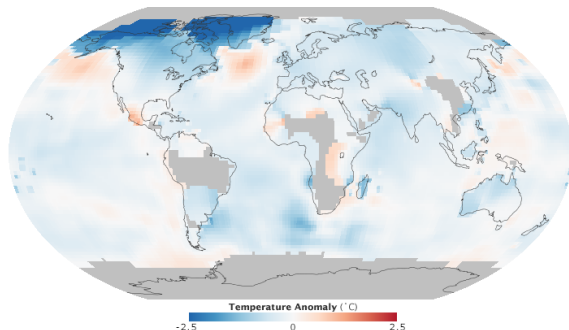


Figure 2.1: Worldwide temperature anomalies 1885-1894 [2]

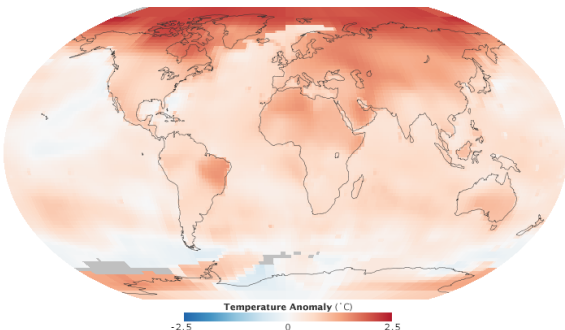


Figure 2.2: Worldwide temperature anomalies 2005-2014 [2]

Geoengineering by solar radiation management is one of those possible interventions. In case temperature trends do not plateau out or start decreasing at a point comfortably under the 2 K temperature increase considered 'dangerous', a temporary intervention to ensure temperatures do not rise further is necessary. In case a program to halt temperature increase is indeed implemented, it is still essential that efforts to reduce greenhouse gas concentrations will follow. These efforts should reduce global greenhouse gas levels gradually, enabling a corresponding gradual decrease in artificial temperature management such that the temperature balance is maintained, with complete elimination of geoengineering eventually. Geoengineering in the form of solar radiation management is not a suitable method to counteract climate change as a whole. From studying volcanic eruptions, a natural analogue to the delivery of sunlight-scattering aerosols in the stratosphere, it could be established that a decrease of overall temperature occurs, however, locally – temperatures in the tropics decrease while polar temperatures increase [1]. Polar ice melting is thus not prevented with solar radiation management. Furthermore, global average precipitation reduces, which is detrimental for desertification, and a risk of increased ozone depletion exists [1, 3]. These effects indicate that temperature reduction cannot be decoupled from other climate effects, and show that geoengineering is

not a suitable measure to be used permanently. A very important thing to realise is that we should not want to employ geoengineering. What we need to do, is take climate change into serious consideration and take action to reduce emissions fast. Assuming this works and we reach the point where the temperature is at its maximum and starts to decrease again, there is a chance that the temperatures around that maximum are dangerously high. In that case, if extreme and unsafe temperatures are reached despite successful efforts to halt climate change, there might come a day when we realise that implementing geoengineering, though very undesirable, is still more desirable than not implementing geoengineering. If used as a means of risk control to temporarily manage temperature until acceptable levels of greenhouse gases are achieved, and not instead of action, geoengineering is justified. The eventual end result of all possible scenarios, whether geoengineering is implemented or not, is the restoration of the climate and temperatures to pre-industrial-like conditions without a continuous need for anthropogenic climate manipulation.

Fig. 2.3 and 2.4 show qualitative representations of the possible scenarios with and without implementation of geoengineering and with or without mitigation by greenhouse gas concentration reduction. In both figures the green continuous lines are the preferred scenarios. When active mitigation works optimally, the threshold temperature increase is not reached, meaning there is no need for geoengineering. Without mitigation, temperatures will rise. When temporary geoengineering is implemented in combination with mitigation strategies, geoengineering helps to keep the temperature below the threshold until greenhouse gas concentration is sufficiently reduced. When geoengineering is implemented, and no mitigation is applied temperatures will rise very rapidly upon halting geoengineering – the moral hazard if geoengineering is wrongfully seen as a solution.

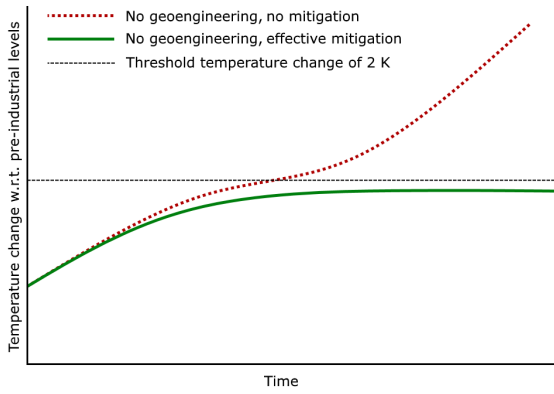


Figure 2.3: Temperature scenarios without implementation of geoengineering

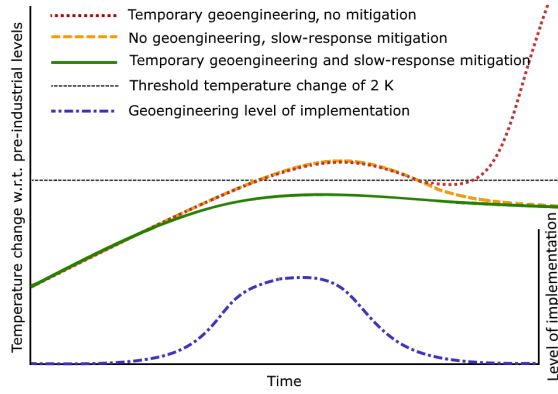


Figure 2.4: Temperature scenarios with implementation of geoengineering

SAGA comes in when a temporary intervention to stabilise temperatures is needed. Solar radiation management using stratospheric aerosols aims to reduce the insolation by reflecting part of the incident sunlight. The reason for injecting aerosols specifically in the stratosphere is the absence of vertical motion, causing the e-folding time to be about a year, whereas tropospheric clouds would fall down much faster [1]. Many methods to deliver the aerosol material to the stratosphere have been identified, among which are shooting of missiles, tethered balloons and aircraft delivery. Preliminary studies indicate tethered balloons are likely to be the most economical option [4], however, the needed technology and methods to implement this strategy are not yet developed and experience with balloon-sustained pipes of lengths that can reach the stratosphere (20 km) is lacking. The most economical solution with a possibility for fast implementation and a high chance of success is a delivery system based on a fleet of purpose-built aircraft. The level of technology and experience in the aircraft industry is very high, enabling fast, reliable and safe development and implementation of an aerosol delivery system. The requirement for fast implementation results from geoengineering being the last resort. Only if dangerous situations are absolutely impossible to be prevented without the implementation of geoengineering, it will be employed. This implies that upon the decision to employ geoengineering is made, action is required fast. As a consequence of this, the technological readiness level and the reliability and safety of solutions is of large importance for all aspects of the SAGA mission.

3. Market analysis

Geoengineering is considered to be a social responsibility. It is therefore difficult to clearly define a market for stratospheric aerosol geoengineering, since the intention is not to commercialise it and make economical profits out of it. However, the policymakers will definitely consider the costs and benefits/drawbacks of the SAGA-project compared to alternatives. Furthermore, for a world-affecting concept such as geoengineering, it is important to obtain an overview of the state-of-the-art of the investigated technology and the present public opinion.

3.1 Funding concept

There are two major development concepts available. For both concepts it is assumed that the implementation of geoengineering needs worldwide support and cooperation to be a success. Thus, a supervising and funding consortium should be established, likely consisting of the world's most influential governments. The development of a geoengineering program using aircraft can then be organised in two ways. Firstly, it is possible to reach out to a number of aerospace companies with requests for proposal and either select one of them, or follow through with a few in parallel. Secondly, it is possible to set up a non-profit transnational engineering division tasked with designing the complete system.

The first concept has been used with success mostly by US government agencies to receive competitive proposals from the private sector. Joint Strike Fighter initial proposal submissions were received from McDonnell Douglas, Northrop Grumman, Lockheed Martin and Boeing¹, from which Boeing and Lockheed were awarded prototype contracts. Similarly NASA currently oversees competition between United Launch Alliance and Space Exploration Technologies both working on *Commercial Crew Program* capabilities². Such an approach offers a promise of competitive costs and reduced risk thanks to multiple independent designs. The drawbacks are: dependence on willingness of the private sector to submit their proposals (which will be the case only if the project offers them positive net present value), possible conflicts of interest when assigning such a large contract and lack of complete control over the project. The private sector could be incentivized to cooperate by offering them the right to retain the intellectual property and technologies developed during the SAGA project, some of which could be promising, but risky ventures, unlikely to be attempted otherwise.

The second concept is reminiscent of the International Space Station programme, which is a joint project among five participating public space agencies³. Intergovernmental treaties and agreements establish the ownership and use of the ISS as it would likely be in the case of the SAGA³. This approach offers more control over the project and a chance to open-source publicly funded technologies – with the benefit of free-of-charge audits by independent experts worldwide and spurring innovation. The main disadvantages are increased risk due to only one design being pursued, and possibility of unmitigated cost explosion as with many other government programs.

When it comes to actual financing, money will most likely come from a public pool provided by the cooperating governments comprising the supervising/funding consortium. The costs should be split fairly, e.g. based on estimated cumulative contribution to global warming. The costs incurred by the governments could be in turn offset by taxing the biggest polluters using Pigouvian “carbon tax”.

To be able to fund their part of the total cost, the governments will seek contributions from investors willing to provide financing, e.g. by buying bonds. Considering that “Failure to sustain the aerosol forcing can lead to sizeable and abrupt climatic changes” [5], the top priority when setting up the project is to establish a very long-term financing structure robust to wars, political shifts and other foreseeable and unforeseeable events. The use of an international consortium composed of the most influential world governments increases the reliability in terms of bond repayment, resulting in the straightforward attainment of an AAA-rating of the bonds. This bond status would lead to extremely low/negligible interest costs, decreasing the overall cost of the project.

¹ URL <https://www.flightglobal.com/pdfarchive/view/1995/1995%20-%200834.html> [Accessed 29/04/2016]

² URL <https://www.nasa.gov/exploration/commercial/crew/index.html> [Accessed 29/04/2016]

³ URL http://www.esa.int/Our_Activities/Human_Spaceflight/International_Space_Station/International_Space_Station_legal_framework [Accessed 29/04/2016]

3.2 Public opinion

In terms of public opinion, a quick search on geoengineering shows that movements opposing the practice already exist. Among these, *Geoengineering Watch* contains a large number of articles, links and videos with the general aim to prove that chemicals are currently being dispersed widely in the atmosphere⁴. The widespread “Chemtrails” conspiracy theory [6] could harm the credibility of the SAGA project. A negative general public opinion could also reduce the willingness of companies to be involved in the project, in addition to the economical aspect. Besides, a negative public opinion could lead to activists interfering with the SAGA operations. Overall, the general public needs to be informed on the benefits and drawbacks of geoengineering and involved in the decision-making process.

3.3 State-of-the-art and cost estimation

Only one company was found to have investigated the design of an aircraft for stratospheric aerosol geoengineering. The company, named Aurora Flight Sciences, was founded in 1989 and currently employs about 375 people [7]. The operating revenue for 2015 was \$62,500,000 and the size of the company is considered as large [7]. In addition, the company has been recognised as a top supplier by Lockheed Martin and awarded with the Supplier Gold award by Sikorsky [7]. With all this in mind, it seems clear that Aurora Flight Sciences is a company that can provide valuable support to the SAGA. Considering what is at stake, the company should be considered as a partner for the SAGA rather than a competitor.

If any single solution emerges as significantly better than alternatives, it has a chance of taking over the entire geoengineering market. Currently no such market exists, but some insights can be extracted from other large, expensive international projects such as Large Hadron Collider (LHC) and International Space Station (ISS), listed in the following.

- Added value is extremely difficult to quantify in financial terms. Benefits coming from ISS, LHC or geoengineering can be negligible (if no discovery/change is made) or virtually priceless (in case of world-changing discovery or rescuing Earth's climate).
- In case of novel design (LHC, ISS), all effort is focused on a single concept after the prototyping phase. One product/product series takes over the entire market (that it created itself).
- Competition is extremely limited due to prohibitive entry-level costs and very high risks associated with low technology maturity.

For the design to be competitive, literature suggests it needs to offer means of sustainably delivering 10 Mt of an albedo-enhancing aerosols per year at a net present cost below \$80 billion[4]. The net present cost is computed assuming a discount rate of 5% and covering a period of 10 years[4]. This cost refers to a delivery of more aerosol per year than SAGA (twice the amount) and the project lasts shorter. However, it can still serve as a useful proxy for the cost bound on the SAGA mission.

Under these assumptions, the net present cost of the SAGA mission amounts to \$146 billion. However, the design can still be considered competitive when taking into account the following notes. To the authors' knowledge, no detailed studies of the cheaper options, namely single-use balloons, reusable balloons, tethered balloons and the combination of fast jets with tankers, exist [4]. This leaves their feasibility questionable, as well as their cost estimates. Assuming sulfuric acid is chosen as aerosol, these options would need systems to handle the aerosol which have not been considered in [4]. Single-use balloons could pose serious sustainability issues. Since about 40 million flights per year would have to be carried, not only more rapidly biodegradable latex would have to be developed, but also a solution would have to be found to limit the rest of the balloon systems' impact on the environment[4]. The latter issue can be avoided by using reusable balloons, however a complex operational plan would have to be implemented to recover those balloons. The operational costs would then likely be higher than what is estimated for SAGA [4]. In addition, both single-use and reusable balloons would cause an impact on the air traffic that was not quantified by [4]. Tethered balloons are a very immature technology compared to aircraft solutions, also with far less short-term implementation possibilities. Finally, the cost estimation for the combination of fast jets and tankers does not consider the challenges of handling the aerosol, which would certainly add both capital and operational costs

⁴ URL <http://www.geoengineeringwatch.org> [Accessed 28/04/2016]

[4] to current estimates. In conclusion, SAGA has a competitive advantage among the cheapest solutions with the most advantageous overall combination of technical feasibility, cost certainty and deployment time. To place the costs into perspective, the operational costs (including depreciation) correspond to 62% of Exxon-Mobil earnings for 2015 and the net present cost corresponds to 0.2% of the world's 2014 GDP. The project can therefore be safely assumed to be affordable for a large consortium of governments.

3.4 Possible alternatives/competition

According to the Aurora research [8], from an engineering perspective, geoengineering is a venture that can prove to be successful and worth the resources – the costs incurred in such projects are estimated to be of similar size to those of other aerospace and large engineering operations.

The analysis of available geoengineering systems concludes that airships offer a range of characteristics that give them an advantage over airplanes, including \$0.5 billion savings and more attractive operating cost. The problem is limited experience with airships at very high altitudes and their questionable resistance to wind and weather. Access to high altitude can be provided through other systems. The one that was found to be competitive and offer the lowest recurring cost per kilogram aerosol is a suspended pipe (tethered balloons) system, however, in order to determine the true feasibility of this system more refined analysis is required, making it difficult to predict development cost. The academic paper proposing the solution as the best approach [4] is not technical in nature and does not put a lot of weight Technical Readiness Level. The technology prototype has not been presented even for lower altitudes and higher altitudes may be outside of the feasibility region. The immature state of the suspended pipe technology makes this solution an inadequate option for quick implementation.

Two extremely high-cost systems which can be definitely written off are rocket- and gun-based systems. The former require a large number of launches, while also being prone to occasional rocket failures, what renders them not cost competitive. The latter in turn is subject to high projectile costs as a large number of shots is required. However, given the projectile payload fraction is increased from around 10% to 50%, the gun costs may become more competitive, yet the yearly costs can still amount to \$20 billion.

New aircraft with a history of operation above 65,000ft represent a significantly more mature high-level technology compared to floating pipe systems or high-altitude airships, which is required to simultaneously allow for flying the aircraft to such high altitudes and making them efficient to operate. As far as existing aircraft are concerned, these could be utilised to reduce acquisition costs, yet the lack of high altitude capabilities, increasing maintenance costs and limited service life reduce their usefulness for geoengineering. One solution would be to modify existing airplanes to improve their high altitude capabilities, however, at the same time this would entail elimination of the cost advantage of using existing systems.

Nevertheless, given enough time for development, pipe systems may be eventually used to replace lower risk aircraft or airships once their useful time has been expended.

3.5 Market analysis conclusion

The goal of the SAGA project is not to take over the market and generate profits. The goal is to deliver the required temperature decrease using albedo-enhancing compounds as cost-efficiently as possible. With this in mind, a case for competitive and economical roll out of aircraft-based geoengineering should be made to decision makers.

As concluded in Section 3.3, purpose-designed aircraft offer a competitive solution from the ones available due to its combination of higher cost certainty, technical feasibility and short deployment time. SWOT analysis of that deployment method is presented in Fig. 3.1. However, considering that geoengineering needs to be carried out on very long time scales, long term plan needs to be proposed. A feasible idea would be to roll out a single series of the SAGA in the short/medium term (10 years enhanced development and certification time and 20-30 years planned operational life). This would offer additional time to develop more advanced and more economical concepts like the suspended pipe system [8] and it puts a strong constraint on the cost (single series, limited production) of the design.

The predicted market share of the SAGA can be very high. Due to the international involvement and responsibility associated with an operation such as the SAGA, one solution, supported by all relevant parties, has the largest chance of success. Thus, assuming that eventually a single system is developed, founded by a supervising international consortium, the market share will be 100%.

	Helpful	Harmful
Internal	<ul style="list-style-type: none"> - Relatively quick to implement - Potentially rapid cooling effect, which could reduce or reverse negative impacts of global warming, including floods, droughts, stronger storms, sea ice melting*, land-based ice sheet melting, and sea level rise* - Easy to modify or reverse - No in-depth studies of purpose-designed aircraft for geoengineering exist 	<ul style="list-style-type: none"> - Lack of similar designs - No CO₂ mitigation - Uncertain climate system impacts - Uncertain ecological impacts - Fallout may contribute to acid rain - Uncertain effects on stratospheric ozone - Continuous implementation required until GHG emissions are reduced - Failure to maintain could lead to rapid temperature rise/climate change - Ocean acidification (via increased CO₂) - Potential for military use of technology - Moral hazard – the prospect of the technology working would reduce drive for climate change mitigation - Moral authority – uncertain who decides whether to implement geoengineering and where to set the thermostat
External	<ul style="list-style-type: none"> - Enhanced international cooperation - Spurring innovation by open-sourcing the design - Benefit of free-of-charge audits by experts in case of open-sourced design documentation - Increased plant productivity* - Increased terrestrial CO₂ sink* - Beautiful red and yellow sunsets* - Persistence of low interest rate environment, leading to very cheap project financing 	<ul style="list-style-type: none"> - Protests/interference by environmental organisations - Technological change making alternatives cheaper or less risky - Ban on geoengineering by some national governments (international disagreements) - Certification issues regarding dangerous payload and unmanned control system - Increase in interest rates, resulting in increased debt maintenance cost which might lead to financing issues

Figure 3.1: SWOT analysis

*effects which have been observed for volcano eruptions

4. Operations and logistic concept description

The goal of SAGA is to deliver 5 Mt of aerosol per year to an altitude of 18.5 to 19.5 km in order to temporarily provide a way to keep global temperatures within acceptable bounds. A very important aspect is the mission operations design: what is the most cost efficient way to ensure optimal dispersion of the aerosol? In Section 4.1 of important mission related variables are discussed.

Based on models of the circulation in the stratosphere - lateral movement from the tropics to the poles-, the optimal location for aerosol injection is identified to be the region between 30 ° N and 30° S latitude at stratospheric altitudes. Using existing literature [8], the optimal payload is determined to be 35 metric tons. From a selection of different operational concepts, a regional based operation system is selected, with ground bases featuring maintenance hubs, refuelling facilities and parking of aircraft. In order to effectively cover the injection area, seven airports are strategically selected as bases of operation in a way that requires an operational radius of 3500 km. The bases are selected based on geographical location, local political stability and local infrastructure.

Consequently, deriving the mission time from the range, it is determined 572 flights per day are required to provide the annual aerosol delivery. The mission time allows for 2 sorties per aircraft per day, resulting in a required fleet size of 344 aircraft to meet the requirement of injecting 5 Tg of aerosol per year. This amount includes a 20% redundancy for maintenance and emergencies.

4.1 General Considerations

In this section the most important variables influencing the operational concept are discussed. They include injection location, payload and dispersion rate.

4.1.1 Injection Location

Laterally speaking, the best location to inject the aerosols into the stratosphere is the tropics, since the stratospheric winds in this zone are optimal for spreading the aerosol [9]. The particles will spread from the equator all the way to the poles. In order to achieve a complete and optimal injection, it is decided to inject the aerosols between 30° North and 30° South latitude [9]. The Hadley circulation will take the particles poleward, and the East-West circulation will spread them longitudinally. Moreover, from the performance analysis follows that dispersing the aerosol at 18.5 to 19.5 km altitude instead of 20 km allows for a significantly improved performance of the aircraft Section 8.2.1. Dispersing the aerosol at 18.5 km instead of 20 km, does not deteriorate the aerosol performance significantly, since optimal altitudes cannot be determined with high accuracy and stratospheric altitudes provide sufficient aerosol effectiveness [1]. Further research is needed to quantify the dependency of aerosol efficiency on altitude.

4.1.2 Payload

Since a fixed amount of aerosol has to be injected into the stratosphere each year, the aircraft payload severely affects the required fleet size. According to Aurora Flight Sciences [8], the most cost efficient payload for regional flights at almost all stratospheric altitudes is 10,000 kg. In the case of a payload delivery of 5 Mt a year, however, a higher payload is more cost efficient because it reduces the required fleet size. For regional flights at 18.2 - 21.3 km the most affordable payload is 40 tons. Since increasing the payload is not feasible due to rapidly increasing structural costs, a payload of 40 tons is taken as the general maximum payload for stratospheric flight. However, using SUAVE Section 8.2.1 it is determined that at 35 tons of payload the aircraft can fly with sufficient mass buffer to deal with the many uncertainties in the design. Therefore, the payload is set to 35 tons.

4.1.3 Dispersion rate

The aerosol dispersion rate is defined as the amount of aerosol dispersed for every meter flown. This rate has a crucial influence on the final particle size of the aerosol [9]. The dispersion rate must be such that the aerosol particles are prevented from coagulating into too large particles. According to [9], the dispersion rate should be in the range from 0.003 kg to 0.1 kg per m, with the optimal value being 0.03 kg per m. The dispersion range of 3,500 km and the dispersion cruise speed of 210 m/s (expanded on later) enable a dispersion rate of 0.01 kg/m, which lies within the specified range.

4.2 Operational concept

In order to meet the aforementioned goal of delivering 5 Mt of payload in the stratosphere, a reusable delivery system featuring ground-based refuelling is chosen. Due to the volume of the operation, a disposable system is not sustainable in both terms of cost and environmental considerations. For a payload of 35 tons per flight, this would require a yearly production of 125000 aircraft. This is an unfeasibly large number, hence the reusable option is chosen. Moreover, a ground-based refuelling concept is chosen in order to reduce risk and cost. Air-to-air refuelling and marine based refuelling would complicate the logistic operation of supplying kerosene and aerosol to the aircraft significantly. It would also induce higher development costs as refuelling boats and aircraft with aerosol storage capacity have to be designed and constructed.

A distinction can be made between regional and transit operations. Transit operations, flying from one airport to the next, require either many airports and small operational radii, or a small amount of airports and large operational radii in order to ensure complete coverage of the tropics. The first option is not feasible since the amount of airports is to be minimised to be cost efficient. For the same distance between two arbitrary airports (so the same amount of airports) in a transit concept only one flight direction is optimal: the one directly flying to the next airport. For all other directions, a larger range is required. Compared to the regional concept worked out in the rest of this chapter, the transit concept requires either significantly more airports or a longer range to obtain lateral and longitudinal coverage of the tropical region between the two specified latitudes. Moreover, with transit flights the airports are not operating independently from each other which increases the damage to the program if one of the airports cannot operate. In contrast, for the regional concept, problems at the independently operating bases do not affect other airports and impose less burden on the program. Overall, the regional concept allows for lower cost, reduced amount of airports, shorter operational range, and more robust operations.

With this regional operations concept, the aircraft will fly to the edge of the operational radius at 13 km altitude. Since the aircraft will have burned a significant part of its fuel at the end of the operational radius, the climb to 18.5 km will be more efficient. After turning and climbing to 18.5 km, the aircraft will disperse aerosol while flying back to base, gradually climbing from 18.5 to 19.5 km altitude followed by a descent back to base. This mission profile proves to be most cost efficient from the performance analysis using SUAVE Section 8.2.1.

4.2.1 Operational range

A program is written to heuristically identify viable operational scenarios as a function of operational radius and number of airports. After iterations concerning nesting the airports and changing the radii, two competing cases are identified, which are displayed in Table 4.1. An operational range of 3,500 km with a fleet size of 344 is chosen.

Decreasing the operational radius any further than 3,500 km causes a steep increase in airports required, e.g. for a radius of 3000 km, 14 airports are required. The final selection is based on cost; the most cost efficient concept is determined by estimating the costs for both scenarios using the methods outlined in Chapter 12.

	Case A	Case B
Number of airports	6	7
Operational radius [km]	5,000	3,500
Fleetsize	477	344
Fleet acquisition cost [Billion USD]	143.1	103.2
Fleet yearly maintenance cost (excluding fuel) [Billion USD]	1.4	1.0

Table 4.1: Total acquisition cost estimations for case A and B

Fleet size

In order to estimate the fleet size, the amount of flights per day is estimated. The flight time of 10.7 hours is calculated using SUAVE Section 8.2.1. The value for the block time equals 11.7, consisting of flight time plus one hour to account for refuelling, reloading, inspection and taxi time [8].

A block time of 11.7 hours results in 2.05 sorties per day. In order to maintain the same time schedule per day and to add time redundancy for unforeseen delays, the amount of sorties per day is set to 2, assuming night flights are permitted. With 250 operational days per year, 2 sorties per day with a 35 ton payload result in 286 individual aircraft required to inject 5 Mt of aerosol per year. Assuming an aircraft availability of 80% [8], a total fleet size of 344 aircraft is required. The fleet size in concept A is determined in a similar manner. Naturally, a longer flying range requires a longer block time allowing less flight per day and thus a larger fleet in order to meet the requirements.

Airport cost

As can be concluded from Table 4.1, Case B features a significant cost reduction with respect to Case A, however, one extra airport is required. Adding an extra airport is costly. It requires installing a system to store and load the aerosol and due to the size and high pace of operations a special maintenance department is needed. Moreover, due to the controversy that might exist around the program, security needs to be increased. Adjustments to the existing airport infrastructure might be required due to the possible unconventional size of the to-be-designed aircraft. All of the above will introduce significant costs. For this reason it is preferred to use a minimum amount of airfields as bases of operations in the first place. However, the cost benefit to choose for case B instead of case A, despite adding an extra airport, is very significant due to the decreased fleet size. Even the cost increase of building and maintaining a newly built airfield, which will exceed the cost of 'leasing' an existing airfield, is less than the cost reduction due to fleet size. The cost reduction of decreasing the fleetsize is displayed in Table 4.1. The cost of building a new airport is \$13.1 billion¹. The operational cost of an extra airport is \$384 million[10]. Resulting from these costs, concept B with an operational range of 3,500 km and seven operating airfields, is the best option.

¹ URL <http://blogs.wsj.com/chinarealtime/2014/12/16/why-beijing-needs-a-new-13-billion-airport/> [Accessed 28/04/2015]

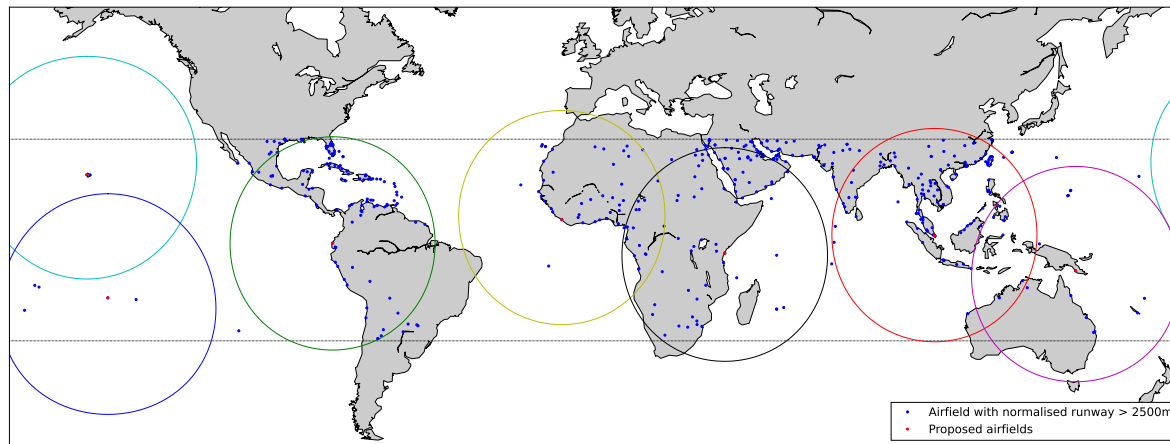


Figure 4.1: Aircraft positioning for an operational range of 3500 km

Airport locations

From the selection criteria for the bases chosen to support these operations, the most pragmatic criteria are the availability of runways with a length of 2,500 m normalised for altitude and locations close to a seaport and in a stable country. The runway requirement is a specified mission criterion. Having an airport close to a seaport allows for easy transport logistics, regarding that large amounts of fuel and aerosol must be delivered to the airport. A stable country is an advantage as it minimises the risk of aborting operations on this airfield due to changing political issues such as strike action, insurgencies and war. The chosen configuration is displayed in Fig. 4.1.

In this configuration, a very significant part of the tropics can be covered. The circles displayed represent an operational radius of 3,500 km. About 36 aircraft will take-off 2 times per day per airport, flying in different directions. Ultimately the entire circle will be covered a few times per year.

The precise airport selection with the ICAO codes are presented in Table 4.2. From this table follows that with a diversion range of 1,000 km, all diversion airports can be reached.

Table 4.2: Selected airports and properties

Airport	ICAO	Location	Runway [m]	Alternate ICAO	Distance [km]
Léopold Sédar Senghor International Airport	GOOY	Dakar, Senegal	3,490	GGOV	371
Paya Lebar Air Base	WSAP	Singapore, Singapore	3,780	WSSS	9
Honolulu International Airport	PHNL	Honolulu, Hawaii, United States	3,753	PHKO	263
Eloy Alfaro International Airport	SEMT	Manta, Ecuador	2,860	SEGU	162
Jacksons International Airport	AYPY	Port Moresby, Papua New Guinea	2,750	YBCS	850
Moi International Airport	HKMO	Mombasa, Kenya	3,350	HKJK	400
Fa'a'a International Airport	NTAA	Tahiti, French Polynesia	3,420	NTTO	920

5. Concept trade offs

The specific constraints of the SAGA mission require an advanced aircraft design. Three concepts are identified, analysed and assessed with respect to their suitability for the SAGA mission. Two analyses were done: In the first, one concept is discarded, after which the result of the second trade-off follows from a more specific comparison of the two remaining concepts. In the following chapter, the three concepts and trade-off criteria are presented in Section 5.1. In Section 5.2 first trade-off table will be shown and the results of a second analysis will be presented, followed by justification based on a summary of the results of the analyses. Finally, a concept choice is made.

5.1 Concepts, trade-off criteria and weights

Three concepts were defined and analysed to determine their eligibility to perform the SAGA mission: a conventional aircraft concept, a blended wing body (BWB) and a twin-body aircraft (TBA). The conventional configuration is a proven design allowing for reduced risks and uncertainties and enabling accurate, detailed examination. Blended wing bodies have good aerodynamic characteristics due to their smooth shape [11]. Twin-body aircraft have good structural characteristics and enable a less concentrated load at the fuselage locations, reducing bending moment [12]. Other options such as designs with unconventionally shaped wings (e.g. Prandtl, C), morphing structures or flying wings were excluded from this selection due to low technological readiness levels (TRL), bad stability characteristics or low efficiency.

The following criteria are used for guidance in the process of selecting the final concept.

1. Applicability to SAGA
 - High altitude performance
 - Aerosol storage capacities

2. Sustainability
 - Noise emissions
 - Operational costs

3. Cost
 - Operational costs
 - Development costs

4. Risk

The criteria are weighted to represent their relative importance in the selection of the final concept. The applicability to the SAGA mission is determined to be of largest importance for the selection of the concept, as a barely usable concept will stagnate development. Within this criterion, a distinction is made between high altitude performance and aerosol storage capabilities, since sustained flight at high altitude poses stringent design requirements on the SAGA. Both criteria related to applicability to SAGA are given the highest weight of 5.

The SAGA mission puts the main focus on its sustainability. The goal is to make the mission as sustainable as possible within reasonable bounds concerning the other mission requirements and constraints, taking into account that a less sustainable design will not immediately abort the mission. This criterion is divided into two categories: noise emissions and operational costs. Reduction in noise emissions lessen the environmental impact of the SAGA, however, this is considered not to be a driving criterion and therefore given a low weight of 1. Operational costs are partially subsumed under sustainability criterion, as they include fuel consumption and thus combustion product emissions and environmental impact cost.

Costs are divided into operational and development costs. Efficiency/fuel consumption is included in operational costs, along with non-sustainability related factors, such as RAMS strategies. The operational cost as outlined in Chapter 12 represents the largest part of the total cost. Therefore, this criterion receives a high weight of 4. Development cost is also of high importance, but is expected to be lower than operational cost. Therefore, it receives a weight of 3.

The last criterion – risk – includes aspects related to the TRL, the reliability of the concept and concept-specific risk items. The reliability of the SAGA must be high, considering the large impact of the program and the possible need for fast and reliable operation at the moment of implementation. Therefore, it is essential that the risks associated with the chosen concept are foreseeable and manageable. Due to the possibility of risk mitigation and risk management, risk is considered not to be most critical, yet still of substantial importance, reflected in a weight of 3.

5.2 Trade-off results and discussion

The final result of both analysis steps is the decision to proceed with the conventional concept, primarily because of its design maturity and the high accuracy level achievable in the next steps of the process.

The first trade off is shown in Table 5.1, on the basis of a separate concept analysis in terms of each of the important design groups: performance, aerodynamics, structures, control and stability, systems and RAMS. A complete, qualitative justification summary for the grading of the concepts is given below, while the reader is referred to earlier-stage design reports for a quantitative and more elaborate discussion.

Table 5.1: Final trade-off table for initial concept selection

Concepts	Applicability to SAGA		Sustainability		Costs		Risk
	High altitude performance	Aerosol storage capabilities	Noise emissions	Operational costs	Development costs		
Conventional	0/+	0	0	0/+	0/+	+/-++	
BWB	0	0/+	+	0	-/- -	--	
TBA	0/+	+	0	+	0	0/+	

5.2.1 Conventional concept analysis

For the conventional concept, generally neutral to high grades are given due to the design maturity and high reliability. The aircraft has good high altitude performance. While the statistically determined aspect ratio AR of 11.6 is not extraordinarily high, conventional designs capable of flying at stratospheric altitudes exist¹, showing that a margin for increasing aspect ratio is present. Propulsion capable of providing the required thrust at high altitudes exists and is compatible with the conventional design. Furthermore, the stability characteristics are very good as conventional configurations are generally inherently stable. The storage capabilities of conventional aircraft are neutral, as it shows neither disadvantages nor advantages related to storage capacity. This also holds for noise emissions: Since conventional engines suffice for this configuration, no benefits concerning noise reduction are present.

The operational costs for the conventional concept score slightly positive, as the standardisation present for this configuration require few adaptations to maintenance and ground operations. However, the high structural weight required for high aspect ratios increases fuel consumption, partially offsetting the mentioned advantages. Development costs also receive a slightly positive score. The existing experience in production and design of conventional aircraft ensures the development costs will not grow unbounded. Conversely, the constraining mission requirements stipulate a very specific design, which will increase development costs as standard procedures will need adaptation. Furthermore, the material cost will be substantial for an aircraft with high aspect ratio, due to the large structural weight.

Lastly, the conventional concept scores very high on risk, as a consequence of the mentioned experience with this product. The extensive amount of research and know-how present results in a very high accuracy of methods and predictions.

¹ URL <http://www.af.mil/AboutUs/FactSheets/Display/tabid/224/Article/104560/u-2stu-2s.aspx> [Accessed 18.06.2016]

5.2.2 Blended wing body concept

The BWB scores neutral on high altitude performance, despite its excellent L/D properties. The airfoil shape causes the possibility of simultaneous occurrence of stall (outboard) and drag divergence (inboard) [13], reducing the feasible design space. Additionally, the stability region of BWBs is small as a result of the absence of a tail, aggravated by the limited amount of sweep possible. Aerosol storage capabilities are slightly above average, as the volume in a BWB structure is high. A disadvantage is the low tolerance to centre of gravity shifts, requiring active sloshing control and liquid pumping. The noise emissions of the blended wing body are good with respect to conventional wing configurations, resulting from the smooth outer geometry and the placement of engines on top of the wing.

The operational costs of the BWB do not score positive, even though efficient aerodynamics and structures reduce fuel consumption. The increased cost due to absence of standardised maintenance procedures and ground operations and the need for active control due to the bad stability characteristics outweigh the fuel related cost reduction. Both the development cost and risk score very low. There is little experience with blended wing bodies, especially of this size [11]. This demands extensive research and testing, contributing to high development costs. In addition, new production procedures must be established, further increasing development costs. The reliability of the existing design methods is low due to a shortage of experimental data, complicating design and development and increasing the time until roll-out. This will interfere with the requirement of immediate and reliable operation when necessary.

5.2.3 Twin body aircraft

The twin-body aircraft concept scores moderately high on most criteria, as it is similar to the conventional configuration. The high altitude performance of the TBA benefits from the possibility of having a higher AR , thus reducing induced drag. The presence of two fuselages, however, increases parasite drag, reducing the benefits of lower induced drag. The possibility of differences in loading between the two fuselages and the spanwise distribution of mass might be detrimental for stability and control characteristics, resulting in a final grade equal to the grade for the conventional configuration. The aerosol storage capabilities are more versatile in a TBA concept, allowing for storage in both fuselages which provides bending relief as well. The noise emissions of the TBA are also similar to the conventional aircraft, as similar engines will be used. This yields a neutral effect on noise emissions.

The operational costs of the TBA score relatively high. The high AR , resulting in more efficient L/D values, reduces fuel consumption. In addition, the distributed loading enabled by two fuselages reduces the bending moment, resulting in a lower structural weight (compared to a conventional model with equal AR), further reducing fuel consumption and thus operational cost. The stability characteristics and maintenance procedures are not significantly different with respect to the conventional concept, resulting in an overall lower operational cost.

The development cost and risk criteria do not score very high, as the TBA is an unconventional design, resulting in larger uncertainties and higher risks. This necessitates more research and testing, in addition to revised production procedures, increasing the development cost. The lack of empirical data and associated limited reliability of methods makes a TBA more risky than a conventional design. The very high similarity with a conventional design, however, increases reliability and keeps the risk within bounds.

Based on this first trade-off, the blended wing concept is discarded, based primarily on its low TRL and the associated unacceptably high risk and development cost. When varying the weights of the criteria to obtain insight in the robustness of the outcome, the TBA and conventional concept outcomes lie too closely together to make a final decision. These concepts are therefore evaluated in more detail.

5.2.4 Second trade-off and final design decision

The second, more detailed analysis resulted in the selection of the conventional concept for further design. The main reason for the selection of this concept is the higher TRL and the associated better availability of analysis and design methods, expected to result in a realistic design with higher reliability.

The in-depth analysis focuses mainly on the difference in AR between the two concepts, which primarily affects their structural weight and drag characteristics. A quantitative analysis of the two concepts is complicated by the difficulty of making a fair comparison. The immediate benefit of using a TBA is the possibility

to achieve higher AR . This makes a comparison of a conventional concept and TBA concept with equal AR invalid, as it undermines the benefit of the TBA.

A second option is comparing a conventional and a TBA concept with the same MTOW. However, this yields the same wing for both concepts, as a higher AR for the TBA wing would enable a more efficient lift generation resulting in differing MTOWs. A comparison that assumes the same wing surface area for both concepts results in a TBA with maximum possible AR , having more efficient lift generation.

However, a TBA concept and a conventional concept with their maximum achievable AR cannot be compared directly either, as the weight of the TBA with larger wing will inevitably be greater. A higher weight increases thrust and fuel consumption, causing a conventional, small AR design to score better where the opposite is expected. A relatively detailed analysis according to this philosophy indeed indicates that a TBA configuration with $AR = 20$ as to be achieved e.g. by Scaled Composites' Stratolaunch² cannot fairly compare against the $AR = 11.6$ conventional configuration. This study concludes that a very large wing area capable of storing all aerosol in the wing is required regardless of the chosen configuration to relieve induced drag pressure on the thrust. That results in enough wing volume to store all aerosol and no required storage in the fuselages. This partly eliminates the improved bending relief performance envisioned for the TBA and does not justify the higher AR that served as the baseline for its higher performance.

At the current stage of the design, these comparison methods therefore could not yield an unequivocal, quantitative conclusion. The tools and expertise to analyse both concepts at the same level of detail are lacking due to the large difference in experience, available literature for both concepts and most importantly, stringent time constraints. Therefore, a final concept selection is made on the basis of the engineering judgement of the design's feasibility.

Even though the analysis does not show that the TBA is inferior, the low availability of reliable modelling and assessment methods for TBA designs is considered to be a crucial obstacle. Its greatest advantage for allowing higher AR – the bending relief provided by the two fuselages – is limited due to the possibility of distributed payload and fuel storage along the wing. Therefore, the uncertainty and risk associated with the TBA do not outweigh its potential upside, resulting in the decision to choose the conventional concept for further development.

The conventional concept however, is not able to meet the mission requirements with the analysed AR of 11.6. Initial concept investigation reveals a number of design drivers, which govern the design of the chosen concept. All mentioned design drivers stem from the overarching constraint of high altitude flight with a heavy payload.

- High induced drag due to high C_L required
- Engine thrust lapse
- Limited payload per flight

The conventional design as selected in Chapter 5 cannot meet the mission requirements with the statistically determined $AR = 11.6$. Therefore, options to increase AR within this configuration using a strut-braced wing design are investigated in the following design steps.

² URL <http://aerospace.vulcan.com/> [Accessed 18.06.2016]

6. Functional analysis

6.1 Functional breakdown structure

In Fig. 6.1, the updated Functional Breakdown Structure (FBS) is shown. It is an AND tree, so it describes the functions that are part of the mission in a cumulative manner. The first block, “Perform mission” (FBS-1), is applicable to the entire fleet of aircraft, while the “Perform flight” (FBS-1.N.1) block is applicable to one sortie of one aircraft.

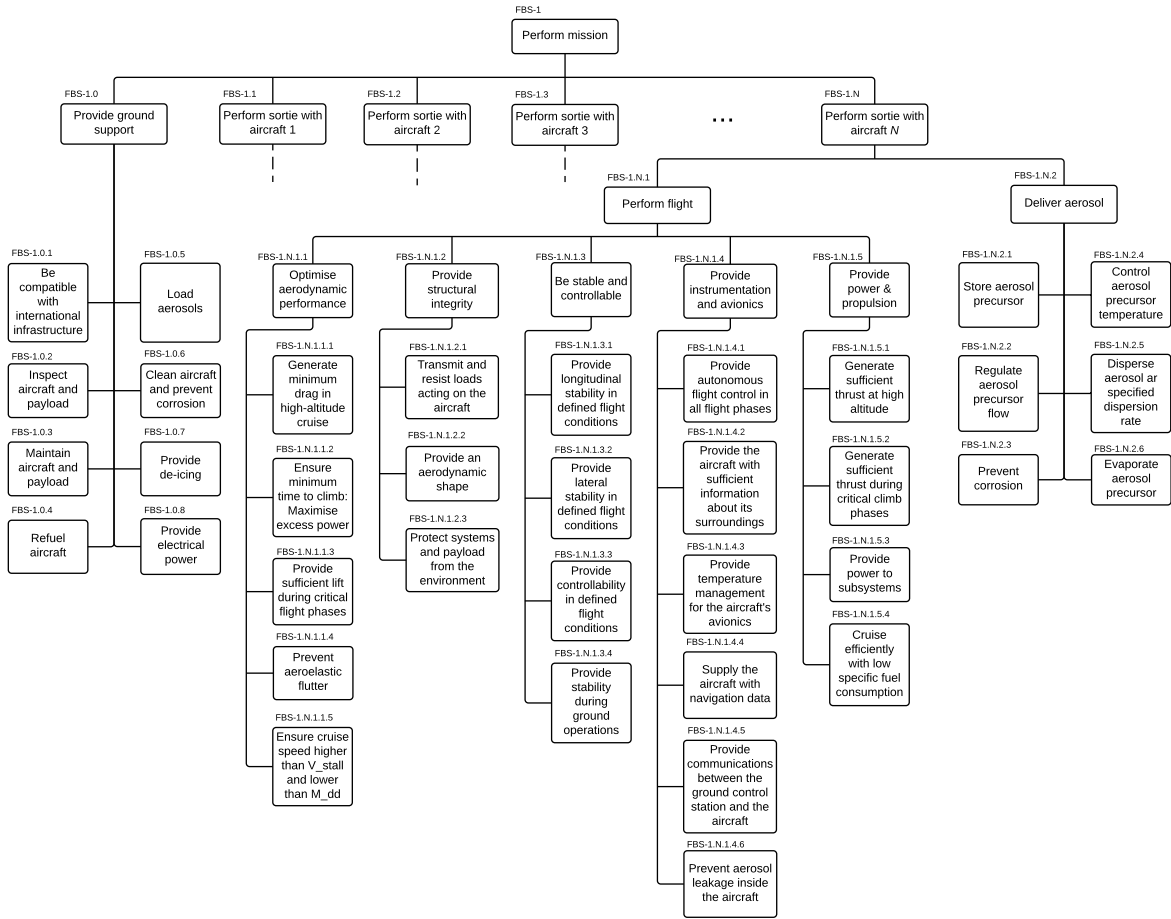


Figure 6.1: Functional Breakdown structure of the mission

6.2 Functional flow diagrams

The Functional Flow Diagrams (FFD) are presented in Figs. 6.2 and 6.3, and they give a timewise breakdown of the mission. The first FFD is applicable to one sortie of the aircraft. It corresponds to block FBS-1.N.1 of the Functional Breakdown Structure from Section 6.1. The second FFD presents the mission outline, which corresponds to block FBS-1 of the Functional Breakdown Structure.

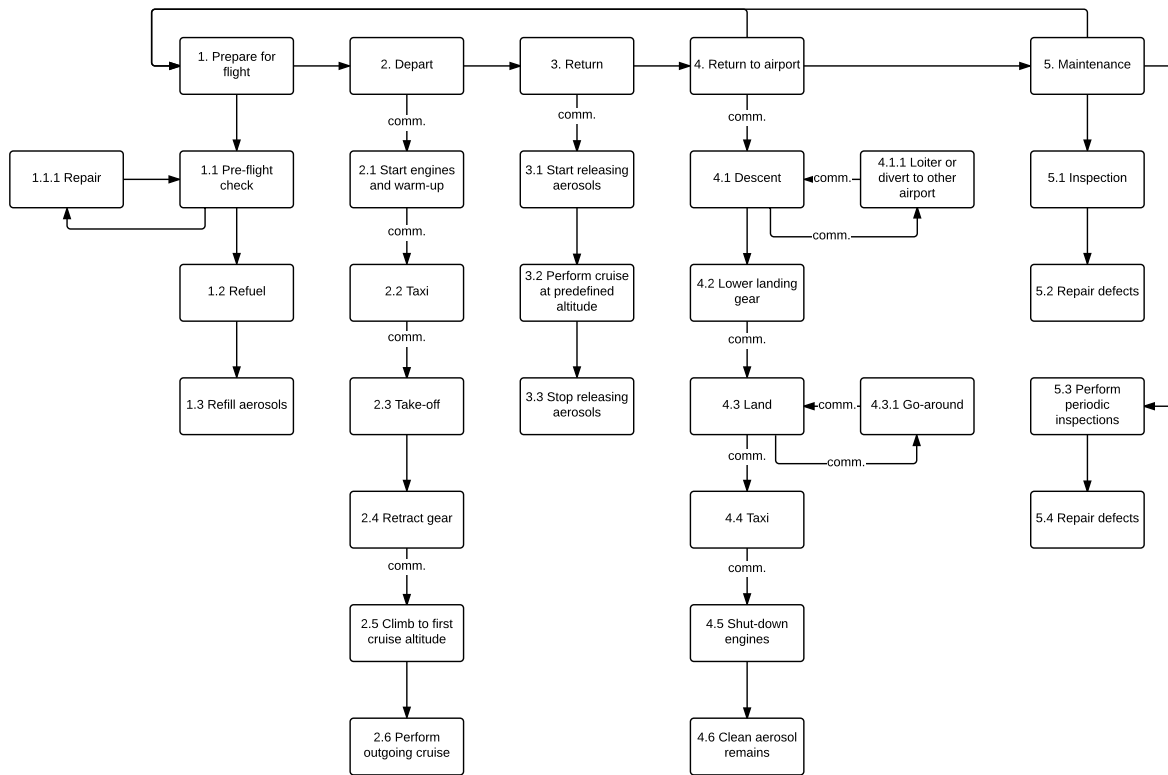


Figure 6.2: Functional Flow Diagram for one aircraft sortie

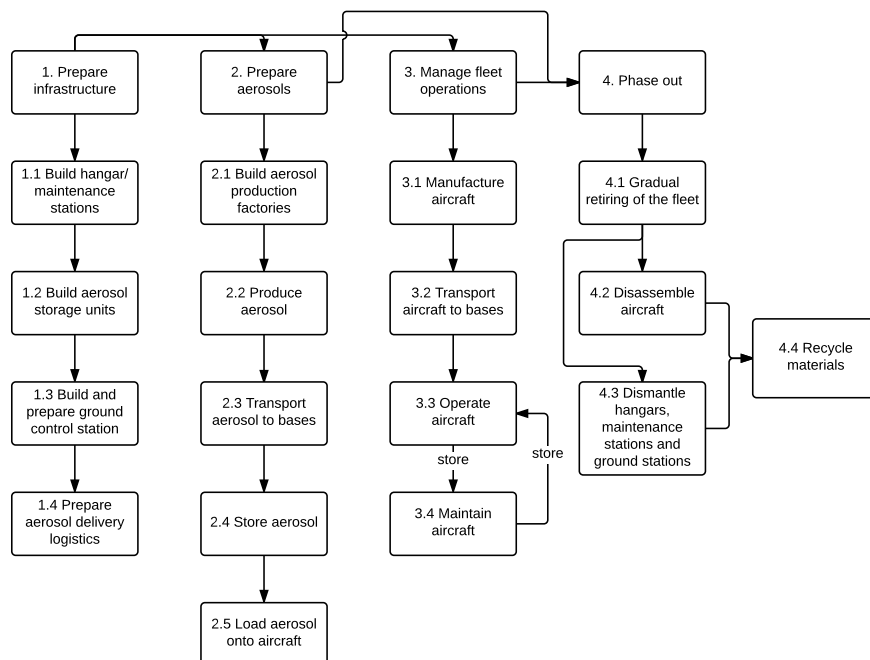


Figure 6.3: Functional Flow Diagram for the mission

7. Final design

After the final concept selection, a final preliminary design is constructed. This final design reflects a number of important technical trade-offs and design decisions to render it feasible. This section presents the final design of SAGA that stems from these decisions and a reflection on the current state of the project. The motivation, consequences and multi-disciplinary optimisation leading to this final design are subsequently outlined in Chapter 8.

7.1 Description of final design

SAGA's technical design is almost entirely driven by its high-altitude, high-payload operation combination. In terms of performance, the aircraft is therefore designed to have a mission range of 7,000 km, the returning 3,500 km of which are spent spraying the 35 ton aerosol payload, divided over segments at 18.5 km, 19 km and 19.5 km altitude. A 1,000 km diversion is added in case of emergency. These mission parameters require a maximum take-off weight of 207,000 kg, including a 13% general weight margin for future design contingency. This translates to a 52,500 kg fuel burn and a 105,000 kg operating empty weight. The low altitude out-going cruise speed is set to 191 m/s, the high-altitude cruise speed is set to 210 m/s.

As will be outlined in Section 8.2, Section 8.3 and Section 8.5, this mission's constrained design space stipulates a 700 m^2 , unswept, strut-braced main wing with $A = 13$, $\lambda_w = 0.5$ and $b = 95.4 \text{ m}$. Engaging a supercritical airfoil, the wing's outgoing cruise stall speed lies at 135 m/s, while the high-altitude, high-speed cruise stall is 192 m/s at $C_L = 1.18$. Drag divergence occurs at 212 m/s in both phases. SAGA does not need high lift devices.

SAGA features four custom-developed, 3.5 m diameter turbofan engines producing 26 kN each at 20 km altitude. With an overall pressure ratio of 34, a bypass ratio of 7.5 and a cruise specific fuel consumption of $1.56 \cdot 10^{-5} \text{ kg/N/s}$, the engines also provide the power for the aerosol heating and dispersion system with a maximum of 1.65 MW during the final cruise. To accommodate for the large wing and thrust, the wing structure comprises a boron-fibre composite, 28 ton wing box with three spars, supported by 19.9 m struts attached at 40% of the semispan to limit tip deflection during the entire mission. It is attached to the outboard engine pylon to minimise its interference with the wing. To prevent static and dynamic aeroelastic failure modes in this configuration, the engines are placed relatively forward at 40% chord.

To further ensure constant control and stability, the sized horizontal tail area is 131 m^2 with $A_h = 5$, $\Lambda_h = 10^\circ$ and $\lambda_h = 0.3$. Similarly, the vertical tail area is set to 39 m^2 , $A_v = 2.5$, $\Lambda_v = 35^\circ$ and $\lambda_v = 0.2$. The wing is longitudinally positioned at 17% of the 40.1 m long, 5.47 m high, elliptical, unpressurised fuselage. For constant control, the elevator is set to 88% of the tail span, the aileron to 40% of the wing span and the rudder to 90% of the vertical tail span.

The high-altitude performance requires SAGA to be an unmanned, autonomously operating aircraft, with one ground controller in charge of 4 aircraft. This entails a 5-level control system redundancy, a satellite communications budget of 1-5Mbps and a sense-and-avoid system.

Finally, SAGA entails a range of subsystems. Most notably, the aerosol handling system comprises a cross-linked polyethylene storage tank for the H_2SO_4 aerosol at 13.9 m semispan of both wings. The tanks do not require slosh baffles, while pumps are installed to guarantee a constant aerosol dispersion rate. Aerosol ground pre-heating to 516 K almost completely eliminates the need for active thermal control; one immersion heater per tank suffices. Evaporation at a rate of 2.1 kg/s is ensured by eight electric resistance immersion heaters in one evaporation chamber per wing. Fuel is stored in inboard wing sections at take off and outboard in cruise for structural reasons. Finally, a 225kW APU is included for emergency operations and an environmental and aerosol monitoring system ensures continuous measuring and control of relevant properties.

The combination of the above parameters yields a feasible design to fulfill the SAGA mission. However, as will be further outlined in Chapter 10, with this final design comes the discovery of a design space with potential for further improvements that were not achievable within the time constraints of the preliminary design

process. This results from freezing several governing parameters such as S and AR at safely obtainable values, before further analysis revealed more structural and aeroelastic leeway than initially expected. While the preliminarily developed design is therefore feasible, SAGA is still very much a living design project with the potential of further optimisation within the discovered design space in future iterations.

7.2 Drawings

To visualise this final design, a CAD model of its geometry was generated in CATIA. In this section, the corresponding design drawings are included. Fig. 7.1 presents the integration of the landing gear into the airframe, while Fig. 7.2 shows a three projection view of the aircraft.

The high fuselage and short gear configuration gives a lower combined weight than a shorter fuselage and a longer gear according to the Class II weight estimation methods. The quadricycle landing gear configuration provides the aircraft with good ground stability while taxiing, but usually results in an inability to rotate at take off [14]. The SAGA is an exception, since its elevators are powerful enough to rotate the aircraft even with a quadricycle configuration. The 3.6 m wheel base provides the aircraft with the ability to perform a ground turn with a radius of 30m at a velocity of 10 m/s. These values were calculated with the method presented in [14]. A tricycle landing gear is not used, since in that case the main gear is located 0.4m behind the centre of gravity in the most critical loading case, which introduces the danger of tip back occurring. Moreover, the main gear in a tricycle configuration will interfere with the strut.

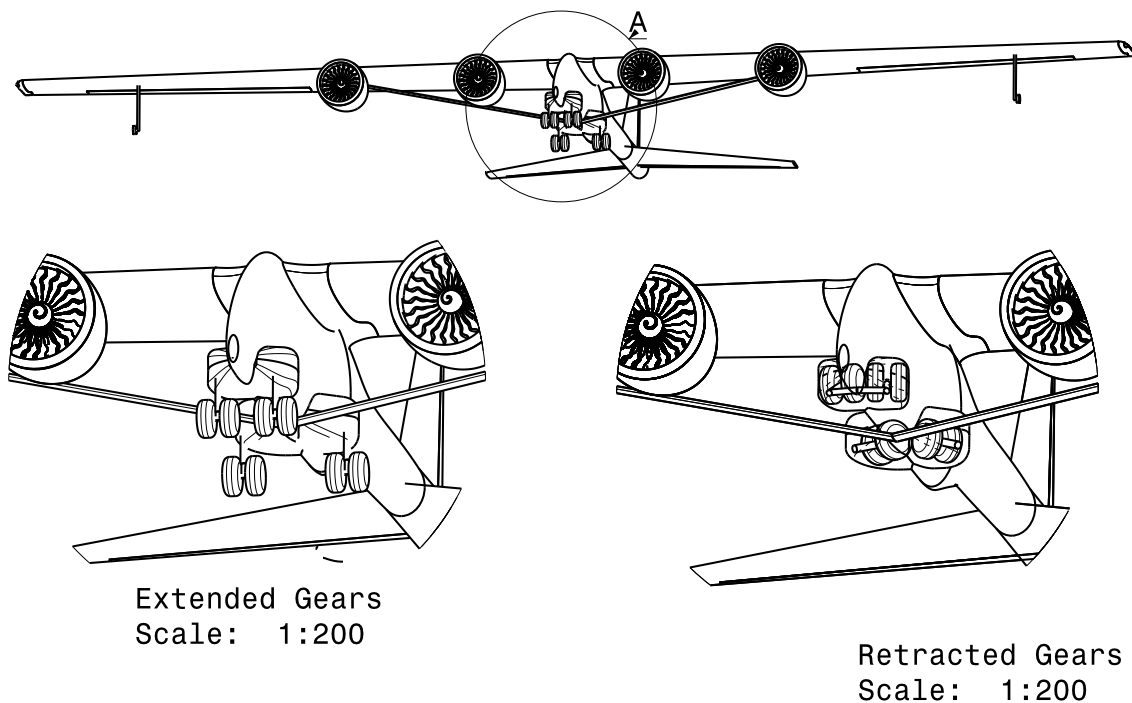


Figure 7.1: Extended and retracted landing gear configurations

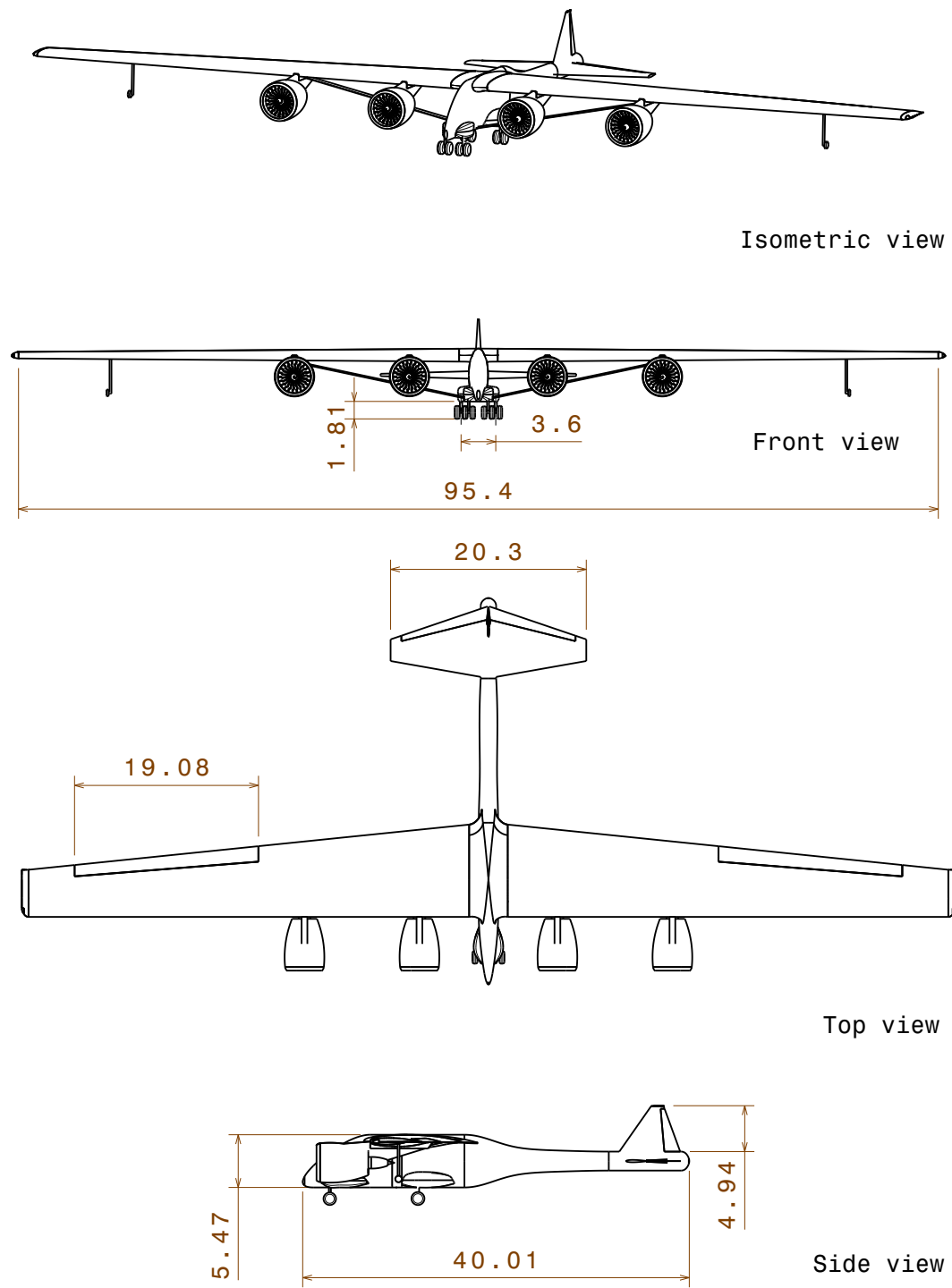


Figure 7.2: Three projection view of the SAGA aircraft. Dimensions are in m

8. Analysis and evaluation SAGA concept

Based on the selected conventional concept in Chapter 5, SAGA underwent a preliminary design process to arrive at the final concept presented in Chapter 7. This section aims to outline all the design choices, motivations and technical sensitivities that played part in that process, along with the verification and validation of the employed analysis methods. The chapter presents the design philosophy and framework for SAGA in Section 8.1, followed by the analysis and design of SAGA in terms of performance in Section 8.2, aerodynamics in Section 8.3, propulsion in Section 8.4, structures and materials in Section 8.5, aeroelasticity in Section 8.6, stability and control in Section 8.7, aircraft systems in Section 8.8 and aerosol systems specifically in Section 8.9.

8.1 Design framework and overview

This section describes the design methodology/framework developed as part of this work. The critical parameters governing the risk-oriented design method used are outlined, and the methodology for the integration of specialised design areas is explained.

8.1.1 Risk-oriented design focus

After selecting the conventional concept based on the motivations described in Chapter 5, the design process has shifted from general to risk-oriented. Initial concept investigation reveals a number of design drivers, which are analysed very thoroughly and govern the design process. The majority of the resources is allocated to the following critical design aspects to ensure a feasible design given the time constraints. All mentioned design drivers stem from the overarching constraint of high altitude flight with a heavy payload.

- High induced drag due to high C_L required
 - Large aspect ratio AR and/or Oswald factor e required to lower C_{D_i}
 - ◊ Difficulty selecting airfoil(s) capable of providing optimal lift distribution (e), sufficient M_{dd} and large t/c (due to structural considerations) simultaneously
 - ◊ Catastrophic aeroelastic effects due to high AR
 - ◊ Excessive structural wing weight due to high AR and the aforementioned
- Engine thrust lapse
 - Insufficient thrust available during cruise or high altitude climb
 - ◊ Oversized, too heavy, inefficient or technologically infeasible propulsion system
 - Insufficient aerosol heating power provided
 - ◊ Aerosol freezing mid-flight
 - ◊ Inability to vaporise the aerosol at the sufficient rate
- Limited payload per flight
 - Cost explosion due to increase in fuel costs, number of required aircraft and airports

The conventional design as selected in Chapter 5 cannot meet the mission requirements with the statistically determined $AR = 11.6$. Therefore, options to increase AR within this configuration are researched in this chapter, resulting in the strut-braced wing with $AR = 13$ presented in Chapter 7. Struts provide structural reinforcement to long slender wings, meaning they can provide structural weight relief in high- AR configurations.

8.1.2 Design methodology

In order to design unconventional aircraft and to accurately model the aircraft performance, it is essential to include information regarding both the aircraft geometry and the governing physics of flight in the performance analysis [15]. To accommodate and appropriately investigate the requirements posed by the very unconventional SAGA mission, Stanford University Aerospace Vehicle Environment (SUAVE) is used for performance analysis in lieu of conventional methods. The latter are used to verify the obtained design and the requirements.

The developed design framework is illustrated in Fig. 8.1. SUAVE, a conceptual design framework under development at the Aerospace Design Lab at Stanford, is used as the mission solver. The SUAVE output is linked through a Python interface to aerodynamic tools – predicting the expected wing performance, and structures programs – producing load and geometry-based weight estimation. The results from the two are sent to the aeroelasticity module for preliminary flutter analysis and control reversal and divergence investigation. The Python interface also connects SUAVE to the propulsion feasibility and engine performance code.

SUAVE handles the mission performance prediction (fuel burn, C_L , thrust required, drag breakdown etc.), stability analysis and take-off and landing field length computation. Aerodynamic prediction is done with vortex lattice methods, empirical data and RANS simulations using SU2 combined with handbook-based drag prediction methods. To obtain an accurate estimate of wing weight and size the primary structure, a code based on Euler–Bernoulli beam theory is used in the structures module. The aeroelasticity module uses methods based on analytical equations as well as NeoCASS software, where analytical methods serve as a verification for the numerical outputs from the NeoCASS package. The numerical propulsion analysis based on analytical methods from theory is extended and verified using the gas turbine simulation program GSP. The design loop is closed with manual and automatic design iteration.

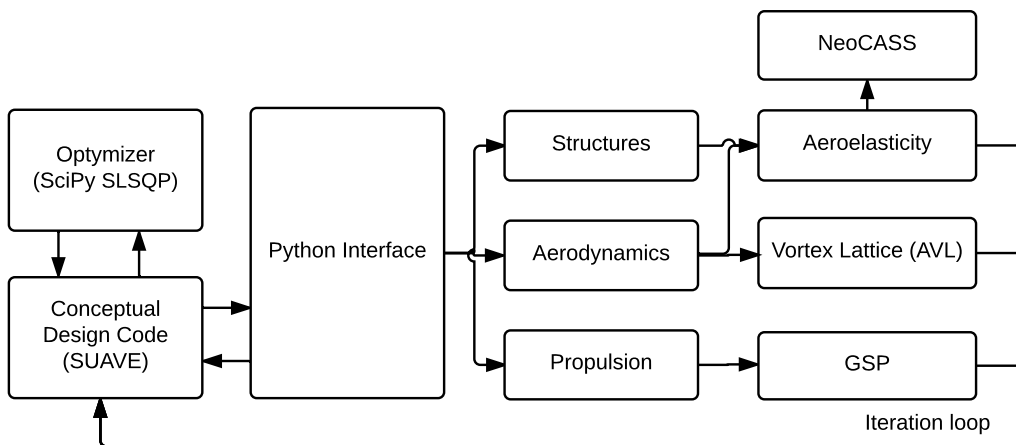


Figure 8.1: Design framework (based on [15])

In an analysis of an unconventional aircraft configuration in an unconventional mission it is not sufficient to investigate one design point. SAGA will operate in different conditions throughout the mission and is designed to be as efficient as possible in all of them. SUAVE is capable of performing multi-disciplinary analyses at multiple levels of fidelity on an aircraft configuration and combining the results from the different disciplines to obtain performance estimates for the aircraft over a simulated mission [15]. SUAVE offers a number of low and medium fidelity analysis capabilities for aerodynamics, structures, weight estimation, stability and propulsion analysis, it allows for optimization studies with the SciPy 'SLSQP' solver and is easily extendable [15]. The overview of SUAVE's capabilities in the form of a class diagram is presented in Fig. 8.2

To solve mission segments, SUAVE implements a pseudospectral collocation method based on Chebyshev polynomials and differentiation [17]. “Pseudospectral methods allow for high accuracy and spectral convergence rates with a small number of control points, a key savings in computational cost when complex physical simulations are required to produce the supporting data.” [17] The SUAVE SciPy wrapper also allows for simple and efficient handling of constraints.

After the mission is solved successfully and all of the constraints are satisfied, subsystem requirements are passed on to the specialist teams and iterated if necessary.

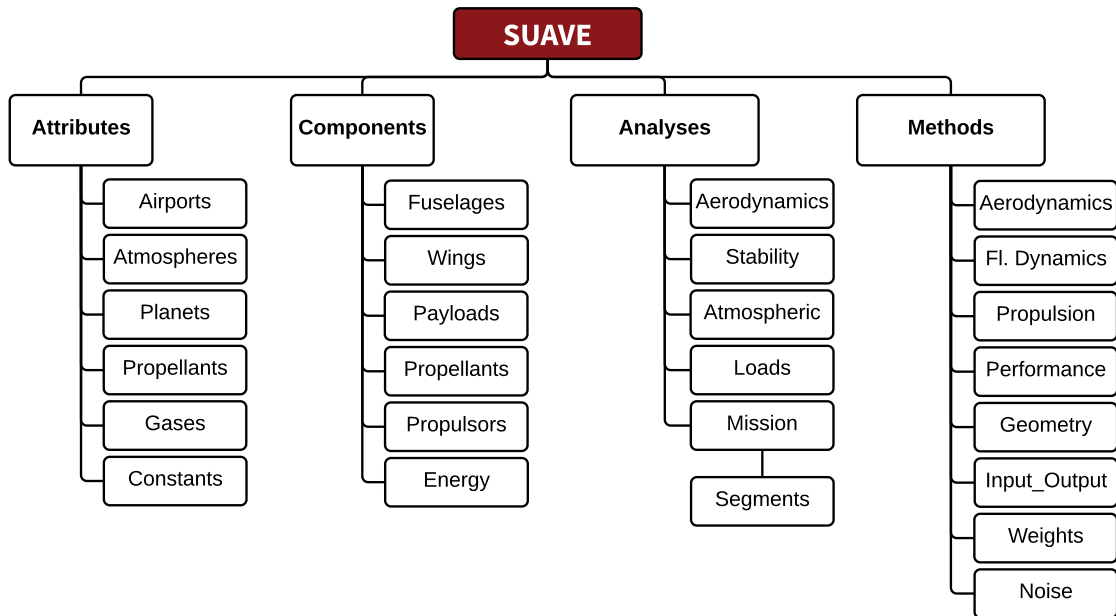


Figure 8.2: Class diagram (based on [16])

8.1.3 Design insights

During the design process, a number of properties of the SAGA design space emerge which differ significantly from conventional transport missions at lower altitudes. The following differences are most remarkable.

- The design space is extremely constrained and results in an aircraft with little disturbance tolerance and a narrow margin of error; e.g. V_s and M_{dd} are very close to each other - V_{EAS} in high altitude cruise is only 61 m/s. This is a common characteristic of high-altitude designs like for example the U-2.
- Usual sizing constraints such as take-off distance or initial climb gradient are not sizing factors in the design, as in case of SAGA the design is almost exclusively dependent on high-altitude flight phase characteristics
- Continuous payload ejection introduces continuous changes in mass that cannot be readily handled by unmodified handbook methods such as e.g. the Breguet-equations. The methods must be re-derived to account for mission characteristics concerning payload ejection. Even then, lack of any reference aircraft flying a similar mission will lead to a less reliable estimate.
- SAGA design is a trade-off between technology readiness level (strut-braced wing and custom engines), dispersion altitude (aerosol effectiveness) and fleet size (cost and sustainability)

SUAVE offers the flexibility of quickly investigating and verifying the feasibility of the design and various missions. This allows for quick judgements on the impact of various design choices based e.g. on quantitative fuel burn estimates. The complete SAGA design specification and analysis toolbox is now available online¹ as an open-source fork of the SUAVE codebase. This transparent approach lets anyone investigate, verify and improve the proposed design, with a goal of spurring interest in the subject, contributing to the future research and advancing the scientific frontier.

8.2 Performance

The performance analysis of SAGA translates the requirements imposed by the mission and operations into concrete requirements for subsystems downstream. In this section, the mission analysis using SUAVE is described (Section 8.2.1), followed by design choices made in Section 8.2.2. Optimised performance results are presented in Section 8.2.3 and verified in Section 8.2.4. The section ends with a sensitivity analysis in Section 8.2.5.

¹ URL <https://github.com/lukekulik/saga-one> [Accessed 20/06/2016]

8.2.1 SUAVE mission analysis

To design and analyse SAGA performance characteristics, the vehicle, the mission and relevant analyses are defined in SUAVE. Firstly, crude manual optimisation and iteration is used to converge to a feasible design; afterwards automatic constrained optimisation is used to further enhance the performance. The SAGA mission is to an overwhelming extent constrained by operational requirements, which are considered first. A check for CS25 requirements is carried out with conventional methods to verify both the design and the requirements. This section summarizes the SUAVE implementation, results and decisions made with respect to the SAGA mission and performance drivers, complemented by the related motivations and consequences.

SUAVE implementation

The program's input consists of more than 50 constants, constraining parameters, iteration parameters and design parameters. A table containing all input parameters and their classification is listed in Appendix A. These inputs are tracked using an interactive tree, shown in Fig. 8.6, as well as passed on to other software packages downstream, where required.

SUAVE is built around principles of flexibility, composability, and extensibility [16]. This allows for extending an already very powerful analysis platform with mission specific components. The following extensions are implemented to increase the design fidelity:

- Aerosol dispersion – this add-on allows to specify the aerosol dispersion rate in kg/s or in kg per mission phase. The resulting decrease in mass throughout the mission yields more realistic lift and drag estimates. The sample outcome of enabling aerosol dispersion is a 12% decrease in fuel burn for $m_{pl} = 35,000\text{kg}$ and more accurate thrust constraints.
- Electrical generator – aerosol heating and evaporation consumes a considerable amount of power (over 1.5MW) and thus increases the fuel burn. Adding a power draw from the low pressure turbine allows to quantify the fuel burn with a power draw input in Watts per mission phase.
- Custom fuel – considering the risk of fuel evaporation at high altitude, a custom fuel class has been implemented to investigate the impact of fuels like JP-7 on the mission. The sample outcome of replacing Jet-A fuel with JP-8 is a 500kg decrease in fuel burn for $m_{pl} = 35,000$.
- Custom class II weight estimation methods - SUAVE has been designed with passenger aircraft in mind. Adjusted statistical methods from [13, 18] have been implemented to account for the unconventional elliptical fuselage, struttured composite wing and on-board unmanned control systems.

8.2.2 Design choices

Before proceeding to automated optimisation, preliminary and iterative search through the design space is carried out. With the input from specialist subteams, this allowed to establish bounds and initial values for design parameters, as well as preliminary estimates for geometric characteristics, which are updated throughout the process. The vehicle design choices with largest impact on design are aspect ratio AR , Oswald factor e , wing area S and design thrust T_{des} . The process of specifying values for these design parameters is iterative and involves plenty of multidisciplinary optimisation.

A maximum aspect ratio of $AR = 13$ is selected for the wing in the preliminary stage. Aspect ratio choice is a balance between the additional fuel burn due to induced drag for low AR and the additional wing weight and structural and aeroelastic issues for high AR . The initial decision to select a bound $AR_{max} = 13$ is intended to keep structural weight within an acceptable range, while keeping induced drag low. The consequence is increased complexity of the required strut-braced structure and increased drag associated with it. A choice of such a high AR increases the development risk, but is necessary to reduce induced drag considering that wing area, Oswald factor are also close to their maximums and cruise speed is just below the Mach drag divergence.

As will be explained in Chapter 10, further design analysis revealed that even larger AR can be achieved in the allocated mass budget, but was excluded from the final design for its uncertainty and time constraints.

The upper thrust bound is set by the propulsion subsystem at 120kN for 4 engines at 19 km altitude – this choice is motivated by maximum feasible parameters of engine components achievable in the near future. The consequence of this very high thrust is the significant (9000+ kg) weight of each engine and its considerable diameter of larger than 3.3 m.

An Oswald factor of $e = 0.95$ was assessed for span efficiency. The Oswald factor has a very significant influence on induced drag, thus maximising it is of critical importance. Preliminary AVL analyses confirmed that with appropriate wing design, $e = 0.95$ can be achieved (see Section 8.3). The negative consequence of this design choice is a significant constraint on airfoil thickness throughout the span - increasing the structural weight of the wing.

Finally, the upper bound on S is set to 700 m^2 . Initially set to keep $b < 100\text{m}$ and $C_{Lcruise} < 1.2$, posterior analysis presented in Chapter 10 validates that this choice minimises the aircraft weight within the feasibility constraints stipulated by C_L .

A number of optimisations are performed on the mission to increase the feasibility. In SUAVE, the mission and the vehicle are defined separately, which enables analysing a range of missions for a given vehicle. To decrease the maximum thrust requirement it is decided to flip the mission legs, such that outgoing cruise is performed first with all payload on board, and the aerosol is released on the way back to the airport. The decreased weight after the first cruise leg due to fuel consumption makes it easier to climb (reduced thrust and C_L requirements) to high altitude as compared to a climb immediately after take-off. In consequence, a somewhat increased fuel burn in the cruise phases is incurred, as the average weight of the aircraft during the mission is greater. However, the reduced C_L and C_{D_i} more than outweigh this increase, causing overall fuel burn to reduce. The dispersion cruise altitude is split into three phases and decreased to the lowest flight level that ensures successful aerosol formation [8]. This is done to decrease the thrust and lift coefficient requirements and to climb only after aircraft has consumed approximately 40% of its fuel.

The first dispersion cruise leg starts at 18.5 km. After a cruise of 1,050 km, a second climb to 19 km follows; subsequently, after a cruise of 1,173 km, a third climb to 19.5 km is performed to the last cruise leg of 1,001 km. The distances are optimised for minimum fuel burn under the mission radius constraints.

Defining climb phases are changed from conventional “constant rate” or “constant gradient” to “constant speed, constant throttle”. This allows for more flexibility in mission analysis, imposes less stringent requirements on the engine and helps to avoid adding 15+ climb phases in constraining phases such as e.g. high altitude climbs from 15 km to 18 km altitude. The consequence is the relative difficulty in executing a climb with non-constant climb rate in practice, which can however be mitigated with an unmanned control system.

Altitude and speed for cruise phases not constrained by operational requirements (outgoing cruise and reserve cruise) are optimised to minimise the fuel burn. Consequence of this approach is that additional constraints have to be set for the mission time to satisfy turnover time specified by operations.

The payload weight is maximised within the zero fuel margin and power provision constraints. Aerosol release is normalised between the cruise phases and checked for sufficient rate in kg/m for adequate aerosol formation.

Finally, a significant 13% zero fuel margin is established to account for the large uncertainty in the design (e.g. oswald factor, structures and propulsion group weight). The margin ensures that the design meets all sensitivity demands. In the case of SAGA, a significant margin does not lead to the often observed self-fulfilling weight increase prophecy, because it is very easy to increase the payload weight or the dispersion cruise altitude with little impact on the overall layout.

Contingency planning

Using a Systems Engineering approach, risk has to be balanced between time, cost/resources and technical performance. After the design space is thoroughly explored, the decision has been made to freeze the MTOW budget with a significant margin – therefore potentially harming technical performance.

The following list presents available options for margin utilisation:

- Contingency for uncertainty in technical parameters
 - Contingency for increase in empty weight
 - Contingency for increase in fuel burn in case of lower aspect ratio AR or Oswald factor e
 - Contingency for using (more/heavier) existing engines to provide sufficient thrust
 - Contingency for increasing wing torsional stiffness to mitigate aeroelastic effects
- Increase payload - marginal cost of increasing the payload weight is minimal (see Section 8.9.3), but it leads to significant capital and operational cost savings

- Increase dispersion cruise altitude - increased altitude may lead to increased aerosol effectiveness and/or increased e-folding time [19].
- Fuel burn increase on a hot day (e.g +15° over expected values)
- Contingency for undetermined unknowns
- Combination of the above

8.2.3 SUAVE results

The SAGA model in SUAVE incorporates necessary constraints to design the vehicle while minimising the fuel burn of the aircraft over the mission defined in Chapter 4. The model uses 11 design variables, incorporating geometric characteristics of the wing, takeoff weight and design thrust at the top of the high altitude climb. The exact methods used to analyse the vehicle are first order methods outlined in [16]. All design variables, their initial conditions, optimised results found using SLSQP in SciPy, upper and lower bounds, and objective results are shown in Table 8.1. Design constraints and their optimised values are presented in Table 8.2.

Table 8.1: Design Variables with Initial conditions, Optimal results, and Bounds

Parameter	Initial	Optimized result	Lower bound	Upper bound
Wing area [m^2]	500	700	400	700
Maximum Takeoff Weight [kg]	210	207	190	215
Design thrust [kN]	100	110	90	120
Outgoing cruise speed [km/h]	200	190	160	220
Spraying cruise speed [km/h]	200	210	160	220
Outgoing cruise altitude [km]	10	13.14	9	15
Spraying cruise (1/3) distance [km]	1000	1050	900	1200
Spraying cruise (2/3) distance [km]	1000	1173	900	1200
Spraying cruise (3/3) distance [km]	1000	1001	900	1200
Outgoing cruise distance [km]	3200	3393	3200	3500
Aspect ratio [-]	11	13	8	13
Design mission fuel burn [kg]	N/A	53,087		

Table 8.2: Constraints for Optimization Study

Constraints	Bound	Optimised result
Max throttle [%]	< 100	97.5
Main mission time [h]	< 11.1	10.73
Design range fuel margin [-]	> 0.13	0.132
Take-off field length [m]	< 2500	1010
Landing field length [m]	< 2500	1740
$C_{L_{\max}}$ [-]	< 1.1	1.01
Spraying range [km]	> 3500	3500.5
Non-spraying range [km]	> 3500	3500.6

As one might expect, the spraying range and non-spraying range approach their bounds since the optimal aircraft will not fly a longer range than required. Similarly, design range fuel margin constraint also approaches the imposed limit to limit any excess weight. Moreover, maximum throttle moves towards 100%, but does not reach it, as the constraining high-altitude climb is throttle-limited at 97.5%. Constraints on take-off/landing field length and main mission time are easily satisfied and are not driving the design. Finally, $C_{L_{\max}}$ constraint is satisfied with a 9% margin, as the induced drag is the largest driver of the design and optimizer aims to reduce lift coefficient as much as possible.

Starting from the initial values, the optimizer aims to obtain lower fuel burn, while satisfying all the constraints. While for all cruise speed and altitude design parameters, an optimum is found, wing area and aspect ration reach their predefined upper bound. This is because induced drag is the largest contribution to fuel burn - both increasing the AR and wing area helps mitigate that to an extent possible. At the same time, the optimal speed is adjusted to achieve the best balance between induced and compressible drag. Design

thrust is minimized under the requirement to provide sufficient thrust for climb at high altitudes. These automatic “design decisions” made by the optimizer match the basic design intuition, which serves as a further validation of the results. Overall, the results of the optimization match general trends one would expect.

SUAVE output graphs

Figs. 8.3 and 8.4 present the SUAVE output for the entire mission including mission profile, weight, fuel burn, aerosol released, specific fuel consumption, mach number, throttle setting, drag, thrust, fuel flow rate and aerosol flow rate. Mission implemented in SUAVE is made up of a number of (climb/cruise/descent) segments, introducing discontinuities in the graph, which however do not impact the analysis, since only integration methods are used for the design objective - fuel burn.

Most relevant aspects in Fig. 8.3 is altitude throughout the mission and time required to achieve that altitude. Secondly, aircraft mass decrease as a function of fuel burn and aerosol release allows to verify the calculated fuel burn and aerosol released. Finally, specific fuel consumption during the entire mission (based on the SUAVE turbofan engine model) gives propulsion subgroup a clear SFC requirement.

Fig. 8.4 includes Mach number and drag figures for the aerodynamics subgroup. Throttle setting and mass rate flow down to the propulsion subgroup as an implicit thrust and efficiency requirement. The throttle setting graph includes the most constraining high altitude climb phases (at around 300, 400 and 500 minutes). Finally, aerosol flow rate together with cruise speed serves as a verification of the requirement SAGA-AC-EQ-13 postulating the required dispersion rate. Moreover, the fact that results show trends and not standalone values serves additional validation purpose.

Payload range diagram has not been included, as it is not relevant for the mission under consideration. If required, an appropriate command in SUAVE¹ will generate it.

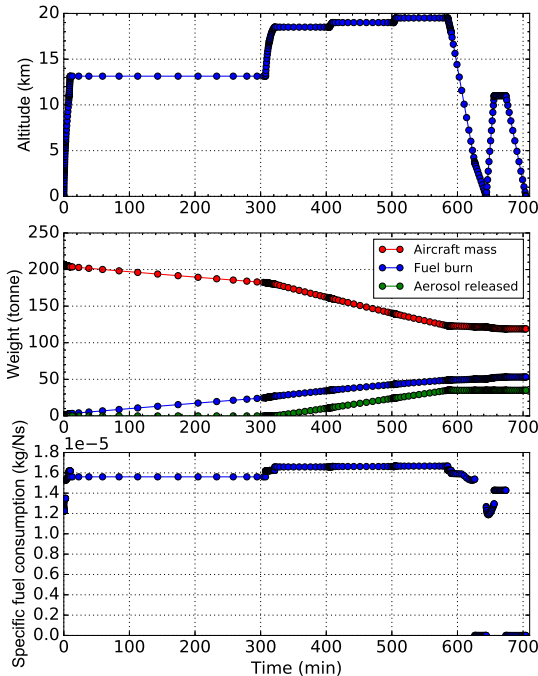


Figure 8.3: SUAVE output: Mission profile; Aircraft, Fuel and Aerosol weights; specific fuel consumption

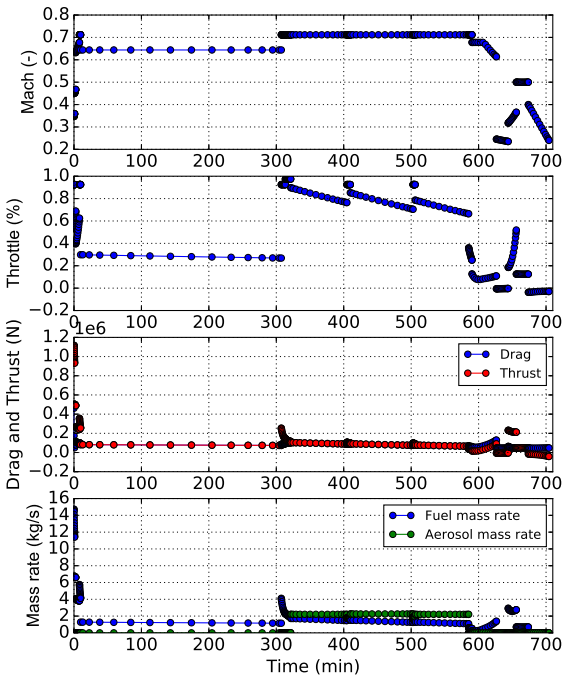


Figure 8.4: SUAVE output: Mach number, Throttle setting, Drag and Thrust, Mass rate of fuel and aerosol

SUAVE has been augmented with custom Class II weight estimation methods to account for unconventional strut-braced composite wing, unmanned concept and no passengers. A major part of the component weights is predicted with the method proposed by Raymer [18]. For the subsystem components, other methods are used as well, since Raymer tends often to take the crew number as the main variable during systems weight estimation. For example, the hydraulic system weight is estimated with Torenbeek's method [20], while the avionics weight is estimated with the method proposed by Gundlach [21]. The mass required for flight computers was approximated by taking a cluster of 500 high performance GPUs², as they would

² URL https://www.amazon.com/EVGA-GeForce-Quieter-Graphics-04G-P4-2983-KR/dp/B00NT9UT3M/ref=sr_1_2?s=pc&ie=UTF8&qid=1467002171&sr=1-2&keywords=nvidia+gtx+980 [Accessed 16.06.2016]

provide sufficient computational power. An overview of the predicted weight budget is presented in Table 8.3 and Section 8.2.3.

Parameter	Value[kg]
Operational Empty Weight	118,882
Wing weight	32,501
Fuselage weight	8,468
Propulsion group weight	41,816
Landing gear weight	6,185
Horizontal tail weight	1,513
Vertical tail weight	947
Rudder weight	379
Systems weight	14,073
Margin	13,000

Table 8.3: Minimum required subsystem performance stemming from mission analysis

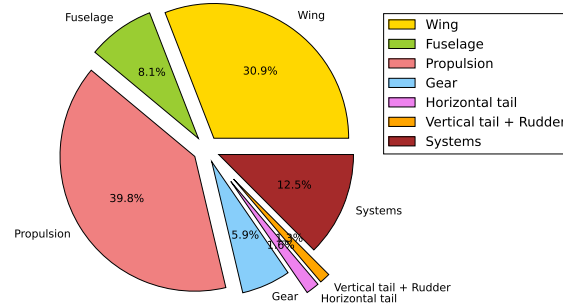


Figure 8.5: Component percentage with respect to OEW

8.2.4 Verification and Validation

SUAVE framework is based on complex, multi-layered code, all interactions of which are very difficult to predict and verify. To complete performance V&V, firstly SUAVE test suite and data export tools are used and then secondly actual design results are verified with handbook methods. If test suite runs successfully, input matches with the design and the independent conventional performance model returns values in line with SUAVE predictions, model is considered to be verified. At the same time, analytical performance calculations serve as requirements verification.

SUAVE code verification

SUAVE as a framework is verified and validated by its original team of developers[16]. To further make sure that everything is working correctly, the integrated unit and integration test suite is executed every week or after a major change in the code has been implemented.

Vehicle definition in SUAVE consists of multiple parameters, scattered around the code. To ensure that the correct configuration is analysed and to track the parameters throughout the specialist teams, an interactive JavaScript mindmap is created – shown in Fig. 8.6

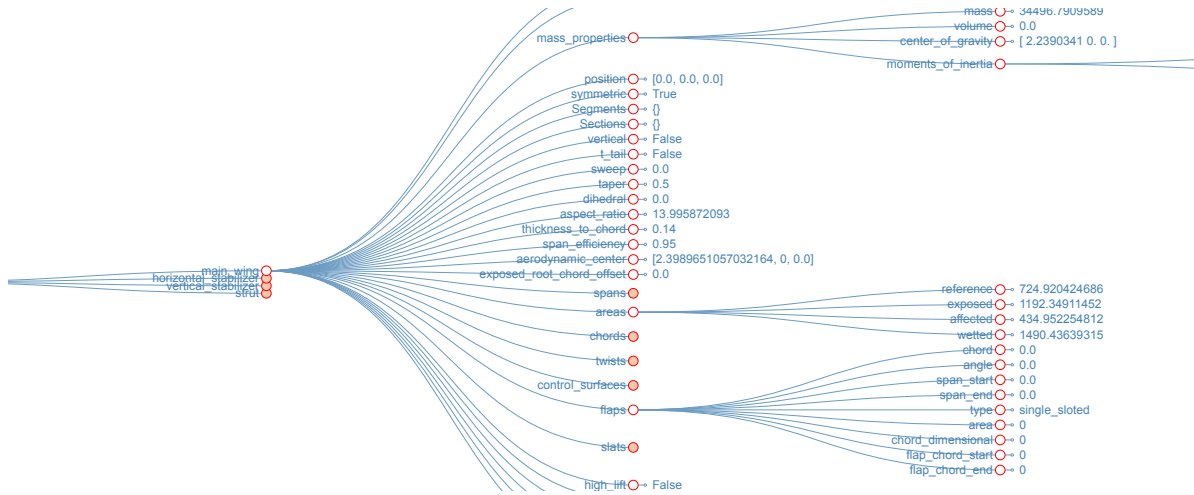


Figure 8.6: SUAVE Vehicle definition data structure sample

Finally, SUAVE plots of engine power, external temperature, force vectors, climb rates, body accelerations, body angle and mass rate versus time are inspected for abnormalities.

Model and requirements verification with conventional model

After the design is finalised, it must be verified that it meets the set performance requirements, coming from both regulations and the mission. The main set of regulation requirements consists of minimum climb gradients during take-off and landing with one engine inoperative and required flight time in the event of aircraft diversion. The main mission specific requirements are take-off and landing distances, service ceiling, and maximum time to altitude.

The climb gradient is defined as the ratio of rate of climb and velocity. It can be calculated with Equation (8.1). An increase in drag coefficient of 0.02 [22] due to the landing gear is considered for the first take-off segment, approach segment, and go-around.

$$G = \frac{c}{V} = \frac{Pa - Pr}{W} \frac{1}{V} = \frac{(T - D)V}{W} \frac{1}{V} = \frac{T - D}{W} \quad (8.1)$$

The climb gradient verification results are presented in Table 8.4. The take-off gradients are obtained using 19% of the maximum available thrust, since this is the minimum amount which the aircraft needs to meet the requirement. This will be described in more detail later in the section.

Table 8.4: Verification results for the climb gradient requirements

	Requirement	Result	Comments
Take-off segment 1	0.5%	7.63 %	Gear, $V_2 = 1.2V_{minTO}$
Take-off segment 2	3.0%	10.25%	
Final take-off segment	1.7%	7.58%	at 1500 m
En-route climb	1.6 %	2.09%	$V_{climb} = 1.2 \cdot V_2 \text{ m/s}$
Approach	2.7%	3.16%	Gear, $V_{app} = 1.25V_{minland}$, $T_{app} = 0.1 \cdot T_{maxOEI}$
Go-around (AEO)	3.2%	6.49%	Gear, $T_{available} = 0.1 T_{max}$

Requirement (CS 25.343 (a)) states that the aircraft shall have a fuel reserve to fly for 45 minutes at a 3,000 m altitude. Since the SAGA is sized to have a diversion range of 1,000 km, it is expected that this requirement will be easily achieved. A simple way to check that is the Breguet Endurance equation:

$$E = \frac{1}{gc_j} \frac{L}{D} \ln \frac{W_{begin}}{W_{end}} \quad (8.2)$$

Using the weight and L/D ratio from Fig. 8.4 as inputs amounts to a total flight time of 280 minutes.

The next set of requirements to be verified consists of the take-off and landing distances. The certification requirements for the screening heights, climb out speed and approach speed are taken into account during the distance calculations. For the take-off distance, the greater distance between 115% of the normal take-off distance and the distance with one engine inoperative is taken. Moreover, the air density used is at 35°C.

It must be mentioned that the lift coefficient at V_{LOF} is achieved by a combination of a wing incidence angle of 3 degrees and a rotation angle of 6 degrees, which results in $C_L = 1.53$. The maximum rotation angle that the aircraft can achieve is approximately 7.5 degrees and the 1.5 degree margin is present in order to prevent the occurrence of tail strikes, as seen in Fig. 8.7. The reason why incidence and rotation angles are used is to lower the lift off speed V_{LOF} in order to reduce the stresses experienced by the gears at take-off and thus simplify their design. Due to the high angle of attack and the excess of thrust at sea level provided by the engines, the take-off distance requirement is easily met when using full thrust. The minimum required thrust to satisfy the requirement is 19% of the maximum achievable thrust. In all cases, the lift-off speed at MTOW is $V_{LOF} = 57.5 \text{ m/s}$

The take-off distance consists of a ground roll and an airborne phase, which are calculated with Equation (8.3) and Equation (8.4), where V_{scr} is the climb-out speed and V_{LOF} is the lift-off speed. Equation (8.5) and Equation (8.6) are used for the landing case [23]. For the landing case an additional drag coefficient of 0.015 is added to account for the effect of lift spoilers.

$$STO_{ground} = \frac{WV_{LOF}^2}{2g(\bar{T} - \bar{D} - \bar{D}_g)} \quad (8.3) \quad STO_{airborne} = \frac{\frac{1}{2g}V_{scr}^2 - \frac{1}{2g}V_{LOF}^2 + h_{scr}}{\sin \gamma_{scr}} \quad (8.4)$$

$$s_{land_{air}} = \frac{\frac{V_A^2}{2g} - \frac{V_T^2}{2g} + h_{scr}}{0.5 \left[\sin \bar{\gamma}_A + \left(\frac{C_D}{C_L} \right)_T \right]} \quad (8.5)$$

$$s_{land_{ground}} = \frac{W}{2g} \frac{V_T^2}{\bar{T}_{rev} + \bar{D} + \bar{D}_g} \quad (8.6)$$

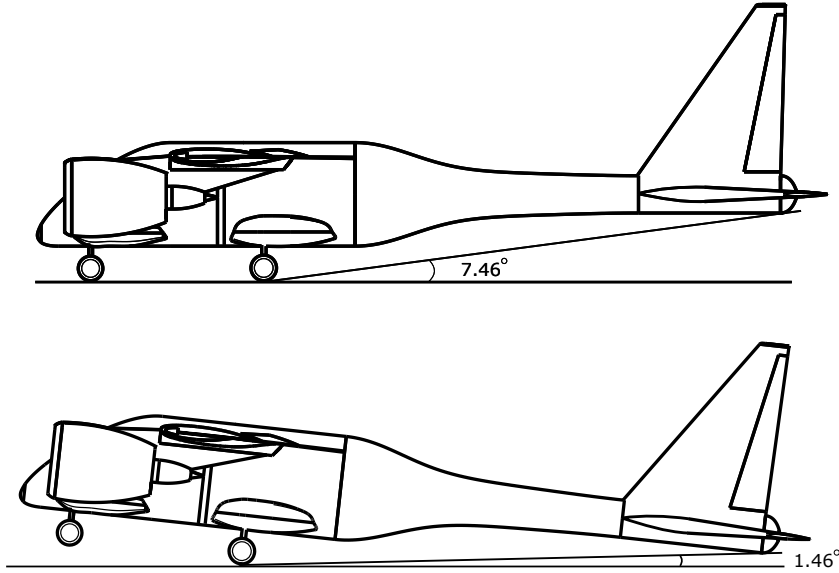


Figure 8.7: Maximum rotation angle of the aircraft and angle margin at actual rotation

The final results are summarised in Table 8.5. The values for μ were taken from [18].

Table 8.5: Take-off and landing distance verification results

Distance	Requirement[m]	Result[m]	Comments[m]
Take-off dry at T_{max}	2500	322	$\mu = 0.03$
Take-off dry at $0.19T_{max}$	2500	2263	$\mu = 0.03$
Take-off wet at T_{max}	2500	324	$\mu = 0.05$
Take-off wet at $0.19T_{max}$	2500	2340	$\mu = 0.05$
Landing dry	2500	1656	$\mu = 0.4$
Landing wet	2500	1880	$\mu = 0.3$

Next, the service ceiling requirement has to be verified. The surface ceiling can be defined as the altitude at which the rate of climb becomes zero. For the calculation of the surface ceiling, the weight is taken as 180 tons, as witnessed by Fig. 8.4. The resulting rate of climb for altitudes between 19 and 20 km can be seen in Fig. 8.8. The reason that the SAGA does not fly constantly at that altitude is the increased fuel burn resulting from such an action.

Finally, the minimum time to altitude has to be verified. It can be found by integrating the inverse of the rate of climb throughout the entire range of altitudes. This is shown in Equation (8.7) [23]. The resulting time to 20 km is 16.4 minutes.

$$t = \int_{H_0}^{H_{end}} \frac{1}{RC_{steady}} dH = \int_{H_0}^{H_{end}} \frac{W}{TV - DV} dH \quad (8.7)$$

8.2.5 Sensitivity analysis

At the current design stage there is a remaining uncertainty when it comes to exact values of the design parameters. Because of that, robustness of the design/model to varied inputs needs to be investigated.

Sensitivity of the results to the most influential design parameters is analysed by means of response surface methodology [24]. The resulting graphs are presented in the following section, with notable results described.

Fig. 8.9 indicates the sensitivity of fuel burn to MTOW and wing aspect ratio. The fuel burn starts to increase rapidly for larger MTOW values at low aspect ratios. Fig. 8.10 further shows the importance of induced drag

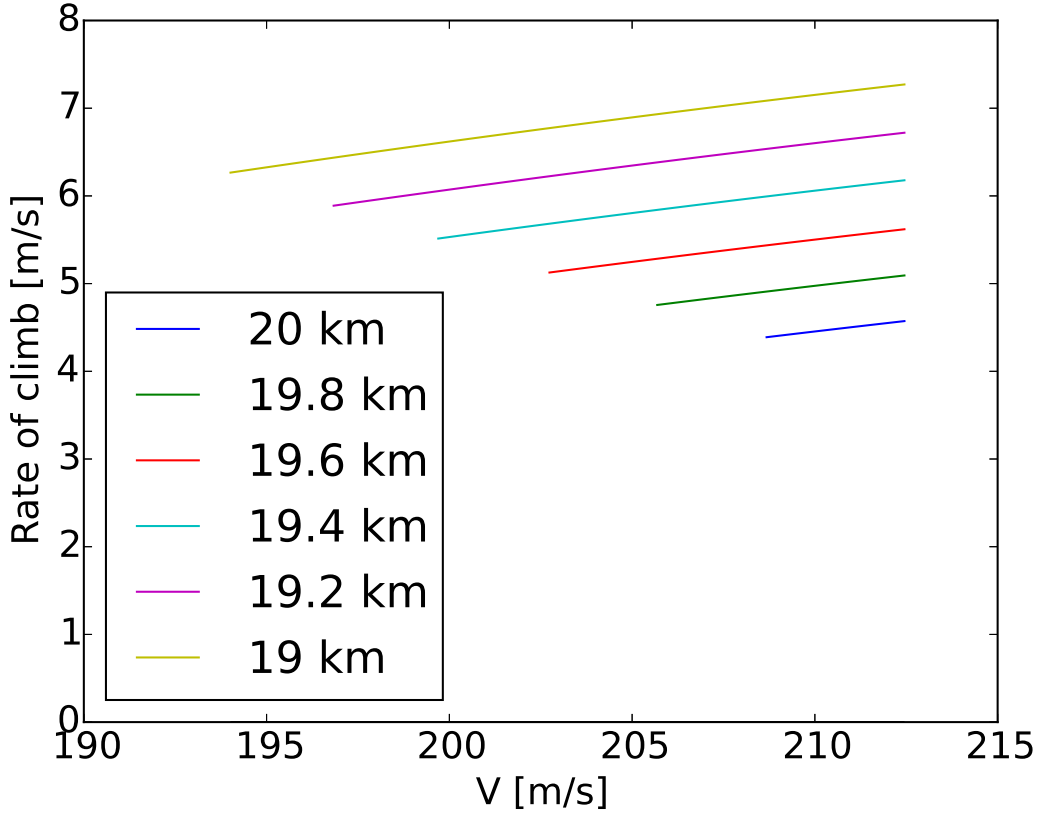
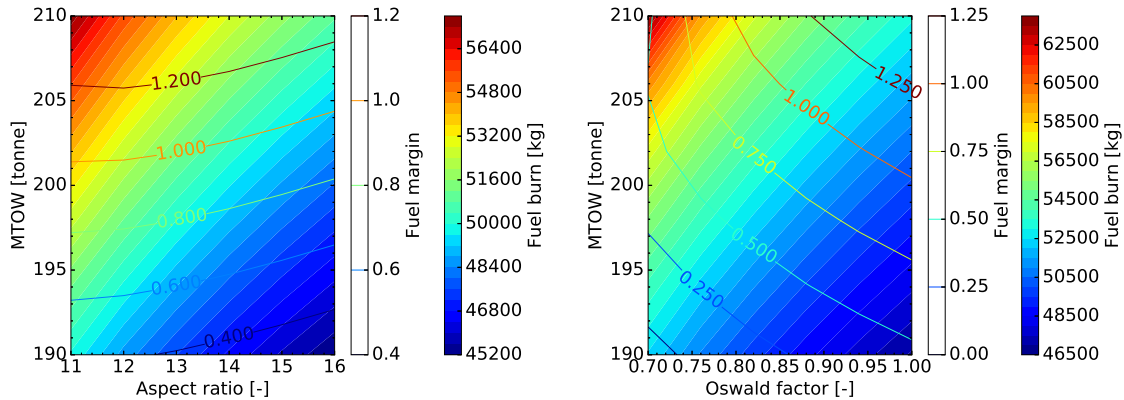
Figure 8.8: Variation of rate of climb with altitude at $W = 180,000$ kg

Figure 8.9: Response surface of aspect ratio vs MTOW (with fuel burn as gradient and fuel margin as contour lines)

Figure 8.10: Response surface of Oswald factor vs MTOW (with fuel burn as gradient and fuel margin as contour lines)

on fuel burn (with oswald factor and MTOW). Contour lines in both graphs indicate fuel margin, where values above 1.0 represent feasible design space in the current configuration.

In Fig. 8.11 it becomes clear that the driving aspect when it comes to fuel burn is induced drag. That is why a larger wing area for a given take-off weight leads to lower fuel burn in a plot. What is not accounted for is the increased operational weight/decreased payload that would result from increasing the wing area. Fig. 8.12 shows the impact on fuel burn as a function of wing area and oswald factor. The sensitivity is particularly high for low Oswald factor and low wing area. Again, only points with fuel margin > 1.0 represent feasible design.

Figs. 8.13 and 8.14 present impact of cruise speed and wing area on fuel burn in outgoing and spraying cruise

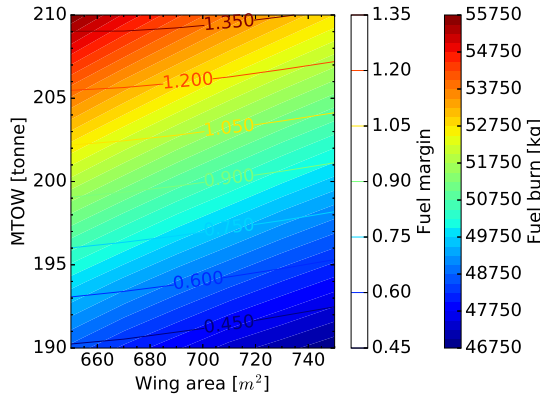


Figure 8.11: Response surface of wing area vs MTOW (with fuel burn as gradient and fuel margin as contour lines)

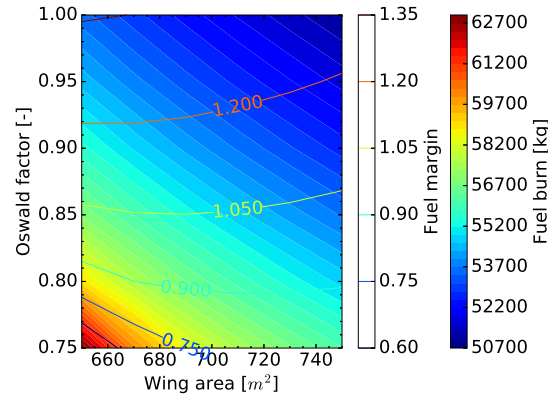


Figure 8.12: Response surface of wing area vs Oswald factor (with fuel burn as gradient and fuel margin as contour lines)

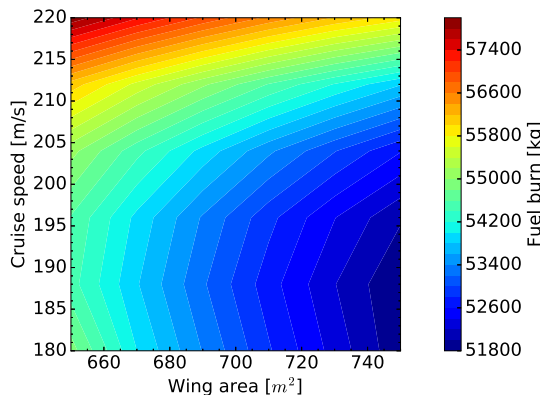


Figure 8.13: Response surface of wing area vs cruise speed (with fuel burn as gradient) (outgoing phase)

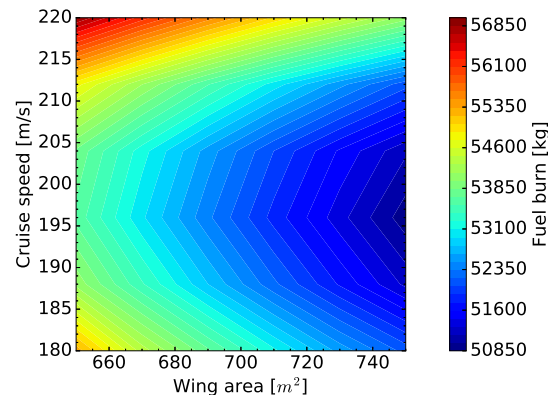


Figure 8.14: Response surface of wing area vs cruise speed (with fuel burn as gradient) (spraying phase)

respectively. Clearly visible at the large wing areas and relatively low cruise speed is the optimum design space offering the lowest fuel burn. The optimal cruise speed increases in the spraying cruise phase due to a change in aircraft weight and increase in altitude.

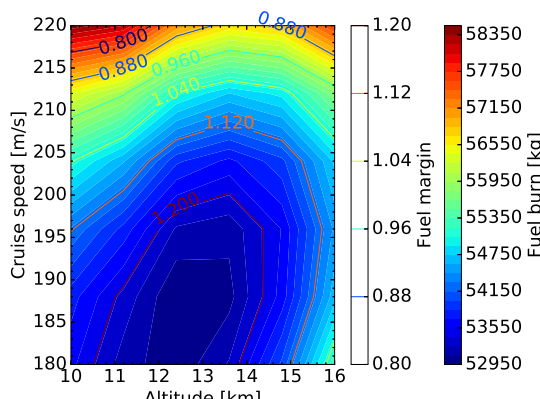


Figure 8.15: Response surface of altitude vs cruise speed (with fuel burn as gradient and fuel margin as contour lines)

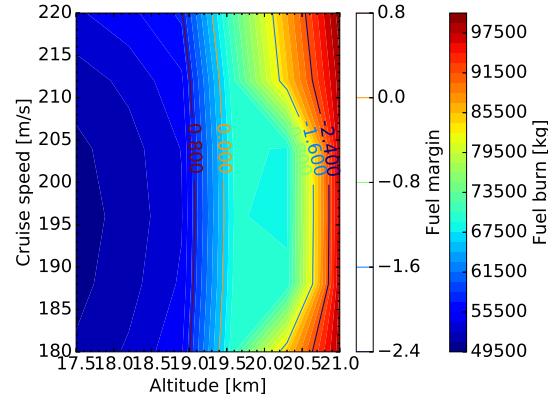


Figure 8.16: Response surface of altitude vs cruise speed (with fuel burn as gradient and fuel margin as contour lines with assumed constant altitude in spray cruise)

Finally, Figs. 8.15 and 8.16 show the impact of cruise speed and altitude on fuel burn in outgoing and spraying cruise phase respectively. For the first case clear optimum can be observed in 12-13km range, while the response surface for the spraying cruise phase serves to show the dramatic increase in fuel burn above $\approx 19.5\text{km}$.

Concluding, the sensitivity analysis of critical design parameters indicates that aspect ratio and oswald factor, parameters influencing induced drag, have a very large impact on the design and they drive the design to an almost unacceptable extent. Moreover, analysis indicates that selecting the appropriate wing area, altitude and cruise speed has a meaningful impact on the fuel burn, but that (given the constrained mission) an optimum can be found.

8.3 Aerodynamics

The aerodynamic analysis and design of SAGA is closely knit with its structural, aeroelastic, performance and propulsive counterparts. In this section, the main aerodynamic design drivers, trade-offs and analyses are presented to deliver a fuel-efficient, low-drag design within the constrained design space. Section 8.3.1 gives an overview of the aerodynamic design drivers, followed by the initial aerodynamic aircraft model in Section 8.3.2. The main wing, tail and strut planform and airfoil design are presented in Section 8.3.3, Section 8.3.4, Section 8.3.5 and Section 8.3.6, while the 3D wing analysis over the span of conditions is included in Section 8.3.7. Finally, a sensitivity analysis and verification and validation is conducted in Section 8.3.8 and Section 8.3.9 respectively.

8.3.1 Aerodynamic design drivers

SAGA is a dedicated high-altitude aircraft, which governs the aerodynamic design. The highest required mission C_L coincides with the dispersion cruise, as opposed to landing and take-off as is common for conventional missions. As the two-term drag polar in Equation (8.8) shows, the corresponding high induced cruise drag is countered by employing a large AR and designing for high Oswald factor e , but still leaves a cruise C_L ranging from 0.805-1.01, even with $S = 700 \text{ m}^2$. The parasite drag C_{D_0} that comes with the concurrently increasing wetted area S_w must also not grow out of proportion:

$$C_D = C_{D_0} + C_{D_i} \quad C_{D_i} = \frac{C_L^2}{\pi Ae} \quad (8.8)$$

The high-altitude region also constrains airspeed, as the high required cruise C_L approaches $C_{L_{max}}$ and the stall speed V_s . Conversely, V_s lies only marginally below the subsonic speed at which supersonic shocks over the airfoil cause drag divergence (the Mach drag divergence number M_{dd}). Exceeding both speed limits prohibits sustained flight at the required cruise altitude and must be avoided in design conditions. This also interferes with in-cruise turning performance.

Finally, the aerodynamic design must meet the prescribed landing and take-off distance requirements, ensure structural feasibility and minimise fuel consumption.

8.3.2 First-order aerodynamic model

For first-order design analysis over the range of conditions encountered during the mission, a conceptual design aerodynamic model as included in SUAVE's aerodynamics library was employed.

This model estimates inviscid wing lift from a Weissinger vortex lattice model [25] with ten spanwise panels and includes a fuselage correction of 1.14 [13]. Compressibility is accounted for with the Prandtl-Glauert correction presented in Equation (8.9), where M_∞ is the freestream Mach number and C_{L_0} the C_L at $M = 0$. Equation (8.10) estimates the lift-curve slope C_{L_α} from the DATCOM method [26]:

$$C_L = \frac{C_{L_0}}{\sqrt{1 - M_\infty^2}} \quad (8.9) \quad C_{L_\alpha} = \frac{2\pi A}{2 + \sqrt{\frac{A^2}{\eta} (1 + \tan^2 \Lambda) - M_\infty^2} + 4} \quad (8.10)$$

$C_{L_{max}}$ is estimated from the method presented in Stanford Aircraft Design, Synthesis, and Analysis course ³. Starting with outboard t/c and Reynold's number Re , this method extrudes those results over the wing by accounting for sweep Λ , taper λ and tail downforce. It includes a 0.2 wing-mounted engine correction and a scaling factor of 1.2 to satisfy CS-25.

Drag estimation

The first-order drag model comprises lift-induced drag, parasite drag, compressibility drag and miscellaneous drag. The last category includes excrescence drag as estimated by ESDU [27], fuselage upsweep drag, control surface gap drag and nacelle base drag, generally an order of magnitude less than the other contributions.

Lift-induced drag follows from the second term of Equation (8.8) and is the dominating drag contribution at high altitude. C_L comes from the inviscid lift estimation. e is translated from the inviscid span efficiency

³ URL <http://adg.stanford.edu/aa241/AircraftDesign.html> [Accessed 11.06.2016]

factor (as determined in Section 8.3.7) through Equation (8.11) [16], where $K = 0.38$ (see Footnote 3) and C_{D_p} is the viscous parasite drag. This component dominates the first term of Equation (8.8), and is computed as the sum of the contributions of the wing, tail, fuselage, engines, pylons and struts. The C_{D_p} estimates are obtained from each component's equivalent skin friction coefficient $C_{f_{eq}}$ scaled by its wetted area:

$$\epsilon = \frac{1}{\frac{1}{e_{inviscid}} + \pi A K C_{D_p}} \quad (8.11)$$

$$C_{D_{p,comp}} = C_{f_{eq}} \frac{S_w}{S} \quad (8.12)$$

$C_{f_{eq}}$ derives from flat plate estimates of the fuselage, tail sections, strut, main wing and landing gear fairings scaled with form factors. S_w and S for each component are presented in the drag budget's breakdown (Table 12.9).

The compressible drag penalty of exceeding M_{dd} is modelled through the regressed relation Equation (8.13) (see Footnote 3). This generally overpredicts compressibility drag with respect to supercritical airfoils, and is calibrated with the ΔM_{dd} increment of 0.06 proposed in Footnote 3.

$$C_{D_{comp}} = 0.00190 \cdot \left(\frac{M_\infty}{0.922 - 1.15t/c - 0.305C_L + 0.333t/c^2 + 0.467t/cC_L + 0.0875C_L^2} \right)^{14.6} \quad (8.13)$$

Finally, the landing gear fairings are modelled as Roskam fuselages [28]. Sensitivity analysis with differing combinations of fairing length, diameter and frontal area showed that increasing $\frac{l_{fairing}}{d_{fairing}}$ is most efficient to minimise the drag impact, resulting in a final fuselage C_{D_0} increment of 0.00001 and 10 kg of additional fuel burn, assumed negligible given that the error of the underlying zero-fidelity estimates is usually significantly larger.

Evaluating this total drag model at the conditions encountered throughout the mission in SUAVE's solver module yields a computationally cheap, mission-spanning drag breakdown, as presented in Fig. 8.18. Combined with the lift estimate and the planforms to be defined in Section 8.3.3, this also assesses L/D , α and C_L throughout the mission as shown in Fig. 8.17.

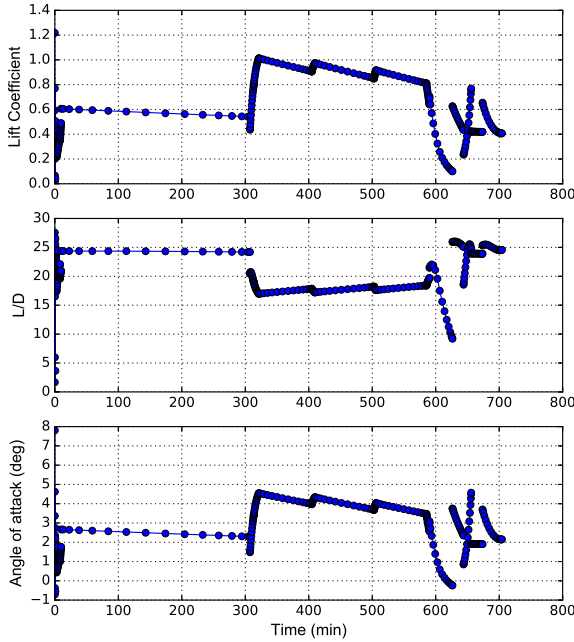


Figure 8.17: C_L , L/D and α over the SAGA mission

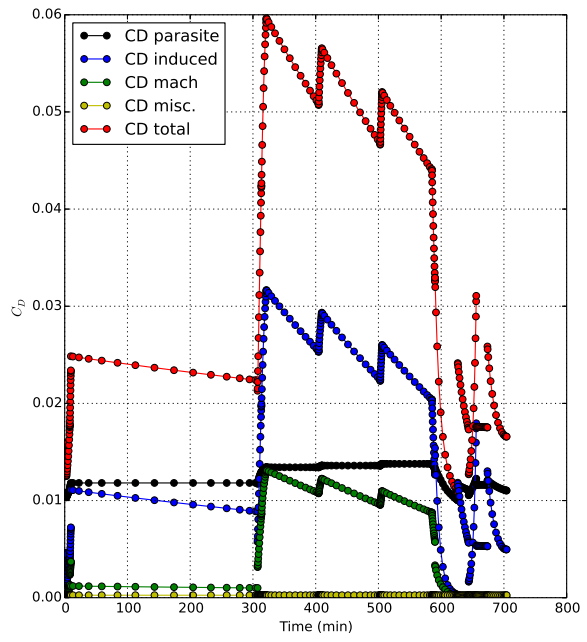


Figure 8.18: Drag breakdown over the SAGA mission

8.3.3 Wing design

SAGA comprises four wing-like surfaces: the main wing, the horizontal tail, the vertical tail and the strut. This section treats the main wing planform and airfoil design, while Section 8.3.4, Section 8.3.5 and Section 8.3.6 describe the horizontal tail, vertical tail and strut design respectively. The final planform design parameters are summarised in Table 8.6:

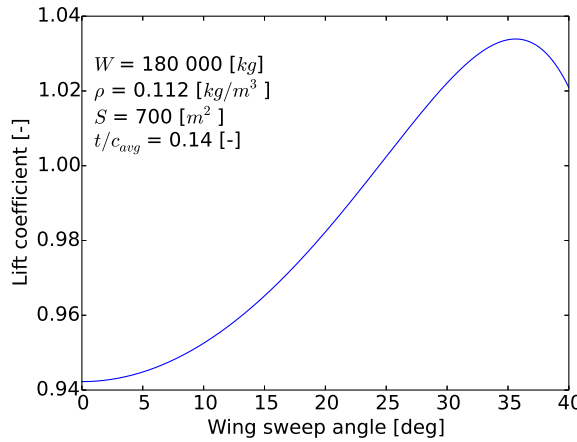
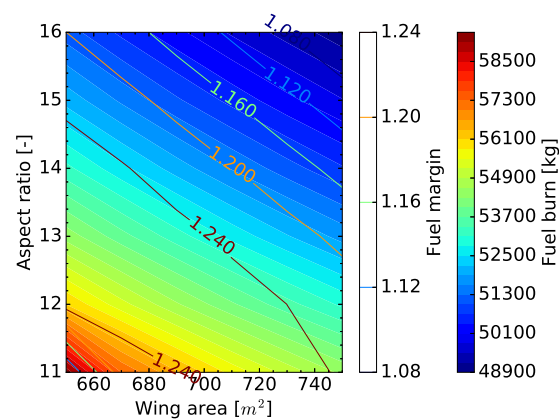
Table 8.6: Main wing, horizontal tail, vertical tail and strut planform parameters

Parameter [Unit]	Main wing	Horizontal tail	Vertical tail	Strut (single side)
$S [\text{m}^2]$	700	131	39	16.3
$AR [-]$	13.0	5.00	2.50	14.6
$b [\text{m}]$	95.4	25.6	4.94	20.3
$\Lambda [\text{°}]$	0.00	10.0	35.0	0.00
$\lambda [-]$	0.500	0.3	0.2	1.00
$C_r [\text{m}]$	9.78	7.87	6.58	1.22
$C_{mac} [\text{m}]$	7.61	5.61	4.53	1.22
$C_t [\text{m}]$	4.89	2.36	1.32	1.22
Airfoil	SC(2)-0714	SC(2)-0012	NACA 63010a	SC(2)-0010

Keeping the design driving C_{D_i} in check requires a high S and AR . This is visualised by Fig. 8.20 and Fig. 8.18. However, to stay within structural feasibility constraints, SAGA's wing parameters were in an earlier design stage constrained to $S = 700 \text{ m}^2$ and $AR = 13$, corresponding to a wing span $b = 95.4 \text{ m}$. Winglets are quickly discarded as an option to increase AR , as they are hard to design right, have a negative aeroelastic impact and may not add significant improvement to the already high AR [29]. The high wing deflections associated with the high b were calculated to affect lift loss by less than 1% and were thus not considered in the required lift calculations.

Main wing sweep Λ

SAGA's main wing will be unswept. Increasing Λ decreases effective airspeed over the wing and postpones M_{dd} . This allows cruise at higher speeds without compressible drag penalty, requiring less C_L and potentially less C_{D_i} . However, for every airspeed the C_L required for maintaining lift equilibrium increases with $\frac{1}{\cos^2 \Lambda}$. This is visualised by Fig. 8.19, which considers the mission point with the highest required C_L , as seen in Fig. 8.17.

Figure 8.19: Required C_L for differing sweep angles at the V_c corresponding to M_{dd} Figure 8.20: Response surface of the predicted sensitivity of AR and S on fuel burn

Assuming the aircraft flies just below M_{dd} , the drag divergence model of Section 8.3.2 predicts that Λ must be of order 33° for the benefit of higher M_{dd} to outweigh the lift loss of the airfoils. To ensure equal AR and S , b then rescales by $\frac{1}{\cos \Lambda}$, a 20% increase for the 33° best-case Λ . As treated in Section 8.5, wing weight reduction is of paramount importance, rendering this span increase infeasible. Since the required mission time is achieved without sweep, its implementation for higher V_c is not necessary. Finally, going past $\Lambda = 40^\circ$ requires M_{dd} as predicted by the model past $M = 0.9$. This falls outside the validity of the model (see Footnote 3), and likely leads to shocks on other exposed surfaces [30].

Taper ratio λ_w

As minimising induced drag is extremely important at the high cruise C_L , achieving as high e as possible is also crucial. For an unswept wing, $\lambda_w = 0.450$ is considered optimal [31] in preliminary design. After optimising for fuel burn in SUAVE and vortex lattice analysis (as explained in Section 8.3.7), this is updated to

an optimum for C_{D_i} at $\lambda_w = 0.5$. Stall is then expected to progress from the back of the TE and not interfere with the ailerons. Setting taper concludes the root, tip and mean aerodynamic chords C_r , C_t and C_{mac} .

Airfoil selection

To ensure the required aerodynamic performance over the mission, the main wing airfoils and their spanwise distribution are selected based on the following criteria:

- M_{dd} high enough for minimum compression drag, comfortably above $M = 0.712$. With $\Lambda = 0$, airfoil M_{dd} is taken as full wing M_{dd} corrected with spanwise Re .
- Design lift coefficient $C_{l_{des}}$ in the range of C_L required by V_c and $C_{l_{max}}$ well higher than the required C_L in cruise and sea level conditions.
- Low α at C_{l_c} to ensure a stall margin and minimise the induced drag.
- Small negative C_m to ensure minimum tail lift for trim.
- L/D as high as possible at the average $C_{l_{des}}$ estimated from the performance analysis.
- t/c above 0.12, as required to keep the wing box weight in check.
- Experimental wind tunnel data on Re and M in the mission's near-transonic critical design conditions, take-off and landing to validate the airfoils' performance.

The C_L considered for both the $C_{l_{max}}$ and $C_{l_{des}}$ analysis is the maximum cruise C_L , as this is both the highest C_L of the mission and the C_L at which most time is spent. As outlined in Section 8.7, this is determined by considering the required maximum aircraft C_L of the three high-altitude cruise phases from Fig. 8.17, corrected for trim for a range of engine and wing placements. Thus, $C_{l_{max}} = 1.05$ at the start of the dispersion cruise is the critical condition, while $C_{l_{des}} = 0.927$ is the averaged C_l for all three high altitude cruise phases.

To perform this analysis efficiently, a tool that automatically checks 1550 airfoils for the $C_{l_{des}}$, L/D , $C_{l_{max}}$ and t/c was developed in Python. The tool runs each airfoil through Xfoil [32] at $M = 0$ (as Xfoil is not designed to handle supercritical Mach numbers) and $Re = 11 \cdot 10^6$ corresponding with the wing M.A.C. in the spraying cruise. $C_{l_{max}}$ and $C_{l_{des}}$ are adjusted down to $M = 0$ through Equation (8.9) to $C_{l_{max}} = 0.72$ and $C_{l_{des}} = 0.65$.

This preliminary analysis resulted in the selection of three supercritical airfoils for M_{dd} and data availability analysis: the NLR7301, NASA SC(2)-0714 and NASA SC(3)-0712. Supercritical airfoils can experience drag creep in off-design conditions and have a narrow α range in their design conditions [33]. However, they are chosen for SAGA as the best, freely available airfoils for high-lift, low-drag transonic performance required by the unswept wing. Wind tunnel test data are available for each of the airfoils [34, 35, 36], supplying their M_{dd} at the high-altitude cruise Re . The relevant design parameters of the airfoils are included in Table 8.7.

Table 8.7: Initial airfoil selection, C_{d_0} and C_{m_0} are drag and moment coefficients at the design C_l

Name	$(\frac{L}{D})_{max}$	$C_{l_{clean,max}}$	$C_{l_{des}}$	t/c	C_{d_0}	C_{m_0}	M_{dd}
NLR7301 [36]	6.25	0.801	0.501	0.165	0.0700	-0.100	0.746
SC(2) - 0714 [34]	70.0	1.20	0.700	0.140	0.0100	-0.160	0.720
SC(3) - 0712 [35]	77.8	1.11	0.700	0.120	0.00900	-0.145	0.740

After a trade-off where every criterion receives a weight from 1-5, the SC(2)-0714 is finally selected. Since generating sufficient lift is the primary requirement to ensure SAGA's feasibility at high altitude and C_{D_i} dominates the design, C_{l_c} and the stall margin $C_{l_{max}} - C_{l_c}$ both receive 5. A pareto wing weight estimation to determine the decreased structural wing weight by increasing t/c and thus reducing C_{l_c} due to a lighter design was performed in conjunction with the structures department and subsumed under C_{l_c} .

The C_d and C_m criteria are evaluated at $C_{l_{cruise}}$. C_d estimates the viscous drag contribution of the airfoil. It receives a weight of 3, as transonic viscous effects such as shock-boundary layer interaction are mitigated through ensuring M_{dd} and this drag is generally subjugated by C_{D_i} . C_m 's weight is 2, since the trim analysis of Section 8.7 shows relative insensitivity to the required C_L . M_{dd} has weight of 4, since it allows higher speed and lower required C_L . The resulting trade-off is presented in Table 8.8:

Based on the trade-off, the NLR airfoil is discarded as main airfoil, as it cannot provide the required lift. However, since the wing weight jeopardised SAGA's feasibility through several design stages before eventually

Table 8.8: Main wing airfoil trade-off table. The column scores are unweighted and with respect to the NLR7301 baseline

Name	$C_{l_{max_req}}$ [5]	Score	C_d [3]	Score	C_m [2]	Score	M_{dd} [4]	Score	Total
NLR 7301	-0.189	1	0.07	1	-0.100	1	0.746	1	14.0
SC(2)-0714	0.190	2.00	0.0100	7	-0.160	0.625	0.720	0.965	36.1
SC(3)-0712	0.09	1.47	0.009	7.79	-0.145	0.690	0.740	0.992	36.0

reducing (further explained in Section 8.5), it was kept as a backup and analysed in several 3D wing models. The SC(3) airfoil outperforms the SC(2) in terms of M_{dd} , cruise drag, and trim, but the thicker SC(2) airfoil $C_{l_{max}}$ is better. This results in almost identical trade off scores for these airfoils. However, since the SC(2) scores the best in the highest weighted category, it is finally selected for SAGA.

8.3.4 Horizontal tail

The horizontal tail area S_h and aspect ratio AR_h are determined in Section 8.7. This is currently extended with selecting a NASA SC(2)-0012 airfoil, setting $\Lambda_h = 35^\circ$ and $\lambda_h = 0.5$. Subscript h indicates horizontal wing parameters.

The tail must generate the required C_{L_h} throughout the mission, stall at a higher α than the main wing to ensure nose down pitch [14] and have ΔM_{dd} of 0.05 higher than the main wing to ensure control even if drag divergence separates the flow over the main wing [37]. As Section 8.7 indicates, C_{L_h} varies with engine placement. This depends on aeroelastic considerations, which again depend on the shear centre as determined in Section 8.5. Therefore, C_{L_h} was considered for a range of engine and wing placements for the three high-altitude cruise phases and landing. Since the main wing does not require high C_M -inducing high lift devices (HLDs), high altitude cruise $C_{L_h} = -0.28 - 0.24$ is sizing. α_s of the main wing is determined through 3D analysis in Section 8.3.7 to lie around 3.5° in those conditions.

On this basis, NASA's SC(2)-0012 symmetric airfoil is selected. Wind tunnel tests at average chord Re in the final high altitude cruise ($Re = 7.2 \cdot 10^6$) indicate M_{dd} at $M = 0.8$, no stall at $\alpha_h = 4^\circ$ for any tested high Mach number and $C_{l_{\alpha=4}} = 0.5$, with $C_d = 0.005$. Since the tail will be fully adjustable (see Section 8.7), the symmetric profile can be rotated to the relevant α_h to ensure trim.

Λ_h is set to 10° . A high Λ_h is beneficial for high stall angle of attack α_s , meeting M_{dd} and inducing leading edge vortices for higher lift. However, it generally reduces C_{L_α} , $C_{L_{max}}$ (assuming no fins) and $C_{L_{\delta_e}}$. The airfoil does not require significant sweep to meet these requirements, but no data predicting its stall angle is currently available. Therefore, $\Lambda_h = 10^\circ$ to bolster the stall margin, while detailed design should encompass stall testing of the airfoil and the effect of leading edge vortices on $C_{L_{h,max}}$ to set the final Λ_h .

Horizontal tail $\Lambda_h = 0.3$ to weigh favourable span loading against premature tip stall based on Λ_h . This sizes C_r , C_t and C_{mac} . No tip stall is predicted at the low tip $Re = 3.35 \cdot 10^6$ and reduced M due to sweep [38].

8.3.5 Vertical tail

The vertical tail planform design comprises many of the same elements as the horizontal tail. S_v and AR_v again flow from Section 8.7, while $\Lambda_v = 35^\circ$, $\lambda_v = 0.2$ and a NACA 63010a are selected to yield a high stall angle β_s , lift curve slope $C_{L_{v,\beta}}$ and $C_{L_{max}}$ to meet the sizing crosswind and OEI requirements. Subscript v indicates vertical tail parameters.

The vertical tail airfoil must be symmetric to ensure $C_{L,v} = 0$ in directional trim. It must be thin to ensure M_{dd} higher than the main wing [14] and stall at β_s above $\beta_{max} = 22.3^\circ$ plus an increment $\beta_v = 2.5^\circ$ that accounts for β_v reduction due to maximum rudder deflection. Finally, its lift curve slope must meet the planform $C_{L_{v,\beta}} = 3.771/rad$. β_{max} and $C_{L_{v,\beta}}$ are specified in Section 8.7. $C_{L_{max}}$ is not assumed sizing for the airfoil, since the rudder design accounts for this.

The Xfoil airfoil selection tool was run for symmetric sections with $t/c < 0.126$ (a 10% decrement from wing t/c [14]) and $\beta_s > 12^\circ$. Re is taken at the average chord, at take-off and landing speeds for OEI and crosswind: $Re_{TO} = 25.7 \cdot 10^6$ and $Re_{landing} = 23.0 \cdot 10^6$ and $M_{TO} = 0.328$ and $M_{Landing} = 0.292$. This results in the selection of the NACA 63010a airfoil. Its $t/c = 0.100$, $\beta_s = 14.0^\circ$ and $C_{l_{max}} = 1.20$. $C_{l_\alpha} = 6.3$ and $C_{d_0} = 0.0045$ [39] at $Re = 20 \cdot 10^6$. Re is on the low side, but had to be extracted from the existing wind tunnel data as Xfoil

mispredicted the existing airfoil reference data and was thus found too unreliable. It should therefore be a conservative estimate of the actual performance.

To meet the β_s and M_{dd} requirements, the vertical tail is swept by 35° . Sweep improves β_s , reduces compressibility drag in cruise and may again induce favourable LE vortices, while lowering vertical tail controllability and $C_{L,\beta}$. To meet $\beta_s = 24.8^\circ$, the method from Corke for the given AR stipulates $\Lambda_v = 35^\circ$ [40]. At this Λ_v , $M_{dd} = 0.81$ according to Equation (8.13), satisfying all the requirements.

Taper $\lambda_v = 0.2$ from Raymer's correlation with Λ_v [18]. This accommodates for Λ_v to minimise induced drag, ensures β_s can be provided and reduces vertical tail weight. $\Lambda_v = 0.2$ corresponds well with large transonic transport aircraft [14]. The ensuing C_r , C_t and C_{mac} are presented in Table 8.6.

8.3.6 Strut

Adding a strut to SAGA has several aerodynamic impacts. Firstly, it adds more wetted area and parasite drag. Secondly, it interferes with wing lift and drag, especially around the attachment points. However, as it reduces the wing weight significantly (as will be explained in Section 8.5), the reduced C_L to sustain high altitude flight still yields a 500 kg positive fuel burn effect.

To estimate this impact, the strut planform was sized from its optimal structural configuration (as explained in Section 8.5). Attached at 40% percent of the semispan and at the bottom of the fuselage, it spans 19.9 m with a cross-sectional area of 0.0175 m^2 to meet the load requirements. As inertia is of secondary importance for the structure, the rest of the planform design aims to minimise aerodynamic impact. As a contingency for transverse loading and aeroelastic effects, skin thickness is set to $t_{sk} = 0.007 \text{ m}$ as proven feasible at the relevant conditions [41]. A proper thickness to area calculation for adequate strut moment of inertia and aeroelastic behaviour should be performed in detailed design.

Given t_{sk} and a straight, unswept planform to minimise transverse strut loading, Equation (8.14) is employed to calculate the strut chord [13]:

$$c_{strut} = \frac{A_{strut}}{(2 + 0.5t/c_{strut})t_{sk}} = 1.40\text{m} \quad (8.14)$$

To minimise the strut interference with the wing, it is attached to the pylon of the outboard engine, at around 0.2 m vertical distance from the wing. This ensures minimum effect on wing lift and drag from the strut [42], but creates a duct-like wing-pylon-strut geometry. In transonic flow, this 'nozzle' can choke and create strong shock waves at the strut trailing edge [43].

NASA's thinnest supercritical airfoil, the SC(2)-0010 symmetric profile is therefore chosen [33] as strut airfoil to minimise this and other drag sources. It does not exceed M_{dd} in cruise, has a small S_{ref} and low C_L . It has also been analysed and found well-performing in literature [43]. To prevent flow acceleration and the nozzle effect at transonic cruise, it is flattened on the nozzle side close to the pylon. The effect this has on loading the strut transversely and on drag must be investigated in further detail in the next design phase and is presently left as a risk.

As the aircraft faces a range of α between $1 - 8^\circ$ during the mission, the strut will inevitably generate force. However, placing it at an incidence angle of -3° with respect to the freestream ensures that this is minimised during the design critical high-altitude cruise, as optimised in SUAVE.

SUAVE estimates the struts' net effect of the drag increment versus the 2 ton wing weight reduction it offers. The struts subtract 500kg of fuel and lower the required $C_{L,max}$ to 1.00 due to the lighter design. Since the strut also ensures a margin for weight feasibility and could permit a higher AR in a future design iteration, they are therefore still recommended for the overall the design in spite of their drag contribution.

8.3.7 Detailed analysis

With the sized wing planform and airfoils, a 3D wing analysis was conducted. This aims to add fidelity to the computationally cheap, first-order estimates from Section 8.3.2 through subjecting the wing planform to a vortex lattice method (VLM) and a viscous analysis. This allows for estimations of e , $C_{D,i}$ and $C_L - \alpha$ of the aircraft at the first point of the take-off, outgoing cruise, the three high altitude cruises, landing and diversion mission segments.

SAGA's wing geometry is therefore implemented in Athena Vortex Lattice (AVL)⁴. Dividing the wing into 20 spanwise and 15 chordwise strips, the wing is automatically analysed from Python over a range of α for every run case. Since a slender body is hard to accurately analyse by placing source and doublet vortices on its surface [44], the fuselage is left out of the analysis and the correction from Section 8.3.2 is used instead. AVL also employs a Trefftz-plane analysis in the far-field to estimate $e_{inviscid}$ as a function of the measured C_{D_i} (Footnote 4). This is subsequently corrected with Equation (8.11) to obtain the viscosity-corrected Oswald factors.

As AVL only performs inviscid analysis, it cannot accurately predict viscous drag or stall. Also, the airfoil's contribution is limited to a correction with respect to thin airfoil theory. To augment a viscous, airfoil-based analysis to the VLM, test data for the SC(2)-0714 airfoil from three different wind tunnel tests are compiled in a database [34, 45, 46], since viscous analysis codes such as Xfoil could not accurately predict or consistently converge for the high M at the cruise Re .

Therefore, for each α strip theory is used to estimate the local spanwise α . The local lift is corrected with the empirical airfoil lift and viscous drag is established at the local M and Re . The values are interpolated from the closest measured M and Re combinations in the database.

The empirical database does not contain data for $\alpha \geq 4^\circ$ at the design $M = 0.712$, between $M = 0.65$ and $M = 0.70$ or the diversion cruise phase $M = 0.500$. Therefore, the database is extended with 2D CFD data generated with Stanford's SU2 software [47]. The analysis is based on SU2's direct Reynolds Averaged Navier Stokes (RANS) solver with a Spalart-Allmaras one-equation turbulence model. It is run on a C-grid with 48,000 grid cells and a farfield boundary at 100 chord lengths in front of the leading edge and 150 chord lengths behind the trailing edge.

The resulting lift and drag polars and minimum e for the different cases are presented below. The take-off and landing cases, as well as the three high-altitude cruise phases are so similar that only the take-off and 18.5 km altitude graphs are included. Moment coefficients were left out of the analysis, since their impact was found relatively insensitive to the stability analysis (see Section 8.7) and focus was placed on the more design driving C_L and C_D . Higher fidelity estimates should be investigated for detailed design.

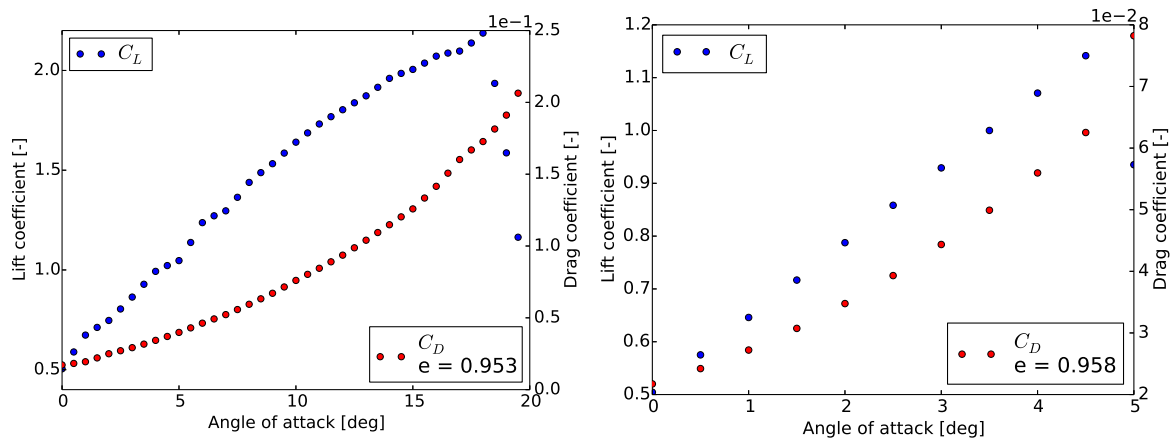


Figure 8.21: Lift and drag polar in take-off conditions: $M = 0.270$, $Re = 26.7 \cdot 10^6 - 53 \cdot 10^6$

Figure 8.22: Lift and drag polar in outgoing cruise conditions: $M = 0.647$, $Re = 17 \cdot 10^6 - 34 \cdot 10^6$

Based on the 3D-wing analysis, several conclusions are drawn: Firstly, high speed, high altitude cruise is indeed the critical condition for the wing. Stall is predicted beyond 3° in all three high-altitude phases, in line with expectations [34]. While the behaviour past stall is not accurately modelled, ensuring α_s is not exceeded can be predicted.

The wing has a considerably wider α -range in take-off and landing. As analysed in Section 8.2.4, the take-off and landing requirements are easily met. As the critical high-altitude cruise is simultaneously the design condition, which the wing can meet, no weight-adding high lift devices are included in the design.

⁴ URL <http://web.mit.edu/drela/Public/web/avl/> [Accessed 17.06.2016]

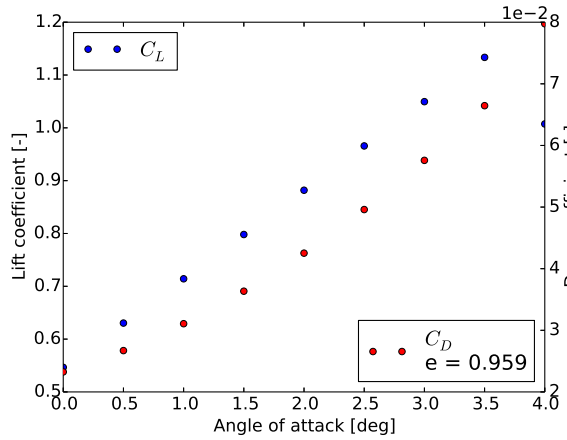


Figure 8.23: Lift and drag polar at 18.5 km altitude: $M = 0.712$, $Re = 8.00 \cdot 10^6 - 16.0 \cdot 10^6$

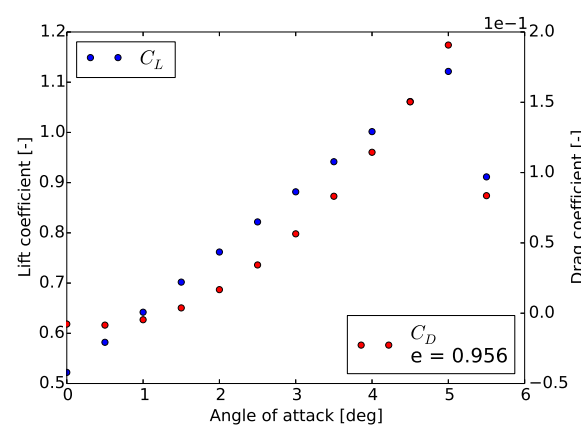


Figure 8.24: Lift and drag polar at diversion: $M = 0.500$, $Re = 21.5 \cdot 10^6 - 42.0 \cdot 10^6$

8.3.8 Sensitivity analysis

The sensitivity analyses affecting aerodynamic design choices have been presented continuously through this section. This includes fuel burn sensitivity with S and AR , C_L sensitivity with respect to Λ , the effect of adding a strut on fuel burn, adding fairings for the landing gear and the effect of t/c on wing weight and overall required C_L . The analysis of Section 8.3.7 further elaborates how C_L and C_D are extremely sensitive to altitude and are operating at the limit of their feasibility range. This section expands on that analysis with stall sensitivity of the wing at the critical first point of 18.5 km altitude cruise.

To estimate the stall sensitivity, the wing $C_{L_{max}}$ is evaluated over a range of cruise speeds and corresponding M and Re ranges. Combined with the required 1g C_L , this spells out Fig. 8.25:

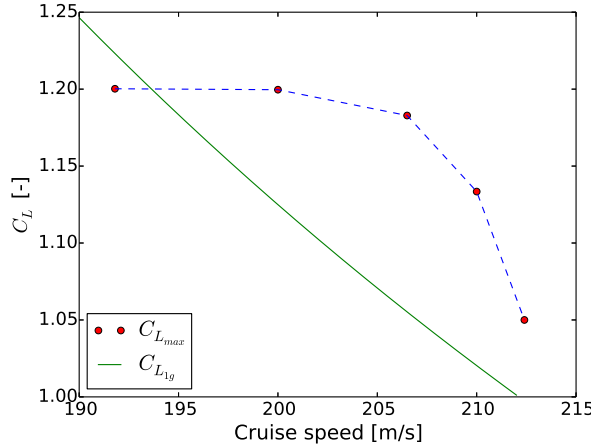


Figure 8.25: $C_{L_{max}}$ and C_L for 1g at the start of 18.5 km cruise 3D analysis. The 200 m/s is based on SU2, the others from windtunnel data

The increased $C_{L_{max}}$ at lower speeds is explained by shock-induced separation occurring at higher α , offsetting a slightly lower lift curve slope further away from M_{dd} . Yet, it also shows how the operating speed envelope between stall and drag divergence is a narrow 17 m/s with stall at 193.5 m/s and drag divergence at 212.4 m/s. SAGA is thus very sensitive to its flight conditions, and may in practice require local mission changes if weather operations differ significantly.

This narrow lift envelope also has pronounced consequences on tip stall and controllability. When making a coordinated turn, the yawing motion may lead to one wing exceeding M_{dd} while the other wing's tip could stall. To mitigate this, vortex generators or tip washout may be applied. However, vortex generators add a critical drag contribution, while washout decreases the span efficiency with negative induced drag impact. Therefore, the current design's feasibility within the narrow lift envelope is investigated.

From Fig. 8.25, excess C_L at an available data point is maximum at $V = 206.5$ m/s. In level flight, the 3D anal-

ysis tool estimates a wing tip stall margin at the wing $C_{L_{max}}$ of $\alpha = 0.223$, indicating that the tip's downwash outweighs the lower Re it operates at in terms of α_s . In Section 8.7 these data are translated to a maximum 1g bank angle and a corresponding yaw rate, to check whether an effective turn can be performed within the lift envelope without tip stall.

8.3.9 Verification and Validation

To verify the programs used in the aerodynamic analysis, a range of unit and system tests were performed. The code blocks importing and processing AVL code and airfoil data were verified to reproduce the same data as manually running the VLM with the same case and the wind tunnel test data. AVL was also unit tested with a rectangular wing to verify that taper improved e . Subsequently, the calculation of C_{D_i} , C_{D_0} , e , C_{L_α} and $C_{L_{max}}$ in Section 8.3.7 was verified as a system test by comparing them to the first-order SUAVE methods presented in Section 8.3.2 at the analysed mission points.

Table 8.9: Verification of aerodynamic parameters. Re and M are equal input in both models. C_{D_0} and C_{D_i} are tested at $\alpha = 3^\circ$. SUAVE is treated as baseline

		Take-off	Outgoing cruise	18.5 km cruise	Landing
$C_{L_{max}}$ [-]	AVL	2.19	1.14	1.13	2.19
	SUAVE	2.15	1.08	1.05	2.08
$\Delta\%$		1.86%	5.56%	7.62%	5.29%
C_{D_i} [-]	AVL	0.0202	0.0293	0.0342	0.0195
	SUAVE	0.017	0.0105	0.0316	0.0120
$\Delta\%$		18.8%	279%	8.23%	62.5%
C_{L_α} [1/deg]	AVL	0.120	0.142	0.168	0.120
	SUAVE	0.149	0.144	0.171	0.139
$\Delta\%$		19.5%	1.34%	1.75%	13.7%
C_{D_0} [-]	AVL	0.00900	0.0150	0.0251	0.00900
	SUAVE	0.0101	0.0128	0.0264	0.00999
$\Delta\%$		10.9%	17.1%	4.92%	9.99%

Table 8.9 shows a good agreement between the models. The only discrepancies larger than 30% arise in the induced drag prediction and are boldfaced. This difference stems from SUAVE estimating $C_L = 0.6$ at the $\alpha = 3^\circ$ outgoing cruise comparison, while the airfoil-AVL combination predicts $C_L = 0.923$ at that α . Since SUAVE accounts solely for airfoil t/c , this likely illustrates the improved fidelity of accounting for the airfoil in the AVL model. Thus, SUAVE likely overpredicts drag and its mission estimates may be conservative. The difference is less for $C_{L_{max}}$ and the design driving high altitude cruise, so the impact is expected to be relatively limited.

Validation of the aerodynamics was carried out throughout the design process. Using empirical wind tunnel test data to validate all aerodynamic predictions, this approach eliminated Xfoil as a reliable analysis tool in the near transonic conditions. Instead, the appropriate empirical data themselves have been consulted as often as possible to ensure the validity of the analysis.

Finally, the SU2 application was validated by running it at the same conditions as the windtunnel-tested data and comparing the pressure distributions and force predictions. The result of the two validation cases are presented in Table 8.10:

Table 8.10: SU2 validation. Case 1 is at $\alpha = 3^\circ$, $Re = 15 \cdot 10^6$, $M = 0.712$, case 2 is at $\alpha = 1.03^\circ$, $Re = 9.98 \cdot 10^6$, $M = 0.704$

	C_l			C_d		
	SU2	NASA	$\Delta\%$	SU2	NASA	$\Delta\%$
Case 1	1.0668	1.0684	-0.150	0.0552	0.0523	5.54
Case 2	0.6795	0.6746	0.726	0.01168	0.01117	4.57

While these data indicate good initial predictions and pressure distribution comparison confirms this for C_L , a proper grid convergence study with three refinement levels should be carried out in a future analysis to assess whether the computed results converge at the expected rate. Subsequently, the observed order of accuracy should also be verified to be similar to the expected order of accuracy where the solution is unknown, using e.g. Richardson extrapolation [48].

8.4 Propulsion and power

In this section, the propulsion and power systems will be discussed. Focus will be placed on propulsion since it is found to be a much higher risk item. It is not the goal of this section to provide an ultimate engine design but rather to investigate the feasibility of current technology to complete the mission successfully.

8.4.1 General design choices

The aircraft fleet will be propelled by turbofans, which are considered the most suitable engine type for SAGA among the available options. The engine choice is mainly driven by the operating speed and altitude [14]. Propeller engines, including turbocharged piston engines and turboprops, are not suitable for operations above M=0.6 and above 11 km altitude⁵ [14]. In addition, engine placement could also pose some challenges, since the rotational plane of the blades should not cross the wings (which could happen with propfans attached on the wing or if sweep was to be added) or critical aircraft systems for safety reasons. A blade detaching from the engine during operations could cause severe damage to the aircraft [18]. Very high altitudes can be reached with electrical engines, however they have only been used for very light aircraft operating at very low speeds⁶ [14]. Propfans are discarded mainly for uncertainty reasons, since they are still in the development stage [49]. In addition, they likely cannot produce enough thrust in the stratosphere due to their very large bypass ratio⁷. Then, ramjets and scramjets are discarded as they are designed for supersonic and hypersonic flights⁸ [14, 50]. Hydrazine engines have been proposed for high altitude aircraft, however, due to their low technological readiness level and the environment concerns they have raised, they are considered unsuitable for SAGA [8, 51, 52]. Since turbofans and turbojets are capable of performing the entire mission, the use of rockets, even for Jet-Assisted Take Off only, would be completely unjustified [14]. Turbojets and turbofans are both suitable options, with the turbofan being more fuel efficient and the turbojet being more weight and cost efficient [14]. Ultimately, the turbofan is chosen since its extra weight and cost are compensated for by the lower fuel required.

With the engine type now defined, its performance analysis will be the core of the rest of the chapter. The present analysis is performed with a Python tool developed to investigate trends and performance in design conditions. The Python program is based on gas turbine theory as explained in [53, 54]. It is supported by the gas turbine software GSP which is used for off-design performance estimation as well as verification purposes. The engine model assumes the fan and the low pressure compressor to be connected to the same spool driven by the low pressure turbine, and the high pressure compressor to be connected to the high pressure turbine by a second spool. A third spool with intermediate pressure components is not included since it was found to increase efficiency but decrease thrust, which was already limited. In addition, a bleed of 5% of the mass flow is taken from before the second compressor to cool the high pressure turbine, following the recommendations found in [55]. The Python model simply assumes the cool and hot air to be mixed uniformly, whereas GSP models Nozzle Guide Vane cooling⁹. In order to provide power for the different subsystems, 2MW is taken from the engines when spraying and 0.2MW in all other phases in both the Python tool and GSP. This includes an assumed generator efficiency of 92% and a margin of at least 15% in case payload requirements are modified in future stages of the design¹⁰.

8.4.2 Engine design

Since the development of a new engine is very costly and as it is recommended to have at least two engine options available, the first analysis considers a number of existing engines to be used for the propulsion system [56]. The results show that six turbofans such as the General Electric GE90 or Pratt&Whitney PW4084, or eight J75 turbojets (engine powering the U-2 which flies at similar altitudes¹¹) are needed to meet the thrust requirements. A preliminary engine design is therefore performed in order to gain a better understanding of the type of specifications suitable for stratospheric flight and to assess whether it is possible to fly with a more efficient propulsion system. In addition, this will allow to determine if technological improvements are

⁵ URL <https://www.grc.nasa.gov/www/k-12/airplane/propeller.html> [Accessed 17/06/16]

⁶ URL <http://www.solarimpulse.com/adventure> [Accessed 17/06/16]

⁷ URL <http://adg.stanford.edu/aa241/propulsion/propulsionintro.html> [Accessed 17/06/16]

⁸ URL <https://www.grc.nasa.gov/www/k-12/airplane/ramth.html> [Accessed 17/06/16]

⁹ URL http://www.gspteam.com/Files/manuals/UM/GSP_UM_11.pdf [Accessed 17/06/16]

¹⁰ URL [http://www.nianet.org/ODM/presentations/Cristian_Angel_-_Honeywell_-_Honeywell_Technologies_for_Hybrid_Electric_Propulsion_\(002\).pdf](http://www.nianet.org/ODM/presentations/Cristian_Angel_-_Honeywell_-_Honeywell_Technologies_for_Hybrid_Electric_Propulsion_(002).pdf) [Accessed 17/06/16]

¹¹ URL http://www.pw.utc.com/J75_JT4_Engine [Accessed 17/06/16]

needed if not more than four engines are to be used and to quantify the gap between the current and the desired technology level. Note that it took around 5 years to develop the GE90 engine, and a similar time frame can be assumed for the purpose-designed engine¹². This should be taken into account in the deployment planning of the fleet. The engines are designed to provide a total thrust of 110kN at 20 km altitude despite the proposed mission never reaching that altitude. This design choice is made to allow the engines to remain suitable if it is decided to climb up to 20 km in the future and provide flexibility for mission changes. It is clear that the engines will be oversized for most part of their operating conditions, however there is no other choice if fuel consumption is to be minimised.

Three parameters were found to drive the engine design: the inlet diameter, the bypass ratio (BPR) and the overall pressure ratio (OPR). The inlet diameter defines how much air mass flow enters the engine and has a significant impact on the thrust. Since the density is extremely low at 20 km, the highest diameter possible is desired, see Fig. 8.35. It was first set to 3.124 m (equal to the current largest engine, the GE90¹³) but has been subsequently increased to 3.5 m to obtain enough thrust at acceptable levels of fuel consumption. This represents a 12% increase with respect to the largest engine and is considered more easily achievable than increasing the components efficiencies or the turbine inlet temperature to the required levels. The second and the third parameter influence thrust and specific fuel consumption opposingly (if specific fuel consumption improves, thrust decreases), as shown in Figs. 8.26 and 8.27.

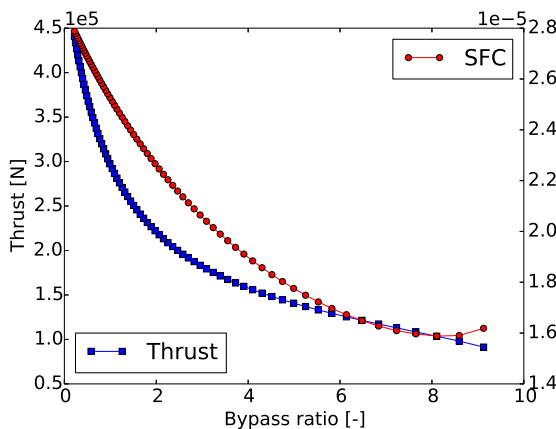


Figure 8.26: BPR effect on thrust and SFC

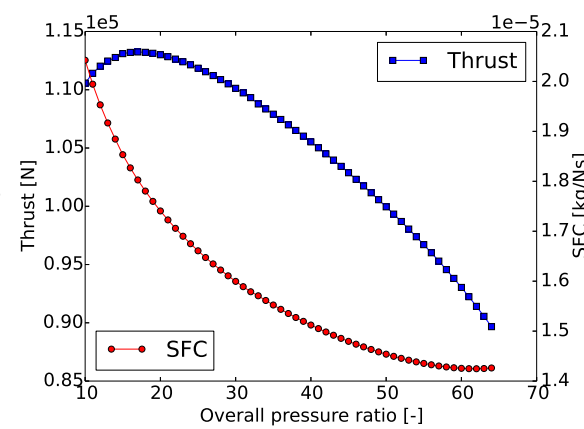


Figure 8.27: OPR effect on thrust and SFC

It can be clearly seen in Fig. 8.28 that for a given thrust, at 20 km altitude, increasing the OPR and decreasing the BPR leads to a more efficient design. However, it has been decided not to reduce the BPR below 7.5, in order to keep the core diameter within reasonable bounds. Such a BPR results in a core diameter of 1.2 m, which is 15% and 20% larger than the PW4084 and GE90, respectively¹⁴. The diameter proposed is nevertheless considered feasible since the core of a turbofan is essentially a turbojet, and the F118 turbojet also has 1.2 m diameter¹⁵. It follows from the BPR of 7.5 that the OPR has a value of 30, see Fig. 8.28. Note that the blue zone in the top-right corner represents an impossible design space. This is also applicable to the next figures showing a similar trait.

To complete the present design of the engine, the pressure ratios of the fan, low pressure compressor (LPC) and high pressure compressor (HPC) are determined. The optimal fan pressure ratio is found to be 1.68, resulting in a HPC pressure ratio of 10.63. Since the fan and the LPC are connected to the same spool, they have the same rotational speed and therefore have usually similar pressure ratios¹⁶. For simplicity, they will be considered equal in the present analysis. This allows to express the HPC pressure ratio as a function of the fan pressure ratio only since the OPR has already been fixed. Fig. 8.29 shows that there is an optimum for the fan pressure ratio where the thrust is maximum and the specific fuel consumption is minimum. Once the fan pressure ratio is changed, the optimum OPR changes and thus some iteration is needed until the optimal values are found.

All values are found to be within current technology, except for the engine size, which has already been

¹² URL http://web.stanford.edu/~cantwell/AA283_Course_Material/GE90_Engine_Data.pdf [Accessed 27/06/16]

¹³ URL http://www.geaviation.com/press/ge90/ge90_19951109a.html [Accessed 18/06/16]

¹⁴ URL <http://www.jet-engine.net/civtfspec.html> [Accessed 18/06/16]

¹⁵ URL <http://www.jet-engine.net/miltfspec.html> [Accessed 18/06/16]

¹⁶ Personal communication, Power & Propulsion Department, Delft University of Technology, the Netherlands

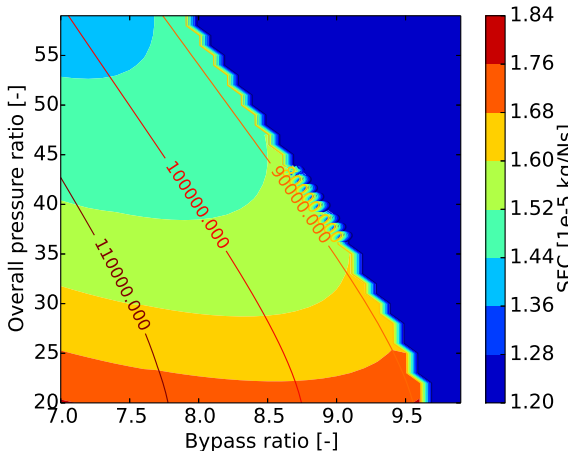


Figure 8.28: Bypass ratio and overall pressure ratio sizing. Lines represent thrust [N]

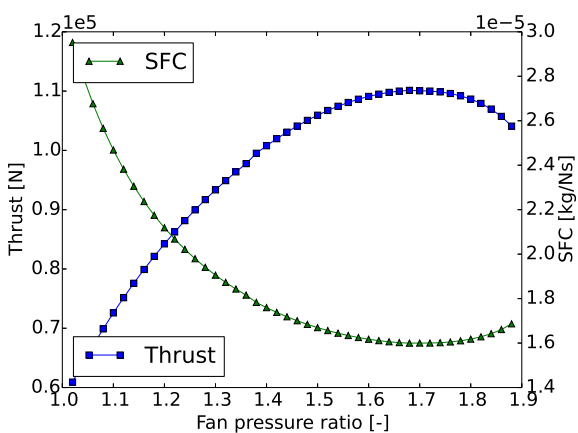


Figure 8.29: Fan pressure ratio sizing

discussed^{14 15 16}[57]. Furthermore, the engine performance is analysed in off-design conditions to verify whether it can cope with the most constraining climb phases and obtain an estimation of the fuel consumption in the main cruise phases. The engine is found to be powerful enough for the critical climb phases – the results are shown in Table 8.11. It should be noted that T04 is the turbine inlet temperature and that temperatures above 1450K are not sustained for long times. In addition, an ambient temperature of 20K above the standard atmosphere value was used under 15 km altitude, a choice explained in Section 8.4.3. Finally, it should be noted that the results can be considered as installed thrust since power is taken from the engines for other subsystems, an inlet and nozzle efficiencies of less than 1 are used, and bleeds as well as ram drag are included¹⁷.

Table 8.11: Off-design engine performance

Flight Phase	h [m]	M [-]	T04 [K]	Thrust [kN]	SFC [kg/Ns]	\dot{m}_f [kg/s]	$\dot{m}_{f,suave}$ [kg/s]
Take-off	0	0.347	1600	275.00	1.367E-05	3.758	3.75
Climb	11000	0.712	1492	101.00	1.553E-05	1.568	1.55
Cruise outgoing	13140	0.647	1202	25.00	1.790E-05	0.448	0.325
Climb	17000	0.712	1700	64.89	1.605E-05	1.041	1.1
Cruise 1	18500	0.712	1346	25.74	1.558E-05	0.401	0.46
Climb	18500	0.712	1357	27.02	1.547E-05	0.418	0.46
Cruise 2	19000	0.712	1345	23.37	1.565E-05	0.366	0.375
Climb	19000	0.712	1376	26.53	1.541E-05	0.409	0.41
Cruise 3	19500	0.712	1330	19.99	1.588E-05	0.317	0.325
Descend	14200	0.68	1143	5.00	3.407E-05	0.171	0.075
Cruise emergency	11000	0.5	1019	14.50	2.071E-05	0.300	0.2

Compressor stall is a risk in high altitude operations and might not be recoverable, it should therefore be avoided at all times [50]. This issue is analysed with compressor maps generated with the gas turbine software GSP. It should be noted that each component has its distinct map, and the available maps with GSP are very limited. The maps are therefore used as generic maps to assess the feasibility of the engine; better results can be obtained with a more extensive map catalogue, since more suitable components can then be chosen. As a brief description, PR means pressure ratio of the compressor, W_c is the mass flow, N_c is the rotational speed with respect to the nominal speed, and η is the efficiency of the compressor. The red line, with highest PR-values, is the surge line and indicates the limit beyond which stall occurs. The performance of the compressors is analysed for the flight phases included in Table 8.11, and plotted on the maps, see Figs. 8.30 to 8.33.

As can be seen in Figs. 8.30 to 8.32, the fan and the LPC seem to operate far from their most efficient region, and the fan even crosses the surge line for the most critical climb phase at 17 km altitude. Since the LPC component used in the calculations is clearly not suitable (although feasible) for the mission, it is considered

¹⁷ URL http://maelabs.ucsd.edu/mae155/07A2_engine-select%5B1%5D.pdf [Accessed 17/06/16]

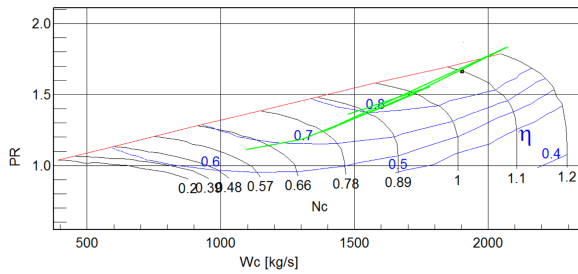


Figure 8.30: Fan side map

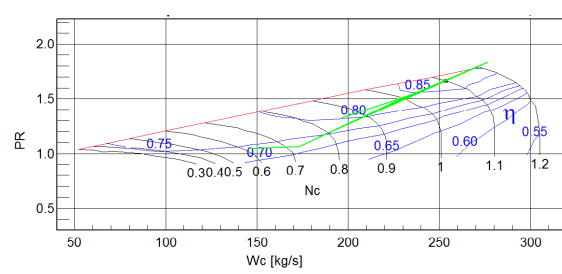


Figure 8.31: Fan core map

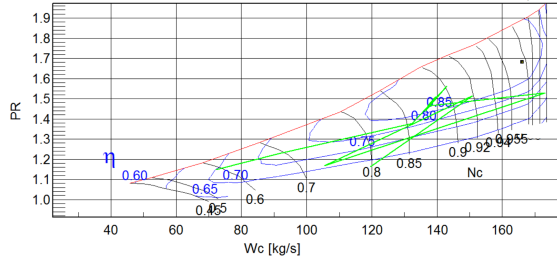


Figure 8.32: LPC map

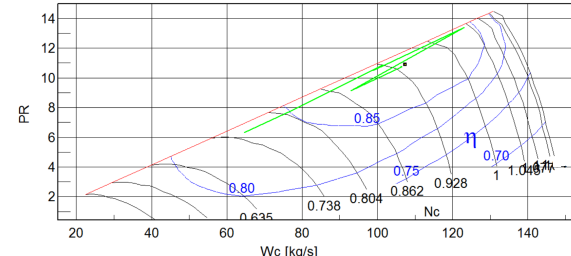


Figure 8.33: HPC map

that a better map is needed before drawing a conclusion on the fan feasibility for this specific flight phase. The maps suggest that the fan and LPC should be designed carefully and that the addition of a gearbox to separate the rotating speeds of the fan and the LPC should be considered. This would allow each component to operate at their own optimum speed and obtain a better efficiency overall. This would also allow the LPC to operate at higher pressure ratios, leading to an increase of surge margin for the HPC. The gearbox for turbofans has already been introduced in new commercial engines and could therefore be implemented to allow the engine to operate more efficiently and reduce the risk of compressor stall, as well as provide a number of other benefits¹⁸. Tables 8.12 and 8.13 summarize the main engine specifications and assumptions.

Table 8.12: Engine main assumptions

Parameter	Value	Unit
R	287.03	J/kg K
LHV_{fuel}	43000000	J/kg
κ_{air}	1.4	J/kg K
κ_{gas}	1.33	J/kg K
$c_{p,air}$	1000	J/kg K
$c_{p,gas}$	1150	J/kg K
PR_{intake}	0.99	-
$PR_{combustionchamber}$	0.96	-
η_{inlet}	0.99	-
$\eta_{compressor}$	0.89	-
η_{fan}	0.86	-
$\eta_{combustionchamber}$	0.995	-
$\eta_{mechanical}$	0.99	-
$\eta_{turbine}$	0.91	-
η_{nozzle}	0.99	-
T04 (max cruise)	1450	K
T04 (max take-off)	1700	K

Table 8.13: Engine specifications

Parameter	Value	Unit
Number of engines	4	-
Engine inlet diameter	3.5	m
Bypass ratio	7.5	-
Fan PR	1.68	-
LPC PR	1.68	-
HPC PR	10.63	-
OPR	30	-
Thrust at 20 km	27.5	kN
SFC at 20 km	1.6e-5	kg/Ns
Estimated mass	9	tons

To conclude this section, a number of additional recommendations are made for future work on the engine design. First, thrust augmentation by injecting the aerosol in the engine was briefly considered in the present analysis. However, the insignificant mass flow of the aerosol with respect to the air mass flow resulted in less than 1% extra thrust. Due to the complexity of injecting the aerosol properly in the engine, the increased

¹⁸ URL <http://www.purepowerengines.com/about.htm> [Accessed 18/06/16]

maintenance efforts that would be needed, and the low thrust increase, it is suggested not to analyse this option further unless resources are available.

Second, the engine weight is estimated to be 9,000 kg, based on the GE90 which weighs around 8,000 kg¹⁴. This estimation takes into account the larger diameter, the lower pressure ratio resulting in lighter components and the absence of thrust reversers. Since simple engine weight prediction methods were found to be highly inaccurate and give disparate results, it is recommended to revise the weight prediction when components start to be defined. A good overview of weight estimation methods can be found in a presentation from Cranfield University¹⁹.

Third, engine technology can be expected to keep improving over the coming years and more specifically, higher turbine entry temperatures of 1550K could be obtained by 2020, based on [49]. This potentially allows to reduce the engine size and the specific fuel consumption. It is therefore suggested to keep up to date with new improvements since new technology enhances efficiency and reduces emissions [49]. NOx reduction is particularly important for SAGA since NOx emissions are known to be damaging for the ozone layer, which has its maximum concentration at 20-25 km altitude [58, 59].

Fourth, the conventional aviation fuel Jet A-1 is used in all calculations, however it was found that some issues with this fuel could arise due to the very low pressure at high altitudes [8]. Evaporation was analysed analytically and the result indicated that the risk of evaporation is low. Since the uncertainty remains, it is recommended to further analyse this potential issue in future research. At this stage, it is proposed to consider an alternative fuel with low volatility, JP-7. This fuel was used by the U-2, has the same mass density and a higher lower heating value compared to Jet A-1²⁰. The latter means that more energy can be extracted from the same mass of fuel, which is beneficial. On the other hand, the JP-7 fuel is likely to be more expensive and needs a special compound to be ignited. This compound, the triethylborane, would require special handling since it is toxic and spontaneously ignites when in contact with air [60, 61].

Finally, it is important to consider the effects of higher concentrations of H₂SO₄ on the engines since SAGA will be spreading sulfuric acid in the stratosphere. It is important to note that engines already spread sulfur components due to the small sulfur content in the fuel [8]. This amount of sulfur content is regulated and cannot exceed 0.3% weight [8, 62]. It is known that clouds of ash and acid gases from volcanic activity can damage aircraft, including windows, paint and engines [63]. An increase of windows crazing was associated to sulfuric acid aerosol injected by the El Chichon volcano in its 1982 eruption, resulting in large increases in window replacement rates [64]. Volcanic eruptions have also caused engine failures and engine replacements, due to ash deposits in the engine that block airflow in the engines or block cooling holes [63]. Also, the fan and compressor blades are likely to be damaged by abrasion [8, 63]. However, these studies focus on volcanic eruption effects, and the conditions do not exactly correspond to the cruise conditions that SAGA would operate in.

Aurora Flight Sciences estimated that the concentrations of sulfuric acid would amount 0.01ppm, which they consider to be negligible compared to sulfate concentrations in polluted areas [8]. This is in line with results found by [65]. Despite the fact that sulfuric acid concentrations would be relatively small at cruise altitude, the long operating time of the aircraft in those conditions might damage the engine materials in the long term. Qualitatively, this means that inspection and maintenance of the engines are of utmost importance for SAGA and will have to be performed more frequently than for conventional aircraft. Also, an engine monitoring system will be installed to perform the maintenance activities more efficiently. Quantitatively, further investigation is needed to obtain more accurate estimations on sulfuric acid concentrations and on engine failure rate increase due to the aerosol influence.

8.4.3 Verification and validation

The performance of the engine in design conditions was verified with the gas turbine software GSP, which is used at NLR. The thrust, fuel mass flow, and specific fuel consumption were all found to be within a 2% accuracy. The level of confidence in the solution is therefore high. Off-design results were verified by comparing fuel consumption values from GSP and SUAVE. The numbers were found to be similar in high altitude flight as can be seen in Table 8.11, however the discrepancy increases at lower altitudes. This suggest that SUAVE underestimates the fuel consumption at low altitudes and overestimates it at high altitudes because its estimation is based on a scaling method. Overall, the results are reasonable and are within reasonable

¹⁹ URL http://www.sawe.org/files/Weight_SAWE.pdf [Accessed 18/06/16]

²⁰ URL <https://www.wbdg.org/ccb/FEDMIL/dtl138219d.pdf> [Accessed 18/06/16]

bounds. Nevertheless, the risk of excessive fuel consumption is present, although it should be noted that off-design calculations depend on the compressor maps. More appropriate maps would therefore likely reduce fuel consumption and better support the fuel budget estimated by SUAVE. The compressor maps were inspected by an academic of the Power and Propulsion department at the Delft University of Technology, and it is suggested to further verify them with data from similar cases during the detailed phase of the components. Validation of the results is not feasible within the scope of this analysis, since it would require more information on existing engines than is publicly available to be able to perform meaningful comparisons. Another option would be to use an already verified and validated CFD tool to estimate the engine performance.

8.4.4 Sensitivity analysis

This section aims to investigate other trends relevant for engine design which were not addressed before. The insights they provide are implicitly used to ensure the accuracy of results obtained before.

Fig. 8.34 shows the significant effect of temperature on the engine. The engine thrust was analysed under the International Standard Atmosphere (ISA) and the ISA+20 (20K higher than standard temperature), thus with lower air density. Engine performance can be very negatively influenced by high temperatures, mostly at temperatures below 16 km, therefore temperature is a crucial parameter to consider. It is worth noting that above 15 km altitude temperatures tend to be even lower than predicted by ISA in the tropics²¹ [66], hence ISA values are always used above 15 km for conservativeness.

In a similar way, Fig. 8.35 confirms that the engine is very sensitive to air mass flow. Increasing the inlet diameter is therefore a very simple and effective way to increase thrust. By varying the engine diameter from 2 to 3.5 m, the thrust is increased by about four times. Another trend which can be observed is the decreasing thrust with increasing bypass ratio for a given engine diameter. This is consistent with results found in Fig. 8.26.

Finally, Figs. 8.36 and 8.37 show how the bypass ratio affects thrust and SFC with altitude. As Fig. 8.36 illustrates, the thrust decrease with altitude does not appear to depend on the bypass ratio in this case. In addition, the thrust decreases at a lower rate at 20 km than it does at 11 km. Fig. 8.37 shows that for each altitude, there is an optimum bypass ratio where the specific fuel consumption is minimised. This optimum decreases with increasing altitude.

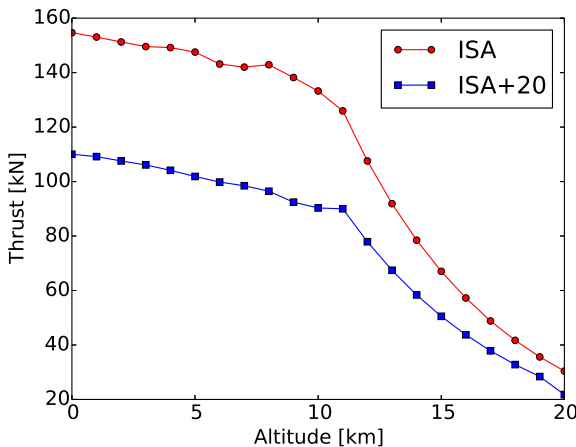


Figure 8.34: Thrust variation with temperature

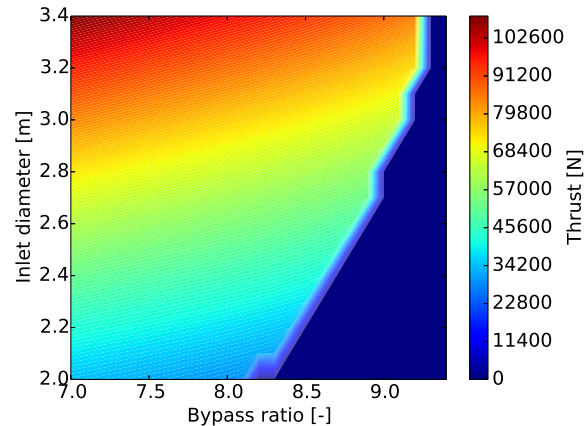


Figure 8.35: Thrust variation with inlet size and bypass ratio

8.5 Structures and materials

In order to cope with all the external loads acting on the aircraft, a sufficiently strong and stiff structure is designed. The major challenge is to provide structural integrity in all design load conditions while reducing the structural weight to a minimum. The most weight efficient design is obtained by an iterative process, varying design parameters such as aspect ratio and wing thickness, comparing a conventional wing to a strut-braced wing and varying the wing box material. Since the wing is by far the highest risk component of the aircraft

²¹Personal communication P. Siegmund, Royal Netherlands Meteorological Institute, De Bilt, Netherlands

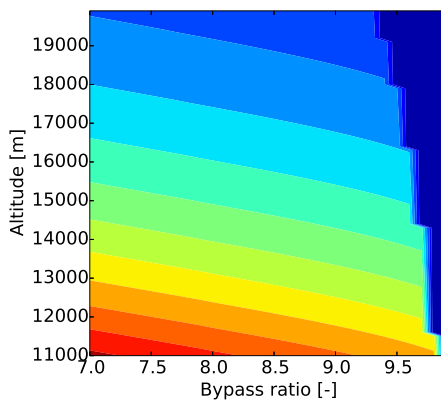


Figure 8.36: Thrust variation with bypass ratio and altitude

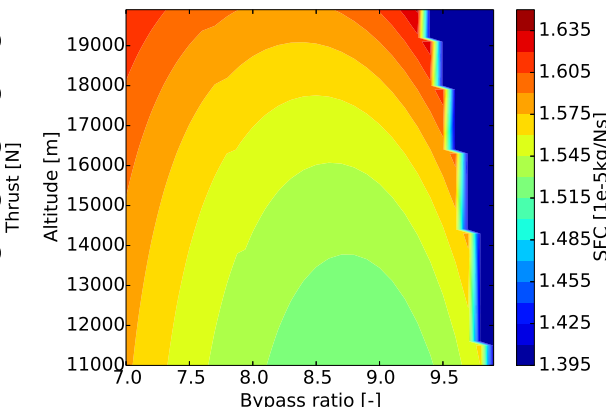


Figure 8.37: SFC variation with bypass ratio and altitude

structure due to the high required aspect ratio, it is analysed thoroughly. The fuselage is non pressurised and the tail is very conventional, therefore the risk related to these components is low and their structures are not analysed in detail. This chapter presents the results of the structural analysis and preliminary structural design of the SAGA wing box, along with the main design drivers, relevant trade-offs and sensitivity analysis.

The results of the design process and the main design drivers are discussed in Section 8.5.1. Next, verification and validation of the wing box model is clarified in Section 8.5.2.

8.5.1 Design choices

During the design process the main driving factors are determined and their influence on the design is investigated. This section describes how for every driving factor a design choice is made in order to ensure the optimal result.

Strut-braced concept

Adding a strut to support the wing structure results in a lighter wing that is still able to cope with the same loads. A disadvantage of struts is an increase in profile drag and interference drag due to strut-wing interference. This effect is however minimised by giving the strut an aerodynamic shape, as explained in Section 8.3. According to [67], the critical loading for struttled wings is compressive buckling. It is chosen to apply a telescopic strut with a damping mechanism, which only engage when a positive load factor is applied [67]. When loaded in tension (in-flight), the strut will take some of the loads of the wing. When loaded in compression, the telescopic structure will retract and no loads will be transferred, requiring strut design for tensile loading only, significantly reducing the structural weight. Next to that, static pull up puts the most stress on the fuselage, see Fig. 8.44, and therefore a tension only strut will already provide a significant weight reduction.

Total struttled wing weight and weight for a wing without struts are plotted against aspect ratio in Fig. 8.38 for both chosen wing box materials. A wing box mass, including wing skin, of 28.2 tons can be obtained using composites for the wing (Boron fibre laminate with epoxy resin), as presented in Table 8.14. As can be seen in Fig. 8.38, strut benefit increases with aspect ratio, especially for composites. For low aspect ratio's struts still provide a significant weight decrease for aluminium wings, but the benefit is lost for composite wings. Their high stiffness makes it difficult to design a suitable strut. Strut material is AL7075 T6, which is chosen for its high yield strength and TRL, although strut material has to be investigated in more detail in further design stages. For aerodynamic reasons an aspect ratio of 13 was chosen (cf. Section 8.2). The reduction in weight when using struts is related to the shear and bending relief provided by the strut force, as shown in Fig. 8.44 and Fig. 8.45, respectively.

Table 8.14: Wing weight with and without struts for composite and aluminium (AR=13)

Material	Unsupported wing weight [tons]	Strut braced wing weight (including strut) [tons]
Aluminium	39.4	32.7
Composite	33.5	27.6

In order to perform optimal sizing of the strut, an algorithm was developed to determine the ideal spanwise

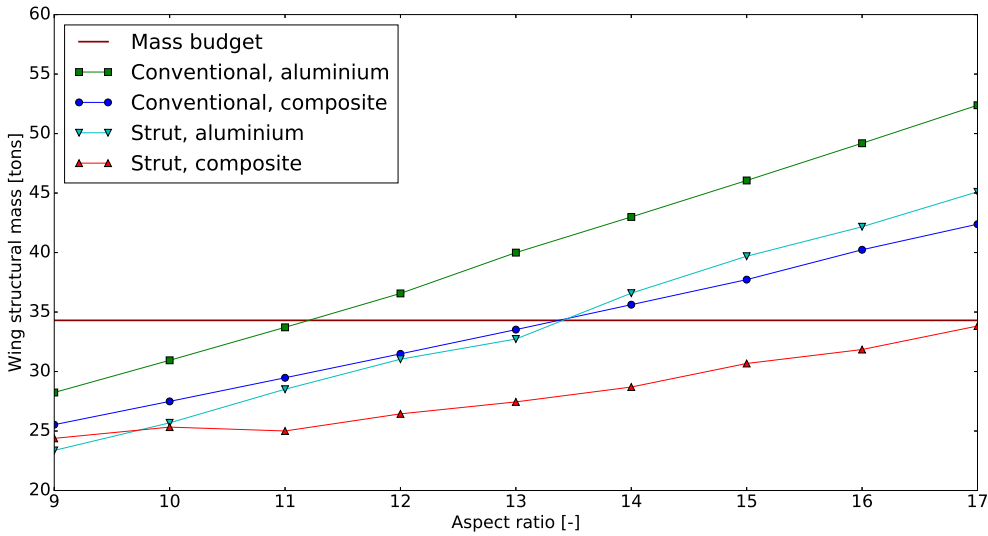


Figure 8.38: Total wing structural mass versus aspect ratio for unsupported and strut braced wings for both the chosen boron fibre laminate composite and aluminium

strut-wing attachment point and cross-sectional strut area. The strut is sized such that it yields when the ultimate load is reached ($n = 3.75$). It is attached at the shear center of the wing and to the engine pylon, and extends towards the bottom of the fuselage, parallel to the wing leading edge. The bottom of the fuselage is chosen as the first attachment point to ensure a maximal angle between the strut and the wing, in order to maximise the vertical component of the strut force. Strut and engine location are forced to coincide to ensure the strut is not attached to the wing directly, thus minimising interference drag. The strut module flow diagram can be found in Fig. 8.39.

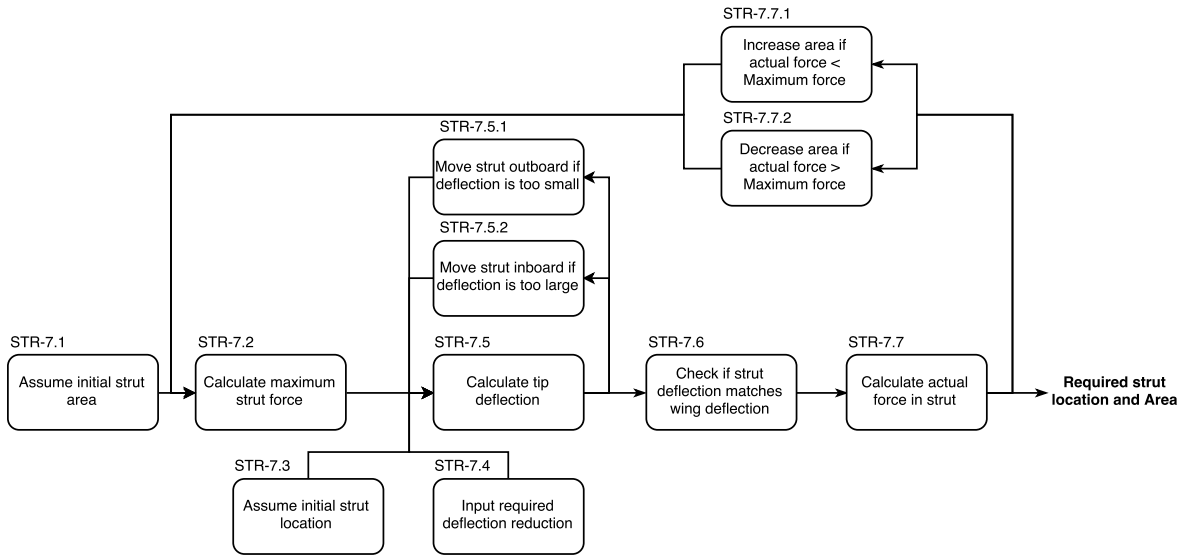


Figure 8.39: Algorithm of the strut sizing

In the analysis, the wing is assumed to be clamped to the fuselage. Since the strut is loaded axially, the force can be decomposed into a horizontal and vertical component acting on the wing, making it impossible to superimpose the deflections [68]. The non-linear structure is solved using Euler-Bernoulli beam theory, given by Equation (8.15). Using tailored Matlab software, a solution for the above equation was found and interfaced with the main Python program [69]. Using an average EI for the entire wing is not accurate, as the tip and root values differ more than 10%. Therefore, the wing was divided into sections where EI does not vary more than 10%, which were modelled as clamped beams with a stiffness equal to the average EI of the

appropriate section. Firstly, all reaction shear forces and bending moments at all clamps are calculated by moving from the tip to the root. Secondly, these reaction forces and moments are applied to the tip of the appropriate inboard beams by moving from the wing root to the wing tip. Slope and deflection boundary conditions are matched as well in order to determine the slope and deflection of the entire wing.

$$EI \frac{d^4 w}{dy^4} + P \frac{d^2 w}{dy^2} = q(y) \quad (8.15)$$

Even though the above loading case greatly increases the complexity of the calculations, it is decided not to ignore the axial load as the following effects are considered significant. The axial force increases when the strut is moved outboard, and this increases the internal bending moment between the strut attachment point and root of the wing. Therefore, outboard strut placement slightly increases the structural weight of the inboard wing compared to the non axial case. Next to that, ignoring the axial force allows the strut to be attached much closer to the tip, as the wing will not buckle as fast. Therefore the absolute value of the shear force will be higher for most of the semispan, and bending moment will in general be lower. Therefore wing weight will be overestimated (29 tons without axial force and 27.6 tons with axial force included), and an inaccurate wing box mass distribution will be obtained. This effect can be seen in Fig. 8.40 and Fig. 8.41 for shear and moment respectively.

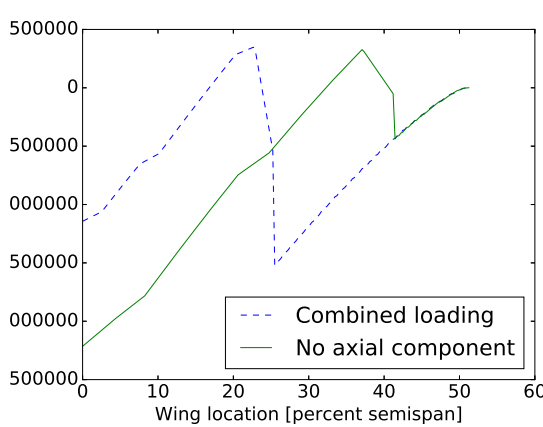


Figure 8.40: Internal shear force with and without axial force

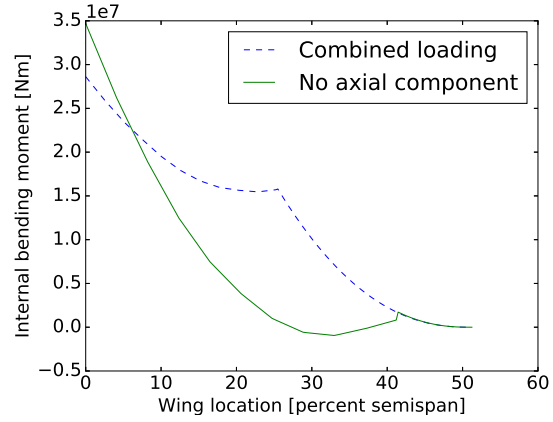


Figure 8.41: Internal bending moment with and without axial force

The force that has to be carried by the strut is always the same for a certain strut cross-sectional area, as it equals the force for yielding, but the spanwise strut attachment point is changed to ensure the tip deflection is within a prescribed limit, see Fig. 8.39. Once this tip deflection requirement is met, the challenge that arises is matching the strut elongation and wing deflection due to the applied force. This is done by increasing or decreasing the strut cross-sectional area accordingly, but this changes the strut yield force, and therefore the wing deflection and strut elongation. Therefore the program is iterated until deflection and elongation match for a certain strut area and location. When the limit on tip deflection is increased and the strut attachment point moves outboard, the wing will eventually buckle due to the axial force becoming too high. Total structural weight decreases until this point is reached though, and therefore that buckling point corresponds to the optimal strut attachment point, as can be seen in Fig. 8.42. For an aspect ratio of 13 and a composite wing, the optimal strut location is 46% semispan, which corresponds to a deflection reduction of 47 percent, a strut area of 0.0185 m², a strut length of 19.9m and a strut weight of 1.26 tons (per wing).

Aspect ratio

The fields of structures and aerodynamics generally lead to opposing ideal design solutions, and a dominant conflict arises when aspect ratio is considered. For aerodynamic reasons a large aspect ratio is preferred, however, structurally this is not always feasible, as it increases the bending and shear stresses in the wing and the wing deflection, resulting in a larger wing weight due to higher required stiffness.

An aspect ratio of 13 is chosen for the wing. This is the lower limit which still allows a sufficient reduction in induced drag, whilst keeping the structural wing weight within the weight budget (see Section 8.2). The benefit of reducing aspect ratio in order to decrease wing box weight is illustrated in Fig. 8.38.

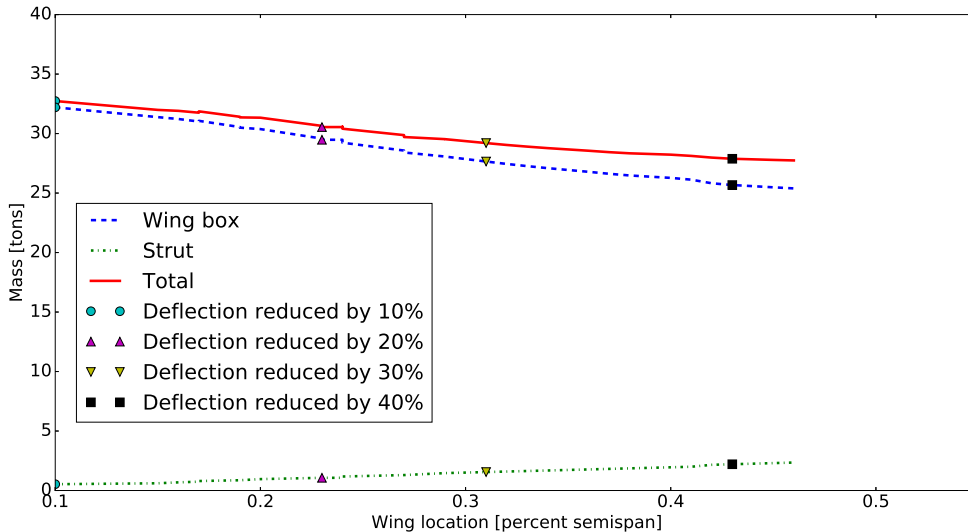


Figure 8.42: Wing box, strut and total masses in relation to spanwise strut attachment point location and tip deflection limit for AR=13 (Composite)

Table 8.15: Limit loads

In flight						
Flight phase	Maneuvering n [-]		Gust n [-]		Fuel weight [kg]	Payload weight [kg]
Start outgoing cruise	2.5		-1.0		2.47 -0.47	49,760 35,000
End outgoing cruise	2.5		-1.0		2.48 -0.48	28,400 35,000
Start dispersion phase	2.5		-1.0		2.27 -0.27	28,400 35,000
End dispersion phase	2.5		-1.0		2.31 -0.31	3,390 0
On ground						
Ground phase	n [-]		Fuel weight [kg]		Payload weight [kg]	
Landing (MLW)	1.3		11,700		35,000	
Taxi bump (MTOW)	1.3		53,000		35,000	

Load cases

The wing box structure is designed such that it can withstand any load it might experience during its lifetime, for which the most critical load cases during flight, landing and take-off were determined. These are summarised in Table 8.15.

The critical loads in flight are the $n=2.5g$ and $n=-1.0g$ static manoeuvring limit loads, extracted from CS25 regulations, which are larger than gust loads encountered during any phase of the flight. The static pull-up load of $2.5g$ is critical when wing inertia relief is the lowest, e.g. at the maximum zero fuel weight. This critical case occurs at the end of dispersion, when all aerosol is sprayed and fuel mass is low. The corresponding loading diagram is presented in Fig. 8.43. The $-1.0g$ loadcase is critical at the start of outgoing cruise, when wing inertia is highest. Landing puts most stress on the structure when the aircraft is at its maximum landing weight, while the taxi bump load case can occur when the aircraft is fully loaded (MTOW). Since load factors are the same for landing and taxi bump, taxi bump is more critical due to the higher fuel weight.

The limit loads are complied with by sizing the wing box for ultimate loadfactors of 3.75 and -1.5 - safety factors of 1.5 are applied, and a taxi bump load of $1.3g$ (taxi bump) . Sizing is an iterative process, which is presented schematically in Fig. 8.46. Loads included are lift, structural weight (wing, fuselage), fuel and payload weight, engine weight and thrust, and strut weight and load. The shear and moment envelopes for both the unsupported and strut-braced wing are shown in Fig. 8.44 and Fig. 8.45 respectively, and these are the loads the wingbox is sized for.

Deflections during static pull up, $-1.5g$ and taxi bump are calculated to ensure aerodynamic performance, stability and control is within acceptable bounds. Also, it is ensured the wing tips and/or engines displacement never exceed the ground clearance limit.

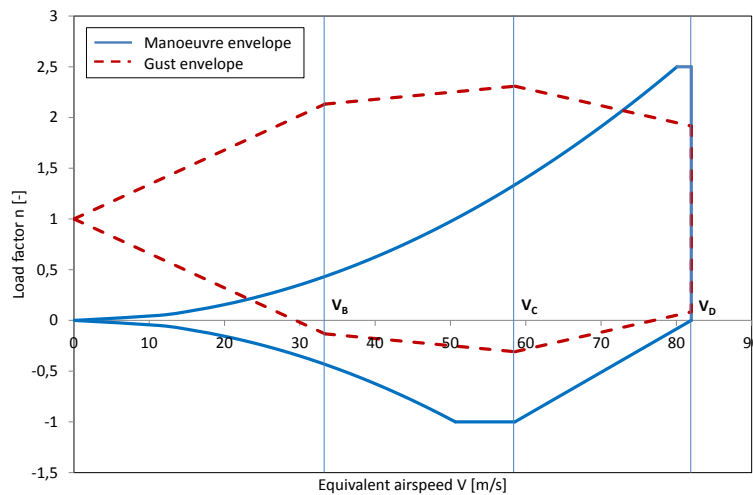


Figure 8.43: Most critical loading diagram (19.5km altitude, end of dispersion phase)

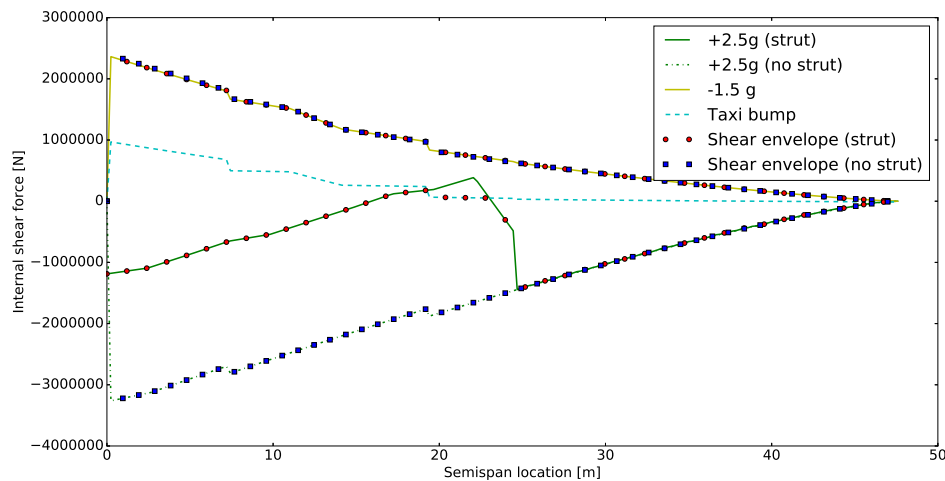


Figure 8.44: Shear envelope (AR=13, Composite)

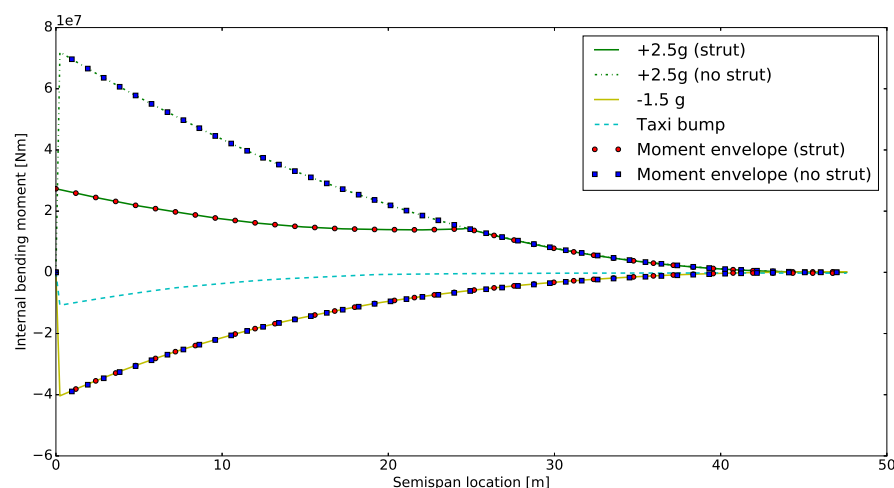


Figure 8.45: Moment envelope (AR=13, Composite)

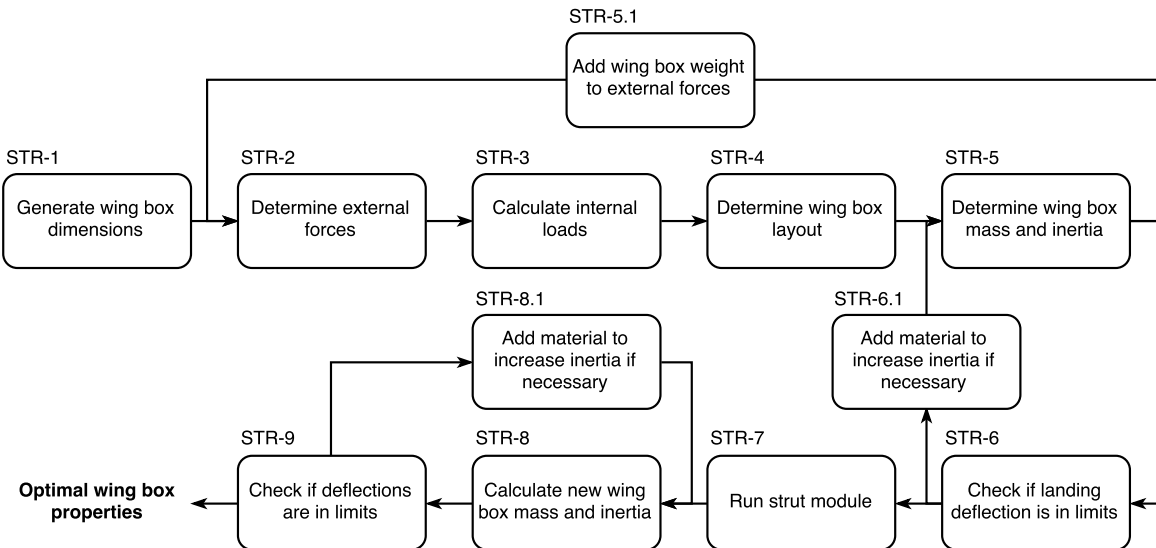


Figure 8.46: Flowchart of the wing box sizing program

Wing thickness

Another conflict between structures and aerodynamics arises for airfoil thickness. In order to postpone drag divergence, thin airfoils (small thickness-to-chord ratio) are preferred, but these greatly reduce the wing moment of inertia. Since the moment of inertia decreases quadratically with airfoil thickness decrease (Steiner term), the increase in bending moment stress due to a decrease in I_x is a significant issue.

Three airfoils are considered: the SC3 airfoil, the SC20714 airfoil and the NLR7301 airfoil with a maximum t/c of 0.12, 0.14 and 0.17 respectively. The SC20714 is selected, as it provides sufficient stiffness while also generating a sufficiently high C_L . This tradeoff is treated in more detail in Section 8.3. The SC20714 was the optimal solution when structural weight and fuel weight due to drag were considered.

Wing box layout

As the high aspect ratio and the wing weight resulting from this aspect ratio are crucial aspects for this specific mission, it is important to investigate structural methods to achieve an acceptable wing weight. In order to investigate if a range of possible aspect ratios for this mission is feasible from a structures point of view, it is decided to size an actual wingbox, optimising for wing weight while achieving an acceptable wing deflection.

The stiffeners are modelled as C-beams with variable width, height and thickness. The thickness of the stiffeners is taken to be same for the webs and flanges. Similarly, the spars are modelled as I-beams with the same variables as the stiffeners. The thickness of the webs and the flanges of the spars is optimised separately. The ribs are modelled as flat plates.

The method sizes the amount or geometry of different parts of the wingbox for different specific failure modes. The flange thickness of the spars is sized for the stress at which the spars yield in tension. The thickness of the spar web is sized for the critical stress at which the spar webs buckle due to shear. The number of stiffeners on the upper side of the wingbox is determined by the buckling of the upper skin during the maximum load case during flight. For buckling of the lower skin the landing case and the negative maximum load case during flight are evaluated. The critical buckling stress determines the amount of stiffeners on the lower side of the wingbox. The skin thickness is sized both for shear stress caused by torsion and for the yield stress. The number of ribs is determined by the critical force at which the stiffeners buckle. Finally, the stress introduced by the engines at maximum thrust is used to size the width of the spars.

Tank position

Since fuel and aerosol provide relief during bending, the tanks are positioned in such a way that the internal loads decrease during the critical load cases. Since the wing is sized for n=3.75 when there is almost no fuel left in the tanks (see Table 8.15), tank position will not have a noticeable influence on that loadcase. Taxi bump and the n=-1.5 loadcase do depend heavily on fuel mass. In Fig. 8.47 it can be seen that deflections

during taxi bump and the negative loadcase increase significantly, while the deflection during static pull up is almost unchanged. Next to that, total wing structural mass increases from 27.6 tons to 29.3 tons (composite, strut) when the fuel tank is moved from the root to the tip. Therefore, the fuel tank is placed at the root.

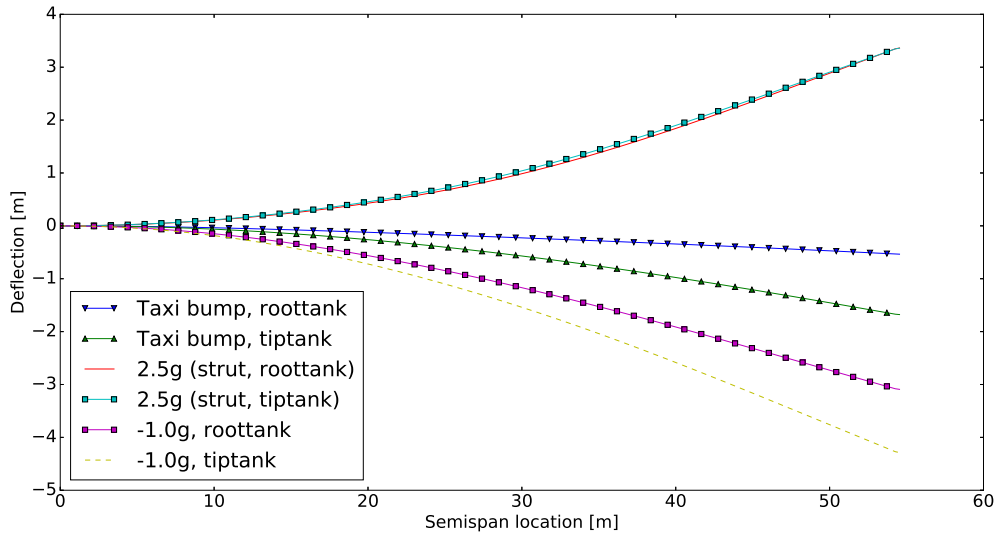


Figure 8.47: Deflections during the critical load cases for both the fuel tank at the tip and the root

8.5.2 Verification and validation

Verification of the moment and shear diagrams, wing slope and deflection is done by comparing the results of the Python program with the results obtained with existing Matlab software [69]. For the conventional wing model, a clamped cantilever beam, a 0% deviation is obtained. The struttured wing model (multiple cantilever beams linked by corresponding boundary conditions) is verified by taking the same EI for every beam and comparing the deflection to a single cantilever beam model with that EI. Again a 0% offset is observed, verifying that all boundary conditions are implemented correctly. Wing box mass is verified by comparing the detailed wing box layout weight to a simplified wing box weight. The latter is calculated assuming a box consisting of two skin panels and two webs, sized to exactly withstand shear, moment and bending stresses, but buckling is not accounted for. Verification of the struttured wing weight is done by ignoring the axial component of the strut force and by using the Python script instead of the MATLAB dedicated combined loading software.

Strut braced wing weight is validated by applying the 15% weight reduction factor predicted by Raymer [18] to the unsupported wing weight and comparing it to the actual calculated weight. This returns a predicted value of 28.5 tons and an actual value of 27.6 tons, which only differ 3.2 percent. Next to that, weight decrease obtained by going from aluminium to composite is 16 percent (both for strut and conventional), which is close to the 20% predicted by Torenbeek [13]. The cause of this difference is the heavy composite that was used (see Section 8.5.3) in order to increase the shear modulus and therefore the torsional rigidity of the wing. Validation with FEM can be done in later design stages, and will yield validation data which is more reliable than the current initial statistical estimates.

8.5.3 Material characteristics

The aircraft industry has been using more and more composites to this day. Also for the SAGA mission, these extremely strong, lightweight materials are beneficial. In this section, the design choices and material selection for the wing box of the main wing are discussed. Also the selection of other aircraft materials is briefly touched. Afterwards, a sensitivity analysis on the composite wing box will follow.

Design choices

Since the high aspect ratio wing requires large bending stiffness, a material with a high E-modulus is used. A trade-off is performed between two fibre composites: an unidirectional high E-modulus carbon fibre (HMCF) laminate²² and an unidirectional boron fibre laminate²³, both with epoxy resin. In both cases the fibre volume is equal to 60%.

The desired properties of these materials can be determined by stacking them in a certain order. For each material, the driving requirement is an axial E-modulus of 110 GPa. The boron fibre proves to be the best solution, since it can provide both a sufficient E-modulus and a high shear modulus, required for aeroelasticity reasons as explained in the sensitivity analysis later in this section. The boron composite requires a stacking sequence of 12 plies in total:

$$[0/45/-45/0/90/0]s$$

where the s indicates the symmetry axis of the laminate, after which the same sequence is mirrored. These three angles are sufficient to obtain quasi-isotropic properties for the material, but other ply angles and stacking sequences can be investigated in the detailed design phase of SAGA to obtain an even better combination of E-modulus and shear modulus.

A drawback of the boron fibre is its high density compared to other composites (2 g/cc compared to 1.57 g/cc for HMCF). However, the weight saving compared to aluminium (2.81 g/cc) is still significant. The properties of the boron fibre laminate are shown in Table 8.16 and were calculated using the Hart-Smith 10% rule discussed in [70]. A safety factor of 2.4 was applied to the failure strain of the composite, taking into account material variability, environmental effects and damage [71]. The resulting strength is used to size the wingbox.

Table 8.16: Directional properties of the composites

Property	Unit	Boron laminate
Tensile E-modulus axial	GPa	110.0
Tensile E-modulus transverse	GPa	50.0
Yield tensile strength axial	MPa	660.0
Yield tensile strength transverse	MPa	300.0
Yield compressive strength axial	MPa	495.0
Yield compressive strength transverse	MPa	225.0
Shear Modulus	GPa	21.2
Poisson ratio	—	0.23
Density	g/cc	2.00

An issue with the use of composites is temperature. If the temperature changes, the material properties change drastically. During flight, the aerosol tank radiates heat as the aerosol is stored at high temperature and evaporated at even higher temperatures. Elevated temperatures higher than 500 K may occur, so a coating or heat treatment will be applied to the composite wingbox. One of the many commercially available solutions is a HI-TEMP 1027 coating from the company PPG²⁴. This coating proves to be able to withstand temperatures up to 900 K.

Another critical part of the aircraft is the aerosol tank inside the wing. In order to prevent failure of the tank by impact from external objects (e.g. bird strikes), the leading edge of the wing will be sized accordingly. Composite materials cannot be used due to their brittleness and low impact resistance²⁵. According to [72],

²² URL http://www.hexcel.com/Resources/DataSheets/Prepreg-Data-Sheets/8552_eu.pdf [Accessed 13/06/2016]

²³ URL http://www.performance-composites.com/carbonfibre/mechanicalproperties_2.asp [Accessed 13/06/2016]

²⁴ URL <https://docs.td.ppgpmc.com/download/11565/22903/Leaflet-PPG-HI-TEMP-1027%2E2%84%A2-> [Accessed 14/06/2016]

²⁵ URL <http://machinedesign.com/materials/basics-aerospace-materials-aluminum-and-composites> [Accessed 17/06/2016]

a bird of 4 lb (1.81 kg) impacting the structure at 261 kts (134.27 m/s) requires a leading edge skin thickness of 2 mm. The material used for the simulation is an aluminium 2014-T6 alloy. Since the SAGA aircraft will fly with a lower speed in the take-off regime (91.9 m/s), the thickness of 2 mm is considered sufficient to prevent failure.

Composites are weak electrical conductors, which may be critical if lightning strike occurs. Commercial solutions exist in the form of a metal foil that is to be applied on top of the composite skin to redirect the electrical charge²⁶. Currents up until 200,000 amps can be conducted using metal foils. If tests show the aluminium skin cannot handle the required level of electrical current, a metal foil can be implemented.

The fuselage does not require pressurisation since the aircraft is unmanned. No pressurisation results in smaller stresses in the fuselage skin compared to commercial aircraft, and hence in a lower required stiffness. Assessing other similar aircraft designs suggests that an aluminium fuselage structure is the most suitable and feasible design option^{27 28}. Moreover, aluminium is not affected by the concentration of sulfuric acid when it flies through an aerosol cloud as aluminium corrosion rate is very low for concentrations up to 40% [73]. Since the actual sulfuric acid concentration in the diffused clouds is significantly smaller, this will not cause any problems. Aluminium alloys are widely used in the aircraft industry, and they can be properly reused and recycled after the end-of-life of the aircraft, which contributes to the sustainability of the design. This is also elaborated upon in Chapter 14.

Stress analyses of the fuselage are not within the scope of the project at this point. The use of other fuselage materials might be required if the analyses dictate so.

Sensitivity analysis

As mentioned before, there is a dependence between E-modulus and shear modulus G. They both ought to be as high as possible to obtain a large bending stiffness for wing deflection and a large torsional rigidity for aeroelastic reasons. E and G are however inversely proportional, and to obtain a large increase in G, the E-modulus has to be decreased significantly. In Fig. 8.48, the relationship between G and E is plotted for an increasing number of plies in 0° direction. As can be seen, the HMCF requires a very low E-modulus to obtain the same G of the boron fibre, which would be detrimental for the long, slender wingbox.

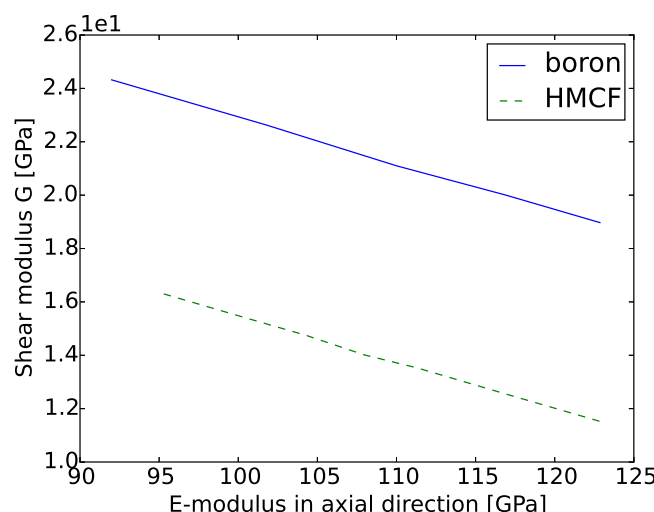


Figure 8.48: Shear modulus versus elastic modulus for HMCF and boron fibre composite

Knowledge about the fatigue behaviour of boron fibres is rather premature due to little long-term application experience with boron. In general, composites perform better in terms of fatigue than metal alloys. Their strength retention stays more constant over time, and their ultimate strength with increasing number of cycles is therefore better than for metals [74]. Fatigue life is included in the safety factor (damage) used to size

²⁶ URL <http://www.dexmet.com/docs/lightning-strike-protection-for-carbon-fiber-aircraft.pdf> [Accessed 17/06/2016]

²⁷ URL http://www.northropgrumman.com/capabilities/rq4block20globalhawk/documents/hale_factsheet.pdf [Accessed 16/06/2016]

²⁸ URL <http://www.dtic.mil/dtic/tr/fulltext/u2/a482086.pdf> [Accessed 16/06/2016]

the wingbox to ensure the requirement of 60,000 flight hours is verified. Nevertheless, there is a lot of uncertainty concerning this topic, and testing of dedicated specimens has to prove that the material can actually survive the mission lifetime. It should also be noted that if fatigue occurs, cracks that start to grow inside the composite structure are hard to detect. Appropriate non-destructive testing methods should be used during the maintenance program to ensure the detection of flaws in the material.

Also sustainability of boron fibres is still rather premature. Industry is currently developing processes to extract fibres from composite laminates and reuse them for other applications. Since it will take a substantial amount of time to build and implement the SAGA fleet, this research can be finalised. By the time the fleet will reach its end-of-life stage and retire, it can make use of these recycling strategies. The end-of-life of the fleet is further discussed in Chapter 14.

8.6 Aeroelasticity

The field of aeroelasticity studies the interaction between structural dynamics and unsteady aerodynamic flow over aircraft structures. Aeroelasticity is a complex and crucial factor in aircraft design and is known to be even more important in the design of high aspect ratio wings. High aspect ratio wings can only provide a limited amount of torsional stiffness in the outboard wing sections, increasing the probability of the occurrence of aeroelastic effects. It has to be assured that these phenomena occur at conditions outside of the flight envelope – according to CS25.629 the speed at which aeroelasticity becomes an issue should be equal to either $1.15 * V_C$ or the dive speed V_D , depending on which one is constraining, i.e. which one has the lowest value [75]. This has to be assured for all configurations and design conditions. Below this speed, the SAGA should provide a safe elastic deformation and no significant loss in stability should occur when approaching the flutter speed.

In this section, the designed wing is analysed for three hazardous phenomena: torsional divergence, control reversal and flutter. Torsional divergence occurs when the application of aerodynamic loads in flight tends continuously increase the deformation of the structure, thereby increasing the load further, eventually leading to failure of the wing. Control reversal refers to the situation where the control devices tend to become ineffective and/or create an opposite effect, making it very hard/impossible to steer the aircraft. Torsional divergence and control reversal are both analysed using simplified equations, which are known from experience to approximate reality well [76]. Next to that, an extensive dynamic flutter analysis is performed. Flutter is an aeroelastic dynamic instability, which is often considered to be the most dramatic aeroelastic phenomenon. When flutter occurs, the elastically deformed structure is extracting energy from the air flow around the wing, leading to sudden catastrophic structural failure. The analysis of flutter of an aircraft is difficult, as the complexity of the aerodynamic flow concerned with an aircraft flying far from its normal operating conditions is high. Convolved unsteady aerodynamics and energy concepts are required to understand and model the flutter phenomenon accurately, which has to be done for several phases of the flight, taking into account variations in fuel, payload, configuration and altitude. However, the aforementioned is beyond the scope of this project concerning the aimed level of detail, and a more simplistic analysis is performed. The results of this section are presented and elaborated on in Section 8.6.1. Verification and validation and a sensitivity analysis are discussed in Section 8.6.3 and Section 8.6.4, respectively.

8.6.1 Results

The results of the torsional divergence, control reversal and flutter analysis are presented in Table 8.17. All phenomena are investigated for the SAGA aircraft design for several phases of flight. In these flight phases, the effects of altitude and corresponding differences in aerodynamic properties are taken into account. The current analysis indicates that no aeroelastic problems occur within the flight envelope and that SAGA meets the certification requirements for the investigated flight phases. The methods used in the analyses, discrepancies between both methods and discrepancies between used models and actual design are elaborated on later.

8.6.2 Recommendations to handle aeroelastic problems

In order for an aircraft to be certified, the critical aeroelastic speed has to be sufficiently different from all speeds encountered in the flight envelope. As can be concluded from Table 8.17, this requirement is met. However, what becomes evident during the analysis, is the complexity of aeroelasticity and the challenges

Table 8.17: Aeroelastic speeds for the SAGA for different flight phases. Analytical solution analyses composite design with struts, NeoCASS uses a conventional aluminium design. (for explanation see Section 8.6.3)

	Certification	Divergence	Control reversal	Flutter (analytical)	Flutter (NeoCASS)
Take-off at sea level	137.5	228.4	245.7	185.3	187.4
Cruise at h = 13 km	267.4	450.4	484.5	364.6	496.9
Cruise at h = 18.5 km	294.1	638.5	686.9	516.0	727.3
Cruise at h = 19 km	294.1	660.2	710.1	533.9	628.5
Cruise at h = 19.5 km	294.1	683.5	735.3	553.8	598.0
Landing at sea level	77.34	228.4	245.7	185.3	152.9

and shortcomings of the used methods when computing these speeds. This leaves an uncertainty in the computed results. Therefore, several solutions are opted below to mitigate the risk of the occurrence of aeroelastic phenomena.

One of the most obvious adaptions to make to the design is an increase in the torsional stiffness of the wing. Torsional stiffness can be increased in several ways, listed below.

- Adding material to the wing box, with which also resistance to bending and torsion by the wing box is added. There is however a certain limit to the addition of material; the point where the disadvantageous increase in wing box mass outweighs the benefit of the additional stiffness. When that point is reached, one should look at other solutions to increase stiffness.
- Reducing the aspect ratio. A lower aspect ratio, however, is detrimental for aerodynamic purposes. In Section 8.6.4 the effect of aspect ratio on aeroelasticity is analysed in more detail.
- Optimised strut sizing and placement. Currently the strut is sized to withstand bending loads and placed in the shear centre, decreasing the wing box stiffness and torsional rigidity of the wing and making the structure more sensitive to aeroelastic problems. In the case of SAGA, the torsional stiffness of the strut-braced wing design is reduced by approximately 4% (depending on whether an aluminium or composite design is selected) with respect to the conventional wing design. Strut attachment to the front spar induces a moment that twists the leading edge down, enabling better aeroelastic resistance [77]. It should be noted however that the strut induces an axial loading case, which is likely to affect the bending and torsional stiffness. This so-called tension stiffening is a geometric non-linear effect that should be considered, in order to conduct a complete aeroelastic analysis [78].
- Appropriate material selection. Currently the material selection is done considering the desired properties for withstanding the tip deflection, implying a high elastic modulus E . However, a high E is achieved at the expense of shear modulus G , the type of strength that is required to provide torsional stiffness. It is found that the torsional stiffness can be impaired by 2-10% due to the implementation of the boron composite (depending on whether a strut-braced wing is design or a conventional concept is selected). A sensitivity analysis of the flutter speed with respect to certain combination of E and G is presented in Section 8.6.4. In the future materials that can provide high shear modulus should be investigated, in order to achieve better aeroelastic characteristics.

Mass balancing is another option that is often used to reduce the problem of flutter. During flight, the wing experiences torsion around the elastic axis. By clever placement of the engines and wing fuel and aerosol tanks the problem of flutter can be decreased, where the reduction in fuel mass during flight must be taken into account to anticipate changes in flutter characteristics during the mission. The mass balancing approach can also be observed in ailerons [79]. To solve the problem of aileron flutter, often a piece of lead is placed at the leading edge of the aileron, making it not only easier to control, but also assuring the centre of gravity to be in front of the centre of pressure, reducing the possibility of flutter. The effect of mass balancing on the flutter performance is analysed and discussed in Section 8.6.4. Static aeroelasticity is not affected by inertia, and therefore the problem of those effects can not be solved using this method.

Alternatively, the problem of flutter can be tackled using an active flutter control system. Research on these systems has been performed since the mid 1960s [80] and nowadays, advanced mechanisms to suppress flut-

ter have been designed and implemented in aircraft²⁹. These active flutter suppressing mechanisms change the deformation shape, modify the stiffness and introduce damping into the vibrating system, resulting in a decrease in oscillation amplitude [81]. These systems can be designed using sensors, actuators and controllers, however, the design of such a system is highly dependent on the specific aerodynamic flow around the aircraft and can not be copied from already existing mechanisms. To design a proper flutter suppressing system, highly accurate aeroelastic models are required [82].

The problem of control reversal can be solved separately from the other phenomena, namely by the design of roll spoilers, so-called spoilerons. This type of control mechanism is a conjunction to the ordinary ailerons. Spoilerons are installed less aft than conventional ailerons, thereby reducing C_{Mac_δ} , which will delay the occurrence of control reversal. Roll spoilers are nowadays applied in a substantial amount of modern airliners³⁰ [76].

It is expected that the above described solutions are sufficient to mitigate the risk of the occurrence of aeroelastic phenomena. However, there is still a huge uncertainty in the presented results, as will be discussed in the following section. More detailed analysis in the complex field of aeroelasticity is required to assure feasibility of the current design of the SAGA.

8.6.3 Verification & Validation

In this section, the methods used for the analysis are briefly introduced and the results are verified and validated.

Static aeroelasticity

The static aeroelastic analysis concerns, as mentioned, torsional divergence and control reversal. These phenomena are analysed using Equation (8.16) and Equation (8.17). These equations are based on the analysis of a simple airfoil, suspended using a linear and a torsional spring, reflecting the equivalent aerodynamic and structural properties of a representative spanwise location, in this case determined to be 80% of the semi-span.

$$q_{div} \leq \frac{K_\theta}{C_{L_a} x_\theta c S} \quad (8.16)$$

$$q_{cr} \leq -\frac{C_{L_\delta} K_\theta}{C_{L_a} C_{Mac_\delta} c} \quad (8.17)$$

These equations provide a first look into the aspects that influence aeroelastic effects. Using the aircraft dimensions at 80% of the span, wing characteristics as presented in Table 8.18 and assuming x_θ is 0.3 times the chord [83, 84], the required torsional stiffness corresponding to a certain divergence speed can be obtained, in this case 264.5 m/s – the critical value in cruise speed range, cf. Table 8.17. The actual torsional stiffness provided by the wing, as specified in Section 8.5, is higher than the value obtained from the specified divergence speed, resulting in higher actual divergence speeds. With divergence speeds higher than CS25 specifies, the certification requirement is satisfied. In the remaining analysis, the torsional stiffness of the designed wing is used.

Table 8.18: Input values for static aeroelasticity calculations.

C_{L_a} [rad ⁻¹]	9.74
C_{L_δ} [rad ⁻¹]	0.039147
C_{Mac_δ} [rad ⁻¹]	-0.010149

Furthermore, as a means of verification, the sensitivity of both divergence and control reversal speed to aspect ratio is investigated. As it is expected that high aspect ratios will impair the aeroelastic performance [85], this design parameter is investigated in more detail to verify the analytical solution and quantify the effect of aspect ratio. For this calculation, S , x_θ and the wing characteristics are assumed to be constant and the torsional stiffness and the chord and span are allowed to vary. The result is shown in Fig. 8.52 and is as expected. This analysis is further discussed in Section 8.6.4.

²⁹ URL http://old.seattletimes.com/html/businesstechnology/2016583947_inpersonfitzgerald24.html [Accessed 15/06/2016]

³⁰ URL http://www.airliners.net/aviation-forums/tech_ops/read.main/27569/ [Accessed 20/05/2016]

Dynamic aeroelasticity

The flutter analysis is performed using an analytical and a numerical approach. The two methods require different input data and also provide different outputs, making comparison between the two analyses difficult. To verify the two methods, the trends observed in both models are compared, which facilitates an estimation of the effects of design adaptations on flutter characteristics.

The analytical method to investigate flutter is based on a multi-body simulation of the wing. As mentioned earlier, flutter is a complex phenomenon and convoluted structural and aerodynamic analysis is required for a high accuracy solution. However, this is beyond the scope of this project, and therefore a more simplistic model is used. By computing the stiffness matrix and mass matrix of the system and calculating the aerodynamic properties, the eigenvalues of the system are identified, from which the damping ratio and frequency are determined. Based on the outcomes, the flutter speed is determined. In this model, several parameters can be varied, such as the wing box dimensions (changing the torsional stiffness), the material properties and the aerodynamic characteristics. The model allows for an initial analysis of the effects of for example altitude and engine placement.

A numerical analysis for the flutter is performed using NeoCASS, an open-source program developed by the Polytechnic University of Milan. NeoCASS helps the user to dimension the structure of the aircraft under development and to investigate its aeroelastic behaviour by means of structural and aerodynamic numerical methods with a physical basis. In contrast to empirical methods, using NeoCASS allows for more unconventional designs, such as a high altitude aircraft like SAGA. For subsonic analysis of flutter and divergence NeoCASS uses a doublet lattice method (DLM)^[86]. The structure of the model is represented by a stick beam model and is sized based on the geometry of the input aircraft and the applied loads. The critical loads imposed on the aircraft model are 2.5g and -1g and input values used for the NeoCASS analysis are stated in Section 8.6.1 in Table 8.19. The flutter analysis is performed for the first twenty flutter modes, including the six rigid modes representing the degrees of freedom of the entire aircraft. The reduced frequencies used for the analysis are in a range of 0 to 0.2, which defines the unsteadiness of a flow. A flow with a reduced frequency above 0.2 is considered highly unsteady^[87]. NeoCASS checks which modes and corresponding frequencies become unstable within a velocity range of 1000 m/s. The flutter diagram for the results at 13 km altitude is shown in Fig. 8.49. The structural model is generated using the AcBuilder Pre-processor, based on a set of geometrical parameters. Unfortunately, the AcBuilder is not able to accurately model complicated designs, such as strut-braced wings or composite designs. This limits the capabilities of NeoCASS using an AcBuilder input to analyse the SAGA design on aeroelastic instabilities to a certain extent. Instead of analysing a strut-braced composite wing, NeoCASS assesses an aircraft with a conventional aluminium wing featuring the same geometry and load cases as SAGA.

Table 8.19: Most important values for AcBuilder Pre-Processor

Spanwise engine location [% of span]	0.15 & 0.4
X-distance engine c.g. to LE [m]	0.2
Fuel + aerosol mass in wing tank [kg]	94000
Wing structure material	Aluminum T-6

An immediate discrepancy is found when comparing the results of the analytical and numerical solution, as NeoCASS outputs significantly higher values for flutter speed than the analytical model. This discrepancy can be explained by several differences between the models. One of these explanations is the different physical bases that are used in both methods, however the consequences of this assumption are difficult to identify. Other possible causes for discrepancies are analysed in the following paragraphs.

Firstly, the fact that the wing is assumed to be clamped in the analytical solution, implies that the wing cannot deflect or rotate at the root section. Therefore, if the flow exerts work on the wing, the elastic potential energy is completely absorbed by the wing. However, in a full aircraft model, the wing is connected to the fuselage, allowing a portion of the elastic potential energy to be transferred to one of the rigid aircraft modes, resulting in motion in one or some of the six degrees of freedom of the aircraft. The presence of a fuselage therefore damps the vibrations and results in higher flutter speeds. In order to quantify the actual difference, NeoCASS is used to compute the results for a clamped model by removing the six rigid modes from the modal base of the flutter analysis and assuming no mass variations. The results are displayed in Fig. 8.50. In this diagram, the flutter velocities for a non-clamped and a clamped wing computed in NeoCASS are presented, as well as the results of the analytical solution for the aluminium design without struts (in which a clamped wing is assumed), for different mass configurations. As the exact distance between the elastic axis and the c.g. in the

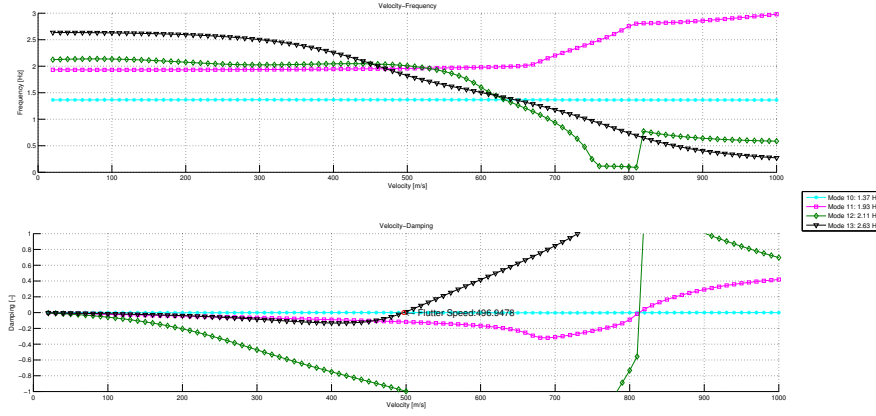


Figure 8.49: Frequency and damping ratio plotted against velocity for the unstable modes; altitude = 13 km (cruise leg 1)

NeoCASS model is not entirely known, a range of x_θ is plotted for the analytical solution. The results show a similar trend line, however it is also observed that the assumption of a clamped wing is detrimental for the flutter performance. Consequently, this suggests that the analytically computed flutter speeds are conservative, imposing more constraints than would be necessary in reality. However, it should be noted that a discrepancy remains between the analytical and numerical solution of a clamped section. Several clarifications – based on the different physical bases of the used methods - can explain the differences. Another explanation could be the level of mass balancing that is applied in both methods. As said earlier, the analytical solution and NeoCASS use different inputs and implementing an equal amount of mass balancing is difficult. However, more in-depth analysis is required to find all possible causes of the discrepancies.

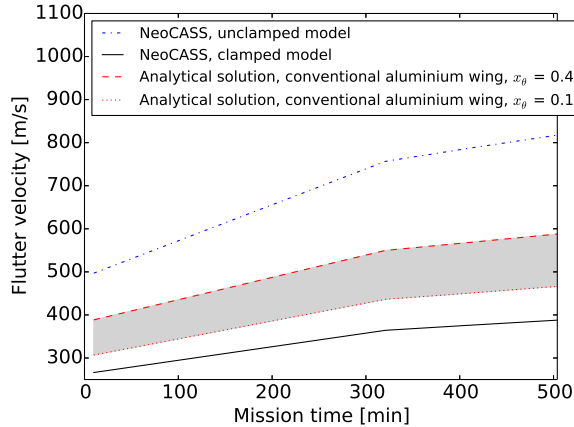


Figure 8.50: Effect of clamped wing assumption

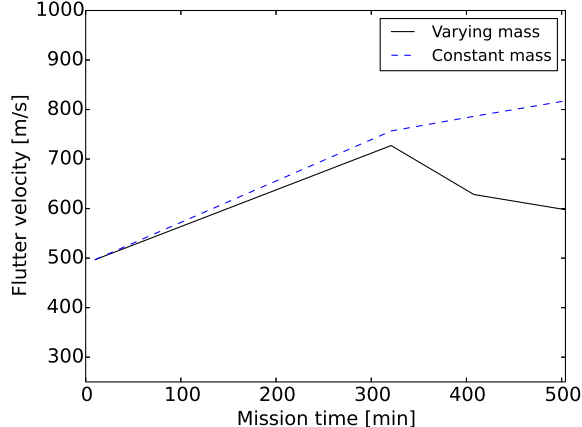


Figure 8.51: Effect of constant mass assumption

Secondly, the way in which mass variations are taken into account in both methods can cause differences between the solutions. In NeoCASS the varying mass during the mission due to fuel consumption and aerosol dispersion is implemented, which is not possible in the analytical solution. The mass decrease is shifting the c.g. of the entire wing aft, decreasing the distance between the elastic axis and the c.g., and reducing the effect of mass balancing as described in Section 8.6.2. This negatively influences the flutter speed. Note that flutter characteristics are affected by the c.g. shift mainly, and only to a lesser extent by the absolute mass decrease. Whether flutter characteristics are influenced positively or negatively depends on the change in distance between c.g. and aeroelastic axis due to mass decrease. In SAGA, the arm of the weight w.r.t the elastic axis decreases, negatively affecting flutter speed. In Fig. 8.51 the varying mass and non-varying mass solution is shown. After approximately 300 minutes the aerosol dispersion starts and indeed a significant reduction in flutter speed is observed in the mass-varying solution. This phenomenon is discussed in more detail in Section 8.6.4.

The last difference addressed is the use of struts and composite material. The wing is, as explained in Sec-

tion 8.6.2, sized for tip deflection. The application of struts and composites is favourable for the wing structural weight, however, it impairs torsional rigidity, as explained in Section 8.6.1. This affect is taken into account in the analytical solution, but implementation of struts and composite materials in the used numerical method is not possible. It is expected that the NeoCASS results would show a similar behaviour to changing inputs due to material and struts, however, the exact effects of the mass change and c.g. shift of the wing are unknown. A lighter wing box implies a larger contribution of the engines and fuel tanks, shifting the centre of gravity more forward. It is at this point uncertain whether this change in centre of gravity would offset the effects on flutter of the reduced wing box size and associated reduced torsional rigidity. Next to that it should be noted that the strut is likely to introduce an asymmetric loading case, leading to hardly predictable aeroelastic responses [78]. This is likely to change the modes and adds large uncertainty to the obtained results. The usage of struts and composites introduces the largest uncertainty when verifying and validating the results.

The flutter velocity of the actual design is predicted to lie somewhere above the analytical outcome, which only models the wing and no fuselage interactions, and somewhere below the NeoCASS outcome, taking into account an assumed negative effect of composites and struts. Although the outcomes are uncertain, this is the best approach available given the complexity of the design and its preliminary state, impeding a complete aeroelastic analysis taking into account all relevant parameters. Despite the uncertainty, it is concluded that flutter will most likely not occur for speeds in the flight envelope of SAGA. It is found both methods are significantly different, however do show similar trends when isolating certain relevant factors.

8.6.4 Sensitivity analysis

In this section, the sensitivity of the aeroelastic characteristics to aspect ratio, material selection and engine placement is investigated. By doing this sensitivity analysis, a feeling for aeroelasticity is further developed, allowing to determine subjects of future research and adaptations.

Aspect ratio

The results of an analysis of the sensitivity of torsional divergence and control reversal to variations in aspect ratio are presented in Fig. 8.52. It shows that a relatively small increase in aspect ratio already significantly deteriorates aeroelastic behaviour. In order to make a flyable design, a limit should be put on the aspect ratio. The aspect ratio of SAGA is 13, resulting in good aeroelastic performance.

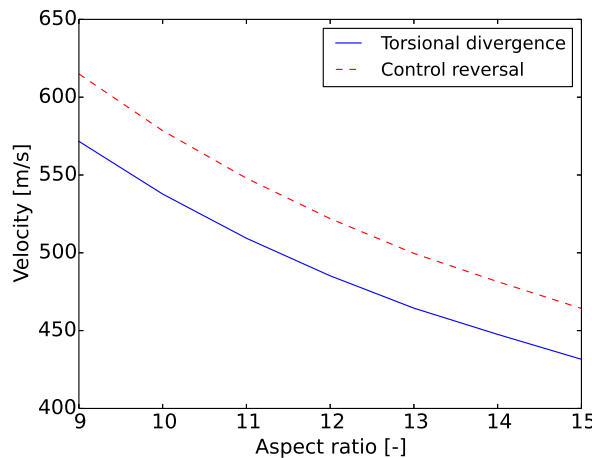


Figure 8.52: The effect of aspect ratio on torsional divergence and control reversal, for a strut-braced composite wing design; altitude = 13 km (cruise leg 1)

The response of flutter to aspect ratio is analysed, using both the analytical solution and NeoCASS. For flutter, a similar behaviour as observed for divergence and control reversal is found, as can be seen in Fig. 8.53 and Fig. 8.54. In Fig. 8.53 the flutter speed for the full model is displayed, along with the results for the analytical aluminium conventional design for different mass configurations. The trend lines are similar, however the discrepancy is obvious, which can be explained by the reasons mentioned in Section 8.6.3. Next to that, in Fig. 8.54 the solution of the strut-braced composite wing is presented, also for different mass configurations. It is observed that the strut-braced composite wing performs worse than the analytically analysed aluminium

conventional wing and it is expected that NeoCASS would have shown a similar reduction, if it were possible to implement struts and composites.

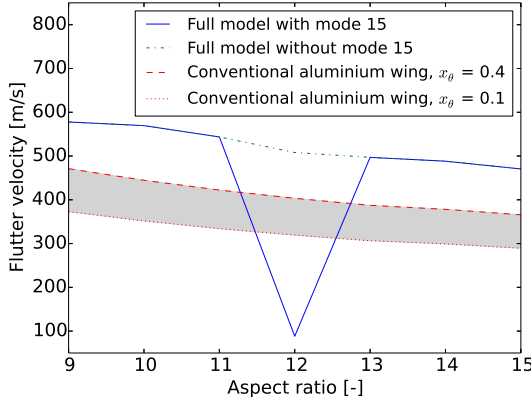


Figure 8.53: The effect of aspect ratio on flutter speed for aluminium conventional design, based on the analytical method and NeoCASS simulation; altitude = 13 km (cruise leg 1)

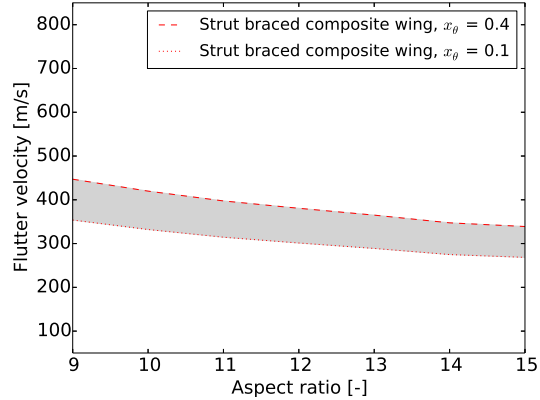


Figure 8.54: The effect of aspect ratio on flutter speed for a strut-braced composite design, based on analytical solution; altitude = 13 km (cruise leg 1)

In Fig. 8.53 an inconsistency w.r.t. the rest of the graph is observed for $AR = 12$. An inferior flutter speed performance is observed for this aspect ratio compared to the surrounding values. Modal analysis shows that for aspect ratio 12, flutter mode 15, with a frequency of 3.4 Hz, becomes unstable. According to deformation plots, the movement of mode 15 is found to be physically feasible, i.e. the deformation can happen given the structural constraints. The explanation for mode 15 becoming unstable is the specific combination of the stiffness and mass distribution of the wing with aspect ratio 12. This is further investigated in Fig. 8.55.

A similar discontinuously low flutter velocity for aspect ratio 12 wings due to unstable mode 15 can be spotted in this graph as well. However, it is observed that by changing the position of the centre of gravity, the extreme drop in flutter velocity can be mitigated and will return to values in trend with the analysis for the other aspect ratios as shown in Fig. 8.53. From this observations two conclusions can be drawn. First of all, with mass balancing, the risk of having an uncertifiable design due to low flutter speeds at apparent 'arbitrary' design points, such as aspect ratio 12 wing, can be controlled by changing the c.g.. The aircraft designer has authority over unexpected instability of modes like mode 15 using mass balancing. Secondly, the flutter performance of the aircraft is sensitive to mass balancing and a small changes in c.g. can cause large fluctuations in flutter speed. Therefore, in detailed design phases, more sophisticated tools are required to perform more advanced and more accurate analysis. Later in this chapter, the effect of engine placement is investigated in more detail.

Fortunately, for aspect ratio 13, this minimum in flutter speed is resolved. However, this analysis shows that the trends following from equations do not always hold and that making assumptions on flutter speed based on continuous trends can cause unanticipated problems. This increases the uncertainty of the flutter analysis from Table 8.17.

Materials

The implementation of composites in the wing is also investigated and it is found that aluminium outperforms boron considering aeroelastic performance, however, 20% decrease in structural wing weight is accomplished when designing a boron wing. As weight is a driving parameter in aircraft design and especially in the design of SAGA, a composite wing design is recommended. From a response surface diagram assessing the combined effect of E and G on flutter characteristics, it is concluded that E has an effect on the flutter speed which is more than 10^6 times smaller than the effect of G . Flutter occurs as a result of coupling of the bending and torsional modes of the wing. The difference in sensitivity to E and G indicates that the effect of G on the torsional frequency is larger than the effect of E on the bending frequency, causing the speed at which the two modes couple to change more with variation in G than with variation in E . During the detailed design phase it is of utmost importance that the feasibility of the design in terms of aeroelasticity is guaranteed, by ensuring that increases in E do not negatively affect G to an unacceptable extent.

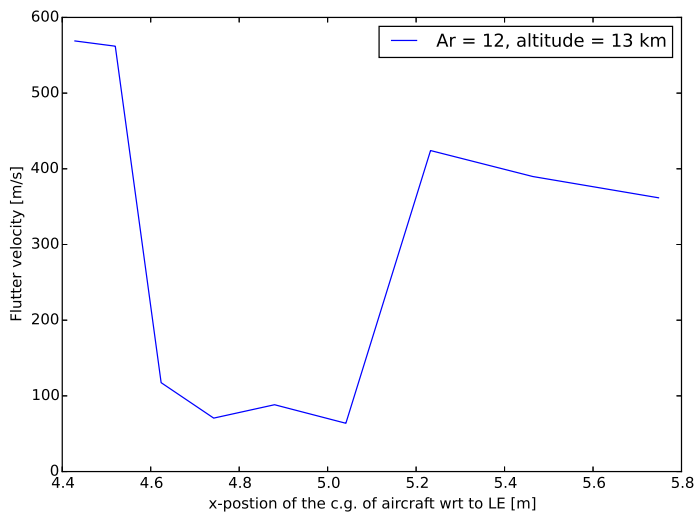


Figure 8.55: The flutter velocity of an aircraft with $AR = 12$ at 13 km altitude for different aircraft c.g. locations

Mass balancing

Mass balancing is often applied as a solution for flutter problems and therefore the variation in flutter speed with placement of engine and wing fuel tanks is analysed. In the analytical solution this is approximated by varying x_g , the distance between the centre of gravity and the elastic axis. For wing boxes of both aluminium and boron, an optimum is achieved at approximately 40% chordwise. This optimum can be explained by the differences in coupling of the bending and torsion frequencies. The engine and wing fuel tank affect the two vibrations in different ways, therefore also changing the ratio between the two. From Fig. 8.56 it becomes apparent that moving the c.g. forward is only beneficial to a certain extent. In addition, the shift in x_g affects more fields than only aeroelasticity, mainly stability & control, which should be able to handle this shift as well.

In NeoCASS, the sensitivity of flutter speed to c.g. position is assessed by varying the engine placement chordwise and spanwise. The results are presented in Fig. 8.57. Fig. 8.57 shows a clear optimum for inboard and forward engine placement, namely at 20% of the span and 1.0 m in front of the leading edge. This is the optimum for an aluminium strutless design. To what extend this optimum holds when considering a strut-braced composite wing is uncertain. Inferring from the properties concerning mode 15, mentioned earlier, a small change in mass distribution or stiffness due to a design change can lead to unexpected instabilities of certain modes which can affect the optimum c.g. position. Additionally, for engine placement to reduce aeroelastic instability, it is beneficial to mount the engine under the wing. This is illustrated by the analogy with a pendulum: a regular pendulum is naturally stable, whereas an inverted pendulum is naturally unstable [14].

8.6.5 Conclusion

From the above described analysis it is concluded that a combination of the analytical solution and the NeoCASS program can be utilised to perform a preliminary analysis of the aeroelastic behaviour of the design, however this analysis is still highly uncertain. For the current design stage, this analysis is considered to be sufficient. However, for the detailed design phase it is recommended to use more advanced tools to more accurately model the extremely important and complex field of aeroelasticity, also taking into account the additional complexity of the implementation of a strut-braced wing. From the conducted analysis it is concluded that aeroelasticity will most likely not cause any problems within the flight envelope. In the past, aircraft with similar aspect ratios have been successfully designed. However, in the unfortunate case where aeroelasticity does cause problems, aspect ratio, material selection and mass balancing can be adapted in such a way that aeroelastic phenomena become less constraining.

8.7 Stability and control

Several aspects of the mission introduce challenges to the stability and controllability of the aircraft. The low density at stratospheric altitudes has a negative effect on the effectiveness of the control surfaces and

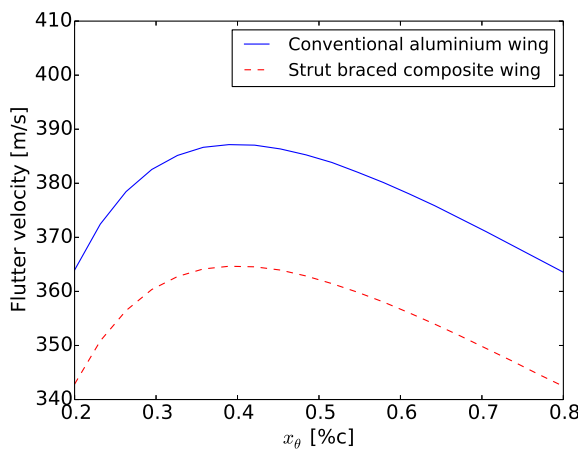


Figure 8.56: The effect of x_θ on flutter speed, for a conventional design computed analytically; altitude = 13 km (cruise leg 1)

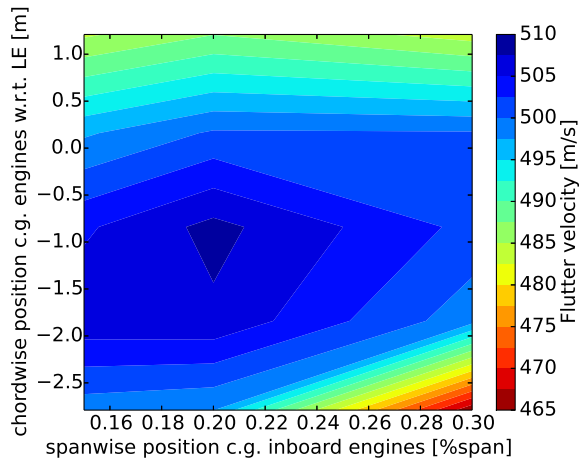


Figure 8.57: The effect of engine placement on flutter speed, for an aluminium design without struts generated by NeoCASS; altitude = 13 km (cruise leg 1)

the damping of the eigenmotions. The large aspect ratio needed to reach this altitude results in a high tip deflection which influences the dynamic behaviour of the aircraft. Another effect of the large aspect ratio is the possible occurrence of control reversal, which limits the roll control of the aircraft in the cruise phase. Sloshing of aerosol and fuel in the tanks can cause significant shifts in centre of gravity which have to be accounted for. Furthermore, the high lift needed at the start of the cruise phase puts stringent constraints on the lift coefficient of the tail in this flight phase.

8.7.1 Tail sizing

Static longitudinal stability and controllability

The first step in the analysis of stability and control is the sizing of the horizontal and the vertical tail. This is done by considering the static longitudinal and lateral stability and controllability of the aircraft in the crucial flight phases. This resulted in a horizontal tail area of 131 m^2 and a vertical tail area of 39 m^2 . Generating a scissor plot is the first step in the evaluation of the static longitudinal stability and controllability of the aircraft. A scissor plot (Fig. 8.58) relates a given horizontal tail area to possible locations of the centre of gravity. These locations are obtained by plotting the horizontal tail area for the critical conditions for both controllability and stability. The limit for stability is achieved by setting the expression for the change in moment coefficient due to a change in the angle of attack to zero. A stability margin of $0.05 \cdot \bar{c}$ is added. For controllability the expression for the moment coefficient is set to zero, representing the trim point. The loading diagram (Fig. 8.59) shows the centre of gravity position for varying payload and fuel.

The area of the horizontal tail was sized using the method from [13], in which the tail arm and the wing position are varied simultaneously in order to obtain the combination for which the tail has to provide the lowest possible lift during the cruise phases and for which the center of gravity range is sufficient to take into account the possible center of gravity shifts due to the location of the aerosol and the fuel. The aspect ratio of the tail is determined from reference values from [88] and is chosen to be lower than the aspect ratio of the wing in order to enable acceptable stall behaviour.

The sizing of the vertical tail for stability and controllability includes the determination of the area and the aspect ratio. The sweep and taper of the horizontal and vertical tail are determined by the aerodynamic characteristics and the tail parameters are given in Section 8.3.4 and Section 8.3.4. For the sizing of the vertical tail, the approach as described in [14] is used. In this approach initial values are estimated from the vertical tail volume coefficient. These values are used in the analysis of the lateral eigenmotions and the requirements on the lateral behaviour of the aircraft treated in the description of the rudder design and adjusted to satisfy the requirements on the eigenmotions and the rudder effectiveness.

Dynamic longitudinal and lateral stability

The area of the horizontal tailplane resulting from the approach described above does not take into account the dynamic behaviour of the aircraft. In general, the static stability and controllability are driving for the

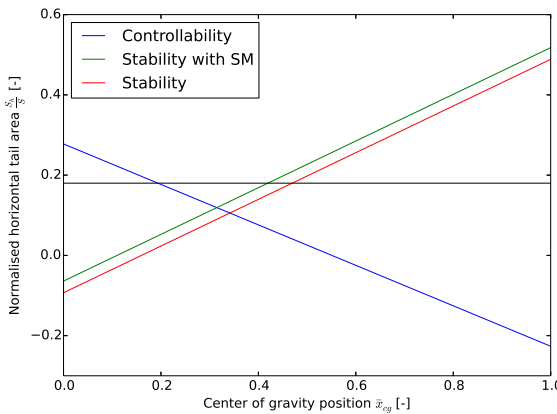


Figure 8.58: Scissor plot and selected normalised horizontal tail area

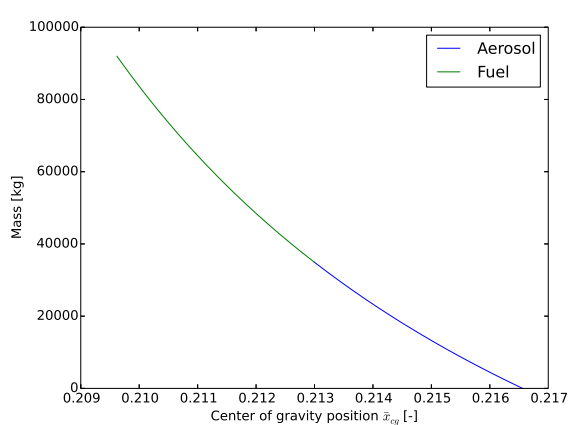


Figure 8.59: Loading diagram

sizing of the horizontal tailplane, hence the initial size is based hereon. The dynamic stability with the determined tail size is analysed and necessary adjustments are implemented [56].

The analysis of the dynamic stability consists of the calculation of the stability derivatives and the analysis of the eigenmotions. The calculated stability derivatives relate the sideforce, rolling moment and yawing moment to the sideslip angle, the rolling velocity and the yawing velocity. The stability derivatives are calculated using the DATCOM method. The DATCOM method takes the geometry of the airplane and the tailplanes as primary inputs. In order to be able to analyse the responses in a numerical model, the linear equations of motion are rewritten to state-space format.

The results of the numerical analysis are shown in Table 8.20. The split columns show the value for low speed and low altitude on the left and the value for high speed and high altitude on the right.

Table 8.20: Eigenmotion characteristics

Eigenmotion	Eigenvalue	Damping [-]	$T_{1/2}$ [s]	Frequency [s^{-1}]	Period [s]	LOA					
Short period	-1.7+0.8j	0.9	0.35	0.5	2.78	0.67	0.683	1.5	1.46	1	1
Phugoid	-0.01+0.3j	0.03	0.03	84	213	0.038	0.007	26.6	140.9	2	2
Aperiodic roll	-2.6+0j	-	-	0.273	1.518	-	-	-	-	1	1
Dutch roll	-0.018+0.33j	0.05	0.015	38.9	176	0.05	0.038	18.37	26.18	3	>3
Spiral	0.0557+0j	-	-	-12.45	-68.9	-	-	-	-	2	1

The requirements on the eigenmotions vary between different classes of aircraft and different flight categories. SAGA is in category III and the flight phases in which it will be operating are B during climb, cruise and descent and C for take-off and landing. The quality of the eigenmotions is analysed using levels of acceptability. Because SAGA is unmanned and controlled by computers it is decided that all behaviour resulting in parameters falling outside the level of acceptability 3 is unacceptable [89].

The requirements on the eigenmotions are taken from [89] and [14]. The acceptability of the symmetric eigenmotions is based on the damping ratio. The acceptability of the aperiodic roll is quantified using the time to half amplitude. The Dutch roll is analysed based on both damping ratio and frequency. The level of acceptability for the aperiodic roll is based on the time to half amplitude. A negative time to half amplitude means that the eigenmotion is unstable and is thus the time to double amplitude.

As can be seen in Table 8.20 the only eigenmotion with a level of acceptability higher than 3 (unacceptable) is the Dutch roll at high altitude. This is to be expected of an aircraft with this mass distribution [90]. It is therefore necessary to implement a yaw damper in the control system to improve the behaviour of the aircraft in the Dutch roll eigenmotion.

8.7.2 Control surface sizing

The effect of control surface deflections on the forces and moments acting on the aircraft is quantified using control derivatives. The control derivatives are calculated using the DATCOM method. The maximum deflec-

tions of the control surfaces are obtained from reference values in order to better constrain the chordwise and spanwise sizing in this phase of the design. For all control surfaces the general approach is to calculate the required effectiveness expressed as a value for the control derivative from the driving flight situations. The maximum deflection and the chordwise and spanwise size are determined to obtain the value for the control derivative. There are many combinations of these parameters which achieve the required control effectiveness. In order to add more constraints to this problem, in further design phases the control forces and the drag induced by the control surfaces can be considered. The design parameters values resulting from control surface sizing are presented in Table 8.22, followed by a motivation for these values. The lay-out of the control surfaces can also be seen in Fig. 7.2

Elevator	Ailerons		Rudder	
$c_e/c_h [-]$	0.19	$c_a/c [-]$	0.22	$c_r/c_v [-]$
$b_e/b_h [-]$	0.88	$\delta_{a,up}$ [deg]	21	$b_r/b_v [-]$
$\delta_{e,up}$ [deg]	16	$\delta_{a,down}$ [deg]	13	δ_r [deg]
$\delta_{e,down}$ [deg]	21	y_{ailin} [-]	0.5	23
		y_{ailout} [-]	0.9	

Table 8.21: Control surface sizes and deflections

Flight situation	$C_{n_{\delta_r}}$ req. [-]
OEI	-0.014
Crosswind landing	-0.021
Spin recovery	-0.016
Coordinated turn	-0.002

Table 8.22: Required rudder effectiveness for various situations

Elevator sizing

The elevator sizes are determined by the take-off rotation requirement and the longitudinal trim requirement. The elevator dimensions and deflections are shown in Table 8.22. The take-off rotation requirement specifies a pitch acceleration during the take-off rotation, which is influenced by the elevator effectiveness in generating a downward force. The pitch acceleration is evaluated at the stall speed in take-off configuration and is set by requirements [14]. The moment required for rotating the aircraft is mainly dependent on tail length, wing position, landing gear placement, elevator size and deflection. The elevator size includes the span and chord, which can both be varied simultaneously with the elevator deflection to achieve the required value for the downward force. The take-off rotation is shown in Fig. 8.7.

The elevator effectiveness for generating an upward force is determined by the longitudinal trim requirement. This required elevator effectiveness is calculated considering moment equilibrium at varying altitudes, velocities and centre of gravity positions.

Aileron sizing

The sizing of the ailerons consists of determining the spanwise location(s), the deflection angles and the chordwise length of the ailerons, which are stated in Table 8.22. The driving requirement for aileron sizing is the requirement for the roll rate expressed as time to roll to 30 degrees. In order to use these requirements to size the ailerons the control derivative $C_{l_{\delta_a}}$ is determined using the DATCOM method. This control derivative is dependent on both spanwise location and chordwise length of the ailerons. Because of the low density at cruise altitude, the roll rate due to aileron deflection is lowest in this flight phase. A combination of spanwise aileron position and chordwise aileron length is chosen such that the roll rate requirement is met at cruise altitude. The maximum time to 30 degrees bank angle required is 2.3 s in flight phase A and 2.5 s in flight phase B. The achieved roll rate in the current design is 2.28 s in flight phase A and 2.43 s in flight phase B. The spoilers fitted for the landing can also be used in an emergency case in which the roll rates originating from requirements are not sufficient. In these cases the spoilers can be deflected at one side. In order to limit the effect of adverse yaw, the downward aileron deflection is lower than the upward aileron deflection.

As discussed in Section 8.6, the phenomenon of control reversal does not occur for the ailerons in the current design. However, if design changes were to change the structural properties of the wing, control reversal could be prevented by using the spoilers on the wing to roll in the critical flight phases for control reversal. Also, the ailerons could be divided into two spanwise positions, using inboard ailerons in flight phases in which deflection of the outboard ailerons would introduce control reversal. The fact that no high lift devices are used provides freedom to the aileron design to vary the spanwise location and size of the ailerons over a large range.

Due to the small velocity range during the cruise phases, the roll performance in these flight phases concerns more than just the roll rate. As in a coordinated turn the outer wing has a higher velocity than the inner wing, there is a chance that the maximum velocity is exceeded by the outer wing or that the velocity is under the lower limit at the inner wing. In Section 8.3.8 the velocity limits for turning are investigated, yielding in a

maximum lift coefficient in the turn of $C_{L_{max}} = 1.18$. The maximum roll angle and the yaw rate for this lift coefficient are obtained from the equations of motion for a coordinated turn. The maximum roll angle in the situation described above is $\phi_{max} = 26.6\text{deg}$. This roll angle corresponds to a turning radius of $R = 8680\text{m}$. As this turn radius does not limit the mission from an operations point of view it is regarded acceptable.

The yaw rate in the situation described above is calculated to be $r = 1.4\text{deg/s}$. From the yaw rate corresponding to the maximum lift coefficient during a turn in the first cruise phase and the span of the aircraft, the velocity changes at the wingtips can be calculated. This resulted in a velocity increase at the outer wingtip of $v_{tip} = 1.2\text{m/s}$ and a velocity decrease at the inner wingtip of equal magnitude. For the velocity margin during this phase in the flight these tip velocities do not pose a problem. However, also as calculated in Section 8.3.8, at this maximum lift coefficient in the described flight situation the margin in angle of attack at the tips is $\alpha = 0.22\text{deg}$. In order to be able to restore the roll angle in this situation, for example to correct for a disturbance, a downward aileron deflection should not cause the inner wing to stall. This can happen because a downward deflection causes the wing to stall at a lower angle of attack. Also, the increased angle of attack increases the drag of the inner wing, resulting in a larger velocity difference between the inner and the outer wing and possibly causing a spin. Using [14] to estimate the effect of an aileron deflection on the stall performance of the wing sections where the ailerons are located, the maximum aileron deflection before wing stall occurs is $\delta_{ail,down} = 2.2\text{deg}$. This maximum deflection angle is relatively small, especially given the low density in this flight phase and the low aileron effectiveness resulting from this density. The maximum deflection angle can be improved by using vortex generators or tip washout. The negative effects of vortex generators and tip washout (increased drag and negatively influenced lift distribution) have to be investigated with respect to the positive effects in further design phases.

Rudder sizing

The size of the rudder is determined by several requirements. The requirements are all analysed and the most stringent requirement determines the size of the rudder. The sizing of the rudder consists of sizing the chord of the rudder and the vertical span of the rudder. These values are stated in Table 8.22. Because the size of the vertical tailplane must accommodate the required size of the rudder, the analysis of the rudder sizing also has an effect on the size of the vertical tail.

Firstly, the rudder must be effective enough to achieve yawing moment equilibrium if an outboard engine fails during take-off, as this is the case which introduces the largest moment. The yawing moment produced by the failure of the outboard engine is calculated considering the thrust per engine, the engine placement and the drag of the inoperative engine. The available yawing moment produced by the rudder is calculated using the equations of motion for equilibrium sideslipping flight. The rudder deflection is set to its maximum and the bank angle is limited to a maximum of 5 degrees by regulations. Iterating until a rudder size is achieved which allows sideslipping equilibrium for a limited aileron deflection gives the rudder size required for the one engine inoperative case.

Secondly, the rudder must be able to align the aircraft with the runway when performing a cross-wind landing with a wind speed of 30 knots. Taking into account the sideforce generated by the sideslip and the rudder deflection during the landing manoeuvre, the value for the minimum rudder effectiveness for a crosswind landing is calculated.

Thirdly, the rudder is sized for the requirement to perform coordinated turns and the requirement to overcome adverse yaw introduced by aileron deflection. The limited effect of the coordinated turn requirement on the rudder design is shown in Fig. 8.60. The maximum rudder deflection for a coordinated turn occurs at low speeds and high roll angles. This required rudder deflection is accounted for in the design for the flight cases that are more critical for rudder design.

Finally, the rudder effectiveness is sized to be high enough to recover from spin. This is quantified using a reference value for the angular deceleration necessary to stop spin within an acceptable time [14]. Because the rudder sizing is dependent on more situations than the other control surfaces, the required rudder effectiveness $C_{n_{\delta_r}}$ is calculated for the situations for the maximum deflection angle, which is set to 25 degrees.

8.7.3 Verification and validation

Verification and validation of the parameters determining the eigenmotions is performed. Verification uses analytical verification methods, whereas validation is performed using output data from SUAVE. The numerical values and the verification and validation data are presented in Table 8.23.

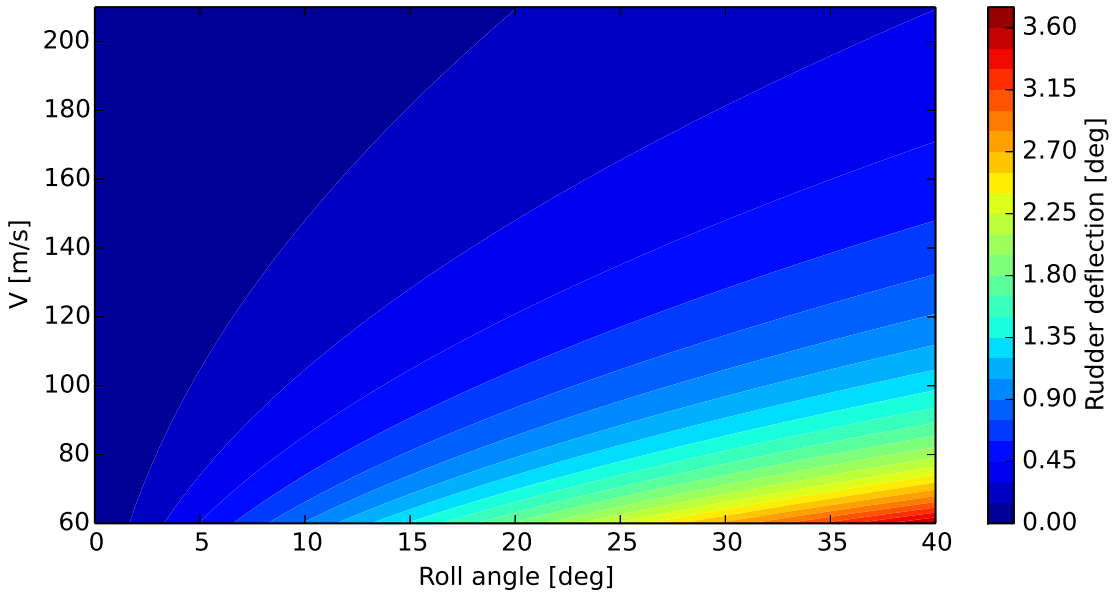


Figure 8.60: Rudder deflection required for coordinated turn for varying velocity and roll angle

Table 8.23: Verification and validation data

Eigenmotion	Parameter	Model	Verification	Diff. [%]	Validation	Diff. [%]
Short period	ω_n [s ⁻¹]	0.67	0.683	0.63	0.65	-6.0 -4.8
	ζ [-]	0.9	0.35	0.88	0.31	-2.2 -11.4
Phugoid	ω_n [s ⁻¹]	0.038	0.007	0.041	0.008	7.9 14.3
	ζ [-]	0.03	0.03	0.031	0.031	3.3 3.3
Aperiodic roll	$T_{\frac{1}{2}}$ [s]	0.273	1.518	0.136	0.597	-50.2 -60.7
Dutch roll	ω_n [s ⁻¹]	0.05	0.038	0.045	0.041	-9.8 7.9
	$T_{\frac{1}{2}}$ [s]	38.9	176	41.9	197	7.7 11.9
Spiral	T_2 [s]	12.45	68.9	13.3	76.9	6.8 11.6
					11.061	45.21 -11.2
						-34.4

Verification

For the verification of the results of the numerical model, a simplified analytical model is used. This analytical method allows for a relatively simple calculation of the eigenvalues of the eigenmotions and the damping and frequency parameters following from the eigenvalues. For the short period oscillation it is assumed that the velocity of the aircraft is constant during this short eigenmotion. The eigenvalues for the phugoid are calculated assuming a constant pitch rate and change in angle of attack. For the aperiodic roll it is assumed that the aircraft only rotates about the longitudinal axis. The Dutch roll is simplified by assuming that the aircraft only yaws and that roll movements can be neglected. Finally, for the spiral eigenmotion it is assumed that all linear and angular accelerations are zero. It can be seen that for most parameters the difference is less than ten percent. In most cases the calculations at high altitude and high velocity the differences are larger than for the results for low altitude and low velocity. The large difference for the aperiodic roll is known to be due to the rather rigorous nature of the simplification [90].

Validation

The results of the numerical model are validated using several parameters related to the eigenmotions from SUAVE. These validation values and their difference in terms of percentage with the values from the numerical model are shown in Table 8.23. The differences between the values from SUAVE and the numerical model are significantly higher than the differences found for verification. For a more in-depth validation of the data in later stages, more advanced validation data is required, for example using CFD or windtunnel tests.

8.7.4 Sensitivity analysis

Horizontal tail lift coefficient during cruise

As the required high lift coefficient at the start of the first cruise phase is a crucial design driver for aerodynamics, it is essential to investigate the effect of several parameters on the horizontal tail lift coefficient of the tail during this cruise phase, to ensure both stable behaviour and sufficient lift generation. If the tail generates a high negative force during this flight phase to counteract the positive pitch moment of the wing, the downforce has to be compensated by lift generation of the wing. This could drive the wing design to an unacceptable extent, which must be prevented. Two important parameters influencing the lift coefficient of the tail are engine position and the wing position. The sensitivity of the tail lift coefficient to these parameters is visualised in Fig. 8.61. The engine position is given w.r.t. the leading edge of the mean aerodynamic chord and is normalised to the mean aerodynamic chord. The wing leading edge position is defined on the horizontal axis from aircraft nose to tail and is normalised by the length of the fuselage. In order to take into account the effect of the centre of gravity shift due to the decrease in aerosol and fuel weight and thus make sure the critical phase is at the start of cruise one, the lift coefficient of the tail is calculated for the start of every cruise phase.

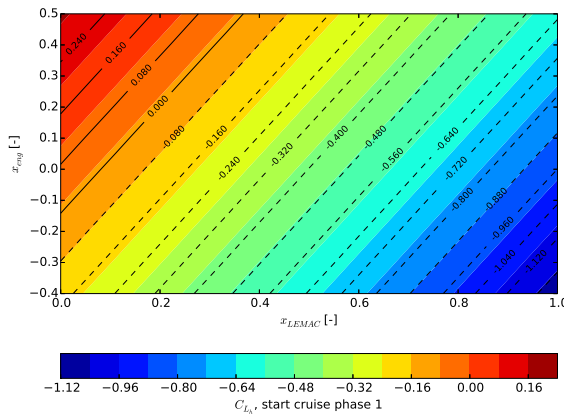


Figure 8.61: Tail lift coefficient during start of first (colored) and third (lines) cruise phase for varying engine and wing position

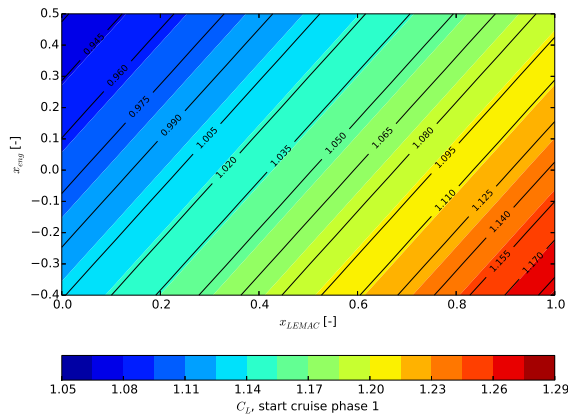


Figure 8.62: Lift coefficient during start of first (colored) and third (lines) cruise phase for varying engine and wing position

Effect of fuel and aerosol sloshing on dynamic stability

In Section 8.7.1 the effect of the position of the fuel and the aerosol on static stability have been accounted for, however the presence of the liquids in the wing also have an effect on the dynamic stability. Investigating the effect of sloshing on the dynamic stability of the aircraft can be done in multiple ways. A preliminary approximation of the eigenfrequency of the aerosol and the fuels in the tanks can be obtained using the methods described in [91]. Using the geometry of the tanks and the amount of liquid in the tanks the eigenfrequency can be calculated. In this approach it is decided to only investigate the fundamental sloshing mode, as this mode is accompanied by the largest mass movement of the aerosols and the fuel. In order to investigate the behaviour of the liquids and compare the eigenfrequencies with the frequency of the short period oscillation in different flight phases, the frequency of the fuel is plotted as a function of the amount of fuel and aerosols in the tank and the tank length in figure Fig. 8.63. Because the tanks are closed the liquids are not able to slosh at 100% level. Therefore, the upper range of the horizontal axis is merely theoretical and not applicable to the tanks in the wing. The range of frequencies of the short period oscillation during the mission is plotted in the hatched area. The current tank length at the position of the aerosol tank is indicated by the vertical line. For the fuel tanks more inboard the tank length is slightly larger and for the fuel tanks more outboard the tank length is slightly shorter. Due to the low frequency of the phugoid it only matches the frequency of the liquids at low levels (around 0.5%). Again, the mass of the fuel and the aerosol at this point is expected to be too low to negatively affect the behaviour of the aircraft.

It can be seen that the frequency of the fuel and the aerosols coincides with the frequencies of the short period oscillation at approximately 70% aerosol or fuel level. As the current tank length results from the spacing of the spars it is not possible to increase the tank length in order to mitigate the risk of coupling between liquid sloshing and the short period oscillation. Decreasing the tank length by installing slosh baffles or by dividing the tank up in more tanks will result in liquid sloshing frequencies which match with the frequency of the

short period oscillation at lower amounts of liquid. If the amount of liquid is lower the effect on the flight behaviour is expected to be less problematic.

In the above description the behaviour of the aircraft and the behaviour of the liquids in the wing are treated separately. In order to obtain a more accurate estimate of the interaction between the sloshing fuel and aerosols the liquids in the wing can be modelled as a oscillating mass. The response of the aircraft can then be calculated using the same linear equations of motion used for the analysis of the eigenmotions. However, instead of treating the motions of the aircraft as an eigenvalue problem, the moving mass of the fuel and the aerosols should be implemented in the equations and be solved using time integration techniques. However, this approach should due to time constraints be implemented in further design phases.

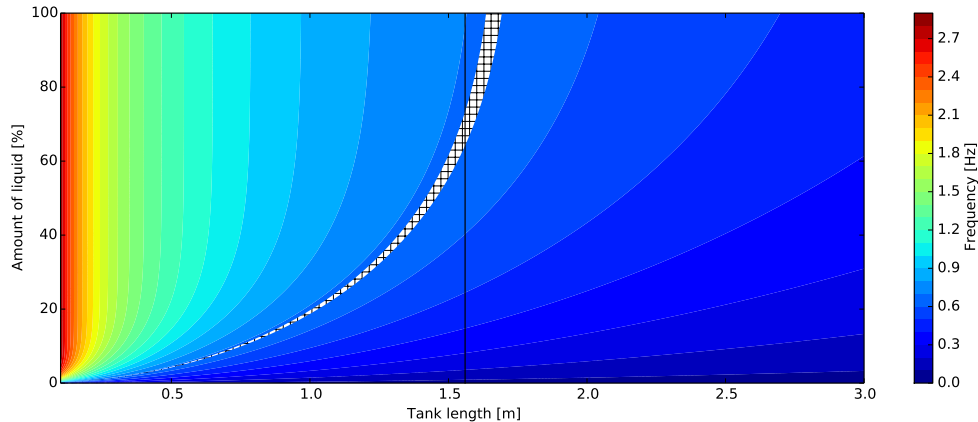


Figure 8.63: Sloshing frequency for the fundamental mode as function of liquid level and tank geometry

Effect of tip deflection and aeroelastic effects on dynamic stability

Dynamic stability is affected by wing deflection. This parameter is strongly dependent on the design choices made concerning the structural characteristics and the aspect ratio of the wing. For lateral stability the wing deflection is modelled as a positive dihedral and has a mostly stabilising effect on the lateral eigenmotions, while the roll performance is slightly worsened by the tip deflection. The phugoid is not expected to be significantly influenced by the wing deflection [90].

More problematic is the effect of the wing deflection on the short period oscillation. An instability can occur if wing bending modes with low frequencies couple with the short period oscillation [92]. This complex phenomenon can be investigated in several ways. In this design phase it was decided to compare the frequencies of the short period oscillation and the symmetric aeroelastic bending modes. The first symmetric bending mode was found to be most important for this phenomenon. The frequency of this bending mode equals the frequency of the short period oscillation at 150 m/s in take-off configuration and at cruise speed in the cruise phases at 19 km and 19.5 km. Ways to mitigate this in further design iterations include changing the frequency of the short period oscillation or the frequency of the problematic mode. The frequency of the short period oscillation can be changed by adjusting the tail parameter, however this solution is rather rigorous and has a large impact on the design and the other subgroups. The behaviour of the short period oscillation might also be changed by using control systems.

8.8 Systems

Several systems are required to complete the mission successfully. Many of them relate to the purpose of the SAGA: aerosol dispersion. The temperature of the aerosol will be monitored in the tank and the heating chamber and the dispersion rate will be continuously checked. Next to that, the aircraft will be able to determine its position and follow a predetermined flight path. It shall be able to perform CAT II/III landings and departures with less than 550m RVR. Lastly, communication between the SAGA and the ground control will be guaranteed at all times.

8.8.1 Fuel system

A conventional pump-fed fuel system is used on the aircraft. The internal tank volume is almost twice as large as the required fuel volume in order to allow the transfer of fuel along the wing span throughout different stages of the flight. For example, during take off and landing fuel is stored in the inboard section of the wing to reduce the wingtip deflection, while during cruise it is stored in the outboard section to provide bending moment relief. Additionally, there is one collector tank per engine, which at all times stores enough fuel to sustain the operation of the engine for fifteen minutes [93].

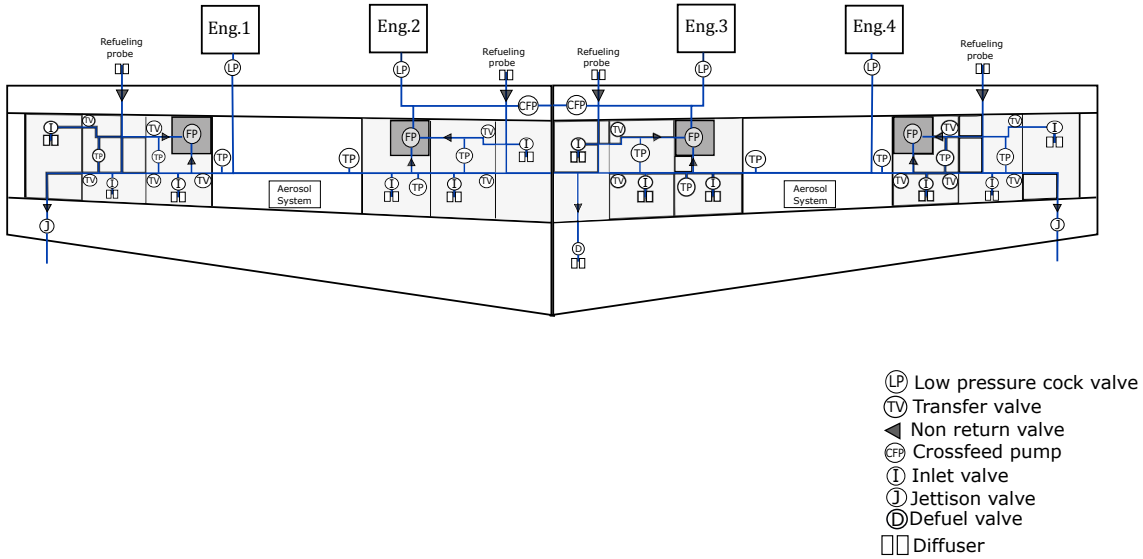


Figure 8.64: Layout of the fuel system

8.8.2 Hydraulic System

In Fig. 8.65 a layout of the hydraulic system can be seen. There are two main systems and one self-sustaining back up system, which relies on electro-hydraulic actuators (EHA). The main systems are powered engine driven pumps (EDP) and air driven pumps (ADP) in combination with an electrically driven pump (El.DP) or a ram air turbine (RAT) as a back up power source. This choice is made in order to increase the aircraft's reliability, as fewer hydraulic components lead to a longer mean time between failure (MTBF) [94]. The option to use mainly electro-mechanical actuators (EMA) in order to decrease the hydraulic system size was considered, but rejected because of the lower reliability levels and potentially shorter life of EMA compared to the chosen system architecture [94].

8.8.3 Electrical system

The electrical system of the SAGA is similar to the system used in the Boeing 787. The power system consists of two 250 kW generators per engine and two 225 kW generators in its APU, which enables the generation of enough power for both the aerosol handling system and the rest of the aircraft's systems. A layout of the electrical system can be found in Fig. 8.66.

8.8.4 Communication system

Fig. 8.67 presents the communication flow diagram with the flow of data through the system and to and from its environment. The diagram contains all elements that are part of the communication chain in blocks and represents data and command flows as arrows, where the content of the flow is annotated as footnotes with those arrows. Significant data rates relevant for the design have been indicated together with the arrow flows descriptions.

The diagram has been created based on [95, 96] with data rate estimates coming from [96]. Dotted boxes are optional and not an essential part of the Flight Computer. They represent the elements that help to increase the system reliability using fault and damage tolerant control [97]. The data/command flows annotated by numbers in Fig. 8.67 are listed in Table 8.24.

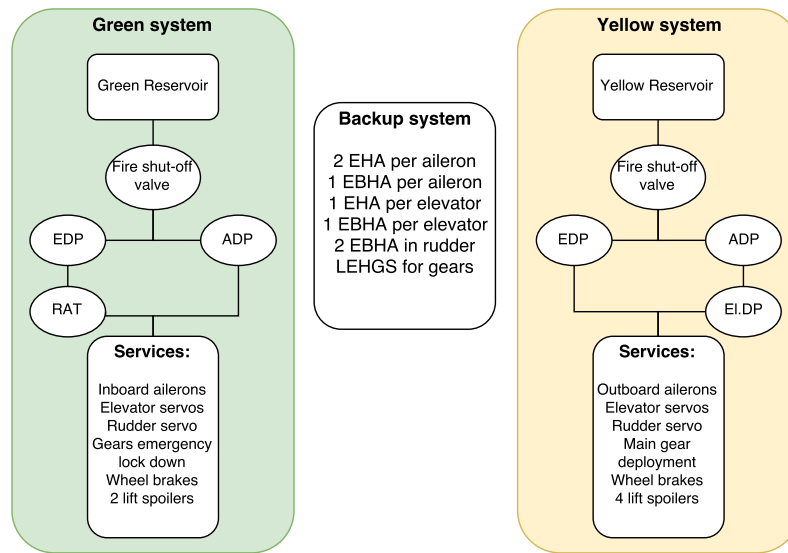


Figure 8.65: Layout of the hydraulic system

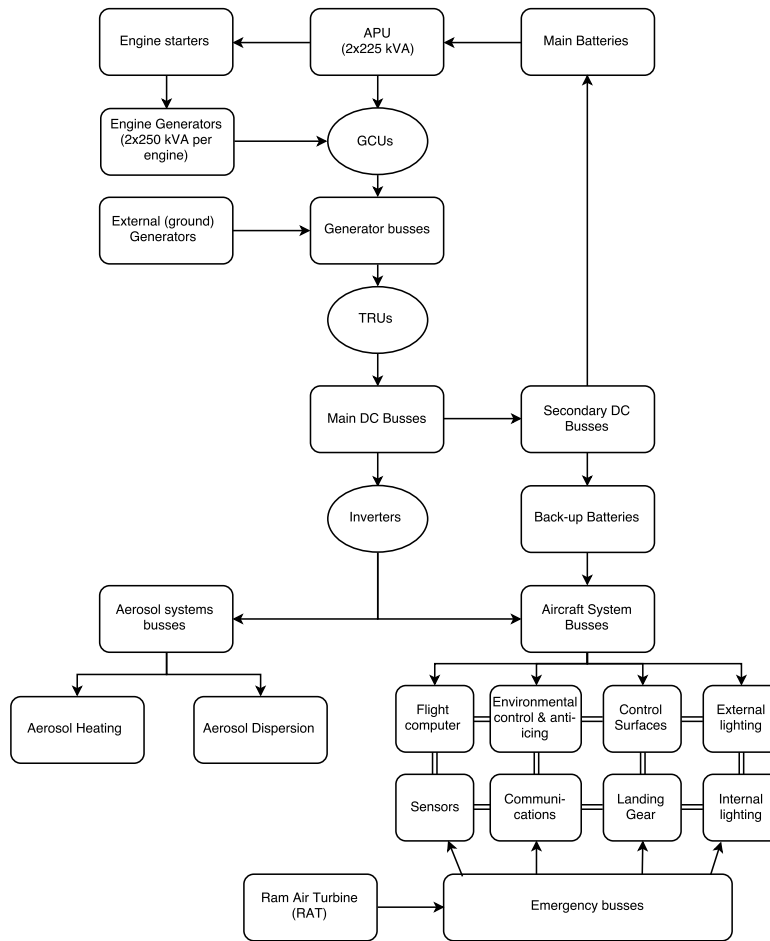


Figure 8.66: Layout of the electrical system

8.8.5 Hardware/software system

The hardware/software system is presented in Fig. 8.68. This system controls the aircraft's systems presented earlier. The software section analyses the data the aircraft receives from the hardware system - sensor data or external communication - and consequently issues commands to relevant systems. The software system is

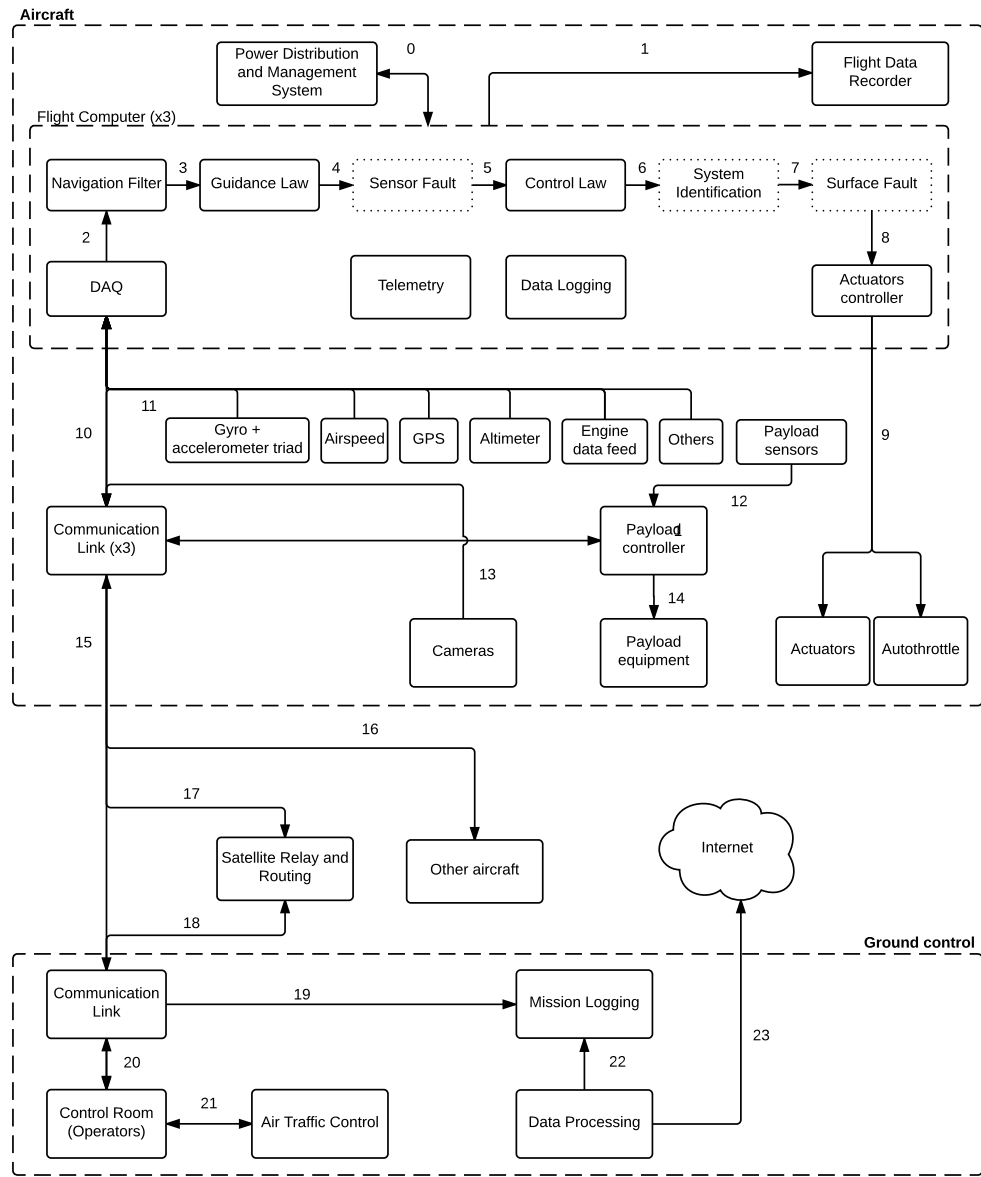


Figure 8.67: Communication flow diagram for SAGA

divided into three main segments: the mission manager (M_{Ma}), flight path manager (FPM), and contingency manager (CM). The M_{Ma} controls the aerosol related systems. The FPM constantly updates the required flight path, based on navigation data, commands from the ground station and inputs from the sense and avoid system, such as relative range and bearing of other aircraft. The CM receives data from the health monitoring system and governs the course of action if certain (combinations of) failure modes occur. The three managers are connected to the flight computer hardware by the virtual autopilot system interface. The latter communicates with the autopilot, which directly controls the aircraft [98].

8.8.6 Data handling system

The function of the data handling system is to transfer and store all of the data coming from both internal and external sources into the flight computer, where it is analysed by the hardware/software system. Furthermore, the data handling system encrypts the communication channels in order to prevent the aircraft's operation by external parties, as this must be prevented given the possible dangers related to the sulfuric acid payload properties. Finally, the data handling system sustains the continuous flow of information between the aircraft and the ground station through the communication system. The data rate that it has to provide is not high, since the aircraft sends and receives mainly parametric data about the state of the aircraft and its systems

Table 8.24: Passed on communication data/commands as shown in the Communication Flow Diagram

#	Data/Commands
0	Power Sensor, Control and Management Data
1	Flight Data Recorded Data Frames
2-7	(Virtual) Data Interfaces between Flight Computer subsystems
8	Control Signal
9	Actuator Commands
10	Target position
11	Sensor data
12	Payload sensor data
13	Imaging data (estimated 75Mbps) [95]
14	Payload equipment commands
15	Encrypted Uplink & Downlink (estimated 5Mbps) [95] via VHF
16	Transponder signal
17-18	Encrypted Uplink & Downlink (estimated 5Mbps) [95] via Satellite
19	Log data
20	Control commands outgoing and status incoming
21	ATC commands and communications
22	Log data
23	External API access

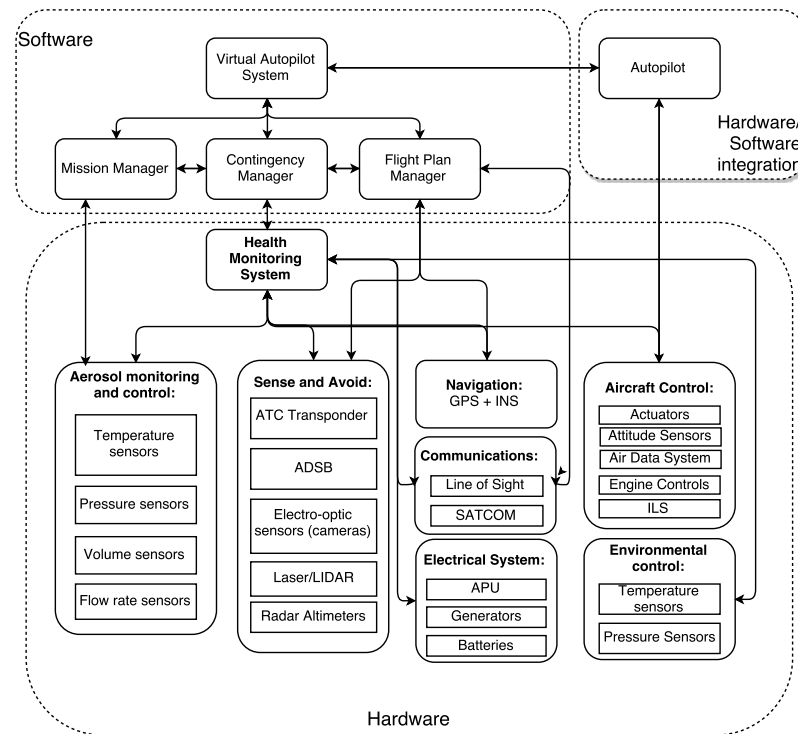


Figure 8.68: Interaction between main hardware and software components

throughout most of the flight, which is in the range of 0 to 5 Mbps³¹. The block diagram of the system is presented in Fig. 8.69.

³¹ URL <http://www.southampton.ac.uk/~jps7/Aircraft%20Design%20Resources/UAV%20Resources/ASE261.09.Comms.ppt> [Accessed 06.06.2016]

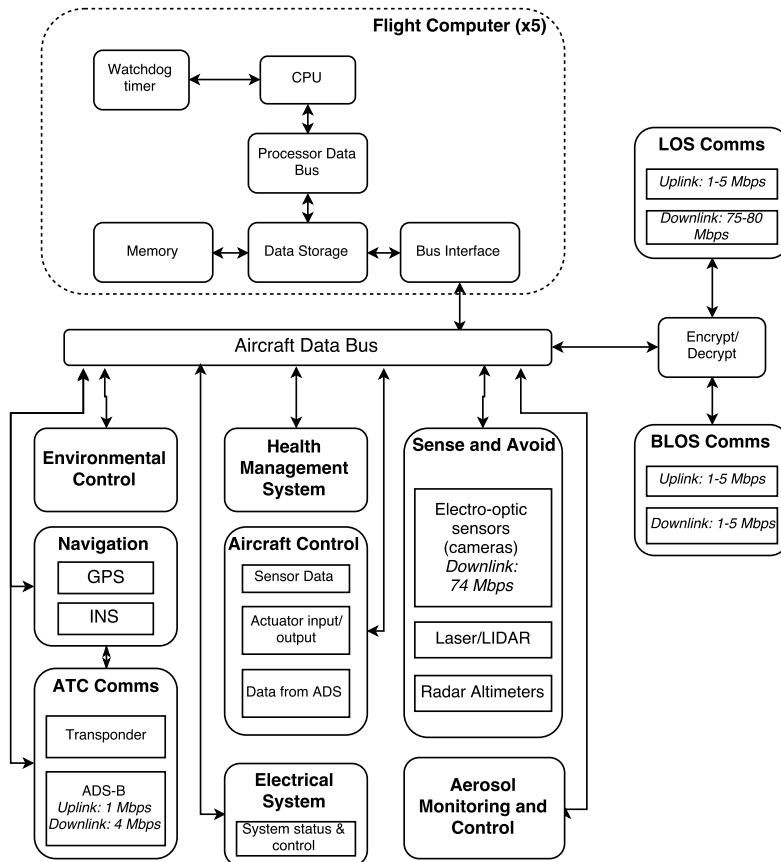


Figure 8.69: Layout of the data handling system

8.9 Aerosol handling system

The SAGA mission is designed to enable the injection of 5 megatons of aerosol in the stratosphere per year. The aerosol material, transportation and dispersion of the payload are therefore an essential aspect of the mission. The goal to decrease solar irradiation must be accomplished by choosing a suitable aerosol material. The aerosol material chosen – sulfuric acid – is a highly corrosive material, imposing constraints on the materials and systems used for aerosol handling. The payload is transported in liquid phase, however, the temperature in the stratosphere is near the freezing point of sulfuric acid. Thermal control is thus required. Furthermore, the requirement to disperse aerosol as a directly condensable gas, creates the need for an onboard heating system to evaporate the aerosol. The design choices made concerning the aerosol will be discussed in the following section, along with the motivations that led to the choices made and their implications.

8.9.1 Aerosol design choices, motivations and consequences

Aerosol material

The aerosol material chosen is sulfuric acid, H_2SO_4 , which will be injected into the stratosphere in gas form. Options for aerosols materials are sulfuric compounds and mineral oxides of different compositions [19]. The main differences between aerosol materials concern effectiveness, environmental impact, technological readiness level and cost.

The concept of solar radiation management using aerosols relies on the establishment of a stratospheric cloud of droplets or particles (from here on used interchangeably) which scatter incident sunlight to increase the Bond albedo of the Earth. The effectiveness of a cloud of aerosol particles depends on the refractive index of the particle compound, particle size and particle concentration [19]. The refractive indices of several possible mineral oxides are higher than the refractive index of sulfuric compounds, theoretically making them more effective in scattering sunlight. However, the presence of a natural analogue for sulfuric acid aerosols –

volcanic activity, known to have significant cooling effects – provides reliability in the prediction of scattering effectiveness [99]. A particle size of around $0.1\text{ }\mu\text{m}$ is optimal, considering high light scattering effectiveness and low infrared absorption, preventing heating of the stratosphere and ozone depletion [19, 3]. In addition, small particles will have a longer life time than large particles, due to their lower descent rate. Mineral oxide particles can be engineered to be of optimal size. Sulfuric compounds will form particles of appropriate size when the aerosol is injected into the stratosphere in the form of a directly condensable gas: gas phase H_2SO_4 [9]. The size of sulfuric aerosol droplets depends on the formation process. The use of non-condensable compounds is inefficient for the forming of aerosols in terms of time and particle size [9]. Assuming a doubling of the CO_2 concentration in the atmosphere is to be counteracted by solar radiation management, using H_2SO_4 instead of SO_2 to achieve the associated solar influx reduction leads to a 50–60% lower injection rate, a reduction of 35% in total injection mass and a sulfur-burden reduction of 40% [9]. Diffusion of engineered solid mineral particles requires research and development of new technologies as carrier gases are required and dispersion needs to be directed, whereas directly condensable H_2SO_4 diffuses automatically and thus has a higher technological readiness level.

The injection of material into the stratosphere influences the environment. One of the main concerns is the possible effect artificially injected aerosols may have on the ozone concentration in the stratosphere. Ozone depletion reactions are dependent on many factors, making it difficult to predict aerosol effects without natural analogues [19, 3]. It is known that higher stratospheric temperatures increase water vapour concentration, facilitating ozone depletion. A sufficiently small particle size is thus essential considering environmental effects as well. Mineral particles can be engineered to be of correct size and can be provided with a chemically inert coating, theoretically decreasing or eliminating reactivity [19]. From the natural stratospheric sulfur analogue was found that volcanic sulfur causes ozone depletion at the poles [100]. This is detrimental, however it is known and can be anticipated; the volcanic analogue enables a more reliable prediction of the effects of aerosol injection. The absence of real-life data on mineral particles creates larger uncertainties about possible reactivity. In addition, the application of inert coatings on microscopic particles is not a mature technique.

The influence of injected stratospheric aerosols on ecosystems is not well known as experiments representing those effects are difficult to conduct [101]. From models and volcanic eruptions is concluded solar radiation reduction in general affects global precipitation levels, regardless of material used [102]. The material-specific effects of deposition of aerosol compounds in surface water and through precipitation can be partly predicted in case compounds naturally present in nature are used. Large amounts of sulfuric acid are brought into the atmosphere by natural and industrial processes and the SAGA mission will only lead to an increase of 4% [1]. Therefore, the contribution to ocean acidification and acid rain due to sulfuric aerosols is not expected to be large. The effect of mineral particles when deposited on Earth is unknown and needs thorough investigation to ensure sustainability of the complete life cycle for both coated and uncoated particle.

Substantial research and development is required to increase the usability of mineral particle aerosols, implying the development cost of this technique is high. In addition, the operational cost is expected to be high due to manufacturing cost, material cost and additional operational difficulties. Sulfuric acid has a much higher technological readiness level. Even though high costs are acceptable in relation to the cost of global warming, sulfuric acid presents the more economical option, and additionally, the uncertainties associated with mineral particles are unacceptably large [19]. Concerning condensable and non-condensable sulfur compounds, the bulk price of H_2SO_4 is about 1/3rd of the price of SO_2 , making H_2SO_4 the more economical option for the sulfuric options³².

Storage configuration

The aerosol precursor material, liquid sulfuric acid, is stored in internal wing tanks at 14.1 m of the semi span. Internal wing tanks are most suitable as the volume capacity of the wing is large enough to accommodate the tanks, bending relief is provided by the weight of the aerosol in the wing and no external changes need to be made to the structure, keeping the outer surface smooth. Several options for aerosol storage were considered, both external and internal. External storage was discarded due to the increase in drag inherent to the installation of extra bodies in the flow. In addition, using external tanks is not necessary as the internal volume of the structure is very large. Different options for internal tanks were identified, based on the location of installation. Fuselage tanks in combination with dispersion from the rear of the fuselage were considered, however, having aerosol systems at the rear of the fuselage would move the centre of gravity backwards, which is detri-

³² URL https://www.alibaba.com/trade/search?fsb=y&IndexArea=product_en&CatId=&SearchText=sulfuric+acid [Accessed 28/04/2015]

mental for stability. Wing storage provides an advantage in the form of bending relief and does not have large effects on the centre of gravity location as wing tanks are located close to the empty-weight centre of gravity location. Summarising, internal wing storage provides most advantages and least disadvantages. The location of the aerosol tank is governed by the requirement of corrosion prevention for the aircraft structure. To ensure the jetstream of highly concentrated sulfuric acid does not come in contact with the structure, the dispersion location must be sufficiently outboard such that maximally deflected streamlines will not be in contact with the most outboard aircraft part; the horizontal tail planes with a semi span of 12.8 m. In the most critical situation – at 18.5 km altitude with a maximum lateral design gust speed of 9.5 m/s [103] and a cruise speed of 210 m/s, the maximum streamline deflection at the tail with respect to the wing is 1.3 m. The end of the tank, where the dispersion system is situated, thus lies 14.1 m outboard.

One tank is installed per wing, which results in a tank volume of 9.6 m³ per wing for a payload of 35,000 kg with a 1% margin for trapped aerosol. In the aerosol tanks, no slosh baffles are required. At 14.1 m spanwise, the width and height of the wing box are 3.3 m and 1.1 m, respectively, resulting in tank dimensions of 3.3x2.6x1.1 m. As the wing has three spars at 14.1 m outboard, the tank is split up into two parts with a width of 1.65 m. To quantify the effects of aerosol sloshing, the maximum centre of gravity shift assuming a simplified case with half-filled tanks and all fuel located at one side shows that the centre of gravity shift at ultimate aerosol position is 0.04 m. This is well within the stability tolerance, thus eliminating the need for additional tank compartmentalisation or slosh baffles. The middle spar divides the tank into two compartments of size 1.65x2.6x1.1 m, resulting in a total tank wall area of 73 m².

Pumps and gauges

The presence of two tanks, separated by the spar, introduces the need for a system connecting the two tanks and controlling the flow between the tanks and between tank and evaporation chamber. Per wing, two electric pulsating pumps are installed. The low aerosol flow per wing, 0.9 kg/s, enables the use of these light, low cost pumps [93]. In addition, pressure gauges and flow gauges are installed to ensure a flow rate of 0.9 kg/s and to ensure all fuel is pumped to one tank during dispersion. For thermal and sloshing purposes, the tanks will be emptied one by one, resulting in one tank being either filled completely or completely empty and one tank with a decreasing aerosol volume. This is beneficial to prevent cooling by maximising the volume per unit wetted tank wall surface area and it decreases the aerosol motion as only one tank is partly filled. In addition, the pressure and flow gauges provide the inputs to an emergency system that shuts off the aerosol flow when the pressure and flow rate deviate from the specified values. The aerosol system layout, showing two aerosol tanks and the smaller evaporation chamber, is presented in Fig. 8.70. Two pipelines are present, connecting the two aerosol tanks and the trailing edge tank to the evaporation chamber.

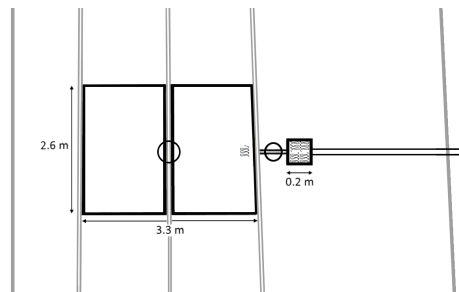


Figure 8.70: Schematic drawing of the part of one wing containing the aerosol systems

Storage tank material

The use of H₂SO₄ in gas form requires specific systems on the aircraft. The aerosol will be transported in liquid form due to volume constraints. H₂SO₄ is a highly corrosive substance, posing constraints on the systems in the aircraft. The storage tank material is to be corrosion resistant and insulating, as the sulfuric acid must be kept at temperatures as high as possible. The chosen tank material is cross-linked polyethylene – XLPE – due to its high corrosion resistance and low weight with respect to metals with the same corrosion resistance. In industry, XLPE tanks are used for storage of highly concentrated sulfuric acid^{33 34}. XLPE is a high density polymer, making it more rigid and corrosion and impact resistant, however the density of 2,200 kg/m³ is still significantly lower than general metal densities in the order of 8,000 kg/m³. Ceramics were considered but

³³ URL <http://www.polyprocessing.com/chemical-storage/sulfuric-acid/> [Accessed 10/06/2016]

³⁴ URL <http://www.rawtanks.com/technical-specs/why-polyethylene.html> [Accessed 12/06/2016]

discarded due to low impact resistance and high density [104]. Also metals can provide corrosion resistance, in combination with high strength and impact resistance and good sustainability characteristics³⁵ [104]. The most suitable metals are stainless steel, carbon steel or cast irons, of which alloys specifically developed for sulfuric acid resistance exist^{36 37} [104, 105]. The major drawbacks of metals are their high thermal conductivity and high density [104]. Composites were discarded due to the small amount of literature available on corrosion resistant composites and the associated low technological readiness level.

Thermal control and insulation

The aerosol will be heated to 516 K (300 K above the stratospheric temperature) on the ground using solar energy and loaded in the aircraft at this elevated temperature. In addition, one immersion heater with a capacity of 120 kW will be installed in the trailing edge tank which will be operational in the last hour of the dispersion cruise only. Finally, two emergency heaters will be present per wing, one in each tank compartment, to be switched on when the temperature drops below a specified minimum threshold value of 300 K. The elevated loading temperature and the thermal insulation of the tank (see below) eliminate the need for continuous background heating in the tank. The chosen aerosol material has an atmospheric freezing point of 283 K [106], which is well above the temperature of 216 K in the stratosphere, which necessitates thermal control during flight. In addition to that, the requirement to disperse the sulfuric acid in gas phase introduces the need to evaporate the aerosol before dispersion. Therefore, the baseline temperature of the aerosol is kept as high as possible, to reduce the power required for evaporation. The temperature of the aerosol in the tank decreases gradually during the outgoing cruise and during dispersion the cooling rate increases as a consequence of the reduction of aerosol volume in the tanks. In the last part of the dispersion cruise, the aerosol in the tanks cools down very quickly and reaches temperatures that pose a risk for freezing. Therefore, the aerosol in the tanks will be heated during the last hour of the dispersion, requiring a power of 90 kW continuously to keep the temperature constant until the end of dispersion. In Fig. 8.71 the mass of the fuel required for evaporation power at the most conservative condition (end of dispersion), as a function of aerosol ground temperature (starting value, x-axis) and aerosol tank wall mass (y-axis) is shown. For a fixed ground temperature, the required fuel mass for evaporation power decreases with increasing wall thickness. The increase in tank mass due to the larger thickness, however, is much larger than the decrease in required fuel mass. Therefore, the overall lightest option is a tank wall with minimum thickness. For the dimensions of the tanks, a minimum XLPE thickness of 2.5 mm suffices, resulting in a double tank wall of two 2.5 mm XLPE walls, separated by an air layer [107]. The thermal conductivity k W/m·K of XLPE is 0.4, whereas air has a k of only 0.02, resulting in a total thermal conductivity of 0.038W/m·K [108] [109]. To provide radiation insulation, a low-emissivity layer of silver is applied to the outside of the tank, reducing the total emissivity of the two XLPE walls ($\epsilon = 0.91$) to 0.025 [108].

The thermal control system contains temperature sensors in every tank, monitoring the temperature and providing input to an emergency system that activates the redundancy heaters when temperatures drop below the specified minimum value of 300 K. In case of unsolvable problems with the temperature or heating system, the emergency system will halt all aerosol operations.

Evaporation

Dispersing the aerosol in gas form requires an onboard evaporation system, able of evaporating the aerosol material at the dispersion rate, equal to 2.1 kg/s. The heating system chosen is electric resistance heating. Electric resistance heating approaches an efficiency of 100%, thus minimising the power required to evaporate the aerosol [110]. The alternative heating options considered - combustion heating, dielectric heating, laser evaporation and electron beam evaporation - were deemed unsuitable. Combustion heating using heated air and heat exchanger loops has an efficiency of lower than 50%, creating a very high power need [111]. Sulfuric acid has very good dielectric properties, making dielectric heating a suitable method [112, 113]. However, the system required for dielectric heating, establishing a continuously rotating electric field, has very low technological readiness level at this scale, making the uncertainties associated very large [113]. Furthermore, the risk of interference of with electric systems renders this method unsuitable. Both laser evaporation and electron beam evaporation require enormous amounts of power or voltage, amounts that are impossible to generate on board of the aircraft[114, 115, 116].

Electric resistance heaters in the form of immersion heaters will be inserted in a small volume of liquid aerosol in the so-called 'evaporation chamber'. The volume of liquid in the evaporation chamber will be 5 litres con-

³⁵ URL <http://www.worldsteel.org/steel-by-topic/sustainable-steel.html> [Accessed 22/04/2016]

³⁶ URL <http://www.bssa.org.uk/topics.php?article=33> [Accessed 22/04/2016]

³⁷ URL <http://www.tampabaysteel.com/metal-products/stainless-steel.html> [Accessed 22/04/2016]

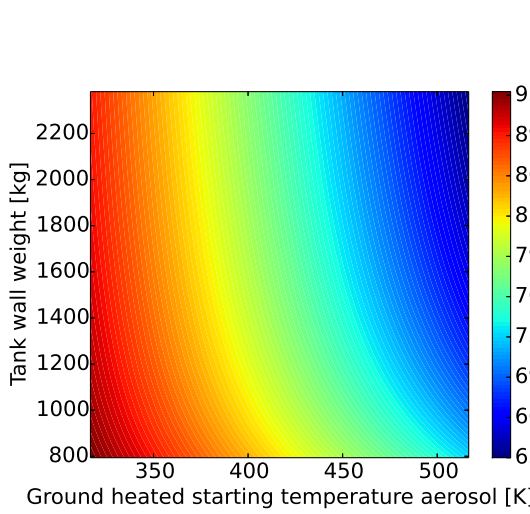


Figure 8.71: Response surface showing the effect of tank wall thickness and starting temperature on fuel required for evaporation power

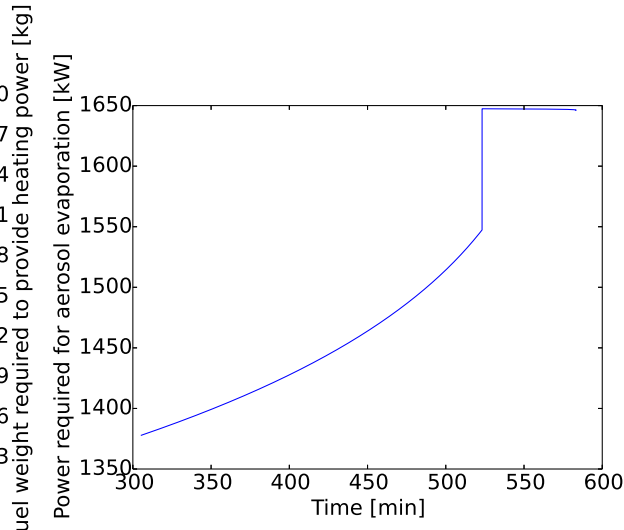


Figure 8.72: Power required for aerosol evaporation during the dispersion part of the mission as a function of time

tinuously, having an evaporation outflow of 2.1 kg/s and a liquid inflow of 2.1 kg/s. The liquid in the evaporation chamber will be boiling continuously, at a temperature of 505 K. The volume of the evaporation chamber is kept as small as possible as the conductive heat losses increase steeply with increasing tank wall area, dominating the required evaporation power. The heating power required during the largest part of the dispersion cruise is the power required to keep the liquid in the evaporation tank boiling is equal to the losses due to conduction, radiation, influx of colder aerosol and the latent heat - energy lost to evaporating molecules. To establish the required evaporation rate of 2.1 kg/s, the power required as a function of mission time is shown in Fig. 8.72. Only the second half of the mission is shown, in which dispersion and thus evaporation is occurring. A margin of 10% is added to account for fluctuations in power and power required for pumping. In addition, to heat the initial, cold volume of 5 l aerosol in the evaporation tank to boiling temperature at the start of dispersion, 279 kJ of energy is required. With the power system installed, an energy of over 2 MJ can be generated easily, meaning the energy required for heating of the volume to boiling temperature at the beginning of dispersion can easily take place in one second. However, taking into account the delay in heating due to imperfect mixing and diffusion, the initial heating will take place in 5 to 10 seconds.

Evaporation chamber

The volume of the evaporation chamber is equal to 1.5 times the volume of liquid aerosol present in the chamber, to account for the expansion of the liquid during boiling and the presence of some vapour in the chamber. This results in a volume of 7.5 litres and a chamber of 0.17x0.17x0.26 m. The high temperature and the movement of the sulfuric acid in the evaporation chamber impose more stringent corrosion resistance requirements on the evaporation chamber material. The small size of the evaporation chamber enables choosing a higher density material with better corrosion properties. The inner wall of the evaporation chamber is made of Monel 400, an alloy of nickel, copper and small amounts of other metals [117]. Monel 400 has very good corrosion resistance properties in combination with low temperature sensitivity and associated constant mechanical properties over a wide range of temperatures. It is specifically suitable for highly corrosive substances at boiling temperatures [117]. The high thermal conductivity of Monel 400, 26 W/mK³⁸, however, requires an insulating layer to reduce the power required to keep the aerosol boiling. A layer of XLPE is applied, separated from the Monel layer by a layer of air. The small chamber size enables a thick insulation layer as the weight increase is negligible compared to the total aircraft weight. The wall composition consists of a 2 mm layer of Monel, a 5 mm layer of air and a 3 mm layer of XLPE, reducing the thermal conductivity to 0.039 W/mK.

In each evaporation chamber, eight immersion heaters are installed, with a maximum required power of 90 kW per heater at the end of dispersion (largest power required) and a power density of 15.5 W/cm² [118]. The mass of the heating system increases with number of heaters, however, the increase in weight when using

³⁸ URL http://www.engineeringtoolbox.com/thermal-conductivity-d_429.html [Accessed 11-06-2016]

eight heaters instead of one heater per wing constitutes an insignificant 0.2 % of the total aircraft weight. Using eight off-the-shelf heaters with a capacity of 120 kW per wing results in a total heater weight of 800 kg³⁹. The benefits of spreading elements throughout the volume in terms of mixing and diffusion, the lower required power per heater and associated lower risk of overheating motivate the choice for eight heaters spread through the substance. The outlet of the evaporation chamber is directly connected to the outside air, as the constant evaporation rate will automatically cause vapour to be released from the evaporation chamber at the same rate. The pipeline connecting the evaporation chamber with the outside air consists of the same material combination as the evaporation chamber, and with a reasonably small diameter, a portion of sulfuric acid gas will have left the line in one second or shorter, causing the cooling rate during this part of dispersion to be negligible.

Dispersion

The dispersion location is at the trailing edge of the wing, 14.1 m outboard. A short rigid tube, attached to the wing and in direct contact with the evaporation chamber leads the vapour from the evaporation chamber to the outside air. This dispersion method introduces little to no additional complexity and the amount of pipelines and pumping is reduced to a minimum, resulting in low system weight and low risk of condensation of the vapour while still within the structure. Several dispersion concepts were considered, including dispersion from the rear of the aircraft and extensible booms or hoses. Dispersion from the rear of the aircraft requires more pumping and pipelines with the aerosol tanks located in the wings. Storing aerosol in the fuselage was discarded for stability reasons (cf. Section 8.9.1). Extensible hoses and booms require additional structural reinforcements and extension/retraction mechanisms leading to higher complexity and weight.

8.9.2 Verification and validation

Most of the analysis done for the aerosol consists of basic physical relations. Numerical programs were used to determine the energy loss throughout the mission for different starting temperatures and thicknesses, for the comparison of heating systems of different compositions and to investigate the effect of various factors on total aerosol systems weight and power required. All outputs were verified using analytical calculations, resulting in discrepancies below 2%, only due to rounding errors. Furthermore, the response of the programs to a change in input was verified with known relations stemming from analytical formulae or physical models, meaning that e.g. an increase in thermal conductivity of the tank walls whilst keeping other inputs constant, should lead to a similar increase in conductive losses. Linear relations used for cost and weight of systems, based on data sheets were verified by personal correspondence with industrial suppliers of XLPE tanks for sulfuric acid storage and industrial immersion heaters confirmed the use of systems as to be implemented in SAGA^{33 34 39} [118]. The values determined from data sheets were compared with values supplied for custom made components. Discrepancies of below 3% were found, indicating the sized components are realistic and commercially available. Additionally, the usage of similar tanks and immersion heaters in industry validate their applicability.

³⁹ URL [Personal communication with Kurval, distributor of Watlow products](#) [Accessed 12/06/2016]

8.9.3 Sensitivity analysis

The aerosol system is dependent on the mission characteristics, in the sense that the requirements on aerosol dispersion follow from the payload and the range over which the aerosol is dispersed. A modification of the payload will affect the aerosol system characteristics, as a different tank volume is required and a different dispersion rate will be used. These parameters affect all operations, as the payload volume and tank wall area determine the cooling rate of the aerosol in the tanks, which affects power, as severe cooling requires more power in the evaporation phase. Furthermore, the dispersion rate of the aerosol, depending on payload and dispersion range, determines the flow through the evaporation chamber, thus determining the amount of evaporation required and the amount of cool flow coming in - the two parameters that dominate the evaporation power requirement. Different power requirements and different tanks result in a variation of aerosol systems weight with payload. In Fig. 8.73 and Fig. 8.75 three plots are shown, showing the required power for aerosol delivery for payloads varying from 10,000 kg to 60,000 kg (8.73 and 8.74) and the total systems mass for the same range of payloads (8.75).

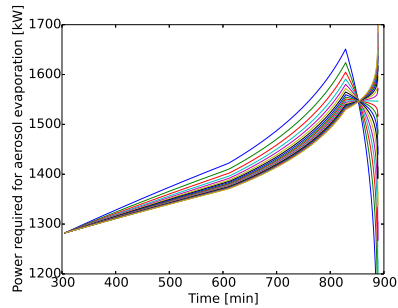


Figure 8.73: Power required for aerosol evaporation during the dispersion part of the mission as a function of time for different payloads

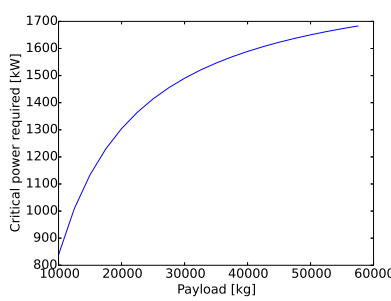


Figure 8.74: Critical (highest) power required for aerosol evaporation as a function of payload

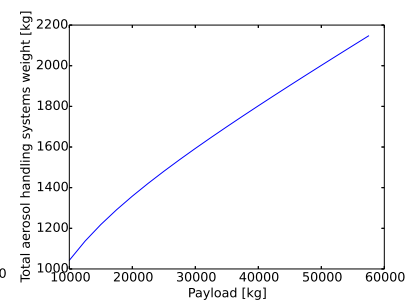


Figure 8.75: Weight of the aerosol handling systems as a function of payload

9. Verification and validation

This chapter provides a summary of the verification and validation of several stages of SAGA's development. SAGA has a highly constrained design space, requires a high level of performance, seeks to achieve a mission of considerable global importance and carries a potentially environmentally hazardous payload. Therefore, ensuring that the methods and results in this preliminary design report are implemented correctly and reflect reality is of crucial importance. The discrepancy handling plan for this process is presented in Section 9.1, while the verification strategies and results are included in Section 9.2 and Section 9.3. The validation strategies and current results are outlined in Section 9.4. Equally important is verifying that SAGA's final preliminary design meets all the predefined requirements for its mission. The requirements compliance matrix and subsequent feasibility analysis are included in Section 9.5 and Section 9.5.1 for this purpose.

9.1 Handling of discrepancies

When comparing calculated results with reference values, it is expected that discrepancies occur. Having this in mind, it is important to define what difference is acceptable. This difference has to take into account the type of verification or validation procedure, implying different thresholds are used. When comparing the calculations to real cases, a threshold of 10 to 15% is used depending on the extensiveness of the assumptions used. In future-stage validation, when simplified cases are compared to complex simulation results (e.g. CFD, X-Plane) this difference is reduced to 10%. Finally, for situations where the same assumptions and same calculations are used, the discrepancy should not be higher than 1%, only to account for decimal accuracy.

If the discrepancies are found to exceed the limits defined, the calculations are analysed. If errors are found, the code is revised. Calculations can also be entirely correct, but simply not accurate enough. In that case, the validity of the underlying assumptions is examined and modified where necessary. If the discrepancies still exceed the acceptability limits, a new method must be used if available and feasible to implement. In the worst case scenario where the results can not be improved to an acceptable level of accuracy, it must be made clear that the results should be used with care and that more investigation is needed. This also applies to evaluating risks and contingencies.

9.2 Verification strategies

Verification is divided into code verification and solution verification. The former concerns itself with ensuring no coding errors such as integer/float division, syntax errors or other unexpected computer processes prevent correct calculations. For this purpose, the design team switched to the PyCharm IDE for Python coding¹, which displays syntax errors and malpractice warnings pre-runtime and incorporates a powerful debugging tool. Print-statements and graph-visualisation of all programs are also carried out in parallel with the coding.

9.2.1 Unit tests

Solution verification is divided in unit tests and system tests. The unit tests considered in this context entail the basic tests conducted at function definition level. At the lowest level, each function featuring in the computations is subjected to a sanity check with comparable, simplified theory. This involves reducing distributed forces to point loads, using average geometries and first-order methods and checking for expected critical points, zeros or asymptotes for all design departments.

9.2.2 System tests

Once the individual units are tested and are verified, system tests are carried out to ensure the results obtained are still correct after integration of the unit code blocks. The system tests performed in the multidisciplinary

¹ URL <https://www.jetbrains.com/pycharm/> [Accessed 19.06.2016]

optimisation context involve both intra-disciplinary integration of calculation procedures and high-level integration of all the disciplines. To save time, this is tested by checking the solution after each block is added to the main code file. If a problem occurs, checking interactions by taking two units at a time is performed until the problem is identified. Finally, when all modules are integrated and the checks have been performed, the systems are tested for robustness to ensure the system responds to changes from the nominal testing values as expected and can handle special cases. Examples include changing the payload mass, the cruise altitude, and the range on the one hand and setting the payload mass to zero, the airspeed below the stall speed and the centre of gravity out of the stability region on the other hand. For the unfeasible cases, the program is to give a warning to the user. In addition, sanity checks are performed with every calculation to ensure local conformation.

SUAVE's zero-fidelity, relatively simple calculation methods with an easily modified input range serve as an adequate verification tool for many divisions. However, since the different technical specialist departments make use of different tools and techniques for their analyses, they also employ specific strategies for their system testing. As SUAVE is validated for conceptual design [16], it is a reliable comparison tool at this stage. However, because SAGA is an unconventional aircraft and SUAVE still relies on first-order methods with limited scope, its validity is critically assessed in the verification.

The performance department, mainly working with SUAVE, employs the integrated SUAVE unit test suite and inspection of the vehicle object tree to verify all the method blocks within SUAVE with the given set of parameters, checking that no method's scope is exceeded. The aerodynamics predictions of VLM-empirical airfoil database calculations are also compared with first order models in SUAVE to verify lift and drag prediction at critical mission points and to gain better understanding of the limits of the SUAVE model. In addition, SUAVE is used along with GSP to verify the propulsion calculations, while the structures department makes use of relevant handbook methods to verify its wing weight predictions. The predicted aircraft eigenmotions are verified with simplified hand-calculations and through SUAVE comparison, as is static aeroelasticity. The flutter analysis in NeoCASS is verified with an eigenvalue analysis, again over the range of critical conditions of the mission.

9.3 Verification results

Since the volume of the results of the conducted unit tests exceeds the present space constraints and were favourable to the extent that system verification was largely successful, this does not warrant a detailed discussion and focus is instead placed on the system tests. The final SUAVE configuration was found to be realistic and sensible, as all internal tests of the features and methods passed the test suite and the data structure fully complies with the final design parameters.

Aerodynamics is largely verified successfully, with the sole large discrepancies stemming from SUAVE's underestimation of the chosen airfoil's performance in outgoing cruise and landing, with no severe impact on the mission predictions. Propulsion verification revealed SUAVE neglects turbine cooling. Once turbine cooling is implemented in SUAVE, the results compare very well to the developed program's predictions.

Aeroelasticity is successfully verified, as similar trends are observed in the models. Discrepancies are traced to differences in the models' assumptions on mass, wing clamping and strut implementation. It should be noted however that these results are with large uncertainty due to the complexity of aeroelasticity and the shortcomings of the methods and that an additional uncertainty is introduced by the implementation of the strut, as the strut is likely to lead to asymmetric, hardly predictable, loading cases.

For stability & control, all eigenmotion predictions were successfully verified, with the exception of the aperiodic roll. The difference between solution and verification found for the aperiodic roll is attributable to the simplifications used for the analytical verification method.

Summarising, the system verification largely confirms the application of the various analysis methods. Whenever this is not the case, a satisfactory explanation of the difference and its impact on the design is included, to the extent that the overall system is considered verified.

9.4 Validation strategies and current results

After the final design has been completed, validation takes place. At this design stage, the validation efforts mostly rest on comparing the aircraft design with relevant references to ensure that the design is realistic.

In the context of performance, this means ensuring the SUAVE analysis stays within the validated scope of its methods. When this is confirmed, it can also serve as a validation platform for all the modules it firstly verifies.

The aerodynamics validation through wind tunnel data rejects Xfoil analyses of the airfoil and took its place directly in the analysis. Propulsion validation is problematic, since existing engine data are hard to access. However, a general comparison with the existing GE-90 engine and intensive consulting with experts confirm the general feasibility characteristics of the engine. The structures wing weight module is validated with several existing slender-wing aircraft and show XXX. NeoCASS's aeroelastic predictions are at this stage validated with reference trend lines and similar aircraft that confirm the predicted trends. Finally, the eigenmotions rely on SUAVE's validated eigenmotion predictions and show significantly larger differences than the verification procedure.

Implementation of the above validates the critical aspects of SAGA's design. However, at the current stage of the project, the level of fidelity cannot be raised to a full-scale, detailed validation. For this purpose, a built prototype has to be available.

To fully validate the aerodynamic properties, the stability and control characteristics and the performance of the engine and the aircraft, a proper validation should be carried out in an upcoming design phase. The aerodynamic and engine characteristics can be validated with the use of a model of the aircraft in a readily available CFD Software. FEM analysis can improve the structural wing analysis. Validation of the stability and control characteristics could be achieved by inserting an aircraft model into a simulator, which makes a prediction of the aircraft's characteristics based on its shape, using aerodynamics theory. An example is the X-Plane simulator, which can create the aircraft model with relative ease. Furthermore, comparisons between actual flight test data and simulation data conclude that it is an accurate tool [119].

9.5 Requirements compliance matrix

The requirements compliance matrices in Tables 9.1 to 9.3 contain all SAGA's requirements and indicate with a tick mark that a requirement is met. When the requirement is not met, the actual value achieved by the design is given. The reference column indicates the section where a given requirement is verified. In case a requirement is not met, the feasibility analysis in Section 9.5.1 presents rationale why the design does not meet the requirement or describes what modifications are necessary.

Table 9.1: Operational requirements

Req. ID	Requirement	✓	Reference
SAGA-AC-AD-01	The lifting surfaces must provide sufficient lift in all mission phases given by performance requirements	✓	Section 8.3.7
SAGA-AC-AD-02	Wing drag divergence shall be below Mach 0.72	✓	Section 8.3.3
SAGA-AC-CS-11	Maximum aircraft center of gravity shift shall be limited to 15% of the mean aerodynamic chord	✓	Section 8.7.1
SAGA-AC-ST-19	The tank and wingbox material shall be resistant to aerosol temperature in all conditions	✓	Section 8.5.3
SAGA-AC-ST-20	Struts supporting the wing should withstand the ultimate load on the aircraft without yielding	✓	Section 8.5.1
SAGA-AC-PR-01	Propulsion system shall provide sufficient thrust for the aircraft in all conditions and mission phases	✓	Section 8.4.2
SAGA-AC-PR-02	Propulsion system shall support the payload electrical power draw in the spraying cruise phase and climbs	✓	Section 8.4.2
SAGA-AC-EQ-11	Aerosol handling system shall be resistant to corrosive effects of the aerosol during aircraft lifetime	✓	Section 8.9.1
SAGA-AC-EQ-12	Aerosol shall remain fluid during flight	✓	Section 8.9.1
SAGA-AC-EQ-13	During dispersion cruise, continuous dispersion rate of 0.01 kg/m shall be maintained	✓	Section 8.9.1
SAGA-AC-ST-14	The structure shall be resistant to corrosive effects of the aerosol after distribution.	✓	Section 8.5.3
SAGA-AC-ST-15	The minimum service life shall be at least 60,000 flight hours.	✓	Section 8.5.3

SAGA-AC-ST-17	The structure shall be able to withstand the payload weight.	✓	Section 8.5.1
SAGA-AC-ST-18	The structure shall withstand the pressure and temperature of the aerosol in any operational scenario.	✓	Section 8.5.3
SAGA-MIS-01	The system shall disperse the aerosols in the tropical region, between 30° N and 30° S latitudes.	✓	Chapter 4
SAGA-MIS-02	The dispersion rate shall be in the range from 0.003 to 0.1 kg m ⁻¹ .	✓	Section 8.9
SAGA-MIS-03	The fleet size shall consist of at least 344 aircraft.	✓	Chapter 4
SAGA-MIS-04	Each aircraft shall be able to carry a payload of at least 35 tons.	✓	Section 8.2.3
SAGA-AC-EQ-04	The aircraft shall be able to perform CAT II/III landings and departures with less than 550m RVR	✓	Section 8.8
SAGA-AC-EQ-05	The aerosol handling system on the aircraft shall monitor the temperature in the aerosol tank	✓	Section 8.9.1
SAGA-AC-EQ-06	The aerosol handling system on the aircraft shall monitor the temperature in the aerosol heating chamber	✓	Section 8.9.1
SAGA-AC-EQ-07	The aerosol handling system on the aircraft shall regulate the temperature in the aerosol heating chamber	✓	Section 8.9.1
SAGA-AC-EQ-08	The aerosol handling system on the aircraft shall monitor the aerosol dispersion rate	✓	Section 8.9.1
SAGA-AC-EQ-09	The aircraft shall support communication between the aircraft and the ground operator.	✓	Section 8.8
SAGA-AC-EQ-10	The aircraft shall be able to determine its position.	✓	Section 8.8
SAGA-AC-PF-01	The aircraft shall have a service ceiling of 20 km.	✓	Section 8.2.4
SAGA-AC-PF-02	The aircraft shall operate from runways less than 2500 m at sea level at all operational conditions.	✓	Section 8.2.4
SAGA-AC-PF-03	The aircraft shall have an operational radius of 3,500 km.	✓	Section 8.2.3
SAGA-AC-PF-04	The aircraft shall have a cruise speed of 210 m/s	✓	Section 8.2.3
SAGA-AC-PF-05	The aircraft shall have a maximum time to altitude of 35 minutes.	✓	Section 8.2.4
SAGA-AC-PF-06	The aircraft shall have a wing loading which ensures that the aircraft can operate throughout the entire range of the desired flight envelope.	✓	Section 8.2.1
SAGA-AC-PF-07	The aircraft shall have a thrust to weight ratio which ensures that the aircraft can operate throughout the entire range of the desired flight envelope.	✓	Section 8.2.1
SAGA-AC-PF-08	The aircraft shall have a lift to drag ratio, which enables it to fly for the required maximum range and endurance.	✓	Section 8.3.2
SAGA-AC-PF-09	The aircraft shall have a specific fuel consumption of less than 23 mg/Ns at 20,000m altitude.	✓	Section 8.4.2
SAGA-AC-SM-01	The aircraft shall perform active system monitoring during operations.	✓	Section 8.8
SAGA-AC-SM-02	The aircraft shall perform active engine monitoring during operations.	✓	Section 8.4.2
SAGA-AC-SM-03	The aircraft's systems shall have a level of redundancy which ensures that no catastrophic failures occur.	✓	Chapter 13
SAGA-AC-SM-05	The aerosol flow shall be automatically shut off in case of a dispersion system failure	✓	Section 8.9.1
SAGA-AC-SM-06	The aircraft shall be equipped with a flight data recorder.	✓	Section 8.8
SAGA-AC-SM-07	The aircraft shall be subject to an A check in the range of 80-120 flight hours.	✓	Chapter 13
SAGA-AC-SM-08	The aircraft shall be subject to a B check in the range of 500-600 flight hours.	✓	Chapter 13
SAGA-AC-SM-09	The aircraft shall be subject to a C check every 24-30 months.	✓	Chapter 13
SAGA-AC-SM-10	The aircraft shall be subject to a D check approximately once every 6 years.	✓	Chapter 13

SAGA-STL-14	The amount of acidity in the precipitation shall have a minimum effect on society and the natural environment, in agreement with all parties.	✓	Section 8.9.1
SAGA-STL-15	The aircraft fleet shall be produced with sustainable materials where possible.	✓	Section 8.5.3
SAGA-STL-16	The factories necessary for production shall be designed for sustainability, by implementation of lean manufacturing and self generation of power resources (solar panels, wind turbines, etc.).	✓	Chapter 15
SAGA-STL-17	A sustainable development strategy shall be defined and implemented.	✓	Chapter 14
SAGA-COST-01	The initial fleet cost shall not exceed 50 billion Euros.	114	Section 12.1
SAGA-COST-02	The total fleet annual direct operating cost, excluding the aerosol cost, shall not exceed 10 billion Euros.	✓	Section 12.1

Table 9.2: CS25 requirements

Req. ID	Requirement	✓	Reference
SAGA-AC-AE-01	The aircraft must be free from aeroelastic instability for all configurations and design conditions (CS 25.629)	✓	Section 8.6.1
SAGA-AC-ST-01	The aircraft shall support limit loads without detrimental permanent deformation.	✓	Section 8.5.1
SAGA-AC-ST-02	The elastic deformation of the aircraft shall not interfere with safe operation.	✓	Section 8.5.1
SAGA-AC-ST-03-B	The aircraft shall experience no vibration and buffeting that would endanger the safety of the flight under any operating condition (CS 25.251 (a))	✓	Section 8.6.1
SAGA-AC-ST-04	The strength requirements of the aircraft shall be met at each combination of airspeed and load factor within the boundaries of the representative manoeuvring envelope and gust load diagram.	✓	Section 8.5.1
SAGA-AC-ST-07	The aircraft shall be strong enough to withstand flight loads combined with pressure differential loads.	✓	Section 8.5.1
SAGA-AC-ST-10	The aircraft shall be able to continue safe flight and landing after impact with a 4 lb bird at V_c at sea-level or 0.85 V_c at 2,438 m. (CS 25.631)	✓	Section 8.5.3
SAGA-AC-ST-11	The aircraft shall be protected against the effects of lightning. (CS 25.581)	✓	Section 8.5.3
SAGA-AC-PF-01	The reference stall speed V_{SR} shall not be less than a 1g stall speed.	✓	Section 8.3.7
SAGA-AC-PF-02	The take off distance shall be the greater distance between the required one engine inoperative (OEI) take off distance and 115% of the distance needed for take off with all engines operative.	✓	Section 8.2.4
SAGA-AC-PF-05	V_{2MIN} shall be higher than 1.13 V_{SR} (CS 25.107 (b))	✓	Section 8.2.4
SAGA-AC-PF-06	The aircraft shall achieve the climb gradient specified by SAGA-AC-PC-03-B at V_2 at all operational conditions. (CS 25.107 (c))	✓	Section 8.2.4
SAGA-AC-PF-07	V_2 shall not be less than V_{2MIN}	✓	Section 8.2.4
SAGA-AC-PF-08	The aircraft at a landing configuration shall have a steady climb gradient of 3.2% with the amount of power/thrust available after 8 seconds after the power/thrust setting was changed from idle to the go-around setting (CS 25.119)	✓	Section 8.2.4

SAGA-AC-PF-09	The aircraft shall have a climb gradient at OEI condition in accordance to the number of engines installed and the take off phase.	✓	Section 8.2.4
SAGA-AC-PC-10	The landing distance shall be the longest distance required to come to a complete stop from a 15m altitude above the runway taken from all operational conditions.	✓	Section 8.2.4
SAGA-AC-PC-11	The approach speed shall be not less than 1.23 times the reference stall speed in landing configuration V_{SR0} .	✓	Section 8.2.4
SAGA-AC-PC-13	The aircraft shall have a fuel reserve enabling it to fly for a maximum of 45 minutes at an altitude of 3,048 m (10 000ft) and speed for maximum range (CS 25.343 (a))	✓	Section 8.2.4
SAGA-AC-CS-01	The aircraft shall be safely maneuverable, controllable and trimmable in about all body axes, in all the possible operating conditions, including transition between the conditions, failure of the critical engine and all configurations.	✓	Sections 8.7.2 and 8.7.4
SAGA-AC-CS-03	At forward centre of gravity position, the aircraft shall be able to perform coordinated turns at constant airspeed without stall warnings or any interference with normal maneuvering at critical weight, altitude and temperature.	✓	Section 8.7.2
SAGA-AC-CS-04	At any speed between stall identification and the speed corresponding to $C_{L,max}$ the aircraft shall be capable to pitch the nose down until the stall regime is exited for all aircraft configurations, HLD or power settings.	✓	Section 8.7.1
SAGA-AC-CS-05	It shall be possible to yaw the aircraft such that a change in heading of 15° is possible with the critical engine inoperative in the opposite direction of that engine, with the power required for level flight at 1.3 times the reference stall speed, at the most unfavourable location of the centre of gravity, with flaps fully extended and at maximum landing weight.	✓	Section 8.7.2
SAGA-AC-CS-06	It shall be possible to make 20° bank angle turns with the critical engine inoperative in both directions at 1.3 times the reference stall speed, with the operating engines at maximum continuous power, at the most unfavourable location of the centre of gravity, with flaps in the most favourable climb position, with the landing gear both retracted and deployed, at maximum take-off weight.	✓	Section 8.7.2
SAGA-AC-CS-07	The aircraft shall be longitudinally, directionally and laterally statically stable.	✓	Section 8.7.1
SAGA-AC-CS-08	The static directional stability with the rudder free shall be positive for any speed within the operating speed range of the aircraft.	✓	Section 8.7.2
SAGA-AC-CS-09	The static lateral stability for any landing gear or flap position, with the ailerons free may not be negative until the minimum control speed, and always gradual and adjustable above the minimum control speed.	✓	Section 8.7.1
SAGA-AC-CS-10	Any short-period oscillations or Dutch roll oscillations occurring anywhere between the reference stall speed times 1.3 and the maximum allowable speed must be heavily damped, both with the stick fixed and the stick free.	✓	Section 8.7.1

Table 9.3: Requirements to be verified in future stages

Req. ID	Requirement
SAGA-AC-PF-04	Control of the airplane at the main engine failure speed V_{EF} shall be maintained with only rudder (i.e. no nose-wheel steering), exerting a control force of 667N, and lateral controls to keep the wings level (CS 25.149 (e))

SAGA-AC-PF-03	The decision speed V_1 shall not be less than the main engine failure speed V_{EF} plus the increase of speed prior to the pilot's reaction (CS 25.107 (a)(2))
SAGA-STL-13	The increase in UV-radiation due to geoengineering shall not be more than 5% [120]
SAGA-AC-ST-03-A	The aircraft must withstand any vibration and buffeting that might occur in any likely operating condition up to dive speed V_D .
SAGA-AC-ST-05	The aircraft shall support a landing with limit descent velocity of 3.05 m/s at the design landing weight.
SAGA-AC-ST-06	The aircraft shall support a landing with limit descent velocity of 1.83 m/s at the design take-off weight.
SAGA-AC-ST-13	The structure shall support a crosswind of at least 20 kts.
SAGA-AC-ST-16	The airframe shall be able to undergo at least one lifetime extension programme.
SAGA-AC-CS-02	The control forces required to meet SAGA-AC-SC-01 shall be within the constraints set by the regulating certification specification for unmanned aircraft or manned aircraft, depending on which of these is chosen.

9.5.1 Feasibility analysis

Some of the initial requirements either cannot be verified at this design stage or cannot be met by the current design. An assessment of the severity of not meeting those requirements and a strategy for mitigating the impact or ensuring satisfaction of the requirement in a future design iteration is given below:

- SAGA-AC-ST-05 and SAGA-AC-ST-06: Converting descent velocity to load factor requires detailed knowledge of the landing gear damping, which is not available at this design stage. Therefore, the structure was sized for a 1.3g deceleration during landing [121].
- SAGA-AC-ST-13: Crosswind will mainly affect the vertical tail and fuselage, which were not analysed in detail yet. A preliminary weight estimation of both these components was made to ensure the tail mass is accounted for in the weight budget, eliminating risk. Next to that, the fuselage is non-pressurised and the tail is conventional, which means they are low risk items.
- SAGA-MIS-05: The reduction of global temperature due to aerosol dispersal at a rate of 5 Tg/year cannot be accurately predicted. However, a dispersion of 5 Tg/year ensures a decrease in radiation of between 1 and 4 W/m² [3, 1].
- SAGA-AC-SM-11: Repair parts shall be available on-site.
- SAGA-COST-01: As explained in more detail in Section 12.1, the capital budget is exceeded by 121%. Depreciating the extra costs over the yearly operating costs for 20 years allows to reduce the extra costs by 29 billion Euros. This is clearly not sufficient to meet the allocated budget. Looking at data from existing projects however suggests that the allocated budget is simply too low to be met.
- SAGA-AC-ST-03-A: Buffeting is very hard to predict and requires detailed analyse of the aircraft structure and aerodynamics. Therefore buffeting has to be investigated in future design stages. The strength of any shock waves is minimised by ensuring the drag divergence mach number is never reached (see Section 8.3.3), therefore buffeting is unlikely to cause major problems.
- SAGA-AC-CS-02: The validation of this requirement can be carried out only after the detailed design of the aircraft's actuation system is made. Moreover, this magnitude of the control forces is influenced by the hinges location, and control surfaces aerodynamic and mass balancing, which are determined in the detail design stage.
- SAGA-AC-PF-04 : This requirement can be satisfied only after the detail design of the actuation system is finished.
- SAGA-STL-13: The increase in UV radiation depends on many variables and is very hard, if not impossible, to predict at this design stage. This has to be done by analysing detailed experimental data later on in the design.

10. Sensitivity analysis

In the design of SAGA as outlined in Chapter 8, each subteam addressed the impact of several high-level design parameters on the specific fields, in order to seek out an optimal design within SAGA's narrow design space. This is included in intra-disciplinary sensitivity analyses, generally aiming for a feasible design optimised for minimal fuel consumption to minimise SAGA's environmental footprint and cost. This chapter aims to summarise and integrate these analyses to a holistic, multidisciplinary sensitivity discussion, drawing a number of conclusions on the final design.

The most notable sensitivity analysis considers the effect of aspect ratio AR on the design. As the main driver of induced drag, fuel consumption and thrust, it features a trade off between reducing fuel weight (Fig. 8.9 and Fig. 8.20), increasing structural wing weight to the limit of design feasibility (Fig. 8.38) and reducing the static and dynamic aeroelastic limit speeds (Fig. 8.53). These studies show that increasing AR of the strut-braced design to 15 could be beneficial, since no flutter, control reversal or torsional divergence is expected in the flight envelope, the structural wing weight increase is estimated to 3.1 tons, outweighed by 4 tonnes of fuel savings and a possibly lighter or existing engine. This will be further explored in a future design iteration, but is kept constant at the current stage due to the associated uncertainties and time constraints.

A second overall sensitivity is the effect of introducing a strut in the final design on drag, wing weight, aeroelasticity, propulsion and fuel burn. As visualised in Fig. 8.38 and explained in Section 8.3.6, a strut designed for maximum wing weight reduction offers an overall 500 kg of fuel weight relief, incorporating the drag it adds and wing weight it alleviates. However, the strut adversely preliminarily affects aeroelasticity-driven torsional rigidity by 4.0%, may induce a nozzle effect with the wing intersection that could cause significant shock-induced interference drag, interfere with the engine outlets and itself become subject to hazardous aeroelastic phenomena. Therefore, its overall sensitivity on SAGA should be investigated further in detailed design.

Altitude is the third sensitivity parameter that affects all disciplines. Higher stratospheric altitudes are beneficial for aerosol e-folding time [19] and particle effectiveness [8]. However, the design analysis shows that C_L is extremely sensitive to altitude change and is operating at its limit without increasing V_c . Changing V_c however, is prohibited by the risk of exceeding M_{dd} . Reducing C_L by increasing S to 750 m² adds 1.5 tonnes of wing weight which outweighs 1.21 tonnes of fuel weight savings (see Section 8.3 and Section 8.5). Increasing altitude also increases required sea level thrust due to thrust lapse and decreased optimal bypass ratio for the engine, though this effect is less severe at higher altitudes and the thrust lapse with altitude appears independent of the bypass ratio. Nonetheless, the impact on engine size and added weight further constrains the already limiting lift, again requiring a larger wing, larger engines and inducing a negative snowball effect that would render the design infeasible. Therefore, the final mission with its 3 climbing segments from 18.5-19.5 km represents the highest achievable altitude with the given weight, reflected in the 17 m/s cruise speed margin.

Finally, the sensitivity of payload mass is considered. Employing the 13% weight margin to increase the payload from 35,000 kg to 40,000 kg offers a potential yearly operational cost reduction of \$898 million at \$111 per barrel of fuel. From a performance perspective, the aerosol heating system is relatively insensitive to added aerosol, adding a maximum 100 kW to the nominal power. This falls well within the excess power range that the engine can provide. However, the added payload adversely affects structural wing weight by 100 kg, as higher tip deflections during landing must be accounted for. This slightly reduces the effective available weight margin to increase the payload. Additionally, the effect this has on aeroelasticity can be adverse if the extra payload is mispositioned, while the extra C_M it adds is seen to increase required tail and already constrained wing lift (see sections Section 8.7 and Section 8.3). Therefore, adding payload is potentially feasible with high cost upside, but requires significant iteration, analysis and time resources and is recommended only if these resources are abundant in a future design stage.

Summarising, the high sensitivity of SAGA's design to aspect ratio, the introduced strut, altitude and payload on all design disciplines highlight the complexity of finding a feasible design space for SAGA and ensuring optimal performance within that design space. The current state of the design meets the feasibility constraints, but, as suggested, could still be improved by increasing AR to 15 and the payload to 40,000 kg. This is left as a recommendation for future, detailed design iterations.

11. Risk identification

In this chapter, technical risks will be identified and classified in terms of severity and likelihood of occurrence. For clarity, the identification and classification will be performed in four separate sections: Aircraft risks, operational risks, aerosol-related risks and remaining design risks. The chapter concludes with an overview of the margins included in several of the design disciplines to actively mitigate the design risks.

11.1 Risk map scales

Risk is the product of likelihood and severity of consequence. As it is at this stage very hard to provide absolute estimates of these two parameters, they will be assessed along mostly qualitative scales. High risk items driving the design were presented previously and taken into account during the design. This chapter summarises the current state of both low and high risks. The consequence of a risk item will be rated as negligible (no reduction in technical performance), marginal (small reduction in technical performance), critical (reduction in technical performance, mission success questionable) or catastrophic (mission failure) [122]. The likelihood of an event will be rated as very unlikely (less than once every ten years), unlikely (more than once every 10 years but less than once every year), likely (more than once every year but less than once every day) or very likely (once or multiple times every day).

For some of the to be identified risks, their position in the risk map does not move after implementation of the mitigation strategies and the associated risk decrease. This can be due to two factors. First, mitigation can sometimes only happen in one direction (either probability or consequence), which can prevent the item to move if it is already in the corner. Second, the probability categories are quite large due to the large lifespan of the project. Therefore, an implemented improvement within the category might not be significant enough to move the item to another position in the risk map.

11.2 Aircraft risks

In this section, the risks associated with flying the defined aircraft mission with the given payload are addressed. In this context, disintegration of the aircraft is considered catastrophic, even though disintegration of one aircraft does not have to lead to a failure of the mission as a whole. This choice is made to avoid underestimating the consequence of an aircraft crash, since it carries a large amount of a highly corrosive substance. Strategies to mitigate the risks are presented with the individual risk items.

1. **Engine failure:** The CS-25 requirements stipulate clearly how the aircraft should operate safely in the case of critical engine failure. Therefore, engine failure is critical, but not catastrophic. The likelihood of an engine failing to the extent that it becomes inoperative, based on the FAA's data between 1992-2005 is in the range of once every million flights [123]. With an estimated 143 thousand sorties a year, this amounts to a statistical estimate of a critical engine failure once every 7 years, thus an unlikely event.

Risk mitigation: Engine failure is mitigated by reducing the likelihood, as an extensive inspection and maintenance program will be implemented. Using an existing engine was investigated and found to be possible. This would decrease the risk of engine failure, however it is preferable to use a purpose-built engine in terms of performance. The custom engine was therefore designed within the bounds of current technology as much as possible, such that existing components can in principle be used. Next to that, investigation needs to be carried out to determine the impact of the sulfuric acid on the engine. This will help to design the inspection and maintenance plans.

2. **Fuel run-out:** Little direct consideration has been given to the glide performance of the aircraft and much of its operation is over water and not in the vicinity of any airport. Therefore, fuel running out is considered catastrophic. On the other hand, the high aspect ratio is beneficial for gliding capabilities and L/D of up to 26 could be achieved. The probability of not reaching an airport is therefore reduced.

Risk mitigation: A fuel management and monitoring system with redundancy and strict operations, as well as careful selection of diversion airports should render this a very unlikely scenario.

3. **Failed landing:** A failed landing, where the vertical speed is too high, the runway too short or the aircraft crashes where there is no runway will likely cause catastrophic damage. Failed landing could also occur in case the aircraft weight exceeds the maximum landing weight. This is now more likely to occur since the landing gear is designed for 80% of the MTOW, down from the 95% planned previously.

Risk mitigation: Failed landing is mitigated by structural requirements on the maximum descent rate, the safety provided by the navigation and communication systems and the lengths of the runways at the airports to be used for operation and diversion. It is therefore unlikely to happen. Fuel dumping systems should be implemented to rapidly decrease the landing weight in case of emergency.

4. **Control system malfunction:** If the control actuators, surfaces or computer fails, the aircraft may become uncontrollable. This would be catastrophic for preserving the aircraft.

Risk mitigation: The quintuple redundancy implemented for these systems, and using safe and well-tested software and actuators yields this very unlikely to ever happen.

5. **Ice- or aerosol buildup:** At SAGA's cruise altitude, the risks of icing are very low since atmospheric moisture occurs mostly at low altitudes [124]. If it occurs, this could result in uncontrollability or critical loss of lift. However, the effect would be critical, but not catastrophic, as descending to lower altitudes could melt the (sulfuric) ice.

Risk mitigation: This risk will be dealt with through the implementation of a de-icing system, which has been considered during the design. Also, aircraft skins that prevent the adherence of these chemical compounds can be applied to the design.

6. **Fatigue failure:** As the aircraft will be in continuous operation, elements such as the aerosol tank, the landing gear and the high aspect ratio wing will very likely be subject to fatigue, which can cause catastrophic failure. The likelihood of this happening is hard to estimate, since it depends on maintenance programmes, the materials and redundancy in the structure and the operation intensity.

Risk mitigation: The consequence of fatigue failure will be reduced by ensuring no single points of failure in the airframe or payload-carrying structure exist, according to the fail safe philosophy. Furthermore, the likelihood of fatigue failure will be addressed through frequent inspection and maintenance of fatigue-exposed elements. Active control ailerons can also help reduce the flutter of the wings¹.

7. **In-air collision:** CS-25 requires the aircraft structure to survive impact of bird-like objects, meaning that impact from a bird or a coagulated cluster of aerosol particles should be marginal. Any collision with a larger object could be catastrophic. Taking bird strikes as an estimate, around 112,000 registered worldwide bird strikes took place between 1990 and 2008². With an estimated 80,000 commercial flights every year³, this amounts to one bird strike per 12.9 flights, which indicates a daily probability of occurrence.

Risk mitigation: A brief analysis conducted after the wing design concluded the risk is marginal. This should be confirmed by further analysis. In addition, close inspection of struck areas on the aircraft and analyses of bird patterns around these airports to avoid flocks can reduce the likelihood.

8. **Navigation or communication system failure:** The navigation and communication system is essential to ensure safe operations. Since the aircraft is unmanned, the failure of these systems is catastrophic, as it can no longer be controlled.

Risk mitigation: Quintuple redundancy again should prevent these systems from ever failing, making it very unlikely.

9. **Power system failure:** If the power system fails, an APU should be ready to take over. Therefore, failure is either marginal or catastrophic if the APU also fails. However, only 4 incidents could be found that had this failure since 1998⁴, making this a very unlikely failure mode. Now that the decision has been made to produce unmanned aircraft, failure of the power system is clearly catastrophic since computers are essential to control the aircraft.

¹ URL http://old.seattletimes.com/html/businesstechnology/2016583947_inpersonfitzgerald24.html [Accessed 20/05/16]

² URL <http://www.nytimes.com/2009/04/25/us/25birds.html> [Accessed 28.04.2016]

³ URL <http://data.worldbank.org/indicator/IS.AIR.PSGR> [Accessed 28.04.2016]

⁴ URL http://www.skybrary.aero/index.php/Aircraft_Electrical_Systems [Accessed 28.04.2016]

Risk mitigation: Inserting an APU in the aircraft will already mitigate the consequence of a power system failure. Adding redundancy such as in wiring and fuses should further reduce the likelihood of a full system failure. Batteries and other power generation systems such as RATS should be installed (extra redundancy) to make sure the critical systems can work, reducing the consequences to critical.

10. **Aircraft becomes unstable:** A flight control computer with a scenario for operating outside the predicted flight envelope can reduce the severity of instabilities. However, the impact could still be critical, as unexpected instability scenarios could render the aircraft uncontrollable. Nonetheless, as CS-25 demands both longitudinal, lateral and directional stability under any scenario, this should never occur, even during rapid c.g. shifts.

Risk mitigation: This risk has been addressed during design, to ensure (with stability margins) that the aircraft will never become unstable, even in the presence of large c.g. shifts as the payload decreases significantly throughout the mission.

11. **Fuel evaporation:** The conventional aviation fuel Jet A-1 is used in all calculations. Jet A-1 could however potentially evaporate due to the low pressure, even though preliminary analytical calculations indicated it would not. Uncertainty remains on that matter, the risk is thus categorised as likely. The consequence would be catastrophic, since it means the aircraft would not be able to reach the altitudes it is supposed to spray the aerosol in.

Risk mitigation: An alternative low volatility fuel could be used. It was proposed to use JP-7, which has better properties than the Jet A-1. It is however likely more expensive and requires a special compound to ignite, as explained in Section 8.4.2.

12. **Dynamic wing failure:** Flutter or buffeting could cause catastrophic structural failure of the wing if the aircraft encounters an aeroelastically unstable region of flight. The same applies for gusts. Since the aircraft flies at high altitude, the Mach range it flies in is very small and its aspect ratio is high, meaning that these phenomena are very likely to occur if no countermeasures are taken. Next to that, the strut placement is likely to introduce dynamic asymmetric load cases, which require advanced tools to predict the aeroelastic response.

Risk mitigation: Giving the wing a proper stiffness and mass distribution, as well as implementing control systems could reduce the impact of this phenomenon. Avoiding aeroelastic speed ranges for the eventual design should reduce the likelihood.

13. **Flight at sub-optimal L/D** Not flying as aerodynamically efficiently as possible is potentially critical to the mission's success, as it could prevent flight at the planned cruise altitude and increase fuel consumption beyond acceptable levels. Since it is very hard to continuously achieve this ratio exactly, this is likely to happen every day.

Risk mitigation: Implementing an autonomous controller with this feature will reduce the amount of sub-optimal aerodynamic performance time. Increasing the C_L range for which the C_D is optimal for the required flight performance can also reduce the likelihood. Finally, good monitoring of the aircraft L/D throughout the project is required to ensure that the desired aerodynamic performance is deliverable.

14. **Unrecoverable stall:** Unrecoverable stall is catastrophic, as it very likely leads to a crash. However, the design requirements state that stall shall be prevented and recoverable, hence this is very unlikely.

Risk mitigation: This risk will be mitigated through careful design. Stall warning systems and automatic corrections in case of dangerous angles of attack will be implemented to reduce the likelihood of occurrence. Also, it was verified control surfaces lie outside of any wake of an aerodynamic surface, ensuring full control of the aircraft and reducing the impact.

15. **Loss of control due to liquid sloshing:** Storing liquids (fuel or aerosol) in a large tank can lead to sloshing effects and dynamic forces as well as dynamic c.g. shifts that can potentially make the aircraft very hard to control. Therefore, this could be of critical impact, as it could prevent the aircraft from operating safely. The aerosol tank is designed to keep c.g. shifts at extreme aerosol locations within acceptable bounds, however, dynamic effects due to abrupt short-duration motions can not be defined completely, leaving a risk for dynamic impulsive sloshing effects.

Risk mitigation: A numerical simulation could be performed under different conditions to define the possible responses of the liquid to impulse disturbances and the response of the aircraft to the liquid

response, for both aerosol and fuel movement. In case of unacceptable results, slosh baffles will be installed were necessary. Pumping in both the aerosol system and the fuel system is installed to prevent the presence of half empty tanks as much as possible, reducing the amount of fuel that is able to move to a minimum.

16. **SO₃ production:** A 100% concentration of sulfuric acid, when heated, decomposes partly into SO₃ and water, where the water stays in the solution with sulfuric acid and the SO₃ forms a gas. This decomposition occurs until a concentration of 98.3 % is achieved in the sulfuric acid solution. SO₃ can cause a violent reaction when in contact with water, thus posing a danger when being present in the tank in gas form. The likelihood of this happening is very high when using 100% H₂SO₄-solution. The consequence would be catastrophic since a violent reaction could lead to important sulfuric acid leakage after damaging the tank.

Risk mitigation: The mitigation of this issue is straightforward. Using an aqueous solution of sulfuric acid with a concentration of 98.3% - an azeotropic solution - decreases the risk significantly. This means, however, that more payload will be needed compared to the 100% concentration case.

17. **Engine cannot be produced:** It could happen that no company wants to produce the engines, or that all decide to charge an excessive price for them. On the one hand, the contract would guarantee a sale of at least 1376 engines. On the other hand, the company would unlikely manage to sell that engine model to airlines since it is optimised for the specific cruise conditions of SAGA. To put the number in perspective, 1600 GE90-115B engines were sold in about ten years, but the number keeps increasing^{5 6}. Since the series is therefore rather small, it is likely to have difficulties finding a manufacturer willing to produce the engine. This would be critical since having to rely on current engines would impact all the design areas covered in this report. Quantifying the impact is beyond the scope of this report and is left as a recommendation, but it is likely to lead to a reduction in payload per flight.

Risk mitigation: Covering for the development costs of the engine would allow the manufacturer to make profits on the engine with a guarantee much higher than for its regular engine programs. Since the engines tend to become larger with time, this program would also allow them to investigate large size engines at no cost. This should make the deal much more attractive for the companies, and reduce the likelihood of the risk item from likely to unlikely. Designing the aircraft for different engine options would reduce the consequence from critical to marginal.

Table 11.1: Risk map for aircraft-related risks

Consequence \ Probability	Very unlikely	Unlikely	Likely	Very likely
Catastrophic	8,9,14	2,4,6	3,11	12,16
Critical		1,5	10,15,17	7,13
Marginal				
Negligible				

Table 11.2: Risk map after implementation of mitigation strategies

Consequence \ Probability	Very unlikely	Unlikely	Likely	Very likely
Catastrophic	2,4,6,11,14,16	3		
Critical	8,9,10	1,15	13	
Marginal	5	17	12	
Negligible				7

⁵ URL http://www.geaviation.com/press/ge90/ge90_20141215.html [Accessed 26/06/16]

⁶ URL <http://www.geaviation.com/commercial/engines/ge90/> [Accessed 26/06/16]

11.3 Operational risks

In this section, risks associated with the operations of SAGA are considered. Items marked with an asterisk are taken from [1].

1. **Political disagreements:** This project is planned to last at least 20 years. Dissension about the execution and continuation of the project might arise which will lead to lack of cooperation and eventually the termination of the project, with disastrous effects for the environment. The chances of this happening are, due to the length of the project and the fast changing multilateral relations, likely.

Risk Mitigation: The risk has to be decreased, because the impact and likelihood are too significant. In order to prevent political disagreement, binding treaties should be made and signed by all stakeholder governments. Moreover, by aligning incentives of different stakeholders, the foundation for a long-term and stable cooperation can be established.

2. **Subversive activities:** Due to the controversy of geoengineering, as well as the sensitivity of the cargo, subversive activities might cause a problem. Activists, terrorists or insurgents could infiltrate the facilities or digitally infiltrate the aircraft control systems and disturb the operations or even use the aircraft and aerosol storing facilities as a chemical bomb. The likelihood of attempts for subversive activities is likely and the effects would be critical.

Risk mitigation: In order to decrease the chances of subversive activities, awareness campaigns can be helpful to inform the public and decrease hostile actions from activists. In addition, security, such as guards and fences, at the operational facilities will have to be increased in order to prevent trespassing. To prevent digital attacks on the communication or control infrastructure, cybersecurity should be outsourced to an independent expert.

3. **International certification problems:** After the research and development of the proposed aircraft, it needs to be certified. There is always a possibility that the final design does not meet the certification requirements for whatever reason. Although this is very unlikely due to the careful requirement analysis and an iterative design process, the results would be catastrophic.

Risk mitigation: There is a only one possibility to mitigate this risk, which is ensuring compliance to the requirements for certification. The aircraft either meets all requirements or it does not, and this makes up the difference between catastrophic effects and no effects at all. Integral control during development to ensure satisfaction of the certification requirements is essential.

4. **Exceeding the budget:** A new and more accurate cost estimation concluded that the capital cost will exceed the allocated budget. Due to unforeseen changes in the operational cost, such as an increased fuel price, the operational budget could be exceeded as well. This is likely to happen if no action is taken to prevent this due to unforeseen cost drivers. Moreover, the consequences would be critical but not catastrophic. Due to the significance of the project, extra funds can be attracted.

Risk mitigation: In order to prevent this from happening, significant cost contingencies should be used in order to have a sufficient buffer and prevent exceeding the budget. Capital cost excess was mitigated by depreciating the extra costs over the operational budget. This excess can be further reduced by obtaining interesting deals with manufacturers, which could happen due to the large number of airplanes/engines involved.

5. **Financing problem:** If the consortium of financiers fails to bring up the budgeted funds, the project has to be terminated. The consequences will be catastrophic, although this is not likely to happen since there is a solid financing strategy.

Risk mitigation: In order to prevent this from happening, significant cost contingencies should be used in order to have a sufficient buffer and prevent exceeding the budget.

6. **Limited availability of aircraft:** Due to insufficient maintenance efficiency, missing parts, bad weather or any other reason that keeps aircraft on the ground, it might occur not enough aircraft are operative to perform the average delivery of aerosol at all times. This is not likely to happen as there is a 20% redundancy in the amount of aircraft.

Risk mitigation: The redundancy was already implemented to ensure sufficient availability. Furthermore, maintenance and inspection activities are of importance to ensure the designed-for 80% availability.

7. **Delivering a too small amount of aerosol:** Delivering a too small amount of aerosol into the stratosphere, thus not meeting the requirements has critical consequences on the program and the environment, although this depends on the amount that is missing.

Risk mitigation: Although this is not likely to happen, meeting the right amount is carefully considered in designing the operational program. If the calculated amount of aerosol is not enough to achieve the desired effects, or simply not met, the number of flights should be increased. First by using the 20% redundancy aircraft, which will gradually be replenished by newly built aircraft with possible improvements in payload capacity.

8. **Manufacturing delay:** If manufacturing is delayed, the project cannot be initiated on the proposed time. This will have a critical effect: the project is behind schedule but can still run properly. If there are no measures taken in order to prevent manufacturing delay, this is likely to happen. Implementation of lean manufacturing can help reduce the likelihood of happening.

Risk mitigation: In order to prevent this from happening, significant time contingencies should be used to have a sufficient buffer and prevent the scheduled manufacturing time.

9. **Airport unavailability:** If, due to natural disasters, political issues or economic reasons, an airport becomes unavailable to act as operating facility, this will have critical impact on the project. This means that a section of the tropics cannot be covered and the workload on the other airports significantly increases. Another possible effect could be the need to move operations to another airport, which is costly. The probability of this happening is likely: even though the airports are carefully selected on political stability, there are 2 bases located in Africa where stability can quickly deteriorate.

Risk mitigation: In order to mitigate this risk, backup airports should already be considered, especially for those in Africa. This enables operations to divert, first to already prepared operating facilities and later to newly established facilities. In addition, communication with and coordination of local governments should ensure smooth and stable collaboration.

10. **Insufficient supply of fuel or aerosol:** If logistic operations fail to deliver the required aerosol and fuel to refuel the aircraft, the project will come to a halt. This will delay the project, which is a critical consequence. However, the chance of this happening is not likely, because the airports are picked at locations with a good infrastructure and seaport access. Moreover, aerosol and fuel tanks are installed at the facilities so reserves can be stored.

Risk mitigation: The communication and cooperation with related companies and parties such as governments should be organised and monitored carefully to minimise the chance of unforeseen problems. Redundancy should be present in orders and a back-up storage of fuel and aerosol should be available.

11. **Moral hazard:** A catastrophic risk is the moral hazard of neglecting the need for reduction of greenhouse gas emission, due to the wrong assumption that geoengineering can solve the global warming problem. This will cause the disruption of natural cycles to continue and the concentration of greenhouse gases to keep rising, meaning the cause of climate change is not eliminated and geoengineering cannot be stopped safely. Especially in the case of a sudden halting of geoengineering, this will cause rapid and extreme climate changes, posing a danger for all ecosystems. Moral problems are likely to happen, especially if large corporations or countries will fund the geoengineering project and at the same time feel justified to increase /or not decrease, their greenhouse gas emissions.

Risk mitigation: Education on the project and emphasis on the temporary character of geoengineering and on the need to find a long-term solution are essential. The negative effects of geoengineering should also be clearly presented to reduce the likelihood of moral hazard.

Table 11.3: Risk map for operational risks

Consequence \ Probability	Very unlikely	Unlikely	Likely	Very likely
Catastrophic	3	5	1	11
Critical		6,7,10	2,4,8,9	
Marginal				
Negligible				

Table 11.4: Risk map after implementation of mitigation strategies

Consequence \ Probability	Very unlikely	Unlikely	Likely	Very likely
Catastrophic	3,5	1,11		
Critical	6,10	2,4,8		
Marginal		7,9		
Negligible				

11.4 Aerosol-related risks

This section presents the risks associated with the aerosol handling, as well as identifies the impact of the identified risks. Mitigation strategies are proposed in order to reduce the likelihood, the consequences or both. Note that failure rates for tanks, pipes, pumps and valves are indicative only. The failure rates are defined after comparison of failure rates under different conditions for each element (the largest value is chosen) however, none represent the specific operating conditions of SAGA. The values should be taken as rough indicative failure rates until further investigation refines these estimates.

1. **Tank leakage:** Since sulfuric acid is a highly corrosive material, a leak could cause the entire aircraft to crash if it is not detected in time. It could also cause only small local damage if the leak is found and repaired quickly. For sustainability and cost reasons, the tank is designed to store sulfuric acid and to have a life of at least 20 years. It is found that the failure rate of tanks for small holes is in the order of 10^{-4} per year per tank⁷. Assuming an exponential distribution, less than one tank would fail over the 20 years. Taking this and the design objectives into account, the chance that a tank will fail is thus unlikely. As explained before, the failure rate is not calculated for the specific operating conditions of SAGA and should be taken as an indicative value. It corresponds to the highest failure rate found for the different investigated conditions. This comment is also valid for the following failure rates. The impact will depend on maintenance and inspection plans that are yet to be defined. However, since in the worst case the aircraft could break due to damage initiated by the leak or sulfuric acid could fall on human infrastructure or humans themselves, the consequence will be considered catastrophic.

Risk mitigation: This risk can be mitigated by implementing a proper inspection and maintenance programme that detects and repairs defects on tanks (or pipes, pumps or valves) to reduce the likelihood even further. In addressing the whole system, redundancy can be added to reduce the effect of a faulty item, such as adding two pumps or placing many valves on the same stream. That way, the impact becomes negligible. In addition, the flow rates should be controlled to allow detection of anomalies. Finally, a thin and light coating could be applied to the aircraft structure surrounding the sulfuric acid storing and distributing system to reduce the impact of leakage.

2. **Pipe leakage:** Pipes were found to fail at very low rate as well, with rates of around 10^{-6} failures per year⁷. The same reasoning can be applied here with respect to the likelihood of failure, thus pipes are placed in the very unlikely category. Although it can be assumed that the impact will be lower since a valve could stop the sulfuric acid to flow by closing the valve upstream, worst case scenarios such as the ones considered above could potentially happen. Therefore, the impact will be considered to be catastrophic.

Risk mitigation: See risk item 1

3. **Tank burst:** As mentioned before, sulfuric acid is very corrosive thus the fuller the tank is at the moment of burst, the worse the impact is. Following the safety philosophy applied throughout the project, the worst-case scenario should be considered. The impact should therefore be considered as catastrophic. Tank burst is really not likely to happen since the tank should not be subject to large loads, and will be designed to sustain temperature and pressure variations. Tank failure in this mode was found to have a failure rate in the order of 10^{-6} per year⁷.

Risk mitigation: See risk item 1

4. **Pipe burst:** The likelihood of a pipe burst is larger than for the tank due to the flow velocity which increases corrosion [104], however the impact is reduced since valves should be able to stop the aerosol

⁷ URL <http://www.hse.gov.uk/landuseplanning/failure-rates.pdf> [Accessed 28/04/16]

to flow in the broken pipe. The worst case scenario would still be catastrophic though, thus the two items are placed in the same risk category.

Risk mitigation: See risk item 1

5. **Valve failure:** Valves are found to fail at small rates, in the order of 10^{-2} per year⁷. However, to account for the high corrosiveness of the sulfuric acid, this item will be categorised as likely to fail. Assuming that valve failure affects the distribution only (no leakage), the impact is critical since an extra flight with another aircraft would have to take place in order to spread the remaining required amount of aerosol.

Risk mitigation: See risk item 1

6. **Pipe blocked:** Dirt, ice, or solidified sulfuric acid (due to low temperatures) could block the pipes. This could happen if some acid remains in the pipe, however it would likely not block the pipe completely. A blocked pipe should only affect the nominal aerosol dispersion and not cause any additional impacts as long as there is a mechanism that stops the acid from flowing in the pipe.

Risk mitigation: The risk can be reduced by implementing a wise design such that the pipes are as short as possible (the aerosol has less time to cool down) or heated such that the aerosol does not reach its solidification temperature. A mechanism to stop the aerosol from flowing into the pipe should be installed such that higher pressures than expected in the pipes do not occur.

7. **Pump failure:** Pump failure rates are very low, in the orders of 10^{-4} or 10^{-5} failures per year⁷. The impact should be considered critical, since the aerosol cannot be sprayed by an aircraft with pump failure and another aircraft will have to catch up, thus affecting the mission performance.

Risk mitigation: See risk item 1

8. **Aerosol ineffective:** The aerosol could turn out to not be as effective as planned. Since effects of sulfuric acid have already been investigated and proven to work with models [9], it is unlikely that the aerosol ends up being ineffective. It is important to be very confident about that though, since the consequence would be that global warming is unaffected and temperatures keep on increasing.

Risk mitigation: The likelihood of this happening could be reduced if further investigation is performed. A small scale test and/or more analysis on models can improve the level of confidence on the aerosol effectiveness. The impact can, however, not be reduced unless other climate control techniques are applied.

9. **Aerosol sub-optimal dispersion rate:** The dispersion rate depends on the internal system (pipes, valves, pumps, etc). Since the internal system will be designed for optimal dispersion rate, the risk is rather low. On the other hand, small deviations from the ideal situation always occur in practice. These small deviations will have a small impact on the stratospheric aerosol effectiveness. Overall, the likelihood is high but with a very small effect, while the likelihood of having a large impact due to internal system failure is already taken into account by previous risk items and therefore not considered here.

Risk mitigation: This risk cannot be really dealt with effectively, except by trying to achieve a system that is as accurate as possible and by taking into account the uncertainty related to the system limited precision in the calculations. Again, only the likelihood can be controlled here.

10. **Aerosol sub-optimal area spread:** It could happen that due to operational constraints, certain areas cannot be reached and a sub-optimal area spread results. It could also happen that currents do not spread the aerosol as planned. The likelihood of the first is likely, while the likelihood of the second is more difficult to predict on long time scales. Overall, this will make a local impact that can reduce the performance of the stratospheric aerosol injection but globally the impact should not be significant.

Risk mitigation: This is another difficult risk to deal with. Likelihood to happen can be reduced by promoting laws that facilitate the airspace access necessary to SAGA. Also, regular climate predictions can be performed in order to update the dispersion plan when necessary. Furthermore, careful tracking of mission parameters such as the range and endurance of the aircraft throughout the project should further reduce this item's likelihood. As before, the impact cannot be changed and only the likelihood can be reduced.

11. **Aerosol too expensive:** Sulfuric acid is usually not used as a final product on its own and therefore the market depends on other industries such as the fertiliser industry⁸. Public access to these market prediction reports is not given, however it is not expected to have a significant price increase that would cause SAGA to go over budget. In case it happens, two scenarios are possible. First, the budget is not exceeded by much and the governments simply agree to pay more, in which case the impact is negligible. Second, the budget is significantly exceeded and the governments decide to use a different aerosol or to decrease the amount of aerosol to be dispersed, in which case the impact is very dependent on the decisions taken. The likelihood is also an unknown since these predictions are not accessible. Overall, this item should be marked as high risk, due to the large uncertainty. The worst case scenario where the program is stopped due to the aerosol price is catastrophic. A slight or slow increase of the sulfuric acid price is more likely to occur than a very large peak that would cause an immediate stop of the program. The probability of the sulfuric acid price being larger than expected will be considered as likely. The item is therefore considered as catastrophic and likely to happen.

Risk mitigation: The price uncertainty can be reduced by obtaining (partial) access to those reports. Even if access was obtained, there would still be uncertainty on the price since unanticipated events could cause a sudden large price change. A way to deal with this is to investigate the use of another aerosol which is compatible with the infrastructure and equipment developed for the sulfuric acid. Another option is to obtain a futures contract, which secures the price for future deliveries.

Table 11.5: Risk map for aerosol-related risks

Consequence \ Probability	Very unlikely	Unlikely	Likely	Very likely
Catastrophic	1,2,3,4	8	11	
Critical	6,7	5		
Marginal		10	9	
Negligible				

Table 11.6: Risk map after implementation of mitigation strategies

Consequence \ Probability	Very unlikely	Unlikely	Likely	Very likely
Catastrophic	3,4,8,11			
Critical	1,2,6			
Marginal	7	10	5	9
Negligible				

11.5 Remaining design risks

As explained in Section 8.1.1, focus in the design was placed on a number of high risk items. However, due to the design state being still rather preliminary, some risks and uncertainties remain present. In this section, the remaining aircraft design risks will be discussed. The risk scale will be the same, however the likelihood of the items will carry a different meaning. Rather than representing the probability to occur during a certain time period, it will represent the authors' perception of the problem's likelihood to occur based on the analysis realised thus far.

1. **Engine performance in hot weather:** Warm ambient temperatures affect the engine performance in two different ways. On the one hand, higher temperatures reduce the amount of energy that can be added to the flow since the temperature limits in the engine remain constant. On the other hand, higher temperatures lead to a lower density which leads to a decrease in air mass flow. Both aspects are detrimental for engine performance, and the performance reduction is significant at lower altitudes. The engines are found to still be able to operate throughout the mission at temperatures constantly 20K higher than ISA. Nevertheless, the fuel consumption will be higher and for that reason the risk is considered critical. High temperatures are expected to be frequent at the latitudes where SAGA will be operating, the risk is thus very likely. At altitudes above 15 km however, the temperatures in the tropics are lower than ISA, increasing engine performance⁹.

⁸ URL <http://www.crugroup.com/market-analysis/products/SulphuricAcidMarketOutlook> [Accessed 28/04/16]

⁹ Personal communication P. Siegmund, Royal Netherlands Meteorological Institute, De Bilt, Netherlands

Risk mitigation: Designing the engines to operate in the most extreme temperatures expected could be considered, although this would lead to an overdesigned engine. Another option that should be considered is to have alternative mission plans to cope with large temperature changes. This would reduce the impact of the risk from critical to marginal.

2. **Excessive aircraft weight:** Excessive aircraft weight could prevent the delivery of the required amount of aerosol, as it would require to decrease payload capacity or fuel to keep the MTOW constant. In the context of the mission, this can become catastrophic. Throughout the design process, weight is also likely to increase if no proper mitigation is undertaken.

Risk mitigation: Weight changes in the areas contributing the most to total weight are monitored continuously during the design process. This allows to make gradual adaptations in weight limits and contingencies and eventually obtain a feasible MTOW.

3. **Heating system power provision:** A very large amount of energy is required for aerosol evaporation and to a lesser extent for maintaining a high enough baseline temperature of the aerosol. This large amount of energy needs to be provided by the engines, which are already constrained by the operating conditions. It would be catastrophic if the engines cannot provide sufficient power, since the aerosol could not be dispersed. Since there are four powerful engines, it is unlikely that single engine failure will fatally affect the power provision.

Risk mitigation: The power required to evaporate the aerosol can only be decreased if the dispersion rate is decreased. This has many drawbacks, such as having to reduce the payload or increasing the range (with its associated weight increase). It is therefore better to find ways to obtain more power during flight. This can be done by decreasing the cruise altitude, which decreases the thrust needed and therefore allows the engine to provide more power. Another option is to rely on the APU to provide the missing power, but it should be noted that it is not the most efficient option since the APU will also consume fuel.

4. **Aeroelasticity:** Static and dynamic aeroelastic instability - control reversal, divergence and flutter - are phenomena of which the occurrence has to be carefully investigated and prevented for high aspect ratio aircraft. It is likely that aeroelastic instability occurs in flight when flying faster than the control reversal/divergence/flutter speed, resulting in structural failure of the wing. The consequences of this are catastrophic.

Risk mitigation: In order to mitigate risk of poor aeroelastic properties of SAGA's high aspect ratio wing, the aspect ratio must be kept as low as possible. Aircraft with the current AR of 13 have been designed before and therefore this design is not rendered unfeasible regarding aeroelasticity. A conflict exists with reducing induced drag, which requires to further increase the aspect ratio. An intermediate value which can result in an acceptable performance for both phenomena needs to be found. Moreover, the wing structure should provide enough rigidity to keep the disastrous control reversal, divergence and flutter speeds above the cruise speed. Possible adaptations to the design, affecting the aeroelastic performance of the aircraft are extensively discussed in Section 8.6.2. As a last resort, active flutter control can mitigate the risk of flutter resulting in structural failure, when flutter speed cannot be raised any further.

5. **Strut failure:** The final design's strut inevitably faces an aerodynamic transverse force, which it currently is not sized for. This force in combination with the design loads could lead to strut failure, which can then lead to wing failure. The consequence is thus catastrophic.

Risk mitigation: The analysis has to be extended to ensure all the critical loading cases are considered. This will allow to reduce the likelihood of strut failure. The consequence could be decreased as well, by adopting a fail safe philosophy for the strut. Finally, the maintenance program should include a regular inspection of the struts to detect small defects on time.

6. **Excessive fuel consumption:** This issue would likely lead to a decrease in payload or range, thus increasing the number of flights and therefore the operational costs. If not managed carefully, excessive fuel consumption could become catastrophic. Results from off-design analysis showed that fuel consumption could be larger than expected. This still has to be confirmed when adequate compressor maps become available. Since there is some margin for extra fuel, the engine would have to consume significantly more before fuel consumption becomes a problem. It is therefore rated as unlikely.

Risk mitigation: Strict contingency management on fuel consumption throughout the design phase reduces the likelihood of fuel consumption to grow excessively. Given the nature of the mission, engine

components can be designed to be able to perform relatively well over a large range of operating conditions rather than very well under one specific condition only. This would allow the engine to consume less fuel in off-design conditions, important for the SAGA program as large parts of the flying mission are performed in off-design conditions.

7. **Stalling or exceeding M_{dd} in cruise:** The extremely narrow 12 m/s speed margin between 1g stall and M_{dd} means the slightest change in local weather conditions or gusts could cause either of the phenomena to occur during cruise. This is very likely to occur (cf. Section 8.4 on hot weather or [125] on cold weather), and could be catastrophic, as it prohibits flight at the required high altitude for effective aerosol dispersion.

Risk mitigation: Monitoring of local conditions, implementing an active overspeed warning, stall warning and recovery control system and implementing cruise slats for a larger stall margin are all options that must be considered in the detailed design phase to increase the speed margin. If these options do not mitigate the risk, the cruise altitude may have to be lowered. This strategy reduces the risk to unlikely, yet still critical.

8. **Strut crossing the engine exhaust:** If the strut is in the wake of the engine, this will be detrimental for the strut since the hot gases will damage it. It would also likely decrease the propulsive efficiency of the engine. Overall, this issue is critical and, considering the current situation in the design, very likely to occur. It is of high importance to avoid this, since a damaged strut which loses its structural benefit only introduces drag and weight.

Risk mitigation: A thorough investigation of engine and strut placement should be performed. It is important to make sure that the increased drag and weight of the strut result in a lighter structure overall and less fuel burn. This is a recommendation to consider in future work. Reducing the consequence of strut failure by making the wing capable of sustaining the same loads alone defeats the purpose of the strut. The likelihood should therefore be decreased by allocating sufficient attention to this risk item in the design.

Table 11.7: Risk map for remaining aircraft design risks

Consequence \ Probability	Very unlikely	Unlikely	Likely	Very likely
Catastrophic	3,6		2,4,5,7	
Critical		1,8		
Marginal			1	
Negligible				1

Table 11.8: Risk map after implementation of mitigation strategies

Consequence \ Probability	Very unlikely	Unlikely	Likely	Very likely
Catastrophic	6	2,4		
Critical	3	5,7,8		
Marginal			1	
Negligible				1

11.6 Design margins

The final design of Chapter 7 incorporates several margins on the technical design disciplines as a contingency for uncertainties in technical parameters and potential design improvements explained in Chapter 10. These margins and factors are individually elaborated in Chapter 8 and collected in Table 11.9 for a complete overview:

Table 11.9: Technical design margins

Margin	Value [Unit]	Explanation
Fuel margin	13 [%]	Overall take-off weight margin to ensure weight compliance
C_L margin	0.1 [-]	Wing lift margin for differing engine and wing locations, local air conditions, lift loss due to tip deflection and model errors
Stability margin	0.05 [%c]	Static longitudinal stability margin
Fleet size margin	20 [%]	Additional aircraft margin for maintenance
Operational margin	115 [days]	Inoperative days during the year
Yield factor	2.4 [-]	Boron material strength due to variability, damage and environment
Load factor	1.5 [-]	Ultimate wing load factor
Weight factor	1.5 [-]	Avionics components safety factor
Weight factor	1.3 [-]	Landing gear weight safety factor
Rotation margin	1.46 [deg]	Rotation angle margin
Power margin	15 [%]	Critical power draw margin from the engine
Aerosol heating margin	10 [%]	Aerosol heating power margin

12. Resource allocation

This chapter will address the development and operational costs of the SAGA project, as well as present a cost breakdown structure diagram to give the reader a quick overview of the major cost components. Budgets will then be addressed for other parameters such as mass and power to complete the discussion on resource allocation.

12.1 Cost breakdown

In order to present the total costs of the delivery system, a cost breakdown structure can be made, listing all the expenses that are part of the system's lifetime. This list, the cost breakdown structure, can be found in Fig. 12.1 (based on [126] and [127]).

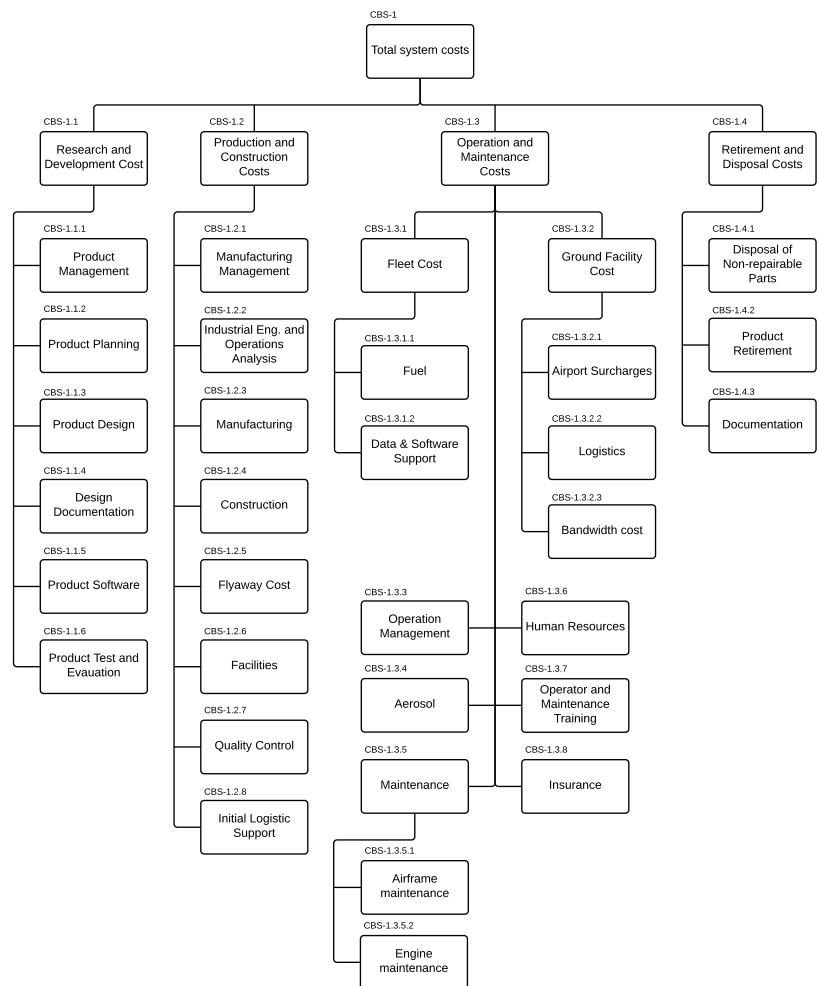


Figure 12.1: Cost breakdown structure

The total system costs can be divided into four different phases:

- **Research and development** The most important aspects of this phase are research, planning of the design, actual development and testing (including documentation).
- **Production and construction** Once the development is complete, the concept can be built. Not only the manufacturing cost is important for this phase, but also the facility cost and quality control after the production is complete. The branch 'flyaway cost' stands for engine, airframe and avionics cost.

- **Operation & maintenance** During operation, a distinction can be made between fleet cost, ground facility cost and the cost that affects both of them. Fuel and software support are only part of fleet cost, while ground facility cost consists of airport surcharges and logistics and bandwidth costs. The cost that applies to both are e.g. aerosol production and storage, maintenance and personnel.
- **Retirement and disposal** After the end-of-life, the aircraft should be disintegrated and recycled as much as possible. Parts that cannot be reused should be disposed and all activities must be documented properly.

To assess the feasibility of the design, a cost estimation is provided in addition to the technical analysis. However, it is challenging to obtain a reliable cost estimation at early stages of the design, where empirical methods have to be used [56]. Therefore, corrections are applied to the methods to account for the unconventional aircraft and mission. The main differences of the SAGA when compared with conventional aircraft affecting the cost estimation are listed below.

- **Aerosol dispersion:** SAGA's fleet disperses their payload in flight. This introduces an additional weight decrease during cruise. In addition, the payload is an extra cost rather than revenue, estimated at \$1.5 billion per year. Furthermore, the payload dispersion requires to fly at much higher altitudes than usual, resulting in different design choices and a more complex aircraft overall.
- **Aircraft systems:** Since no passengers are carried on board, the number of aircraft systems is reduced. For example, no air conditioning, pressurisation or entertainment is installed. On the other hand, the aerosol demands a very large amount of power that exceeds the power available in current most electric commercial aircraft such as the B787¹. Due to the absence of pressurisation and the payload fitting entirely in the wing, the fuselage differs greatly from normal passenger/cargo aircraft.
- **Wing design:** The wing does not only need to accommodate the fuel and the aerosol tanks, but also needs to be designed for high altitude subsonic flight and the support of large powerful engines. This means that the aspect ratio of the wing is larger than for freighter aircraft with comparable payload, and struts are used to ensure structural integrity at low structural weight. In addition, the composite material used adds significant extra costs to the unconventional wing design. A complex maintenance program has to be designed that accounts for the strut, the composite materials and the aerosol tanks.
- **Airport operation:** The 95 m wing span is likely to hinder the use of already existing hangars and might also complicate the manoeuvrability of the aircraft on airfields. Furthermore, special services might need to be provided to the aircraft on ground to load the heated aerosol into the aircraft. This is however considered an indirect operating cost and therefore not accounted for in the calculations.
- **Autonomous control system:** Unmanned aircraft require a higher level of redundancy than manned vehicles (still most conventional) and the infrastructure to operate autonomously. This was found to be beneficial from a cost perspective, however the methods need to be adapted to account for such a different operating mode.

To obtain more confidence in the estimates, two methods are used and compared to each other, as shown in Table 12.1. Worst-case numbers are assumed where relevant to obtain an upper bound. In addition, the estimates are compared to a recent case - the A380 - to put the values in perspective. No real case value is given for the operational costs since these highly depend on how the airlines choose to use the aircraft. In addition, operational cost is only calculated using an in-house estimation since statistical methods are found to rely too heavily on conventional aircraft. It should be noted that although the comparison vehicle is certainly not one-to-one comparable to SAGA, the high level of complexity of the A380 indicates that the results are in the right order of magnitude.

Method 1

Method 1 corresponds to Roskam's cost estimation set of equations for research and development cost and acquisition cost. Operations and maintenance cost depends too much on a conventional flight profile, therefore it is considered more reliable to use a combination of in-house calculations and Liebeck's method [56, 129].

¹ URL http://www.boeing.com/commercial/aeromagazine/articles/qtr_4_07/article_02_3.html [Accessed 17/06/16]

Table 12.1: Cost estimation in billion dollars, assuming a program duration of 20 years

	Method 1	Method 2	Airbus A380²	IATA Conference[128]
Research & development cost	9.9	33	25	n/a
Acquisition cost per aircraft	0.28	0.33	0.4	n/a
Total initial cost	106	146	163	n/a
Operations	6.8	6.8	n/a	n/a
Maintenance	1	15	2 ³	1.7
Insurance	0.16	0.22	n/a	n/a
Total yearly DOC	8	22	n/a	n/a

Although it is relatively old, Roskam's method allows to take into account most of the complexity of SAGA aircraft, as well as many different elements of the cost breakdown structure. **Research and development costs** are calculated based on the sum of seven cost elements: airframe engineering and design (\$177 million), development support and testing (\$62 million), flight test airplanes (\$3 billion), flight test operations (\$66 million), test and simulation facilities (+10%), R&D profit (+10%) and financing cost (+5%), resulting in a total of \$4.4 billion. An additional \$5.5 billion is assumed for the development of the engine. This value is based on the average between Pratt & Whitney's innovative Geared Turbofan⁴ with a development cost of \$10 billion and a common engine development cost of around \$1 billion⁵, as SAGA's engine is new but not as innovative as the state-of-the-art Pratt & Whitney's engine. It is assumed that engine development costs will have to be covered in order to make companies interested in producing the engine, as outlined in Section 11.2. Paying the development costs of the purpose-designed engine and using it still results in a lower cost compared to using an existing engine.

Acquisition costs are calculated in a similar manner, with airframe engineering and design (\$177 million, note: same name and amount as in the R&D phase, however a different cost item), airplane production (\$85 billion), production flight test operations (\$27 million), financing costs (+0.5%) and, assuming a manufacturer profit margin of 10%, a total of \$98 billion is obtained [56]. This method assumes an engine cost of \$35 million⁶ and avionics cost of \$70 million[8, 56], both having a significant impact on the end result.

For the **operational cost**, it is assumed that the main contributions come from the fuel, aerosol, ground control station and bandwidth link. Since the allocated yearly budget excludes aerosol, its assumed cost of \$1.5 billion⁷ is not included in the calculations. The annual fuel cost is dependent on the fuel consumption and the volatile Jet A-1 price. Because of the significant volatility of the fuel price, a range is used based on the minimum and maximum price in the last five years. Using the expected annual fuel cost, this results in an upper bound of \$6.6 billion per year. Although it is expected SAGA cannot be insured due to the large costs involved, as holds for the ISS as well, a project comparable in size, an insurance cost estimation is included for conservativeness and completeness. Insurance costs are assumed to be 2% of the total yearly direct operating cost (DOC), based on Roskam [56]. The need for satellite bandwidth results from the long aircraft range. Since relatively high bit rates are required, it is assumed that a Ku-band satellite communications (SATCOM) system is used. As a baseline, the Ku-band SATCOM costs for the Global Hawk used by NASA are used⁸. The results are a SATCOM budget of \$440,000/year per aircraft, resulting in \$126 million for 286 aircraft (the amount of flying aircraft, 80% of the total fleet). These costs will vary, however, as they strongly depend on the specific contract. Therefore it assumed that the SATCOM costs will vary in the interval of \$100 to \$200 million per year. Attempts for negotiating better contract conditions can be made due to the international nature of the SAGA mission and with SAGA's large fleet of aircraft, economy of scale can be applicable, potentially leading to lower prices.

Part of the operational cost is represented by labour cost of the ground station crew. The different crew members and their respective labour rates are given in Table 12.2. One operator will be responsible for several aircraft because of the high degree of aircraft automation and because operators of SAGA aircraft will have to process less information than common UAV operators, since nowadays most UAV missions are related to surveillance or combat operations, which are more variable and uncertain than the SAGA mission. Therefore, the labour rate of a SAGA operator potentially is lower, or less operators could be needed, leading to

⁴ URL <http://goo.gl/0fqp0h> [Accessed 26/06/16]

⁵ URL <http://goo.gl/3T8eK4> [Accessed 26/06/16]

⁶ URL <https://blog.klm.com/8-things-you-probably-dont-know-about-jet-engines/> [Accessed 17/06/16]

⁷ URL https://www.alibaba.com/trade/search?fsb=y&IndexArea=product_en&CatId=&SearchText=sulfuric+acid [Accessed 28/04/2015]

⁸ URL https://airbornescience.nasa.gov/content/SATCOM_Requirements_and_Costing [Accessed Accessed on 18/05/2016]

lower costs. Due to control based on management by consent (the aircraft gives an operator a set of suggestions and executes one of them after being instructed to do so), one operator can control up to four aircraft simultaneously [130]. Therefore, an operating fleet of 286 aircraft needs at least 72 pilots. However, with a flight duration of approximately 12 hours, one flight takes up two work shifts, doubling the amount of pilots. Hence, the total yearly cost for the aircraft operators will be \$46 million. This value takes into account that some flights may be longer than normal. All other crew members are involved in the maintenance and support of the station. It is assumed the total support and maintenance time for the ground station is 60 days per year, and that technical specialists work eight hours per day, which is a conservative estimate [131]. The rest of the crew works nine hours per day for the entire active period of the mission. The crew yearly costs are presented in Table 12.2, resulting in a total of \$54.1 million.

Table 12.2: Yearly costs for ground control station crew. Labour rates are taken from [131]

Crew Member	Labour rate [\$/h]	Amount per base	Total yearly cost [\$M]
Operators	106	18	46
Operations director	126.47	1	2.7
Operations engineer	95.7	2	2.7
Mission manager	119.85	1	1.7
Technical Specialist I	128.52	1	0.432
Technical Specialist II	95.72	1	0.322
Technical Specialist III	73.33	1	0.247
Total	n/a	n/a	54.1

Maintenance costs are estimated with Liebeck's method, which separates airframe and engine maintenance costs [129]. The airframe maintenance cost is estimated using a statistical relationship based on the weight of the airframe, time per flight and amount of flights. The airframe weight is assumed to be equal to the operational empty weight less the weight of the engines. A labour rate of \$25 per hour is assumed [129]. In addition, to account for the maintenance training cost, the management, administration and planning the airframe, the maintenance overhead or burden is estimated to be 200% of the labour cost [129]. The labour cost, material cost and overhead for the airframe maintenance are summed and amount to \$83 million, including a 15% margin to account for unconventional maintenance tasks.

The engine maintenance cost is estimated using a statistical relationship based on propulsion unit weight, number of engines, time per flight and amount of flights. The same assumptions on labour rate and burden hold. The labour cost, material cost and overhead for the engine maintenance are summed and amount to \$848 million, including a 15% margin to account for the ambient sulfuric acid damage to the engines.

Method 1 results in a development and acquisition cost of \$103 billion and a yearly operational cost of \$8 billion.

Method 2

Cost estimation method 2 is based on Raymer [18], who uses the Development and procurement costs of aircraft (DAPCA) model, which is applicable to a wide range of aircraft types and therefore assumed to be usable for the SAGA. The total costs are divided into research, development, test & evaluation costs (RDT&E), operation & maintenance costs (O&M) and airline economics [18]. The latter is not applicable to SAGA and is therefore not considered. The other two costs are considered below.

Raymer considers **research and development cost and production cost** simultaneously in Research, Development, Test & Evaluation (RDT&E). As a rough estimate, for large scale production, research and development represents approximately 25% of the total cost and actual production 75%. The DAPCA method estimates the expected hours required for development and production, by making a division between engineering (airframe design and analysis, test engineering, configuration control and system engineering), tooling (all preparation for production), manufacturing (direct labour to fabricate the aircraft), and quality control groups (inspection of tools, fixtures, subassemblies and complete aircraft). The estimated hours are multiplied by the estimated hourly rate for labour cost. In addition, the cost for development and actual testing of the aircraft is included, plus the material, engine (using the previously assumed cost of \$35 million) and avionics costs. The \$5.5 billion development cost of the engine is also included. Besides that, a correction factor of 1.8 is applied for the use of composites. This method gives a value for RDT&E of \$146 billion.

The **operation and maintenance costs** consist of fuel cost, crew salaries, insurance and maintenance. The fuel cost was previously estimated to be at most \$6.6 billion per year, using a straightforward method which

does not require revision by another method. Crew salaries as calculated according to Raymer are not considered to be applicable as SAGA does not employ pilots and flight attendants of the kind Raymer assumes and therefore the crew cost estimated in method 1 is adopted, yielding a crew cost of \$54.1 million. Insurance cost is estimated to be 1% of the total yearly DOC. The maintenance expenses are calculated using a statistical relation. The maintenance costs are assumed to be dependent on the amount of flight hours and the number of cycles, but also on airframe and engine costs [18]. The maintenance cost amounts to \$15 billion per year for the entire fleet.

Method 2 results in a development and acquisition cost of \$146 billion and a yearly operational cost of \$22 billion.

The two cost estimation methods used provide different results, leading to uncertainty in the cost estimation. Nonetheless, a final budget is specified, amounting to **\$126 billion initial cost** and **\$9 billion operational cost**. The verification data for the initial cost correspond sufficiently well to the estimations of the two methods, resulting in setting the final initial cost value equal to the average of the two estimation methods. The large discrepancy between the two values for maintenance cost indicates taking the average is not reliable. Verification data from two different sources show that a maintenance cost of around \$2 billion is realistic, resulting in the assumption that method 1 provides a more reliable value for maintenance cost. A conservative value of \$2 billion is assumed to hold for SAGA, resulting in a total yearly DOC of \$9 billion. With these values, the initial budget requirement of \$57 billion is exceeded by 121% and the yearly operating budget requirement of \$11 billion is met with a margin of 18%. The margin in operational costs could be used to depreciate the excess in initial cost in order to better meet the budget requirements and remain competitive versus alternatives.

Depreciation

There is a deficit in the capital budget, but a surplus in the yearly operational budget. This positive margin in yearly operational budget can be used to relieve the deficit in capital. A part of the initial equipment cost can be depreciated annually over the duration of the program. The assumed program length is 20 years, and an interest rate of 2.2% is expected⁹. The debt constant, i.e. a constant yearly down payment of loan principal and interest, is set equal to the yearly budget surplus. Since there is a yearly budget surplus of \$2 billion, this allows of depreciating a capital amount of \$32.1 billion, resulting in a initial cost of \$ 93.9 billion and a yearly operational cost of \$ 11 billion¹⁰. Bar charts showing the costs before and after depreciation are shown in Figs. 12.2 and 12.3.

To conclude this section, an explanation for exceeding the budget is given. The initial cost budget is exceeded by 121% which is considered unacceptable. With depreciation included, the initial cost budget is exceeded by 65% and the yearly operational cost budget is exactly met. Verification data from the existing A380 indicate an even higher initial cost. Therefore, it is concluded the allocated budget of \$57 billion for an unconventional innovative aircraft is not realistic and that the initial cost budget requirement is set to \$100 billion. With this value, the initial cost budget is met with a margin of 6.5%. It should be noted that the methods are in general highly dependent on certain inputs such as airframe, engine and/or avionics costs. The highest values were assumed for conservativeness, but the guarantee of orders consisting of large numbers will probably enable beneficial contracts. Uncertainty remains at this point, however, due to the discrepancies of estimation methods and the uniqueness of SAGA aircraft.

Sensitivity analysis

In Fig. 12.4 the sensitivity of the DOC to payload and fuel price is given. First of all, the payload has a direct effect on the operating cost of the mission. The straightforward explanation for this is that a larger payload per aircraft requires less flights to the stratosphere to disperse the annual required 5 Mt of aerosol. Therefore, the fleet size and flight hours are reduced, causing maintenance costs as well as fuel burn to decrease, which drives the operational costs down. The payload in the SAGA design is set at 35 tons and the yearly operational cost budget equals \$11 billion, lines representing these values are shown. With a payload of 35 tons, a fuel price of \$143 per barrel is the maximum price possible to still meet the budget. In the last 5 years, the fuel price for Jet A-1 has not exceeded a \$ 110 per barrel. It can thus be concluded with reasonable certainty that the payload weight of 35 tons allows for an affordable yearly operations budget.

⁹ URL <https://www.treasury.gov/resource-center/data-chart-center/interest-rates/Pages/TextView.aspx?data=longtermrate> [Accessed 27/6/2016]

¹⁰ URL <http://www.double-entry-bookkeeping.com/periodic-payment/how-to-calculate-a-debt-constant/> [Accessed 27/6/2016]

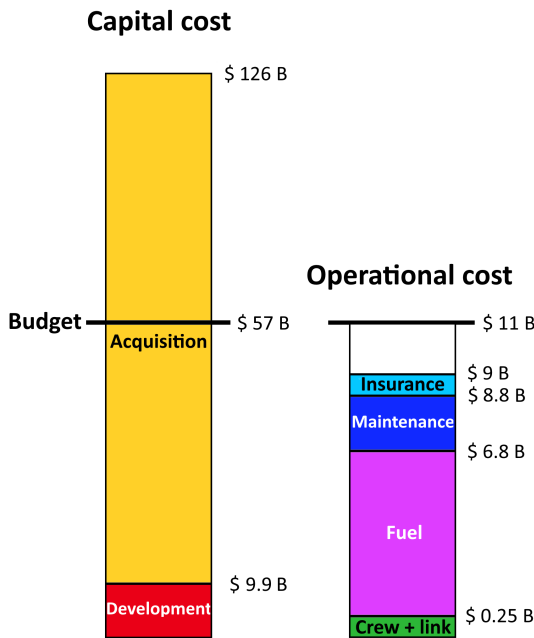


Figure 12.2: Composition of initial and operational cost before depreciation is implemented

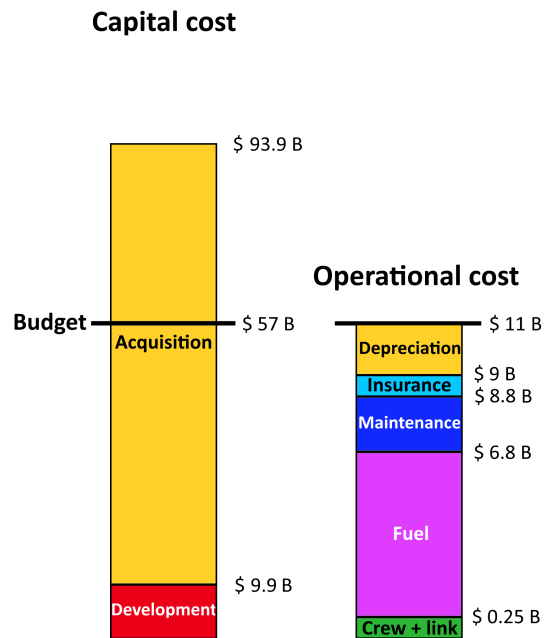


Figure 12.3: Composition of initial and operational cost after depreciation is implemented

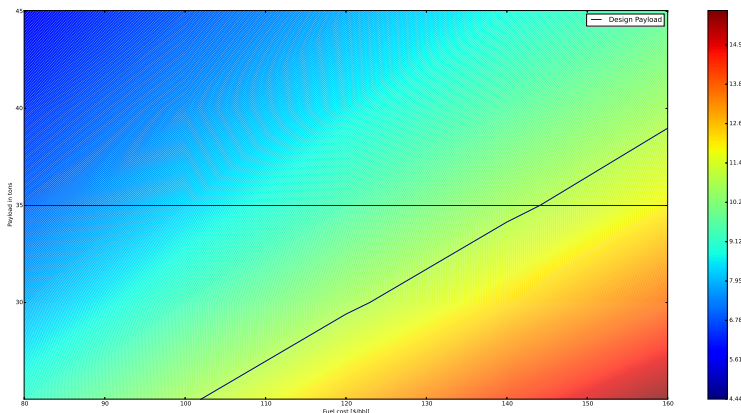


Figure 12.4: Response surface of the annual operational cost and the budget (black line) plotted against the fuel price and the payload per aircraft. White line corresponds to the design payload.

12.2 Budget breakdown

To ascertain the final product achieves its specified performance within the allocated budget, a Technical Performance Measurement (TPM) is carried out. Uncertainty is always present during product development. As the design process advances, this uncertainty usually grows in an unfavourable and undesired way. In this section, the budget breakdown of five TPM parameters that are most applicable to SAGA will be presented:

- Weight (both operational empty weight and maximum take-off weight)
- Power
- Cost (both capital cost and operational cost)
- Drag
- Fuel burn

A contingency allowance is allocated to each of these TPM parameters for different stages of the development, as can be seen in Table 12.3 [122]. Currently, the design has met the end of the preliminary design stage.

Table 12.3: Contingency budget

Design maturity	Contingency [%]						
	EOW	MTOW	Power	C. cost	O. cost	Drag	Fuel burn
Conceptual (Class I) estimate	20	30	20	25	30	20	30
Preliminary (Class II) estimate	10	20	15	15	20	10	20
Final preliminary estimate	5	10	8	13	15	5	15
<i>Post DSE</i>							
Detailed estimate	3	3	5	8	10	3	8
Qualification measurement	1	1	1	1	1	1	1
Flight measurement	0	0	0	0	0	0	0

Contingencies are usually derived from previous similar product development processes. Since the SAGA mission is not a conventional mission, not many similar product development processes exist, hence this is not possible. Therefore, the contingencies for the conceptual design stage are very large, accounting for the expected large uncertainties. As the design process continues, a thorough risk assessment allows contingencies to be defined more precisely.

The TPM parameters are analysed and their breakdown is presented in Tables 12.4 to 12.10. The current state of the parameter is described by four values [122]:

- **Actual value (AV):** the most accurate estimate of the parameter in the specific design stage
- **Current value (CV):** the actual value including a contingency
- **Specification value (SV):** the predefined value (sometimes stemming from requirements), including all approved waivers
- **Target value (TV):** the specification value minus the contingency

If applicable, these values are used to determine the margins ($TV - AV$) that the TPM parameters have at the current design stage. If the margin is positive, no action is required. If the margin is negative, either the design should be changed or the specification value should be chosen differently. For parameters that were not given a specification value at the beginning of the conceptual design, this value is missing in the analysis.

The OEW and MTOW breakdown are presented in Tables 12.4 and 12.5. During the Class I estimate, no weights were allocated to the individual aircraft components, but only to the entire aircraft. The Class II estimation contains the component weights as calculated with the Raymer method. The values that were obtained at the end of the preliminary design, including the numerically calculated structural wing weight, are also included.

A reserve margin of 7.21 tons is taken into account for the Class II weight estimation to divide over the components that would be heavier than estimated. As can be seen in the tables, the initial specification (and therefore the target value) was modified several times because a negative margin was obtained. This can be attributed to the little knowledge about the unconventional design of SAGA in early stages. After thorough consideration and major design changes after the class II estimation, the specification values have been changed to obtain a positive margin again. The margin is visualised by Fig. 12.5, showing the timewise relation of actual and target value. For the sake of simplicity, specification and current values are left out.

The power budget is presented in Table 12.6. Also here, a low initial specification value was selected due to the low design maturity, which results in a negative margin during the early preliminary estimate. The specification value was changed afterwards, and now the margin is met again.

In Tables 12.7 and 12.8, a negative margin of 50.67 billion dollars and 0.36 billion dollars per year is found for the capital and operational cost, respectively. In order to ensure that the design will meet the target (or in the end the specification) value, the cost will be depreciated as described in Section 12.1. Another possibility is to reduce the uncertainty in cost estimates, so the budget breakdown can be made more precisely.

In Tables 12.9 and 12.10, the drag and fuel burn breakdown are indicated. These TPM parameters are not given a specification value, since they are already optimised for using SUAVE.

Table 12.4: Operational empty weight breakdown

Aircraft component	Class I OEW [tons]	Class II OEW [tons]	Preliminary OEW [tons]
Wings	n/a	18.20	27.60
Engines	n/a	40.00	41.82
Fuselage	n/a	5.66	8.47
Landing gear	n/a	12.70	6.19
Horizontal tail	n/a	3.69	1.51
Vertical tail	n/a	1.72	0.95
Rudder	n/a	n/a	0.38
Systems	n/a	10.82	14.07
Contingency value	20%	10%	5%
Actual value	64.52	92.79	100.99
Current value	77.42	102.07	106.04
Specification value	85.00	85.00	110.00
Target value	68.00	76.50	104.5
Margin (TV – AV) [tons]	3.48	-16.29	3.51

Table 12.5: Maximum take-off weight breakdown

Aircraft component	Class I MTOW [tons]	Class II MTOW [tons]	Preliminary MTOW [tons]
OEW	64.52	92.79	100.99
Fuel	41.84	60.00	53.09
Aerosol	40.00	40.00	35.00
Margin	0	7.21	0
Contingency value	30%	20%	10%
Actual value	146.33	200.00	189.08
Current value	190.23	240.00	207.99
Specification value	160.00	200.00	215.00
Target value	112.00	160.00	193.50
Margin (TV – AV) [tons]	-34.33	-40	4.42

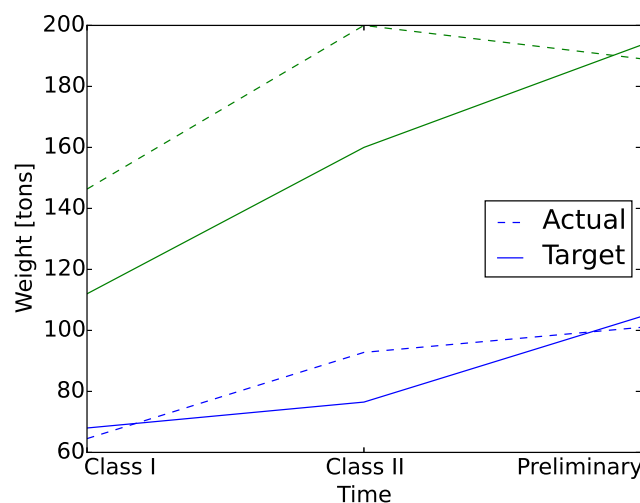


Figure 12.5: Target and actual values for MTOW (upper lines) and OEW (lower lines)

Table 12.6: Power breakdown

System	Conceptual estimate [kW]	Initial preliminary [kW]	Final preliminary [kW]
Exterior lights	n/a	3.85	3.85
Avionics	n/a	18.50	18.50
ECS	n/a	1.60	1.60
Fuel system	n/a	6.50	6.50
Hydraulic system	n/a	8.50	8.50
Flight control system	n/a	5.00	5.00
LOS communications	n/a	0.82	0.82
SATCOM	n/a	1.20	1.20
Aerosol evaporation	n/a	2,000	1,500
Contingency value	20%	15%	8%
Actual value	30.40	2045.97	1545.97
Current value	36.48	2352.87	1669.65
Specification value	40.00	40.00	2000
Target value	32.00	34.00	1840
Margin (TV – AV) [kW]	1.6	-2011.97	294.03

Table 12.7: Capital cost breakdown

Item	Cap. cost [billion dollars]
R&D	14
Acquisition cost	86
Contingency	13%
Actual value	100
Current value	113
Specification value	56.7
Target value	49.33
Margin [billion dollars]	-50.67

Table 12.8: Operational cost breakdown

Item	Op. cost [billion dollars]
Fuel	6.6
Communications	0.126
Maintenance	2.73
Ground facilities	0.541
Contingency	15%
Actual value	10
Current value	11.5
Specification value	11.34
Target value	9.64
Margin [billion dollars]	-0.36

Table 12.9: Drag breakdown

Aircraft component	Form factor [-]	S_w [m ²]	S_{ref} [m ²]	C_{D_0} [-]	Percentage [%]
Wings	1.33-1.48	1430	700	0.00504	52.0
Strut	1.19-1.25	58.0	28.3	0.00056	5.8
Engines	1.21	59.3	8.16	0.00088	9.1
Pylons	n/a	n/a	n/a	0.00017	1.8
Fuselage	1.69-1.80	283	34.4	0.00143	14.6
Horizontal tail	1.21-1.27	269.9	131	0.00107	11.0
Vertical tail	1.20-1.26	80.0	39.0	0.00028	2.9
Miscellaneous	n/a	n/a	n/a	0.00026	2.7
Actual value	-	-	-	0.00969	100

Table 12.10: Fuel burn breakdown

Flight phase	Fuel burn [kg]	Percentage
Climb 1	701	1.3
Climb 2	664	1.2
Climb 3	1299	2.4
Final outgoing	486	0.9
Cruise outgoing	21664	39.5
Climb 5	1047	1.9
Climb 6	974	1.8
Cruise 1	8501	15.5
Climb 2.1	413	0.8
Cruise 2	8552	15.6
Climb 2.2	238	0.4
Final cruise	6168	11.2
Descent 1	163	0.3
Descent 2	1316	2.4
Final descent	0	0
Reserve climb	1918	3.5
Reserve cruise	747	1.4
Reserve descent 1	0	0
Actual value	54851	100

13. Reliability, availability, maintainability and safety analysis

In order for the SAGA mission to be successful, the aircraft must be reliable, have a high availability rate, be maintainable and safe to operate. In order to check if the aircraft meets these requirements, a reliability, availability, maintainability and safety analysis is performed and described in this chapter. The chapter starts with an analysis on the required reliability level in Section 13.1, which is then followed by an outline of the safety critical functions in Section 13.2. Next, the redundancy philosophy is presented in Section 13.3 and the expected reliability and availability levels in Section 13.4 and 13.5. Finally, the maintenance activities are briefly explained in Section 13.6.

13.1 Required level of reliability

The required level of reliability for an unmanned aircraft can be based on an expected level of safety (ELS), expressed in ground fatalities per flight hour. It can be calculated with the model proposed by Weibel [132], shown in Equation (13.1). It takes into account the ELS, aircraft size, population density, probability of impact, and mitigation against impact. To make a first order estimate on the required Mean Time Between Failure (MTBF), it is assumed that the probability of impact is one and no mitigation is applied. MTBF in this context means failure of a system or component that places an aircraft out of service. Furthermore, the ELS is taken to be 10^{-7} fatalities per hour, as proposed by Weibel. The exposure area is taken to be two times larger than the area for the Heavy UAV class in [132], since the SAGA has almost two times longer wingspan than the given reference aircraft, the MD-11¹. Finally, the population density is taken to be 400 people per square kilometer.

$$ELS = \frac{1}{MTBF} A_{exp} \rho P_{pen} (1 - P_{mitigation}) \quad (13.1)$$

The final result is a MTBF of 5.7 million hours which is higher than the US required reliability level of 1 million hours for heavy UAVs [133]. Therefore in the detailed design phase the SAGA must be designed to meet this goal.

13.2 Safety critical functions

The first step to achieving the required reliability level is to identify the functions which are safety critical for the unmanned aircraft system. Failure to perform these functions can lead to loss of the aircraft and consequently ground casualties. The identified safety critical functions and the reasons for choosing them are presented below:

- **Provide autonomous flight control in all flight phases:** Due to the operational control concept (one operator supervising four aircraft), the aircraft cannot be flown manually. Therefore, a complete system failure of the autonomous flight control system leads to losing the aircraft.
- **Provide the aircraft with sufficient information about its surroundings:** The autopilot needs information about the environment surrounding the aircraft (relative position, bearing and velocity of nearby aircraft, distance to ground, surrounding atmospheric conditions, etc.) in order to function properly and prevent collisions.
- **Provide temperature management for the aircraft's avionics:** Avionics cannot operate outside of their specified temperature range. Multiple system failures can result if thermal control fails.

¹ URL <https://janes.ihs.com/Janes/Display/1337870> [Accessed 17/06/2016]

- **Supply the aircraft with navigation data:** Inability of the aircraft to determine its position and direction can render it unable to return back to base or to land on a reserve airport, which results in aircraft loss.
- **Provide communications between the ground control station and the aircraft:** Inability of the ground station to track and command the aircraft severely increases the mission risk. Unanticipated deviations from the nominal mission requiring operators pose a problem in case no communication is possible.
- **Prevent aerosol leakage inside the aircraft:** Due to its corrosive nature, the aerosol can damage the aircraft structure and systems. Strategies for the mitigation of that risk are presented in Section 11.4.

13.3 Redundancy philosophy

Redundancy strategies for the systems concerning the identified safety critical functions are made, to provide an adequate level of safety for these critical functions. Every system has a specific strategy, which is presented below.

- **Flight control system (FCS):** The FCS has quintuple (5 level) redundancy. This level is chosen since it consists of four main flight computers working in parallel and one back up computer, which has the same hardware but runs on different software. During normal operations the main flight computers are synchronised with each other. Every computer proposes an output, which is voted against the outputs of the other three and if it deviates significantly from the rest, it is excluded from the control process. The same principle is applied to the actuators as well. Similar systems are applied in the F-16C and the Space Shuttle [134].
- **Sense & avoid system (S&A):** The Sense & avoid system is comprised of different suites of sensors, which have different functions - mainly aircraft detection and avoidance and ground avoidance. For aircraft avoidance, a combination of a transponder, an ADS-B system, electro-optic sensors and a LiDAR system is used, which ensures that the aircraft has information about the relative range, velocity, bearing and position of other aircraft. For ground avoidance, two look-down and two look-forward radar altimeters are installed in order to ensure that the aircraft can measure terrain proximity even in non-level flight.
- **Instrument landing system (ILS):** Three independent ILS systems are installed on the aircraft.
- **Environmental control system (ECS):** Two independent ECS systems from different manufacturers are installed on the aircraft. If one fails the other automatically takes over. MTBF = 20,000 hours²
- **Navigation system:** The navigation system uses two GPS receivers³ and two GPS/INS integrated systems⁴. The INS system acts as a back-up to the GPS and is constantly being calibrated. If the GPS receivers fail or the aircraft moves outside the satellite coverage area, the INS is capable of bringing the aircraft back to base.
- **Communications system:** The communications system consists of two modules: Line-of-Sight (LOS) communications and satellite communications (SATCOM). The LOS module has three antennas - two main antennas and a back up antenna working in a different frequency spectrum. The SATCOM module has one main Ka-band antenna for nominal uplink/downlink data transfer, one smaller back-up antenna for receiving commands from the ground station, and two smaller INMARSAT antennas for aircraft status and location updates, which act as a back-up to the main system. If all communications between the aircraft and the ground station are lost, the aircraft will abort its mission and fly a predetermined flight plan back to base, until it is in the coverage of the LOS system.

² URL <http://www.fairchildcontrols.com/products/thermal-management-systems> [Accessed 16.06.2016]

³ URL https://www.thalesgroup.com/sites/default/files/asset/document/thales_navigation_topstar_lpv_rnp_ads-b_2015.pdf [Accessed 16.06.2016]

⁴ URL <http://www.northropgrumman.com/Capabilities/LN251INSGPS/Documents/ln251.pdf> [Accessed 16.06.2016]

13.4 Expected reliability level

An in-depth reliability estimate of the aircraft cannot be performed at this stage of the design. In order to do that, the design must be in its detailed stage, when all of its systems are designed. However, a first order reliability estimation can be performed for some of the aircraft systems, which is based on the level of redundancy and the MTBF figure of existing systems of similar type.

The reliability of the entire aircraft is calculated with Equation (13.2), where R_i is the reliability of one system. A system's reliability is calculated with Equation (13.3), where j is the level of redundancy and R is the reliability of one system block. The reliability of one system block is calculated for a given time interval with Equation (13.4). The results are shown in Table 13.1. [131]

$$R_{aircraft} = \prod_1^i R_i \quad (13.2)$$

$$R_{system} = 1 - \prod_1^j (1 - R_j) \quad (13.3)$$

$$R_{block} = \exp\left(-\frac{t}{MTBF}\right) \quad (13.4)$$

Table 13.1: Reliability of some of the aircraft systems for a single flight

System	Components	Redundancy	MTBF [h]	Reliability
FCS	Flight Computer	5	3000	Approx. 1
	Interface Unit	5	6000	Approx. 1
				0.9999997
Navigation	Main GPS ³	2	60,000	Approx.1
	GPS/INS back up ⁴	2	22,000	0.9999997
	ECS module ²	2	20,000	0.9999997
Combined reliability of these subsystems			$41.4 \cdot 10^6$	0.999999

Compared to the reliability of the entire aircraft, which is 0.999997982 for one flight, the rest of the systems must have a combined reliability of 0.999998623 (MTBF = 19.2 million hours). Note that the accuracy of these numbers is higher than can be guaranteed at this stage, but required to show the difference between aircraft reliability and system reliability.

There is some uncertainty associated with these numbers. Since the flight control system is autonomous, its reliability may differ significantly from the reliability of a manual system. This reliability difference can only be determined when the autonomous system is designed. The difference is dependent on the accuracy of the flight dynamics model of the aircraft throughout the entire flight envelope. Moreover, it is also affected by the accuracy of the sensors in the S&A system, the location of the components in the air data system (static ports and Pitot tubes) and their accuracy in extreme conditions, such as at high angles of side slip.

In order to quantify the reliability uncertainty of the autonomous system, it must be modelled and run through simulations for all operational conditions. The behaviour of the system is constantly analysed, and a sensitivity analysis of the inputs (flight dynamics model, sensor accuracies, etc.) must be made. After this has been completed, the overall flight control system reliability can be determined.

13.5 Expected availability level

The aircraft availability can be divided into inherent availability, dependent on the aircraft's MTBF, and achieved availability, dependent on the Mean Time Between Maintenance (MTBM). These values are calculated with Equation (13.5) and 13.6, where \bar{M}_{ct} is the mean corrective maintenance time (or mean time to repair) and \bar{M} is the mean active maintenance time [131]. Given the high required MTBF, the inherent availability is expected to be high (in the range of 0.89-0.95, dependent on the repair time).

$$A_i = \frac{MTBF}{MTBF + \bar{M}_{ct}} \quad (13.5)$$

$$A_o = \frac{MTBM}{MTBM + \bar{M}} \quad (13.6)$$

13.6 Maintenance activities

The maintenance activities are divided into two categories: scheduled activities and unscheduled activities. The scheduled activities consist of daily checks, including visual inspection of the aircraft, checking fluid levels and taking reports from the aircraft health monitoring system. They are followed by type-A checks, during which the structure is visually inspected for damage, deformation and corrosion, the landing gear retracting mechanism is lubricated, and gear brake pressures are checked. Type-A checks usually require 10 to 20 man-hours⁵.

Next, a type-B check is performed, during which the aircraft systems are inspected tested separately. Some aircraft components may be examined in more detailed as well, but no detailed disassembly is performed. The aerosol tanks are also examined for corrosion. Type-B checks are carried out between 500 to 600 flight hours and take approximately 100 to 200 man-hours to perform⁵.

The maintenance heavy check is the type-C check, where a thorough inspection of specific parts of the airframe with specialised tooling is carried out. It is done once every 24-30 months. The functioning of the aerosol system is also tested. During a type-C check, the aircraft will not be able to participate in the mission from 3 to 5 days⁶. If major issues with the aircraft are found during this check, the aircraft is sent for repair at a maintenance facility located at the base.

The last type of check is the type-D check. The aircraft is subject to a type-D check approximately once in every 6 years. During the D check the aircraft is completely disassembled and overhauled. The most detailed inspection of the structure takes place, using non-destructive testing methods. This is the longest maintenance activity, which requires 30,000-50,000 man-hours, or four to six weeks⁷.

Some unexpected maintenance activities can also occur. Examples of these are repairing of system failures reported by the health monitoring system prior to a flight, or maintenance activities performed after an emergency situation (engine failure, fire, etc.)

⁵ URL https://www.aa.com/content/images/aboutUs/newsroom/fs_aircraft_maintenance_procedures.pdf [Accessed 17.06.2016]

⁶ URL <http://www.aviationpros.com/article/10388655/whats-this-a-check-c-check-stuff> [Accessed 18.06.2016]

⁷ URL <http://www.lufthansa-technik.com/overhaul> [Accessed 18.06.2016]

14. Sustainability strategy and analysis

Geoengineering by means of injecting aerosols into the stratosphere is a technology to be used for an environmental purpose. The accumulation of greenhouse gases in the atmosphere and the associated rise of temperature place a burden on the environment and society. The proposed technology presents a temporary intervention to avoid unacceptable temperature increase. In combination with methods to decrease or prevent the accumulation of greenhouse gases, this method can be implemented to halt global warming, until the amount of greenhouse gases has reduced to acceptable levels and geoengineering is no longer required. The purpose of geoengineering is to reduce damage to the environment and mitigate the effects of unsustainable practices. For an optimal implementation of geoengineering, sustainability should be integrally included in each step of the process. In the following, it is described how sustainable development is applied in the design process of the SAGA.

14.1 Strategies for sustainability

During a design process, certain methods can be used to enhance the performance and sustainability of the finished product. Two strategies used by the SAGA team are Design for X (DfX) strategies, and concurrent engineering (CE).

The most important DfX strategy for SAGA is Design for Environment (DfE). Environmentally friendliness is a key aspect of the project. A careful life cycle analysis of the mission (LCA), as performed in Chapter 4, allows for a quantification of the environmental impact of the design. Other DfX strategies applied to SAGA are Design for Cost (DfC) and Design for Reliability (DfR) [135, 136].

In concurrent engineering, parallel and simultaneous activities of all group members on all design areas contribute to the overall success of the design. The SAGA team works together with physical presence of all group members at all times. The working environment enhances the workflow, since all information is available at once. If someone is absent or not available right away, use can be made of the dedicated online networks that are being used by the team. The advantage of concurrent engineering is not only to provide a facility and framework for the project, but it is also a tool to provide the team with a common understanding about the DfE strategies. A sustainable design strategy is integrally implemented from the beginning of the project and carefully monitored throughout the design process.

14.2 Sustainable conceptual design choices

Several design concepts are established during the conceptual design. By implementing the sustainable development strategy in the requirements, meeting the requirements in the design implies sustainability is ensured, however, thorough examination of the concepts is required to assess and compare their sustainability level. To select the final design concept, a trade-off is performed. Implementing the sustainable development strategy is done by assigning a high weight to criteria that influence sustainability. Examples of aspects influencing sustainability are the mass, engine characteristics & emissions, production & manufacturing methods and materials. During the trade-off, all aspects affecting sustainability are considered carefully and taken into account in the grading of concepts. The concept designs are graded on the trade-off criteria, thus selecting appropriate criteria and weights related to sustainability ensures sustainability of the selected concept.

After trading off the concepts and selecting a design, the requirements are revised and specified for the concept. As in earlier design phases, requirements explicitly addressing sustainability are set up, as well as requirements implicitly containing sustainability aspects, thus implementing the sustainable development strategy in the set-up of new requirements. In the risk assessment, environmental risks are taken into account, and risk management aims to minimise environmental risks and ensure sustainability as well as possible.

One of the most important aspects concerned with the SAGA mission is the selection of the aerosol material, which is done with great attention to sustainability. In the selection process, criteria focused on environ-

mental impact are considered to be crucial. Different usable compounds are analysed on their chemical characteristics and effect on the environment.

During the development of a preliminary concept of operations sustainability is considered as well. The operational concept is optimised for costs, which inherently implies optimisation for sustainability as cost is highly dependent on required amount of flights and thus on fuel consumption. For example, the range flown by the aircraft fleet will be optimised such that the minimum amount of kilometres is flown to disperse the aerosol, reducing both costs and environmental impact induced by SAGA. Another aspect of operations, the fleet size, represents an important influence on sustainability. An analysis with respect to sustainability of having a large fleet with low payload in comparison to a small fleet with high payload was conducted. From this analysis the optimal combination of fleet size and payload to balance the multiple factors such as cost, effectiveness and sustainability is selected, leading to a list of aircraft requirements. Furthermore, all other system requirements are set up with the general goal of sustainability.

In the resource allocation, globally three categories can be distinguished: land, labour and capital. Sustainable development is mainly applicable to the 'land'-category, representing material use and fabrication processes. The resource 'capital' is a means to realise requirements. In the target cost determination, enough budget was reserved to facilitate sustainable development. As this project has little commercial interest, less constraints concerning budget for sustainability are present for there is no dominant competitive element. Indeed, governments or transnational entities looking to use a geoengineering aircraft will likely require a service that guarantees environmentally friendly operations. This enables larger budgets to account for sustainability.

14.3 Sustainable preliminary design choices

The focus of SAGA is to obtain a light weight vehicle. Use of composite materials reduces the structural wing weight by approximately 15%, and the strut-braced concept saves an additional 18% of weight. Even though the design is more expensive than an aluminium wing, it is very beneficial for fuel burn and emissions. The impact of SAGA on the environment is therefore smaller by choosing appropriate materials and structural concepts.

DfE strategies for propulsion are implemented by making the engine more efficient. Using SUAVE, the fuel consumption is minimised to obtain the lowest possible emissions. The use of bio-fuel, which may yield even better emission characteristics, can be investigated in future detailed design stages.

On the ground, the use of large hangars is required to store the aircraft that are in maintenance or out of service. These facilities can be equipped with systems to generate green energy. The large roofs of hangars is a suitable place to install solar panels to provide energy to e.g. the heating of the aerosol. Grounded aircraft will be cleaned to prevent the accumulation of dirt. Cleaner aircraft have less emissions due to the lower drag [137].

A last important consideration about the life cycle of SAGA is the disposal of the fleet at the End of Life (EoL). Numerous companies have implemented a 3R strategy, in which Reuse, Remanufacturing and Recycle strategies propose a sustainable EoL solution. SAGA is a very unusual mission in various ways, which makes it hard to establish a reuse policy for the aircraft. Most of SAGA's aircraft components will not be applicable to other designs, making them superfluous when the mission is over. However, giving the aircraft another purpose is possible. A portion of the fleet can be used for scientific high-altitude measurements. The increasing demand for private space travel can also be exploited, where SAGA can be used to launch satellites or other vehicles from the stratosphere (cfr. Stratolaunch²), reducing launcher fuel and costs and therefore yielding more sustainable space exploration [135]. Remanufacturing of certain parts can be beneficial for future aircraft concepts, since SAGA is a conventional aircraft design. After EoL, certain parts can be disassembled and remanufactured in other aircraft. In addition, recycling of materials contributes to the sustainability of the design. Parts made of metal alloys can be cast in different shapes and be used in different industries. In any case, incineration and landfilling will be reduced as much as possible, or preferably eliminated completely from the mission.

14.4 Environmental effects of SAGA

The implementation of SAGA is proposed to halt the temperature increase of the Earth temporarily, in order to buy the world population time to stabilise the greenhouse gas concentrations in the atmosphere. By dis-

persing sulfuric acid (H_2SO_4) into the stratospheric layer of the atmosphere, radiation will be scattered back into space, reducing warming of the Earth. This, often labelled as dangerous, human interference in the climate system, is likely to experience opposition. To objectively assess the sustainability and environmental aspects of SAGA, its impacts are analysed and placed in the appropriate context in the following paragraphs.

First, the current situation and predicted forecasts are presented and discussed. In Chapter 2 a qualitative prediction of possible scenarios is presented. In this analysis several situations are modelled, including both worst and best case scenarios. It should be noted that the need for geoengineering is not necessarily present yet with the current state of the greenhouse gas concentration. Based on historical data, the mitigation of greenhouse gas emissions by the implementation of a sustainable life style can still prove to be sufficient to keep temperatures below the limit increase of 2K set in 2009 at the Climate conference in Copenhagen. However, also the potential of geoengineering becomes clear in Fig. 2.4. The dispersion of aerosol can show to be an excellent method to ensure the global temperature does not exceed the limits set in 2009 in Copenhagen, providing humanity with the time to take responsibility and reduce emissions.

It should be noted that the effect on the climate system due to the implementation of the SAGA, is hard to predict. Several studies have been conducted to investigate the consequences of aerosol dispersion, however, all are considering different circumstances and different kinds of implementation, complicating the comparison. Therefore, the Geoengineering Model Intercomparison Project (GeoMIP) was developed, in which four possible scenarios of geoengineering are researched by several modelling groups using different climate models, allowing for an analysis of the consequences of geoengineering [138]. The cases were implemented in 11 different climate models. This research resulted in slightly varying outcomes, as expected, as all models are based on different climate nmodels. However, some trends can be observed:

- All models show a similar response to aerosol dispersion regarding temperature decrease, indicating that it is possible to predict the consequences in temperature changes quite accurately [1].
- In all models it is noticed that a sudden halt in aerosol dispersion would cause a fast and large increase in temperature. It is therefore important to carefully guide the implementation of SAGA, preventing the need for a sudden stop of aerosol dispersion and thereby mitigating this risk [1].
- One of the observed consequences of aerosol injection is change in precipitation patterns. Temperature changes and precipitation variations can not be modelled independently, and also the composition of the atmosphere (and thus stratosphere) affect precipitation patterns. The affects on precipitation need to be investigated carefully, as this can heavily affect agriculture and water supplies. A certain limit on changes in this aspect should be established and a compensation for the affected parties should be provided. [1] [139].

All models and scenarios predict a very slow response of temperature to geoengineering, and only slight variations in temperature values between the models are observed. Besides the temperature variations, it is observed in all models that a sudden halt of aerosol dispersion will rapidly increase the temperature, as mentioned, which is visualised in Fig. 2.4. This emphasises that aerosol dispersion should be gradually ramped down at the end of the project, provided that CO_2 levels allow this.

The annual dispersion of 5 Tg of sulfuric acid seems to be an enormous amount, however the annual volcanic sulfur dioxide emission (SO_2) is 13 Tg. Besides these natural emissions, industries diffuse an additional 100 Tg of SO_2 every year. Assuming that SO_2 will entirely react to H_2SO_4 , the addition to sulfuric acid levels by SAGA is only 4.4%. The sulfuric compounds that are dispersed, however, are brought to an altitude of 20 km. This dispersion in the stratosphere makes the sulfur effective in scattering back of sunlight, whereas volcanic and industrial sulfur are not injected at this desired high altitude [1].

As said earlier, the SAGA mission is designed to alleviate some of the consequences of increasing greenhouse gas emissions, but is not considered to be a solution to the global warming problem. In order to make the project successful, it is of utmost importance that global carbon dioxide emissions are cut down in parallel to the dispersion of aerosol. The additional CO_2 emissions due to SAGA are investigated to quantify the effect of this project, in order to show its potential. It is found that SAGA will cause an additional 2.0% fuel consumption in aviation and an extra CO_2 exhaust of 1.5% [140]¹. Considering that aviation is responsible for 2% of the global fuel consumption, the worldwide fuel consumption is only increased by 0.03%².

¹ URL https://www.eia.gov/environment/emissions/co2_vol_mass.cfm [Accessed 05/06/2016]

² URL <http://www.atag.org/facts-and-figures.html> [Accessed 05/06/2016]

From the above it is concluded that the SAGA shows much potential, however that more in-depth research is required to form a deliberate opinion on this rather controversial topic. It is concluded that SAGA has no substantial polluting effect on the environment. Taking into account that the uncertain response of the climate can possibly result in dangerously high temperatures, a situation in which implementing geoengineering is the best option available might occur. In that case, it is invaluable knowledge that geoengineering implemented by SAGA presents a feasible intervention. With or without implementation of SAGA, a considerable adaptation in human life style is required to diminish greenhouse gas emissions. SAGA can prove to be a good supplement to this, but cannot be considered a substitute.

15. Production plan

The production plan, based on manufacturing, assembly and integration concepts, is elaborated upon in this chapter. This chapter describes all the steps that still have to be taken from the end of the design stage until the moment the aircraft will be flying. First, a discussion on the main considerations of the manufacturing process is presented. It is followed by the core flow diagram of the SAGA manufacturing process.

15.1 Main considerations

The production of the aircraft fleet is affected by several factors including, but not limited to, design, manufacturing processes, economy of scale, and organisational concept [141]. The way each parameter affects the production process is explained in the following list.

- **Design:** Manufacturing costs can be reduced if parts are designed in such a way that they do not require complex tooling. In addition, feasible tolerances in the detailed design and smart divisions of the aircraft into sections can facilitate the production of the manufacturing, assembly and integration [142].
- **Manufacturing processes:** The selection of manufacturing processes depends on the series size, the part size, the accuracy required and the time available [142]. Some manufacturing processes also require more expensive equipment than others.
- **Economies of scale:** The series size is an important factor for SAGA, as it significantly affects cost. The fleet size is small compared to commercial aircraft series. Implementing SAGA requires approximately 350 aircraft, whereas most commercial aircraft series are larger in number. Due to the small fleet size, outsourcing the production is recommended as will be explained in Section 15.2. The small fleet size also has an impact on the available manufacturing processes, as some are only feasible economically if the series is large and others are particularly suitable for small series [142].
- **Organisational concepts:** Apart from the successful lean manufacturing strategy, several other concepts exist [143]. Six sigma, agile and total quality management are three possible alternatives, which can be used in combination with each other and with lean manufacturing. Lean manufacturing aims to eliminate waste and therefore reduce lead times [144]. This is desirable to increase the production rate, discussed in Section 15.2. Since the production is to be outsourced, it is convenient to find a company that has implemented successful six sigma strategies since this allows to save money [144]. In case of SAGA, a stable (predictable) demand can be assumed such that agile manufacturing is not needed [145, 146, 147]. In addition, quality management can also be discarded since the mission requires only a single purchase.

15.2 Manufacturing, assembly and integration of SAGA

In Fig. 15.1, the timewise (from left to right) production plan of the SAGA mission can be found. It starts from part manufacturing¹ (batch processes), after which the different parts will be joined together to sub-assemblies and finally the aircraft structure (line manufacturing). The final step is to provide integration with aircraft systems.

Particular attention has to be paid to the manufacturing of the wingbox, aerosol subsystem and the integration of the systems into the aircraft. The wingbox is a long and slender assembly, and it will have to carry large bending moments. The fibres of the boron composite used for the wing box will be made available by external companies in a pre-impregnated ply. The layup of the laminate is done by hand, since the wing structure is very long and slender. An automatic layup would require very precise machinery and would increase cost with a substantial amount [148]. Moreover, since the fleet size is very small, an investment in automatic

¹It should be noted that the indicated parts are only a small fraction of the actual parts needed.

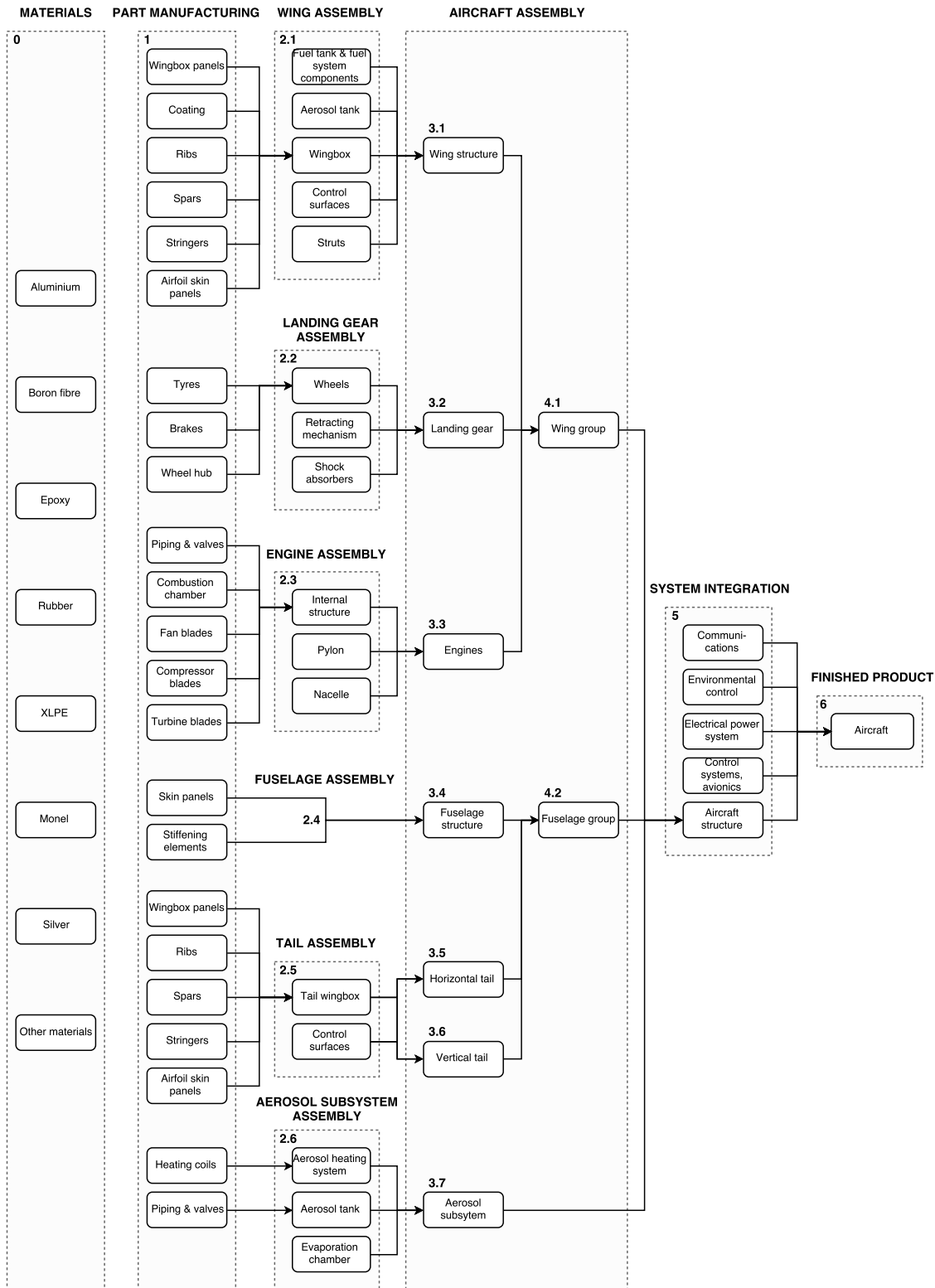


Figure 15.1: Timewise manufacturing, assembly and integration diagram

layup is not economically beneficial. After the stacking is completed, the composite is cured in an oven or autoclave, after which it can be integrated into the main wing.

The aerosol subsystem is the most critical part of the mission, since the aircraft is designed around it. The heating system requires good insulation, since the radiated heat might affect other components. It might be necessary to apply specific long-term ceramic coatings to the aerosol assembly so it doesn't affect the performance of other systems or assemblies.

Finally, integration has to be addressed carefully since the aircraft is unmanned and therefore a working connection between systems is crucial. Also due to the absence of a pilot, the integration is expected to be very complex as a consequence of the required redundancy levels.

Due to the small size of the fleet, it is convenient to outsource the production, as mentioned. Not only a large investment in equipment, but also additional costs for in the recruiting and training personnel are drawbacks of in-house production. The SAGA aircraft fleet will be assembled in line production, where many aircraft manufacturers already have years of experience [142]. Vertical integration is therefore not suitable for SAGA, since it would require large investments and would prevent the project from using more competitive (less costly, more efficient) options [149]. A larger level of control would be needed, however, for the critical components of the aircraft, including the aerosol tank. Besides, it is likely that the proposed consortium funding SAGA will want to be responsible for part of the production process for economical reasons [142]. This will complicate the production planning/process and will require a compromise between efficient work share and each country's economical interests. As a last note, it should be mentioned that the requirements stated above shall also be met when outsourcing the production.

Sustainability is an important factor for the production of the fleet and defined in the stakeholder requirements. For this reason, in the production process the use of toxic substances should be minimised, and the use of green energy and recycled material in the production should be maximised. Lean manufacturing will certainly help to improve the sustainability of the production by for example reducing processing waste, transportation and rework. These ideas, among others, should be exploited where relevant and based on existing facilities, it is decided that the production site shall generate at least 50% of its energy needs from renewable energy.

Based on current values from industry, it is estimated that it would take 3.5 years to produce the amount of aircraft needed per day (fleet without spare aircraft) and four years to finalise the production of the complete aircraft fleet^{2 3 4 5}. These values are based on the new Airbus A350 and Boeing 787, since the orders for both aircraft are very large for the current production rate. Therefore, it is assumed that the production rate corresponds to the current maximum achievable and is not scaled down due to low demand. Moreover, both companies adopt the concept of lean manufacturing^{6 7}.

² URL http://www.boeing.com/commercial/?cm_re=March_2015_-_Roadblock_-_Orders+%26+Deliveries/#/orders-deliveries [Accessed 18/05/16]

³ URL <http://boeing.mediaroom.com/2014-01-24-Boeing-Rolls-Out-First-787-Dreamliner-at-Increased-Production-Rate> [Accessed 20/05/16]

⁴ URL <http://aviationweek.com/paris-air-show-2015/airbus-plans-increase-a350-production-rate-13-month> [Accessed 20/05/16]

⁵ URL <http://www.airbus.com/presscentre/corporate-information/orders-deliveries/> [Accessed 20/05/16]

⁶ URL <http://uk.businessinsider.com/r-boeing-looks-to-car-industry-expert-for-jet-production-savings-2015-4?r=US&IR=T> [Accessed 20/05/16]

⁷ URL <http://www.airbus.com/innovation/proven-concepts/in-manufacturing/> [Accessed 20/05/16]

16. Future planning

16.1 Project design and development logic

In Fig. 16.1 and Fig. 16.2 the project logic diagram is shown. The project logic diagram shows the order of activities to be performed in the post-DSE phases.

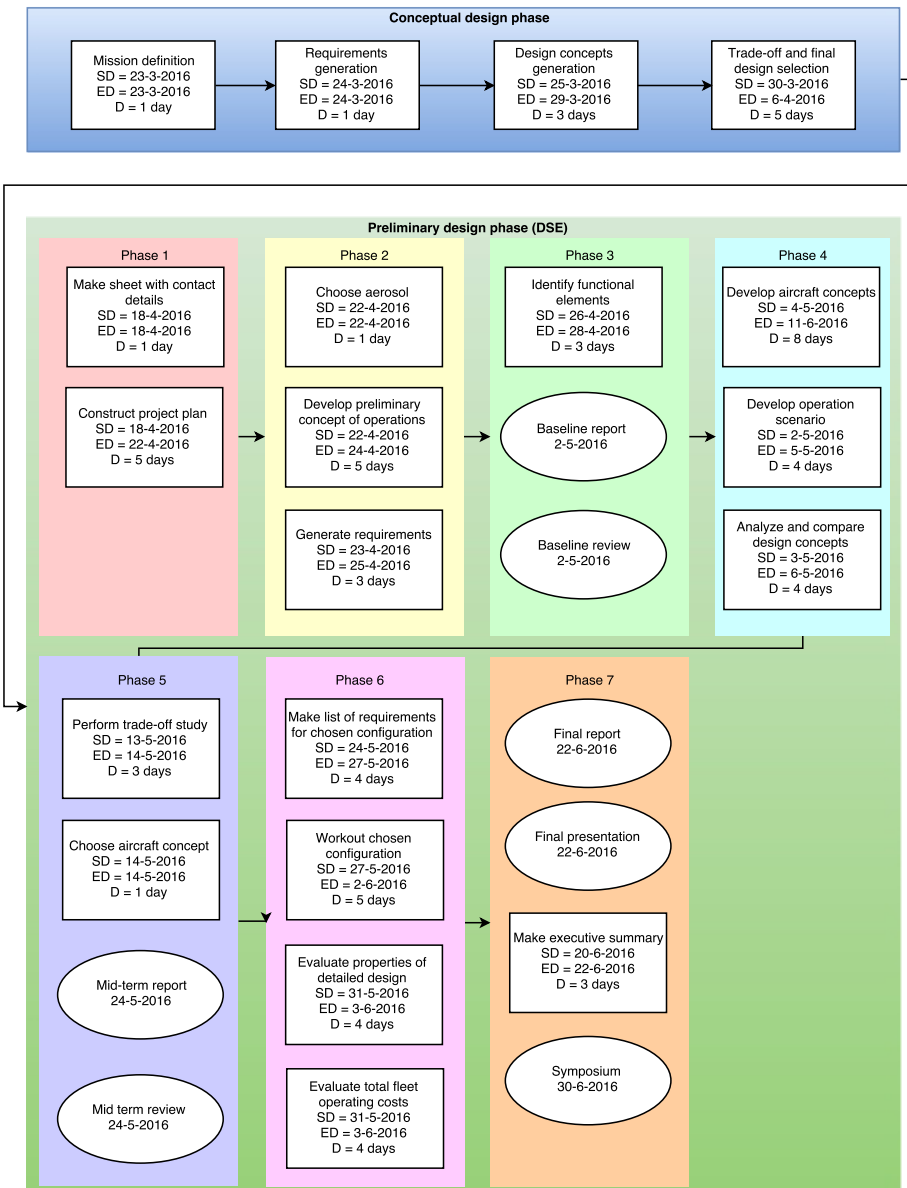


Figure 16.1: Project logic diagram

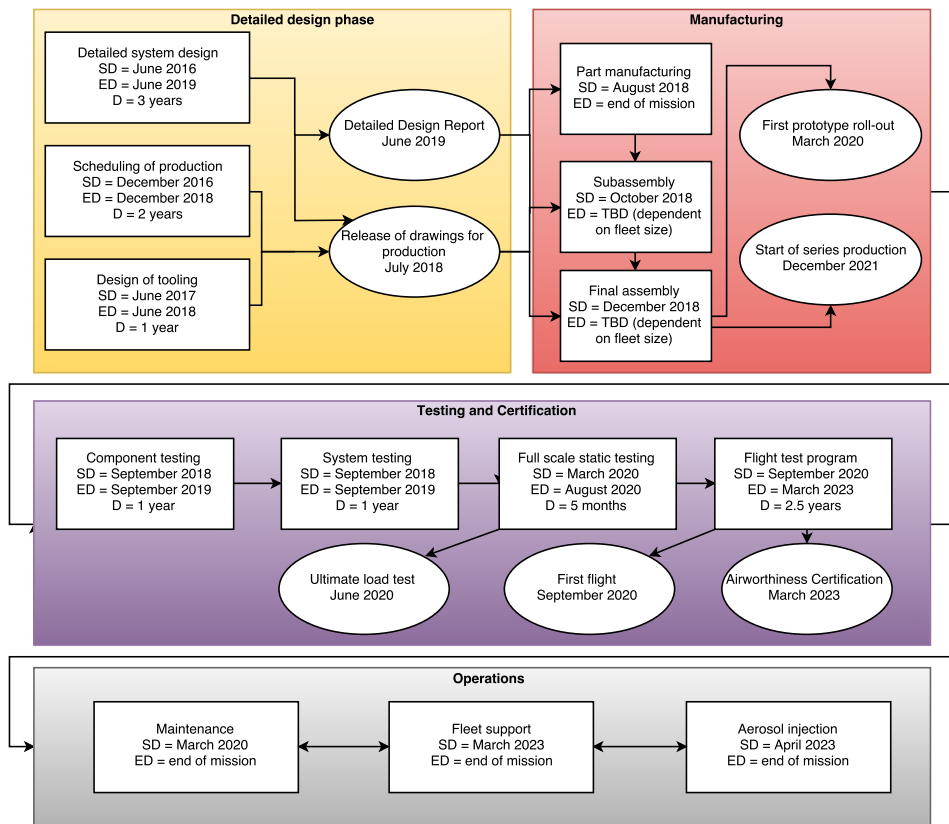


Figure 16.2: Project logic diagram (continued)

16.2 Project Gantt chart

The project Gantt chart is shown in Fig. 16.3 and shows the post-DSE activities in Gantt chart format.

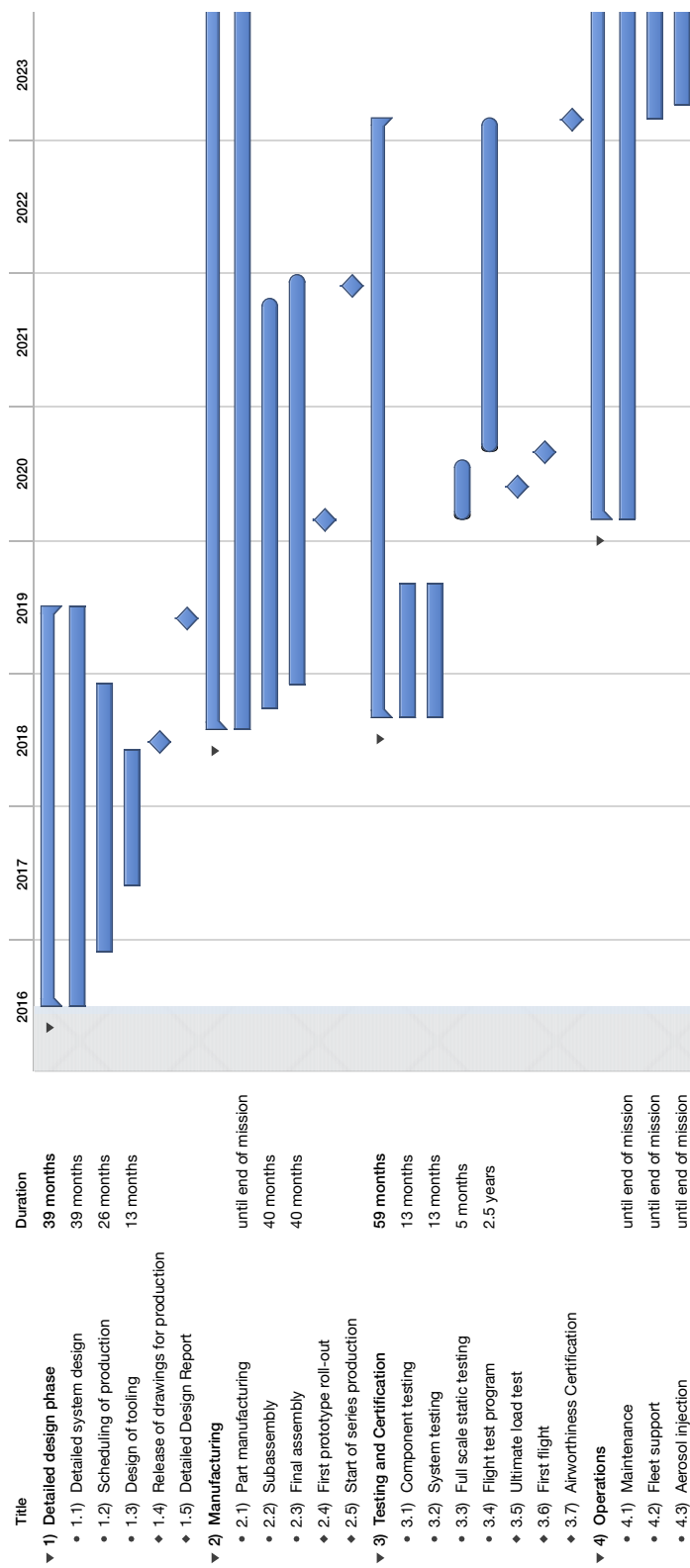


Figure 16.3: Post-DSE Gantt chart

17. Conclusion and recommendations

Current models of the climate show a possibility exists that the response of society to counteract rising global temperatures is not implemented fast enough or does not become effective fast enough to ensure temperatures remain within safe bounds. In this case, an intervention might be necessary to temporarily halt temperature increase until preventive long-term solutions are effective. Stratospheric geoengineering, more specifically, solar radiation management (SRM), offers such a temporary solution. A possible implementation of SRM is the injection of aerosols in the stratosphere, producing stratospheric clouds which reflect part of the incoming sunlight. This report aimed to describe the preliminary technical and operational design a fleet of purpose-built Stratospheric Aerosol Geoengineering Aircraft (SAGA) to deliver five megatons of aerosol per year to altitudes between 18.5 and 19.5km to gain insight in the cost and impact of such a system.

The design of an aircraft delivery system for stratospheric aerosol geoengineering has provided insights in the practical aspects of geoengineering. This report proposes a feasible implementation method for SRM by the injection of aerosols into the stratosphere. The design approach focused on feasibility and practicality is intended to augment the current research on climate engineering.

The high altitude and high payload requirements drive the design of all aspects of the SAGA mission. First of all, the operational scenario, employing a fleet of 344 unmanned aircraft, enabling 572 flights per day, is established with focus on most efficient delivery of the required 5 Mt of sulfuric acid aerosol to the stratosphere.

Sulfuric acid will be ejected from the aircraft in gas phase to facilitate efficient aerosol particle formation. Transport of the aerosol at elevated temperature in combination with on-board evaporation enable gas phase dispersion, and introduce a compelling power requirement. Aerosol dispersion will occur in the tropical region at altitudes between 18.5 and 19.5 km. The high altitude at which dispersion takes place governs the aircraft design. This altitude demands efficient lift generation and considerably high thrust.

The need for efficient lift generation results in a design featuring a high aspect ratio of 13 in combination with a wing surface area of 700 m². The structural integrity of this long and slender wing is ensured with the help of a strut-braced wing design. Aerodynamic, structural and aeroelastic characteristics create a very narrow design space, resulting from their conflicting requirements. The wing design as mentioned enables good lift-to-drag performance at a low structural weight. In addition, the risk for aeroelastic phenomena is acceptably low. Purpose-built engines are proposed to efficiently provide thrust and power to SAGA aircraft. Four engines, each providing over 600 kN thrust at sea level, facilitate completion of the constraining mission profile and provide a sufficient amount of power to the aerosol systems.

The costs of SAGA are estimated to amount to an initial capital cost of \$93.9 billion and a yearly operational cost of \$11 billion, which are acceptable amounts considering the costs of global warming. Although aircraft are not identified to be the most economical method for stratospheric aerosol delivery, the high technological readiness level enables fast and reliable implementation. The context in which geoengineering is applied calls for a safe and high confidence method, provided by SAGA.

17.1 Recommendations

In future iterations and design stages, the most highly constrained aspects of the concept design can be improved. High altitude flight can be performed more efficiently with a higher aspect ratio. The use of composites and a strut-braced design enable higher aspect ratios than 13 to be achieved in future design iterations. An increase of aspect ratio, however, introduces the need for more in-depth aeroelasticity analyses to ensure safe operations within the flight envelope.

In addition, the weight margin present in the current design possibly enables higher altitude flight for higher aerosol effectiveness or higher payload, reducing operational cost and emissions. However, detailed investigation of uncertainties in parameters is recommended, and (part of) the weight margin is reserved for required improvements identified in detailed design. Some examples of aspects requiring detailed analysis and possibly design modifications are the potential implementation of a gearbox between the fan the low pressure compressor in the engines for higher engine efficiency; more accurate fuel consumption estimates, perhaps

leading to a change in fuel weight; and detailed investigation of aeroelastic phenomena, likely requiring wing box design modifications to increase torsional stiffness.

In order to quantify the environmental impact of the injection of sulfuric acid or other aerosol compounds into the stratosphere, thorough experimenting and modelling is required. Ozone depletion, deposition through precipitation and climate effects other than temperature reduction will inevitably affect the environment. Before a geoengineering intervention using stratospheric aerosols is implemented, examination of these aspects is required to guarantee geoengineering is a safe operation.

Bibliography

- [1] Robock, A., *Geoengineering of the Climate System, Stratospheric Aerosol Geoengineering*, Issues in Environmental Science and Technology, The Royal Society of Chemistry, 2014.
- [2] Carlowicz, M., "World of Change - Global Temperatures," *Earth Observatory*, 2014.
- [3] Heckendorf, P., Weisenstein, D., Fueglstaler, S., Luo, B. P., Rozanov, E., Schraner, M., Thomason, L. W., and Peter, T., "The impact of geoengineering aerosols on stratospheric temperature and ozone," *Environmental Research Letters*, Vol. 4, No. 4, 2009, pp. 108–120.
- [4] Davidson, P., Burgoyne, C., Hunt, H., and Causier, M., "Lifting options for stratospheric aerosol geoengineering: advantages of tethered balloon systems," *Philosophical Transactions of the Royal Society of London A: Mathematical, Physical and Engineering Sciences*, Vol. 370, No. 1974, 2012, pp. 4263–4300.
- [5] Goes, M., Tuana, N., and Keller, K., "The economics (or lack thereof) of aerosol geoengineering," *Climatic change*, Vol. 109, No. 3-4, 2011, pp. 719–744.
- [6] Oliver, J. E. and Wood, T. J., "Conspiracy theories and the paranoid style (s) of mass opinion," *American Journal of Political Science*, Vol. 58, No. 4, 2014, pp. 952–966.
- [7] Global, M., "Aurora Flight Sciences Corporation," Tech. rep., Mint Global, 2015.
- [8] Sciences, A. F., "Geoengineering cost analysis," Tech. rep., University of Calgary, 2011.
- [9] Pierce, J. R., Weisenstein, D., Heckendorf, P., Peter, T., and Keith, D. W., "Efficient formation of stratospheric aerosol for climate engineering by emission of condensable vapor from aircraft," *Geophysical Research Letters*, Vol. 37, No. 18, 2010, L18805.
- [10] The Auditor, S. o. H., "Department of Transportation Airports Division State of Hawaii (An Enterprise Fund of the Staet of Hawaii)," Tech. rep., KPMG, 2014.
- [11] Liebeck, R., "Future Trends in UAS Avionics, Design of the Blended Wing Body Subsonic Transport Aircraft," *Journal of Aircraft*, Vol. 41, No. 1, feb 2004.
- [12] de Jong, S. and Slingerland, R., "Analysis of the Twin-Fuselage Configuration and its H-cabin Derivative," *AIAA's Annual Aviation Technology, Integration, and Operations (ATIO) Tech*, 2003.
- [13] Torenbeek, E., *Advanced Aircraft Design*, John Wiley & Sons, Ltd, 2013.
- [14] Sadraey, M. H., *Aircraft Design: A Systems Engineering Approach*, John Wiley & Sons, 2012.
- [15] Variyar, A., Economou, T. D., and Alonso, J. J., "Multifidelity Conceptual Design and Optimization of Strut-Braced Wing Aircraft using Physics Based Methods," *54th AIAA Aerospace Sciences Meeting*, 2016, p. 2000.
- [16] Lukaczyk, T., Wendorff, A. D., Botero, E., MacDonald, T., Momose, T., Variyar, A., Vegh, J. M., Colombo, M., Economou, T. D., Alonso, J. J., et al., "SUAVE: An Open-Source Environment for Multi-Fidelity Conceptual Vehicle Design," *16th AIAA/ISSMO Multi-disciplinary Analysis and Optimization Conference*, 2015, p. 3087.
- [17] Botero, E., Wendorff, A., MacDonald, T., Variyar, A., Vegh, J. M., Lukaczyk, T., Alonso, J. J., Orra, T. H., and Ilario da Silva, C., "SUAVE: An Open-Source Environment for Conceptual Vehicle Design and Optimization," *54th AIAA Aerospace Sciences Meeting*, 2016, p. 1275.
- [18] Raymer, D., *Aircraft Design: A Conceptual Approach*, American Institute of Aeronautics and Astronautics, Inc., 2006.
- [19] Pope, F. D., Braesicke, P., Grainger, R. G., Kalberer, M., Watson, I. M., Davidson, P. J., and Cox, R. A., "Stratospheric aerosol particles and solar-radiation management," *Nature Climate Change*, Vol. 2, No. 10, 2012, pp. 713–719.
- [20] Torenbeek, E., "Synthesis of Subsonic Airplane Design: An Introduction to the Preliminary Design of Subsonic General Aviation and Transport Aircraft, with Emphasis on Layout, Aerodynamic Design, Propulsion and Performance," *Delft University Press*, 1976.
- [21] Gundlach, J., *Multi-Disciplinary Design Optimization of Subsonic Fixed-Wing Unmanned Aerial Vehicles Projected Through 2025*, Ph.D. thesis, Virginia Polytechnic Institute, February 2004.
- [22] Roskam, J., *Airplane Design Part I: Preliminary Sizing of Airplanes*, DARcorporation, 1985.
- [23] Voskuil, M., "Take-off and Landing, Flight and Orbital Mechanics Lectures 4 and 5," Unpublished lecture notes.
- [24] Bauer Jr, K. W., Parnell, G. S., and Meyers, D. A., "Response surface methodology as a sensitivity analysis tool in decision analysis," *Journal of Multicriteria Decision Analysis*, Vol. 8, No. 3, 1999, pp. 162.
- [25] Durston, D. A., "LinAir: A Multi-Element Discrete Vortex Weissinger Aerodynamic Prediction Method," Tech. rep., NASA, 1993.
- [26] Hoak, D. E., e. a., "The USAF Stability and Control DATCOM," Tech. rep., Air Force Wright Aeronautical Laboratories, 1960.
- [27] ESDU, "ESDU 94044 - Excrescence drag levels on aircraft," Tech. rep., IHS, 2007.
- [28] Roskam, J., *Airplane Design Part VI: Preliminary Calculation Aerodynamic, Thrust, and Power Characteristics*, DARcorporation, 2000.
- [29] Steenhuizen, D., "AE2102 Wing Design Part 3," unpublished lecture slides.
- [30] Wallace, L. E., *Engineering Science to Big Science*, chap. 5: The Whitcomb Area Rule: NACA Aerodynamics Research and Innovation, NASA, 1998, pp. 144–147.
- [31] Nila, M. and Scholz, D., "Estimating the Oswald factor from basic aircraft parameters," *Deutscher Luft- und Raumfahrtkongress 2012*, 2012.
- [32] Drela, M., "XFOIL: An analysis and design system for low Reynolds number airfoils," *Low Reynolds number aerodynamics*, Springer, 1989, pp. 1–12.
- [33] Harris, C. D., "NASA Supercritical Airfoils: A Matrix of Family-Related Airfoils," *NASA Scientific and Technical Information Division*, 1990.
- [34] Jenkins, R., "NASA SC(2)-0714 airfoil data corrected for sidewall boundary-layer effects in the Langley 0.3-meter transonic cryogenic tunnel," *NASA-TP-2890*, 1989.
- [35] Johnson, W. and S., H. A., "Pressure Distributions From High Reynolds Number Tests of a NASA SC(3)-0712(B) Airfoil in the Langley 0.3-Meter Transonic Cryogenic Tunnel," *NASA Scientific and Technical Information Branch*, 1985.

- [36] Panel, F. D., "Experimental Data Base for Computer Program Assessment," Tech. rep., NATO Advisory Group for Aerospace Research and Development, 1979.
- [37] Scholz, D., *Aircraft Design Course Notes*, chap. 9: Empennage General Design, Hamburg Open Online University, 2016, pp. 1–17.
- [38] Mineck, R. E. and Lawing, P. L., "High Reynolds Number tests of the NASA SC (2)-0012 airfoil in the Langley 0.3-meter transonic cryogenic tunnel," *NASA Technical Memorandum*, 1987.
- [39] Loftin Jr, L. K., "Theoretical and experimental data for a number of NACA 6A-series airfoil sections," *NACA Research Memorandum*, 1946.
- [40] Corke, T. C., *Design of aircraft*, Pearson College Division, 2003.
- [41] Carrier, G., Atinault, O., Dequand, S., Hantrais-Gervois, J., Liauzun, C., and Paluch, B., "Investigation of a strut-braced wing configuration for future commercial transport," *28th International Congress of the Aeronautical Sciences*, 2012, p. 15.
- [42] Ko, A., Mason, W. H., Grossman, B., and Schetz, J., "A-7 strut braced wing concept transonic wing design," Tech. rep., VPI-AOE-275, Virginia Polytechnic Institute and State University, 2002.
- [43] Ko, Andy, M. W. and B., G., "Transonic Aerodynamics of a Wing/Pylon/Strut Juncture," *21st AIAA Applied Aerodynamics Conference*, AIAA, 2003, p. 9.
- [44] Welstead, J. R., Reitz, B. C., and Crouse Jr, G. L., "Modeling Fuselage Aerodynamic Effects in Aircraft Design Optimization," *Aerospace Sciences Meeting including the New Horizons Forum and Aerospace Exposition*, 2012, pp. 9–16.
- [45] Harris, C. D., McGhee, R. J., and Allison, D. O., "Low-speed aerodynamic characteristics of a 14-percent-thick NASA phase 2 supercritical airfoil designed for a lift coefficient of 0.7," *NASA technical memorandum*, 1980.
- [46] Harris, C. D., "Aerodynamic characteristics of a 14-percent-thick NASA supercritical airfoil designed for a normal-force coefficient of 0.7," *NASA Technical Memorandum*, 1975.
- [47] Palacios, F., Economou, T. D., Aranake, A. C., Copeland, S. R., Lonkar, A. K., Lukaczyk, T. W., Manosalvas, D. E., Naik, K. R., Padrón, A. S., Tracey, B., et al., "Stanford University Unstructured (SU2): Open-source analysis and design technology for turbulent flows," *AIAA paper*, Vol. 243, 2014, pp. 13–17.
- [48] Richardson, L. E., "The Approximate Arithmetic Solution by Finite Differences of Physical Problems Involving Differential Equations, with Application to Stresses in a Masonry Dam," *Transactions of the Royal Society of London*, Vol. 210, No. A, 1910, pp. 307–357.
- [49] Haselbach, F. and Parker, R., "Hot End technology for advanced, low emission large civil aircraft engines," *28th International Congress of the Aeronautical Sciences*, Vol. 2, 2012, p. 3.
- [50] CA, A. F. T. P. S. E. A., "Volume 1. Performance Flight Testing Phase. Chapter 7. Aero Propulsion." Tech. rep., Air Force Test Pilot School Edwards AFB CA, 1991.
- [51] Richardson, M., Gudino, J., Chen, K., Luong, T., Wilkerson, D., and Keyvani, A., "NASA/USRA High Altitude Research Aircraft," Tech. rep., NASA, 1990.
- [52] Rivera, J., Nunes, A., McRae, M., Wong, W., Ong, A., and Coble, S., "NASA/USRA high altitude research aircraft. Gryphon: Soar like an eagle with the roar of a lion," Tech. rep., NASA, 1991.
- [53] Melkert, J., "AE-2203 Propulsion and Power - Lecture-5 : Aero Engines-3," retrieved as ppt, mar 2015.
- [54] Cohen, H., Rogers, G. F. C., Saravanamutto, H. I. H., and (r.) Saravanamutto, H., *Gas turbine theory*, Longman Scientific & Technical Harlow (England), 1996.
- [55] Tiemstra, F., *Design of a Semi-Empirical Tool for the Evaluation of Turbine Cooling Requirements in a Preliminary Design Stage*, Ph.D. thesis, TU Delft, Delft University of Technology, 2014.
- [56] Roskam, J., *Airplane Design Part 8: Airplane Cost Estimation: Design, Development, Manufacturing and Operating*, DARcorporation, 1990.
- [57] Spittle, P., "Gas turbine technology," *Physics education*, Vol. 38, No. 6, 2003, pp. 504.
- [58] Krupa, S. V. and Manning, W. J., "Atmospheric ozone: formation and effects on vegetation," *Environmental Pollution*, Vol. 50, No. 1-2, 1988, pp. 101–137.
- [59] Stolarski, R. S., Baughcum, S. L., Brune, W. H., Douglass, A. R., Fahey, D. W., Friedl, R. R., Liu, S. C., Plumb, R. A., Poole, L. R., and Wesoky, H. L., "The 1995 scientific assessment of the atmospheric effects of stratospheric aircraft," *NASA Publication Reference*, 1995.
- [60] Kimmel, E., Leahy, H., Kinhead, E., and Wall, H., "The Acute Inhalation Toxicity of Triethylborane Spontaneous Oxidation Products: Immediate and Delayed Exposure," Tech. rep., DTIC Document, 1990.
- [61] Graham, R. H., *SR-71: The Complete Illustrated History of the Blackbird, The World's Highest, Fastest Plane*, Zenith Press, 2013.
- [62] Pueschel, R. F., Verma, S., Ferry, G. V., Howard, S. D., Vay, S., Kinne, S. A., Goodman, J., and Strawa, A. W., "Sulfuric acid and soot particle formation in aircraft exhaust," *Geophysical research letters*, Vol. 25, No. 10, 1998, pp. 1685–1688.
- [63] Casadevall, T. J., Delos Reyes, P., and Schneider, D. J., "The 1991 Pinatubo eruptions and their effects on aircraft operations," *Fire and Mud: eruptions and lahars of Mount Pinatubo, Philippines*, 1996, pp. 625–636.
- [64] Bernard, A. and Rose, W. I., "The injection of sulfuric acid aerosols in the stratosphere by the El Chichón volcano and its related hazards to the international air traffic," *Natural Hazards*, Vol. 3, No. 1, 1990, pp. 59–67.
- [65] Shepherd, J. G., "Geoengineering the climate - Science, governance and uncertainty," *Royal Society*, 2009, pp. 32.
- [66] Mattingly, J., *Aircraft Engine Design*, AIAA education series, American Institute of Aeronautics & Astronautics, 2002.
- [67] Naghshineh-Pour, A., *Structural Optimization and Design of a Strut-Braced Wing Aircraft*, Master's thesis, Virginia Polytechnic Institute and State University, 1998.
- [68] Crandall, Dahl, L., *An Introduction to the Mechanics of Solids*, McGraw-Hill, Inc., 1978.
- [69] Yang, B., *Stress, strain, and structural dynamics: An iterative handbook of Formulas, Solutions, and MATLAB toolboxes*, Elsevier, Inc., 2005.
- [70] Richardson, D., "The Fundamental Principles of Composite Material Stiffness Predictions," Unpublished lecture notes.
- [71] Kassapoglou, C., "Advanced Design and Optimization of Composite Structures I," Unpublished lecture notes.
- [72] Walvekar, V., *Birdstrike analysis on leading edge of an aircraft wing using a smooth particle hydrodynamics bird model*, Master's thesis, Visvesvaraya Technological University, 2007.
- [73] Craig, B. and Anderson, D., *Handbook of corrosion data*, ASM International, 1995.
- [74] Strong, A., *Fundamentals of Composites Manufacturing. Materials, Methods, and Applications*, Society of Manufacturing Engi-

- neers, 2008.
- [75] European Aviation Safety Agency, *Certification Specifications for Large Aeroplanes CS-25*, amendment 5 ed., September 2008.
- [76] Hulshoff, S., "AE4930 Aeroelasticity," retrieved as PDF.
- [77] Gern, F. H., Naghshineh-Pour, A. H., Sulaeman, E., , and Kapania, R. K., "Structural Wing Sizing for Multidisciplinary Design Optimization of a Strut-Braced Wing," *Journal of Aircraft*, Vol. 38, No. 154-163, feb 2001.
- [78] Nguyen, N., Ting, E., and Lebofsky, S., "Aeroelasticity of Axially Loaded Aerodynamic Structures for Truss-Braced Wing Aircraft," *56th AIAA/ASCE/AHS/ASC Structures, Structural Dynamics, and Materials Conference*, 2015, p. 1840.
- [79] Kehoe, M. W., "A Historical Overview of Flight Flutter Testing," Tech. rep., National Aeronautics and Space Administration, oct 1995.
- [80] Livne, E., "The Active Flutter Suppression (AFS) Technology Evaluation Project," retrieved as powerpoint slides, mar 2014, The William E. Boeing Department of Aeronautics and Astronautics University of Washington, Seattle, WA.
- [81] Raja, S. and Upadhyay, A. R., "Active Control of Wing Flutter Using Piezoactuated Surface," *Journal of Aircraft*, Vol. 44, No. 1, feb 2007, pp. 71-80.
- [82] Tewari, A., *Aeroservoelasticity*, Birkhäuser, 2015.
- [83] Dubcová, L., Feistauer, M., Horáček, J., and Sváček, P., "Numerical simulation of airfoil vibrations induced by turbulent flow," *Journal of Computational and Applied Mathematics*, Vol. 218, No. 1, 2008, pp. 34 – 42, Special Issue: Finite Element Methods in Engineering and Science (FEMTEC 2006)Special Issue: Finite Element Methods in Engineering and Science (FEMTEC 2006).
- [84] Bergami, L., *Aeroelastic Stability of a 2D Airfoil Section equipped with a Trailing Edge Flap*, Danmarks Tekniske Universitet, Risø Nationallaboratoriet for Bæredygtig Energi, 2008, Risø-R-1663(EN).
- [85] Yoon, N., Chung, C., Na, Y.-H., and Shin, S., "Control reversal and torsional divergence analysis for a high-aspect-ratio wing," *Journal of Mechanical Science and Technology*, Vol. 26, No. 12, 2012, pp. 3921–3931.
- [86] Cavagna, L., Ricci, S., and Travaglini, L., "NeoCASS: an integrated tool for structural sizing, aeroelastic analysis and MDO at conceptual design level," *Progress in Aerospace Sciences*, Vol. 47, No. 8, 2011, pp. 621–635.
- [87] Wright, J. R. and Cooper, J. E., *Introduction to aircraft aeroelasticity and loads*, Vol. 20, John Wiley & Sons, 2008.
- [88] Rocca, G. L., "AE3221-I Lecture 4 - Design for Aircraft Longitudinal Stability," unpublished lecture slides.
- [89] Hodgkinson, J., *Aircraft Handling Qualities*, Blackwell Science, 1999.
- [90] Mulder, J., van Staveren, W., van der Vaart, J., de Weerdt, E., de Visser, C., in 't Veld, A., and Mooij, E., "Flight Dynamics Lecture Notes," Unpublished lecture notes.
- [91] Institute, S. R., Abramson, H., Aeronautics, U. S. N., and Administration, S., *The Dynamic Behavior of Liquids in Moving Containers: With Applications to Space Vehicle Technology*, NASA SP, Scientific and Technical Information Division, National Aeronautics and Space Administration, 1966.
- [92] Su, W. and S. Cesnik, C. E., "Nonlinear aeroelasticity of a very flexible blended-wing-body aircraft," *Journal of Aircraft*, Vol. 47, No. 5, 2010, pp. 1539–1553.
- [93] of Transportation, U. D., *Aviation Maintenance Technician Handbook - Airframe*, Vol. 2, Federal Aviation Administration, 2012.
- [94] Van Den Bossche, D., "The A380 flight control electrohydrostatic actuators, achievements and lessons learnt," *25TH International congress of the aeronautical sciences*, 2006, pp. 1–8.
- [95] Elkaim, G. H., Lie, F. A. P., and Gebre-Egziabher, D., *Handbook of Unmanned Aerial Vehicles*, chap. Principles of Guidance, Navigation, and Control of UAVs, Springer Netherlands, Dordrecht, 2015, pp. 347–380.
- [96] Heppe, S. B., *Handbook of Unmanned Aerial Vehicles*, chap. Problem of UAV Communications, Springer Netherlands, Dordrecht, 2015, pp. 715–748.
- [97] Edwards, C., Lombaerts, T., and Smaili, H., "Fault tolerant flight control," *Lecture Notes in Control and Information Sciences*, Vol. 399, 2010.
- [98] Angelov, P., *Sense and avoid in UAS: research and applications*, John Wiley & Sons, 2012.
- [99] Robock, A. and Mao, J., "The Volcanic Signal in Surface Temperature Observations," *Journal of Climate*, Vol. 8, No. 5, 1995, pp. 1086–1103.
- [100] Solomon, S., "Stratospheric ozone depletion: a review of concepts and history," *Reviews of Geophysics*, Vol. 37, No. 3, 1999, pp. 275–316.
- [101] Dykema, J. A., Keith, D. W., Anderson, J. G., and Weisenstein, D., "Stratospheric controlled perturbation experiment: a small-scale experiment to improve understanding of the risks of solar geoengineering," *Philosophical Transactions of the Royal Society of London A: Mathematical, Physical and Engineering Sciences*, Vol. 372, No. 2031, 2014.
- [102] Haywood, J. M., Jones, A., Bellouin, N., and Stephenson, D., "Asymmetric forcing from stratospheric aerosols impacts Sahelian rainfall," *Nature Climate Change*, Vol. 3, No. 7, 2013, pp. 660–665.
- [103] European Aviation Safety Agency, *Certification Specifications for Large Aeroplanes CS-25*, amendment 3 ed., September 2007.
- [104] Davis, J., *Corrosion: Understanding the Basics*, A S M International, 2000.
- [105] Panossian, Z., Almeida, N. L. d., Sousa, R. M. F. d., Pimenta, G. d. S., and Marques, L. B. S., "Corrosion of carbon steel pipes and tanks by concentrated sulfuric acid: A review," *Corrosion Science*, Vol. 58, 2012, pp. 1 – 11.
- [106] for Biotechnology Information, N. C., "PubChem Compound Database; CID=1118," 2004–2016, accessed May 2016.
- [107] ASTM, *D1998-15 Standard specification for polyethylene upright storage tanks*, ASTM International, 2015.
- [108] N/A, N/A, American Society of Heating, Refrigerating and Air-Conditioning Engineers, Inc., 2009.
- [109] Lee, K. Y., Yang, J. S., Choi, Y. S., and Park, D. H., "Specific Heat and Thermal Conductivity Measurement of XLPE Insulator and Semiconducting Materials," *2006 IEEE 8th International Conference on Properties applications of Dielectric Materials*, June 2006, pp. 805–809.
- [110] Yane, D., Base, H., and James, J., "High efficiency ultra-pure fluid heater," July 27 1999, US Patent 5,930,458.
- [111] Fakheri, A., "Heat exchanger efficiency," *Journal of Heat Transfer*, Vol. 129, No. 9, 2006, pp. 71268–1276.
- [112] Campos, D. C., Dall'Oglio, E. L., de Sousa Jr., P. T., Vasconcelos, L. G., and Kuhnen, C. A., "Investigation of dielectric properties of the reaction mixture during the acid-catalyzed transesterification of Brazil nut oil for biodiesel production," *Fuel*, Vol. 117, Part B, 2014, pp. 957 – 965.
- [113] Gabriel, C., Gabriel, S., H. Grant, E., H. Grant, E., S. J. Halstead, B., and Michael P. Mingos, D., "Dielectric parameters relevant to microwave dielectric heating," *Chem. Soc. Rev.*, Vol. 27, 1998, pp. 213–224.

- [114] Veiko, V. P., Skvortsov, A. M., Huynh Cong, T., and Petrov, A. A., "Laser ablation of monocrystalline silicon under pulsed-frequency fiber laser," *Scientific and Technical Journal of Information Technologies, Mechanics and Optics*, Vol. 15, No. 3, 2015, pp. 426 – 434.
- [115] Esenaliev, R. O., Karabutov, A. A., Podymova, N. B., and Letokhov, V. S., "Laser ablation of aqueous solutions with spatially homogeneous and heterogeneous absorption," *Applied Physics B*, Vol. 59, No. 1, 1994, pp. 73–81.
- [116] Sree Harsha, K. S., *Principles of Physical Vapor Deposition on Thin Films*, Elsevier, Oxford, 1st ed., 2006.
- [117] Special Metals Corporation, *MONEL alloy 400*, feb 2005.
- [118] Watlow Electric Manufacturing, *Immersion heaters - Firebar/Watrod flange immersion heaters*, Feb. 2013.
- [119] Babka, D. W., "Flight Testing in a Simulation Based Environment," Tech. rep., American Institute of Aeronautics and Astronautics, 2011.
- [120] Bais, A. F., McKenzie, R. L., Bernhard, G., Aucamp, P. J., Ilyas, M., Madronich, S., and Tourpali, K., "Ozone depletion and climate change: impacts on UV radiation," *Photochem. Photobiol. Sci.*, Vol. 14, 2015, pp. 19–52.
- [121] Niu, M. C.-Y., *Airframe Structural Design*, Commlit Press Ltd., eighth ed., 1995.
- [122] Curran, R. and Verhagen, W., "AE3221-I Lecture 8 - Risk Management & Reliability Engineering," unpublished lecture slides.
- [123] Federal Aviation Agency, "2nd Technical Report on Propulsion System and APU-Related Aircraft Safety Hazards," Tech. rep., Aerospace Industries Association, 2005.
- [124] Smetana, F. O., *Flight vehicle performance and aerodynamic control*, AIAA, 2001.
- [125] Nielsen, J., Larsen, N., Cairo, F., Donfrancesco, G. D., Rosen, J., Durry, G., Held, G., and Pommereau, J.-P., "Solid particles in the tropical lower stratosphere," *Atmospheric Chemistry and Physics*, Vol. 7, No. 3, 2007, pp. 685–695.
- [126] Curran, R., Raghunathan, S., and Price, M., "Review of aerospace engineering cost modelling: The genetic causal approach," *Progress in Aerospace Sciences*, Vol. 40, 2004, pp. 487 – 534.
- [127] Dhillon, B., *Life Cycle Costing: Techniques, Models and Applications*, Gordon and Breach Science Publishers S.A., 1989.
- [128] *FY2013 Maintenance Cost Preliminary Analysis*, Lecture Notes in Computer Science, Athens, Greece, 2014, IATA.
- [129] Liebeck, R. H., Andrastek, D. A., Chau, J., Girvin, R., Lyon, R., Rawdon, B. K., Scott, P. W., and Wright, R. A., "Advanced subsonic airplane design and economic studies," Tech. rep., NASA, apr 1995.
- [130] Elkaim, G. H., Lie, F. A. P., and Gebre-Egziabher, D., *Handbook of Unmanned Aerial Vehicles*, chap. Human Factors Perspective on Next Generation Unmanned Aerial Systems, Springer Netherlands, Dordrecht, 2015, pp. 2406–2423.
- [131] Gundlach, J., *Designing Unmanned Aircraft Systems: A Comprehensive Approach*, American Institute of Aeronautics and Astronautics, 2012, Chapter 16.
- [132] Weibel, R. E., *Safety Considerations for Operation of Unmanned Aerial Vehicles in the National Airspace System*, Ph.D. thesis, Department of Aeronautics & Astronautics, June 2005.
- [133] Amina Malik, F. L., "Evaluation of Equivalent of Level of Safety for Civil and Commercial Applications of Remotely Piloted Aircraft Systems," *Air Transport and Operations Symposium 2015*, 2015, p. 7.
- [134] Christopher Edwards, Thomas. Lombaerts, H. S., *Fault tolerant flight control : a benchmark challenge*, Springer, 2010.
- [135] Gehin, A., "A tool to implement sustainable end-of-life strategies in the product development phase," *Journal of Cleaner Production*, 2008.
- [136] Curran, R. and Verhagen, W., "Concurrent Engineering & Design for Lifecycle," retrieved as PDF, apr 2016.
- [137] Airbus, "Sustainable Aviation: Aviation Environmental Roadmap," Unpublished document.
- [138] Kravitz, B., Robock, A., Boucher, O., Schmidt, H., Taylor, K. E., Stenchikov, G., and Schulz, M., "The Geoengineering Model Inter-comparison Project (GeoMIP)," *Atmospheric Science Letters*, Vol. 12, No. 2, 2011, pp. 162–167.
- [139] Ammann, C. M., Washington, W. M., Meehl, G. A., Buja, L., and Teng, H., "Climate engineering through artificial enhancement of natural forcings: Magnitudes and implied consequences," *Journal of Geophysical Research: Atmospheres*, Vol. 115, No. D22, 2010, D22109.
- [140] ICAO, "ICAO Environmental Report," Tech. rep., International Civil Aviation Organization, 2010.
- [141] Bolz, R., *Production Processes: The Productivity Handbook*, Industrial Press, 1977.
- [142] Sinke, J., *Production of Aerospace Systems*, TU Delft, 2016.
- [143] Ramaswamy, D., *The role of lean manufacturing principles and strategic alternatives in achieving business goals*, Ph.D. thesis, Massachusetts Institute of Technology, 2006.
- [144] Andersson, R., Eriksson, H., and Torstensson, H., "Similarities and differences between TQM, six sigma and lean," *The TQM Magazine*, Vol. 18, No. 3, 2006, pp. 282–296.
- [145] Mason-Jones, R., Naylor, B., and Towill, R., "Lean, agile or leagile? Matching your supply chain to the marketplace," *International Journal of Production Research*, Vol. 38, No. 17, 2000, pp. 4061–4070.
- [146] Naylor, J. B., Naim, M. M., and Berry, D., "Leagility: Integrating the lean and agile manufacturing paradigms in the total supply chain," *International Journal of Production Economics*, Vol. 62, No. 1-2, 1999, pp. 107 – 118.
- [147] Hines, P., Holweg, M., and Rich, N., "Learning to evolve: A review of contemporary lean thinking," *International Journal of Operations & Production Management*, Vol. 24, No. 10, 2004, pp. 994–1011.
- [148] Hexcel, "HexPly Prepreg Technology," January 2013.
- [149] Hurtt, D. N., Kreuze, J. G., et al., "Cost Management: Is Vertical Integration the Answer?" *Journal of Corporate Accounting & Finance*, Vol. 11, No. 3, 2000, pp. 29–36.

Nomenclature

Abbreviations

ΔT	temperature difference	[K]
$\frac{L}{D}$	lift to drag ratio	[–]
FR_{sys}	failure rate of system	[ground fatalities per hour]
OEW_0	line intersection for empty weight fraction from statistics from reference aircraft	[N]
Re	reynolds number	[–]
ADP	air driven pump	[–]
APU	auxiliary power unit	[–]
ATC	air traffic control	[–]
AVL	athena vortex lattice	[–]
AWO	all-weather operations	[–]
BPR	bypass ratio	[–]
BWB	blended wing body	[–]
c.g.	centre of gravity	[m]
CE	concurrent engineering	[–]
CFD	computational fluid dynamics	[–]
Dfc	design for cost	[–]
Dfe	design for environment	[–]
Dfr	design for reliability	[–]
DME	distance measuring equipment	[–]
DOC	direct operating cost	[–]
DOT	design option tree	[–]
EASA	european aviation safety agency	[–]
EDP	engine driven pump	[–]
FBS	functional breakdown structure	[–]
FFD	functional flow diagram	[–]
GCU	generator control unit	[–]
GISS	goddard institute for space studies	[–]
GPS	global positioning system	[–]
HLD	high lift device	[–]
HPC	high pressure compressor	[–]
ICAO	international civil aviation organisation	[–]
ILS	instrument landing system	[–]
INS	inertial navigation system	[–]
ISA	international standard atmosphere	[–]
ISS	international space station	[–]
KE	kinetic energy	[J]
LAAS	local area augmentation system	[–]
LGHEGS	landing gear electro-hydraulic generation system	[–]
LHC	large hadron collider	[–]
LHV	lower heating value	[J/kg]
LORAN	long range navigation	[–]
LPC	low pressure compressor	[–]
MLS	microwave landing system	[–]
MSLBS	microwave scanning beam landing system	[–]
MTBF	mean time between catastrophic failure	[flight hours]
MTOW	maximum take-off weight	[–]
NAA	national aviation agencies	[–]
OEI	one engine inoperative	[–]
OEW	operational empty weight	[–]
OPR	overall pressure ratio	[–]
PR	pressure ratio	[–]
RAMS	reliability, availability, maintainability, safety	[–]
RAT	ram air turbine	[–]
RC	rate of climb	[m/s]
RVR	runway visible range	[–]
SA	spallart-almaras turbulence model	[–]
SAGA	stratospheric aerosol geoengineering aircraft	[–]
SAM	sollar array management	[–]
SATCOM	satelite communications	[–]
SFC	specific fuel consumption	[kg/Ns]
SRM	solar radiation management	[–]
SU2	stanford university unstructured	[–]
SUAVE	stanford university aerospace vehicle environment	[–]
T04	turbine inlet temperature	[K]
TBA	twin body aircraft	[–]
TRL	technological readiness level	[–]

TRU	transformer rectifier unit	[–]
UAV	unmanned aerial vehicle	[–]
VFR	visual flight rule	[–]
VHF	very high frequency	[–]
VLM	vortex lattice method	[–]
VOR	vhf omnidirectional range	[–]
WAAS	wide area augmentation system	[–]
WBS	work breakdown structure	[–]
WFD	work flow diagram	[–]

Greek Symbols

α	angle of attack	[deg]
γ_A	flight path angle at approach	[rad]
β	angle of sideslip	[deg]
ϵ	dielectric loss factor	[F/m]
ϵ_0	vacuum permittivity	[F/m]
η	efficiency	[–]
γ_A	flight path angle at screening altitude	[rad]
Λ	sweep angle	[rad]
Λ_h	horizontal tail sweep angle	[rad]
Λ_v	vertical tail sweep angle	[rad]
λ_{fus}	fuselage slenderness ratio	[–]
ω	angular frequency	[rad/s]
ϕ	roll angle	[deg]
ρ	density	[kg/m ³]
ζ	damping ratio	[–]
ϕ_{hi}	roll angle	[deg]

Roman Symbols

\bar{D}_g	average drag due to ground friction during take off/ landing	[N]
\bar{D}	average drag at take off/landing	[N]
\bar{T}_{rev}	average reverse thrust during landing	[N]
T	average thrust at take off/ landing	[N]
κ	specific heat ratio	[–]
λ	main wing taper ratio	[–]
λ_h	horizontal stabilizer taper ratio	[–]
λ_v	vertical stabilizer taper ratio	[–]
a	laser beam radius	[m]
A_I	area of impact	[m ²]
A_{exp}	exposed ground area	[m ²]
AR	aspect ratio	[–]
C_D	aircraft drag coefficient	[–]
C_L	aircraft lift coefficient	[–]
C_M	moment coefficient	[–]
c_p	specific heat ratio at constant pressure	[J/kgK]
c_p	specific heat	[J/K]
C_{D0}	zero lift drag coefficient	[–]
C_{Di}	aircraft induced drag coefficient	[–]
C_{Dp}	aircraft parasite drag coefficient	[–]
$C_{D0,tank}$	zero lift drag coefficient of an external tank	[–]
C_{feq}	equivalent skin friction coefficient	[–]
C_{ftank}	skin friction coefficient of an external tank	[–]
$C_{L\delta}$	change in lift coefficient due to aileron deflection	[rad ⁻¹]
$C_{M\delta}$	change in moment coefficient due to aileron deflection	[rad ⁻¹]
$C_{M\delta}$	lift curve slope	[rad ⁻¹]
C_{mac}	mean aerodynamic chord	[m]
C_r	root chord	[m]
c_{strut}	strut chord	[deg]
C_t	tip chord	[m]
d_f	diameter of an external tank	[m]
E	endurance	[s]
E	young's modulus	[N/m ²]
e	elementary charge	[C]
e	oswald factor	[–]
$e_{inviscid}$	inviscid oswald factor	[–]
G	climb gradient	[%]
g	gravitational acceleration	[m/s ²]
h_{scr}	screening altitude	[m]
K	scaling parameter	[–]
k	wall conductivity	[W/mK]
K_θ	torsional stiffness	[Nm/rad]
l_f	length of an external tank	[m]
l_h	moment arm of horizontal tail	[m]
M	mach number	[–]
m	mass	[kg]
M_{dd}	drag divergence mach number	[–]
m_{pl}	payload mass	[kg]

n	ultimate load factor	[–]
P_a	power available	[W]
P_a	power available	[W]
P_r	power required	[W]
P_r	power required	[W]
P_{pen}	probability of penetration	[–]
q	dynamic pressure	[Pa]
R	range	[m]
r	yaw rate	[deg/s]
R_p	radius of a person	[m]
S	wing surface area	[m ²]
s	wall thickness	[mm]
S_h	area of horizontal tail	[m ²]
S_w	body wetted area	[–]
S_{front}	aircraft frontal area	[m ²]
$S_{wet,tank}$	wetted area of an external tank	[m ²]
t/c	wing thickness to chord ratio	[–]
T_{app}	approach thrust	[m/s]
T_{des}	design thrust	[N]
U	voltage	[V]
V	airspeed	[m/s]
V_1	decision speed	[m/s]
V_s	1g stall speed	[–]
V_{EAS}	equivalent airspeed	[m/s]
V_{app}	approach speed	[m/s]
V_{climb}	climb out speed	[m/s]
V_{cr}	cruise speed	[m/s]
V_{EAS}	equivalent airspeed	[m/s]
V_{EF}	main engine failure speed	[m/s]
V_{LOF}	lift off airspeed	[m/s]
V_{scr}	airspeed at screening altitude	[m/s]
V_{SR}	reference stall speed	[m/s]
W	aircraft weight	[N]
$W_{engines}$	engines weight	[N]
W_{f1}	fuel weight for the first cruise phase	[N]
W_{f2}	fuel weight for the second cruise phase	[N]
W_{f3}	fuel weight for the third cruise phase	[N]
$W_{f,tot}$	total fuel weight	[N]
W_{lg}	weight of landing gears	[N]
W_{pl}	payload weight	[N]
W_{TO}	take off weight	[N]
x_θ	distance between centre of gravity (c.g.) and elastic axis	[%c]
A	total tank area	[m ²]
b	wing span	[m]
E	elastic modulus	[GPa]
E	laser beam energy	[J]
G	shear modulus	[GPa]
g	gliding distance	[m]
I	moment of inertia	[m ⁴]
P	vapour pressure	[Pa]
Q	energy loss/input energy	[J]
R	gas constant	[J/kgK]
T	vapour temperature	[°C]
T ₂	time to double amplitude	[s]
T _{1/2}	time to half amplitude	[s]
V	airspeed	[m/s]
v	kinematic viscosity	[m ² /s]

List of Figures

2.1 Worldwide temperature anomalies 1885-1894 [2]	2
2.2 Worldwide temperature anomalies 2005-2014 [2]	2
2.3 Temperature scenarios without implementation of geoengineering	3
2.4 Temperature scenarios with implementation of geoengineering	3
3.1 SWOT analysis *effects which have been observed for volcano eruptions	7
4.1 Aircraft positioning for an operational range of 3500 km	11
6.1 Functional Breakdown structure of the mission	16
6.2 Functional Flow Diagram for one aircraft sortie	17
6.3 Functional Flow Diagram for the mission	17
7.1 Extended and retracted landing gear configurations	19
7.2 Three projection view of the SAGA aircraft. Dimensions are in m	20
8.1 Design framework (based on [15])	22
8.2 Class diagram (based on [16])	23
8.3 SUAVE output: Mission profile; Aircraft, Fuel and Aerosol weights; specific fuel consumption	27
8.4 SUAVE output: Mach number, Throttle setting, Drag and Thrust, Mass rate of fuel and aerosol	27
8.5 Component percentage with respect to OEW	28
8.6 SUAVE Vehicle definition data structure sample	28
8.7 Maximum rotation angle of the aircraft and angle margin at actual rotation	30
8.8 Variation of rate of climb with altitude at $W = 180,000 \text{ kg}$	31
8.9 Response surface of aspect ratio vs MTOW (with fuel burn as gradient and fuel margin as contour lines)	31
8.10 Response surface of Oswald factor vs MTOW (with fuel burn as gradient and fuel margin as contour lines)	31
8.11 Response surface of wing area vs MTOW (with fuel burn as gradient and fuel margin as contour lines)	32
8.12 Response surface of wing area vs Oswald factor (with fuel burn as gradient and fuel margin as contour lines)	32
8.13 Response surface of wing area vs cruise speed (with fuel burn as gradient) (outgoing phase)	32
8.14 Response surface of wing area vs cruise speed (with fuel burn as gradient) (spraying phase)	32
8.15 Response surface of altitude vs cruise speed (with fuel burn as gradient and fuel margin as contour lines)	32
8.16 Response surface of altitude vs cruise speed (with fuel burn as gradient and fuel margin as contour lines with assumed constant altitude in spray cruise)	32
8.17 C_L , L/D and α over the SAGA mission	35
8.18 Drag breakdown over the SAGA mission	35
8.19 Required C_L for differing sweep angles at the V_c corresponding to M_{dd}	36
8.20 Response surface of the predicted sensitivity of AR and S on fuel burn	36
8.21 Lift and drag polar in take-off conditions: $M = 0.270$, $Re = 26.7 \cdot 10^6 - 53 \cdot 10^6$	40
8.22 Lift and drag polar in outgoing cruise conditions: $M = 0.647$, $Re = 17 \cdot 10^6 - 34 \cdot 10^6$	40
8.23 Lift and drag polar at 18.5 km altitude: $M = 0.712$, $Re = 8.00 \cdot 10^6 - 16.0 \cdot 10^6$	41
8.24 Lift and drag polar at diversion: $M = 0.500$, $Re = 21.5 \cdot 10^6 - 42.0 \cdot 10^6$	41
8.25 $C_{L_{max}}$ and C_L for 1g at the start of 18.5 km cruise 3D analysis. The 200 m/s is based on SU2, the others from windtunnel data	41
8.26 BPR effect on thrust and SFC	44
8.27 OPR effect on thrust and SFC	44
8.28 Bypass ratio and overall pressure ratio sizing. Lines represent thrust [N]	45
8.29 Fan pressure ratio sizing	45
8.30 Fan side map	46
8.31 Fan core map	46
8.32 LPC map	46
8.33 HPC map	46
8.34 Thrust variation with temperature	48
8.35 Thrust variation with inlet size and bypass ratio	48
8.36 Thrust variation with bypass ratio and altitude	49
8.37 SFC variation with bypass ratio and altitude	49

8.38 Total wing structural mass versus aspect ratio for unsupported and strut braced wings for both the chosen boron fibre laminate composite and aluminium	50
8.39 Algorithm of the strut sizing	50
8.40 Internal shear force with and without axial force	51
8.41 Internal bending moment with and without axial force	51
8.42 Wing box, strut and total masses in relation to spanwise strut attachment point location and tip deflection limit for AR=13 (Composite)	52
8.43 Most critical loading diagram (19.5km altitude, end of dispersion phase)	53
8.44 Shear envelope (AR=13, Composite)	53
8.45 Moment envelope (AR=13, Composite)	53
8.46 Flowchart of the wing box sizing program	54
8.47 Deflections during the critical load cases for both the fuel tank at the tip and the root	55
8.48 Shear modulus versus elastic modulus for HMCF and boron fibre composite	57
8.49 Frequency and damping ratio plotted against velocity for the unstable modes; altitude = 13 km (cruise leg 1)	62
8.50 Effect of clamped wing assumption	62
8.51 Effect of constant mass assumption	62
8.52 The effect of aspect ratio on torsional divergence and control reversal, for a strut-braced composite wing design; altitude = 13 km (cruise leg 1)	63
8.53 The effect of aspect ratio on flutter speed for aluminium conventional design, based on the analytical method and NeOCASS simulation; altitude = 13 km (cruise leg 1)	64
8.54 The effect of aspect ratio on flutter speed for a strut-braced composite design, based on analytical solution; altitude = 13 km (cruise leg 1)	64
8.55 The flutter velocity of an aircraft with $AR = 12$ at 13 km altitude for different aircraft c.g. locations	65
8.56 The effect of x_θ on flutter speed, for a conventional design computed analytically; altitude = 13 km (cruise leg 1)	66
8.57 The effect of engine placement on flutter speed, for an aluminium design without struts generated by NeoCASS; altitude = 13 km (cruise leg 1)	66
8.58 Scissor plot and selected normalised horizontal tail area	67
8.59 Loading diagram	67
8.60 Rudder deflection required for coordinated turn for varying velocity and roll angle	70
8.61 Tail lift coefficient during start of first (colored) and third (lines) cruise phase for varying engine and wing position	71
8.62 Lift coefficient during start of first (colored) and third (lines) cruise phase for varying engine and wing position	71
8.63 Sloshing frequency for the fundamental mode as function of liquid level and tank geometry	72
8.64 Layout of the fuel system	73
8.65 Layout of the hydraulic system	74
8.66 Layout of the electrical system	74
8.67 Communication flow diagram for SAGA	75
8.68 Interaction between main hardware and software components	76
8.69 Layout of the data handling system	77
8.70 Schematic drawing of the part of one wing containing the aerosol systems	79
8.71 Response surface showing the effect of tank wall thickness and starting temperature on fuel required for evaporation power	81
8.72 Power required for aerosol evaporation during the dispersion part of the mission as a function of time	81
8.73 Power required for aerosol evaporation during the dispersion part of the mission as a function of time for different payloads	83
8.74 Critical (highest) power required for aerosol evaporation as a function of payload	83
8.75 Weight of the aerosol handling systems as a function of payload	83
 12.1 Cost breakdown structure	104
12.2 Composition of initial and operational cost before depreciation is implemented	109
12.3 Composition of initial and operational cost after depreciation is implemented	109
12.4 Response surface of the annual operational cost and the budget (black line) plotted against the fuel price and the payload per aircraft. White line corresponds to the design payload.	109
12.5 Target and actual values for MTOW (upper lines) and OEW (lower lines)	111
 15.1 Timewise manufacturing, assembly and integration diagram	123
16.1 Project logic diagram	125
16.2 Project logic diagram (continued)	126
16.3 Post-DSE Gantt chart	127

List of Tables

4.1 Total acquisition cost estimations for case A and B	10
4.2 Selected airports and properties	11
5.1 Final trade-off table for initial concept selection	13
8.1 Design Variables with Initial conditions, Optimal results, and Bounds	26
8.2 Constraints for Optimization Study	26
8.3 Minimum required subsystem performance stemming from mission analysis	28
8.4 Verification results for the climb gradient requirements	29
8.5 Take-off and landing distance verification results	30
8.6 Main wing, horizontal tail, vertical tail and strut planform parameters	36
8.7 Initial airfoil selection, C_{d_0} and C_{m_0} are drag and moment coefficients at the design C_l	37
8.8 Main wing airfoil trade-off table. The column scores are unweighted and with respect to the NLR7301 baseline	38
8.9 Verification of aerodynamic parameters. Re and M are equal input in both models. C_{D_0} and C_{D_i} are tested at $\alpha = 3^\circ$. SUAVE is treated as baseline	42
8.10 SU2 validation. Case 1 is at $\alpha = 3^\circ$, $Re = 15 \cdot 10^6$, $M = 0.712$, case 2 is at $\alpha = 1.03^\circ$, $Re = 9.98 \cdot 10^6$, $M = 0.704$	42
8.11 Off-design engine performance	45
8.12 Engine main assumptions	46
8.13 Engine specifications	46
8.14 Wing weight with and without struts for composite and aluminium (AR=13)	49
8.15 Limit loads	52
8.16 Directional properties of the composites	56
8.17 Aeroelastic speeds for the SAGA for different flight phases. Analytical solution analyses composite design with struts, NeoCASS uses a conventional aluminium design. (for explanation see Section 8.6.3)	59
8.18 Input values for static aeroelasticity calculations	60
8.19 Most important values for AcBuilder Pre-Processor	61
8.20 Eigenmotion characteristics	67
8.21 Control surface sizes and deflections	68
8.22 Required rudder effectiveness for various situations	68
8.23 Verification and validation data	70
8.24 Passed on communication data/commands as shown in the Communication Flow Diagram	76
9.1 Operational requirements	86
9.2 CS25 requirements	88
9.3 Requirements to be verified in future stages	89
11.1 Risk map for aircraft-related risks	95
11.2 Risk map after implementation of mitigation strategies	95
11.3 Risk map for operational risks	97
11.4 Risk map after implementation of mitigation strategies	98
11.5 Risk map for aerosol-related risks	100
11.6 Risk map after implementation of mitigation strategies	100
11.7 Risk map for remaining aircraft design risks	102
11.8 Risk map after implementation of mitigation strategies	102
11.9 Technical design margins	103
12.1 Cost estimation in billion dollars, assuming a program duration of 20 years	106
12.2 Yearly costs for ground control station crew. Labour rates are taken from [131]	107
12.3 Contingency budget	110
12.4 Operational empty weight breakdown	111
12.5 Maximum take-off weight breakdown	111
12.6 Power breakdown	112
12.7 Capital cost breakdown	112
12.8 Operational cost breakdown	112
12.9 Drag breakdown	113

12.10 Fuel burn breakdown	113
13.1 Reliability of some of the aircraft systems for a single flight	116
A.1 SUAVE input and useful output	141

A. SUAVE inputs and outputs

In this chapter, a list for the most critical inputs and outputs used in the SUAVE environment is presented. This list can be seen in Table A.1

Table A.1: SUAVE input and useful output

Input	Conventional
hline MTOW [kg]	207 000
$m_{payload}$ [kg]	35 000
n_{ult} [-]	2.5
n_{lim} [-]	1.5
S [m^2]	700
A [-]	13
Λ_{TE} [deg]	0
λ (taper)	0.5
t/c [-]	0.14
c_{flap} [m]	0
A_h [-]	5
S_h [m^2]	139
Λ_h [deg]	10
λ (taper) [-]	0.3
t/c_h [-]	0.12
A_v [-]	2.5
S_v [m^2]	39
Λ_v [deg]	35.0
λ [-] (taper)	0.2
t/c_v [-]	0.10
d_{fus} [m]	3.88
l_{fus} [m]	40.046
$N_{engines}$	4
Bypass ratio [-]	7.5
OPR [-]	51
Total design Thrust (iteration) [kN]	250
Climb1 [h_{end} [km], V_{EAS} [km/h], c [m/s]]	[3,368, 55.55]
Climb2 [h_{end} [km], V_{EAS} [km/h], c [m/s],]	[6, 396.7, 29.4]
Climb3 [h_{end} [km], V_{EAS} [km/h], c [m/s]]	[11, 410, 14.88]
Climb4 [h_{end} [km], V_{EAS} [km/h], c [m/s]]	[13.14, 367.2, 20.98]
Cruise outgoing [h_{end} [km], V_{EAS} [km/h], c [m/s]]	[13.14, 329.4, 0]
Climb5 [h_{end} [km], V_{EAS} [km/h], c [m/s]]	[17, 272.5, 10.72]
Climb6 [V [h_{end} [km], V_{EAS} km/h], c [m/s]]]	[18.5, 242.6, 3.16]
Cruise spraying-1 [h_{end} [km], V_{EAS} km/h], c [m/s]]]	[18.5, 242.6, 0]
Climb7 [h_{end} [km], V_{EAS} [km/h], c [m/s]]]	[19, 233.3, 1.67]
Cruise spraying-2 [h_{end} [km], V_{EAS} km/h], c [m/s]]]	[19, 233.3, 0]
Climb8 [h_{end} [km], V_{EAS} [km/h], c [m/s]]]	[19.5, 224.6, 2.78]
Cruise spraying-3 [h_{end} [km], V_{EAS} km/h], c [m/s]]]	[19.5, 252.4, 0]
Reserve cruise [h_{end} [km], V_{EAS} km/h], c [m/s]]]	[11, 297, 0]